# Myeloperoxidase Enhances DNA Damage Induced By Drugs Targeting DNA Topoisomerase II

**Mandeep Atwal**

**Doctor of Philosophy**

**Institute for Cell and Molecular Biosciences**
**Faculty of Medical Sciences Newcastle University**

**July 2017**

## Abstract

Topoisomerase II (TOP2) poisons are effective anti-cancer agents used to treat a wide range of neoplasms. However, TOP2 poisons are subjected to enzymatic conversion which leads to metabolites with altered DNA damaging properties. Myeloperoxidase, present exclusively within developing myeloid progenitors and granulocytes, is capable of the biotransformation of TOP2 poisons to metabolites that are potentially more genotoxic in nature. Whilst TOP2 poisons are valuable chemotherapeutic agents, their use is associated with myelosuppression and with the risk of developing therapy related acute myeloid leukaemia. The reason that myeloid progenitor cells are particularly susceptible to TOP2 poison associated genotoxicity is unclear, however the presence of myeloperoxidase could potentially make myeloid progenitor cells more vulnerable to TOP2 poison mediated damage. This lead to the hypothesis that myeloperoxidase inhibition could protect developing hematopoietic cells from TOP2 poison associated genotoxic and/or cytotoxic damage. Data generated in this thesis supports the proposed hypothesis as expression of myeloperoxidase significantly enhanced the accumulation of TOP2 poison induced TOP2-DNA covalent complexes and the level of DNA breaks within myeloid cell lines. The use of two potential clinically relevant inhibitors of myeloperoxidase showed that reduction in myeloperoxidase activity reduced the abundance of TOP2 poison stabilised TOP2-DNA complexes and DNA breaks. Furthermore, depletion of glutathione to mimic conditions experienced during chemotherapy, resulted in a myeloperoxidase dependent increase in TOP2 poison mediated DNA damage. Taken together these results show inhibition of myeloperoxidase could protect developing hematopoietic cells from TOP2 poison mediated damage without compromising the effectiveness of these drugs as anti-neoplastic agents.

**Acknowledgements**

I would like to start by thanking my supervisors, Dr. Ian G. Cowell and Professor Caroline. A. Austin for their continuous support and guidance throughout this project and in the writing of my thesis. Their support was invaluable for this project and for my development as a scientist, and thank you is not enough to express my gratitude. I would like to thank all the team members within the Austin lab for their support and the many memories that I will cherish from working with them. I would also like to acknowledge and thank Breast Cancer Now for funding my PhD project (Grant 2012 November PhD11).

Additionally, I would like to thank Dr. Angelica Mariani for the synthesis of etoposide catechol and etoposide quinone which were used to conduct experiments shown in Chapter 5, section 5.3.3, Figures 5.7 and 5.8; and also for support Angelica has provided.

The work shown in Chapter 3 Section 3.3.7 (Figures 3.17 to 3.19) was conducted jointly with a graduate student, Miss Emma L. Lishman under my guidance.

The work presented in Chapters 3, 4 and 5 has been published in the following research article:

Atwal, M., Lishman, E.L., Austin, C.A. and Cowell, I.G. (2017) 'Myeloperoxidase Enhances Etoposide and Mitoxantrone-Mediated DNA Damage: A Target for Myeloprotection in Cancer Chemotherapy', *Mol Pharmacol*, 91(1), pp. 49-57.

# Table of Contents

## Abbreviations

| | |
|---|---|
| $1e^-$ | One electron oxidation |
| aa | Amino acids |
| 4-ABAH | 4-Aminobenzoic acid hydrazine |
| AML | Acute myeloid leukaemia |
| APL | Acute promyelocytic leukaemia |
| ATCC | American type culture collection |
| ADP | Adenosine diphosphate |
| AMPPNP | Adenylyl-imidodiphosphate |
| ATP | Adenosine triphosphate |
| AZD | AstraZeneca |
| bp | base pairs |
| BSA | Bovine serum albumin |
| BSO | Buthionine sulfoximine |
| CLN | Calnexin |
| CLP | Common lymphoid progenitor cell |
| CML | Chronic myeloid leukaemia |
| CMP | Common myeloid progenitor cell |
| CO2 | Carbon dioxide |
| CRT | Calreticulin |
| CTD | C-terminal domain |
| CYP | Cytochrome P450 |
| DAPI | 4',6-Diamidino-2-phenylindole |

| | |
|---|---|
| dH2O | Distilled water |
| DMEM | Dulbecco's modified eagle medium |
| DMSO | Dimethyl sulfoxide |
| DNA | Deoxyribonucleic acid |
| DSB | Double-strand break |
| DTT | Dithiothreitol |
| ECACC | European Collection of Cell Cultures |
| ECAR | Extracellular acidification rate |
| ECL | Enhanced chemiluminescence |
| EDTA | Ethylenediaminetetraacetic acid |
| EP | Erythrocyte progenitor cell |
| FBS | Foetal bovine serum |
| FCCP | Carbonyl cyanide 4-(trifluoromethoxy)phenylhydrazone |
| FDA | Food and Drug Administration |
| FISH | Fluorescence in situ hybridisation |
| FITC | Fluorescein isothiocyanate |
| G418 | Geneticin |
| GAPDH | Glyceraldehyde 3-phosphate dehydrogenase |
| GFP | Green fluorescent protein |
| GHKL | Gyrase, Hsp90, Histidine Kinase, MutL domain |
| GMP | Granulocyte-macrophage progenitor cell |
| GSH | Reduced glutathione |
| GST | Glutathione S-transferase |
| H2AX | H2A histone family, member X |

| | |
|---|---|
| H2O2 | Hydrogen peroxide |
| HCl | Hydrogen chloride |
| HEPES | 4-(2-hydroxyethyl)-1-piperazineethanesulfonic acid |
| HMG | High-mobility group |
| HOCl | Hypochlorous acid |
| HR | Homologous recombination |
| HSC | Haematopoietic stem cell |
| IC50 | Half maximal inhibitory concentration |
| IDMEM | Iscove's Modified Dulbecco's Modified Eagle's Medium |
| IgG | Immunoglobulin G |
| kb | kilobases |
| $k_{cat}$ | Catalytic rate constant |
| $K_D$ | Dissociation rate constant |
| KCl | Potassium chloride |
| kDa | kilodaltons |
| LMPP | Lymphoid-primed multi-potent progenitor cell |
| LPO | Lactoperoxidase |
| m-AMSA | Amsacrine |
| MAPK | Mitogen-activated protein kinase |
| MEF | Mouse Embryonic fibroblasts |
| MEP | Megakaryocyte-erythrocyte progenitor cell |
| MgCl2 | Magnesium chloride |
| MkP | Megakaryocyte progenitor cell |
| MLL | Mixed lineage leukaemia |

| | |
|---|---|
| MPO | Myeloperoxidase |
| MPO inhibitor II | 4-(5-Fluoro-1H-indol-3-yl)butanamide |
| MPP | Multi-potent progenitor cell |
| MS | Multiple sclerosis |
| $MH_2X$ | Mitoxantrone |
| NaCl | Sodium chloride |
| NADPH-oxidase | Nicotinamide adenine dinucleotide phosphate oxidase |
| NaPO4 | Sodium phosphate |
| NCBI | National Centre for Biotechnology Information |
| NET | Neutrophil extracellular traps |
| NICE | National Institute for Health and Care Excellence |
| NK | Natural killer cell |
| NMR | Nuclear magnetic resonance spectroscopy |
| NS | Non-significant |
| nt | Nucleotides |
| OCR | Oxygen consumption rate |
| PAGE | Polyacrylamide gel electrophoresis |
| PARP-1 | Poly (ADP-ribose) polymerase-1 |
| PBS | Phosphate buffer saline |
| PDB | Protein Data Bank |
| PF | Pfizer |
| PF-1355 | [2-(6-(2,5-dimethoxyphenyl)-4-oxo-2-thioxo-3,4-dihydropyrimidin-1(2H)-yl)acetamide) |
| PI | Protease inhibitor cocktail |

| | |
|---|---|
| PML | Promyelocytic leukaemia |
| PMS | N-methyl dibenzopyrazine methyl sulphate |
| Por | Porphyrin |
| QTK | Glutamine, Threonine, lysine loop |
| PPR | Proton production rate |
| RARA | Retinoic acid receptor alpha |
| RNA | Ribonucleic acid |
| RPMI | Roswell Park Memorial Institute medium |
| RT-PCR | Reverse transcription polymerase chain reaction |
| RUNX | Runt-related transcription factor |
| SA | Succinylacetone |
| SDS | Sodium dodecyl sulphate |
| SEM | Standard error of the mean |
| SWI/SNF | SWItch/Sucrose Non-Fermentable chromatin remodelling complex |
| t-AL | Therapy-related leukaemia |
| t-AML | Therapy-related acute myeloid leukaemia |
| t-APL | Therapy-related acute promyelocytic leukaemia |
| TARDIS | Trapped in Agarose Immunostaining assay |
| TBE | Tris-borate-EDTA buffer |
| TBS | Tris buffered saline |
| TBS-T | Tris buffered saline and 0.1% Tween20 |
| TOP1 | Topoisomerase I |
| Top1 | yeast Topoisomerase I |

| | |
|---|---|
| TOP2 | Topoisomerase II |
| Top2 | yeast Topoisomerase II |
| TOP2A | Topoisomerase II alpha |
| TOP2B | Topoisomerase II beta |
| TOP3A | Topoisomerase III alpha |
| TOP3B | Topoisomerase III beta |
| TOPRIM | TOpisomerase/PRIMase domain |
| (v/v) | volume per volume |
| WCE | Whole cell extract |
| WHD | Winged helix domain |
| WHO | World Health Organisation |
| (w/v) | weight per volume |
| XTT | 2,3-bis-(2-methoxy-4-nitro-5sulphenyl)-(2H)-tetrazolium-5-carboxanilide |

## List of figures

## List of tables

# Chapter 1. Introduction

## 1.1 Topoisomerase II (TOP2)

Topoisomerases are critical cellular enzymes present in all domains of life. Their function is to relieve DNA topological stress allowing normal DNA processes such as transcription, replication and chromosome segregation to occur efficiently. Humans encode six topoisomerases (TOP) known as TOP1, TOP1mt (mitochondria specific), TOP2A, TOP2B, TOP3A and TOP3B. Topoisomerases catalytic mechanism involves the cleavage of a DNA segment followed by either a DNA strand passage (TOP2 and TOP3) or a controlled DNA rotation event (TOP1) and the subsequent re-ligation of the cleaved DNA molecule. Due to topoisomerases being essential nuclear enzymes functioning in processes such as cell proliferation and their ability to catalyse DNA strand breaks, human topoisomerases are targeted in chemotherapy regimens. The focus of this thesis will be on human topoisomerase II (TOP2) and will be discussed in detail herein.

### *1.1.1 TOP2 isoforms and cellular roles*

Humans express two isoforms of TOP2 known as Topoisomerase II alpha (TOP2A) and Topoisomerase II beta (TOP2B) (EC 5.99.1.3) that are encoded on separate genes and differentially regulated in cells (TOP2A 17q21-22; TOP2B 3q24) (Tsai-Pflugfelder *et al.*, 1988; Chung *et al.*, 1989; Drake *et al.*, 1989; Austin and Fisher, 1990; Jenkins *et al.*, 1992). The isoforms share an overall 68% amino acid identity. The N-terminal region and catalytic portions share 78% amino acid identity, whereas the C-terminal region shares only 34% identity between the two isoforms (Austin *et al.*, 1993).

TOP2A (170kDa) is essential for the survival of proliferating cells and its expression (protein and mRNA) is tightly regulated during the cell cycle (Woessner *et al.*, 1991; Pendleton *et al.*, 2014). TOP2A protein expression is at its highest during the G2/M phase of the cell cycle and remains low in G1 to mid-S phase (Heck *et al.*, 1988; Felix *et al.*, 2006) (Figure 1.1.A). The cell cycle regulation of TOP2A protein

expression is due to key post-translational modifications and changes in mRNA stability with a 15-fold elevation in mRNA levels at late S-phase (Wells *et al.*, 1995b; Goswami *et al.*, 1996). This also correlates with a peak in TOP2A activity at M-phase and activity is dependent on phosphorylation of residues within the C-terminus (Corbett *et al.*, 1993; Chikamori *et al.*, 2003; Li *et al.*, 2008). Defects in phosphorylation of TOP2A or inhibition of TOP2A activity can result in S-phase arrest (Ishida *et al.*, 1996; Li *et al.*, 2008; Wu *et al.*, 2016).

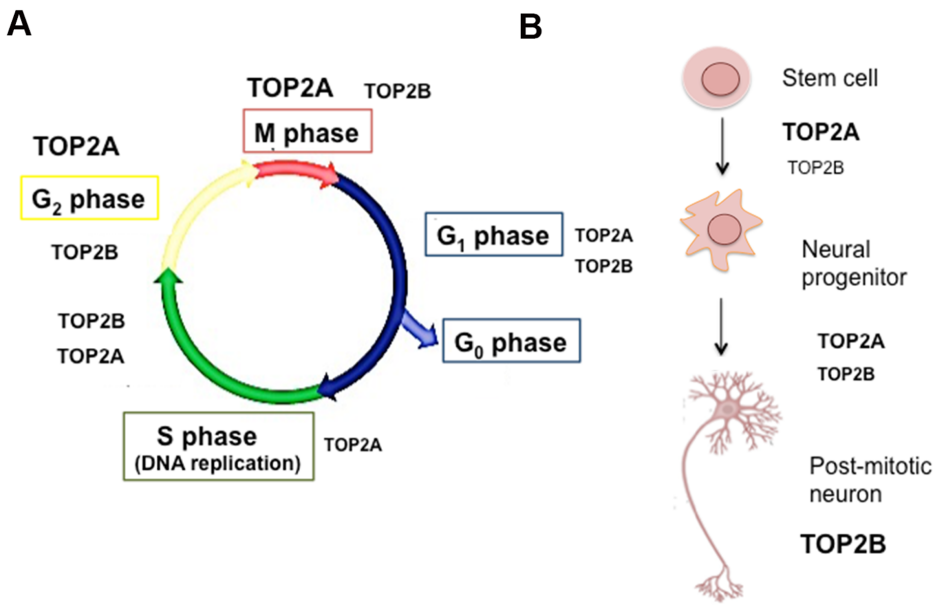


**Figure 1.1 (A) Cell cycle changes in TOP2A and TOP2B levels and (B) Switching of TOP2A and TOP2B expression in cell differentiation.** (A) The cell cycle is divided into four phases; G1 (stage of metabolic changes to prepare cells for chromosome duplication), S phase (DNA replication to duplicate chromosomes), G2 (undergo metabolic changes to prepare the cell for mitosis and to check duplicated chromosomes), M phase (nuclear division followed by cell division by cytokinesis). During the cell cycle phases, TOP2 expression is dynamically regulated both at the mRNA level and by post-translational modifications to regulate TOP2 activity and cellular distribution.

In contrast, TOP2B (180kDa) levels remain constant once cells enter the cell cycle, after cell cycle exit TOP2B levels can drop by ~60% (Woessner *et al.*, 1991; Meyer *et al.*, 1997) (Figure 1.1.A). TOP2B is the predominant isoform in post-mitotic differentiated cells whereas; TOP2A expression is almost absent in quiescent and terminally differentiated cells (Woessner *et al.*, 1991; Thakurela *et al.*, 2013). However, in foetal tissues TOP2A is strongly associated at sites of proliferation compared to TOP2B, but TOP2A also present in foetal cells which have differentiated (Zandvliet *et al.*, 1996).

TOP2B plays an essential role in transcriptional regulation and is required for proper neural and retinal development and in the transcriptional regulation of ligand inducible genes (Manville *et al.*, 2015; Calderwood, 2016). Studies conducted using mouse embryonic stem cells induced to differentiate into post-mitotic glutamatergic neurons showed TOP2A and TOP2B expression can 'switch' during cell differentiation. This study showed TOP2A levels were high during the stem cell to neuronal progenitor stage. Once stem cells had differentiated into post-mitotic, neurons TOP2A levels were undetectable and this was accompanied by an increase in both TOP2B mRNA and protein expression (Tiwari *et al.*, 2012) (Figure 1.1.B).

### *Role of TOP2A in DNA replication, S-phase transcription and chromosome condensation and segregation.*

#### *DNA replication*

DNA replication is initiated at multiple sites across chromosomes. Dynamic protein and DNA polymerase containing structures form around a DNA segment during replication and are termed replication forks. Replication forks consist of cellular machinery required to replicate DNA, including DNA helicases that use ATP to unwind the DNA helix, separating parental strands (Branzei and Foiani, 2010). Unwinding of the DNA duplex creates differences in the topology and conformation of the replicating DNA creating torsion stress. This results in positive supercoiling ahead of the replication fork and precatenanes (wrapping of two replicated strands) behind the replication fork (Peter *et al.*, 1998) (Figure 1.2.A).

DNA cannot resolve supercoiling stress by itself and the presence of chromatin structure (nucleosomes) prevents the diffusion of positive supercoils therefore, hindering the progression of replication (Mondal *et al.*, 2003). The cleavage and religation activity of TOP1 and TOP2 can relax positive supercoiling ahead of the replication fork sustaining the progressive action of the replication machinery (Figure 1.2.A). Precatenanes do not pose a major threat to replication machinery however as these structures form by winding of daughter chromosomes around each other, this would create a problem during chromosome segregation in mitosis.

Precatenanes are substrates for TOP2A. Studies conducted in *Xenopus* egg extracts showed TOP2 is dispensable for plasmid DNA replication, but the plasmid is associated with increased positive helical stress. Furthermore, by mapping the TOP2 cleavage site (using stabilisation of TOP2-DNA complexes by the TOP2 poison

etoposide) showed TOP2 predominantly acts behind the replication fork (Lucas *et al.*, 2001).

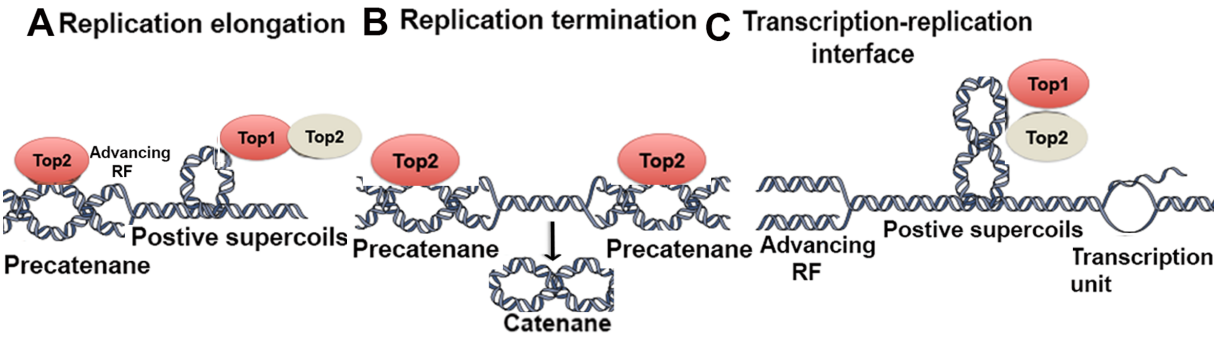


**Figure 1.2 Requirement of TOP2 to relieve positive supercoiling during different stages of replication.** (A) During the progression of the replication fork (RF), the unwinding action of ATP-dependent helicases creates positive supercoiling ahead of the replication fork and behind the replication fork precatenanes develop causing a problem for chromosome segregation. (B) At replication termination, the progression of two replication forks closes the gap separating the two forks creating positive supercoils, the merging of two replication forks at termination creates catenated sister chromatid junctions which are resolved by TOP2. (C) Replication forks colliding with transcription factories in S-phase can slow down replication and TOP1/TOP2 can create DNA looping to insulate the transcription machinery preventing collision with replication forks. TOP2 is labeled as Top2 and TOP1 as Top1 as the yeast nomenclature are used, the alternative dark red to off white colouring associated with Top2 or Top1 is used to show which topoisomerase is shown to function more predominantly in the different progresses of replication (red=major role; off white=minor role according to reported data). Figure adapted with permission from Branzei and Foiani 2010.

Studies have suggested that TOP2A has a more predominant role at the final stages of DNA replication and this coincides with the high expression of TOP2A at late S-phase (Figure 1.1). Earlier studies have shown that TOP2 (Top2) mutant yeast were defective at the stages of DNA replication termination but not in replication elongation (Brill *et al.*, 1987). At replication termination, two replication forks fuse creating interlinked catenanes (interlocked DNA molecules) and require separation by TOP2 prior to segregation (Sundin and Varshavsky, 1980; Sundin and Varshavsky, 1981) (Figure. 1.2.B). Experiments conducted using yeast TOP2 (Top2) showed that during S phase, Top2 is recruited to sites of chromosomal termination regions (TERs) to prevent chromosomal fragmentation during replication fork fusion. Top2 mutants displayed delayed replication termination, exhibited un-replicated regions and had chromosome entanglements resulting in chromosomal breakage during segregation (Wang, 2002; Fachinetti *et al.*, 2010).

Another role of TOP2A in S phase is to prevent collision of replication forks with transcription hubs. TOP2 solves this problem by binding to intragenic regions (DNA

located between genes) using the HMG protein Hmo1 (High mobility group of proteins). TOP2 is thought to insulate transcription bubbles from replication forks in S phase by looping DNA to concentrate transcription machinery and to maintain chromosome stability (Bermejo *et al.*, 2009) (Figure 1.2C). However, TOP1 may play a more predominant role over TOP2A in S-phase transcription (Tuduri *et al.*, 2009).

During the process of DNA replication, TOP2A has a role in relaxing DNA supercoils and but also maintaining genomic stability. Sites of replication termination and intragenic regions (region between genes) are fragile sites within chromosomes and are frequently associated with phosphorylated H2Ax sites (marker of DNA damage). The binding of TOP2A to these regions is suggested to protect DNA from aberrant breaks induced by torsion stress created by the movement of cellular machinery (Bermejo *et al.*, 2009; Fachinetti *et al.*, 2010).

***Chromosome segregation and condensation***

DNA replication has been reported to prime the accumulation of TOP2A to heterochromatin in late S phase, as failure of DNA replication results in loss of the tight association of TOP2A with chromosomes (Cuvier and Hirano, 2003; Gonzalez *et al.*, 2011). The processes of chromosome segregation and condensation are dependent on TOP2A. At the concentrations expressed in cells, TOP2B cannot compensate for the loss of TOP2A protein expression. In the G2/M phase TOP2A is required to facilitate the untangling of catenations, condensation and segregation of chromosomes (Holm *et al.*, 1985; Uemura and Tanagida, 1986; Adachi *et al.*, 1992; Buchenau *et al.*, 1993). TOP2A binds tightly to chromatin as studies showed that during S phase and metaphase TOP2A is harder to extract using sodium chloride (350mM) whereas the equivalent concentration of salt can extract more than 90% TOP2B but only 52% of TOP2A is extractable (Meyer *et al.*, 1997).

The recruitment of TOP2A to chromosomes is partly dependent on its interaction with the chromatin remodeller complex BAF (mSWI/SNF). Specificity the interaction of TOP2A is with BAF's ATPase subunit, BAF250a (Dykhuizen *et al.*, 2013). However, authors also identified regions of genome where TOP2A binds independently to BAF.

TOP2A also is essential for anaphase sister chromatid separation. In Drosophila cells, depletion of Top2 resulted in 2.5 fold decrease in chromosome compaction and chromosomes were described to be morphologically abnormal (Chang *et al.*, 2003).

During the M (mitotic) phase of the cell cycle, TOP2A dynamically associates with mitotic chromatin and remains associated until anaphase being highly concentrated at the centromeres where it has a structural role and causes chromatin hyper-compaction. Disruption of TOP2A's catalytic function results in deficient chromosome hyper-compaction slowing progression through the G2/M phase (Earnshaw and Heck, 1985; Tavormina *et al.*, 2002).

TOP2B is also reported to distribute weakly along chromosomes, contributing to the initial shortening of chromosomes (Taagepera *et al.*, 1993; Christensen *et al.*, 2002; Null *et al.*, 2002; Farr *et al.*, 2014). However, the mechanisms of TOP2B in the localisation and shortening of mitotic chromosomes are not yet fully understood. However, it could be that localisation of TOP2B across the arms of chromosomes causes initial compaction to aid in TOP2A-mediated chromatin hyper-compaction.

***Transcription***

Both isoforms of TOP2 play roles in transcription. TOP2A is involved in both transcription initiation and transcription elongation. TOP2B plays a predominant role in regulating transcription at signal-dependent promoter and regulatory regions of genes in response to ligands.

***Transcription elongation***

During transcription, the progression of DNA through RNA polymerase II generates positive supercoiling ahead of RNA polymerase II and negative supercoiling behind. This is referred as the 'twin supercoiled domain' generated during transcription (Liu and Wang, 1987; Wu *et al.*, 1988). If positive supercoiling were not resolved then this would result in hyperwinding of the DNA structure upstream of the template, blocking transcription. The relaxation activity of TOP2A is reported to be required during transcription elongation by the association with RNA polymerase (Schultz *et al.*, 1992).

Studies conducted in yeast showed, yeast deficient in Top2 or when Top2 activity was inhibited using etoposide or ICRF-193, transcription of nucleosome free DNA continued but transcription was inhibited for DNA wrapped in chromatin. This supports the hypothesis that in the presence of nucleosomes diffusion of positive supercoils is inhibited (Mondal and Parvin, 2001; Mondal *et al.*, 2003). However, earlier studies conducted in yeast suggested that Top2 is crucial for termination of

DNA replication and chromosome segregation but is dispensable for transcription (Brill *et al.*, 1987).

***Initiation of transcription***

A study conducted by Bunch and colleagues report that TOP2 may be required for the pause and release of RNA polymerase II at the transcription start site (Bunch *et al.*, 2015). The pause and release activity of RNA polymerase II at the promoter-proximal site before elongation is an important step in gene regulation and 'primes' genes for rapid induction. TOP2A and TOP2B mediated DSB seems to be an important step in pause-release activity of RNA polymerase II. As the catalytic inhibition of TOP2 resulted in retention of RNA polymerase II at transcription start sites and reduced the level of γH2Ax signal (marker of DNA damage). However, the level of retention of RNA polymerase II was greater for serum inducible genes. Additionally, TOP2A also plays a role in RNA polymerase Iβ transcription by inducing DSB in the promoter region to facilitate the assembly of the pre-initiation complex (Ray *et al.*, 2013).

***The role of TOP2B in regulating transcription of ligand inducible genes***

TOP2B has been reported to play role in regulating the transcription of hormonally and developmentally regulated genes and gene networks (Ju *et al.*, 2006b; Perillo *et al.*, 2008; Li *et al.*, 2014; Madabhushi *et al.*, 2015). Binding of TOP2B at promoter regions is required for neural and retinal development and the survival of post-mitotic cells. Furthermore, deficiency of TOP2B in mouse models has shown to lead increased DNA damage and contributes to neurodegeneration (Heng *et al.*, 2012).

Studies have shown that TOP2B is recruited to promoter regions of ligand dependent genes where it may have a role in the regulation of transcription. Furthermore, Non-homologous end joining (NHEJ) factors are associated with promoter regions indicating TOP2B may catalyse the formation of DNA break that requires repair.

A study conducted by Ju and colleagues showed that in the absence of estrogen, TOP2B and Poly[ADP-ribose] polymerase 1 (PARP-1) are located in a co-repressor complex on the promoter region of pS2 (estrogen regulated gene). Other components of the co-repressor complex include histone deacetylase 3, nuclear receptor co-repressor, nucleolin, nucleophosmin and heat shock protein 70. However, stimulation with 17-β estradiol resulted in a dynamic and rapid recruitment of TOP2B, PARP1 and components of the NHEJ system (DNA-PK/Ku86/Ku70) to

promoter of pS2 together with RNA polymerase II and the eviction of components within the co-repressor complex (except TOP2B and PARP-1).

TOP2B catalysed the formation of a DNA strand break between linker regions of nucleosomes and following this PARP-1 was activated to cause the exchange of nucleosomes to allow changes in chromatin architecture allowing nuclear receptor and transcription activation (Ju *et al.*, 2006a). A further study evaluated the hormone dependent recruitment of TOP2B/PARP 1 to the pS2 gene requires the chromatin remodellers BAF (mSWI/SNF) (Trotter *et al.*, 2015). Subsequent studies showed TOP2B DSB positively regulates androgen and glucocorticoid stimulated genes in response to ligand stimulation (Haffner *et al.*, 2010; Trotter *et al.*, 2015). However, TOP2B recruitment to the promoter of the RARA gene (retinoid nuclear receptors which regulate myeloid differentiation) is associated with transcriptional repression (McNamara *et al.*, 2008).

### *1.1.2.Structure of TOP2*

TOP2 functions as a dimeric enzyme with each monomeric unit consisting of three structural domains (Austin *et al.*, 1995) (Figure 1.3). The N-terminal domain is the site of DNA entry and consists of ATPase domain that is sub-divided into a N-terminal nucleotide binding domain (a member of the GHKL superfamily) and a C-terminal transducer domain. The central domain is referred as to the breakage-reunion core comprising of DNA-binding and the catalytic centre and is target for anti-cancer TOP2 poisoning agents. The C-terminal domain is the site for nuclear localisation signals and post-translational modifications and but is also important in regulating catalysis (Austin *et al.*, 1993; Wells *et al.*, 1995a; Ishida *et al.*, 1996; Cowell *et al.*, 2000; Kim *et al.*, 2002; Lindsey *et al.*, 2014; Yoshida *et al.*, 2016).

Separate protein structural determination of the breakage-reunion and ATPase units of *Saccharomyces cerevisiae* Top2, showed the dimeric enzyme has a two-fold symmetry (Berger *et al.*, 1996b) (Figure 1.3). In addition, the quaternary assembly of TOP2 was shown to make three major interfaces/gates that work in a coordinated manner allowing DNA cleavage and gated strand passage. These interfaces at which the protomers of the dimeric enzyme contact each other are known as the N-gate (N-terminal domain), DNA gate and C-gate (within breakage-reunion domain).

The N-gate is formed by the ATPase domains, as mentioned earlier this domain is sub-divided into nucleotide binding and transducer domains. The nucleotide-binding domain comprises of a GHKL ATP binding fold, which is also present in proteins such as gyrase B, Hsp90 and histidine kinases. The nucleotide binding and transducer domains form the ATP binding pocket (one ATP binds per monomer). Upon ATP binding, dimerisation occurs between the nucleotide GHKL domains of the two protomers, in particular an N-terminal coil region within the nucleotide domain, termed the N-terminal strap wraps around the symmetry axis to contact the neighbouring promoter. The C-terminal of the transducer domain is a key component consisting of an α/β fold and a conserved QTK loop, which forms a salt bridge and contacts the γ-phosphate of ATP. (Wigley *et al.*, 1991; Classen *et al.*, 2003; Wei *et al.*, 2005).

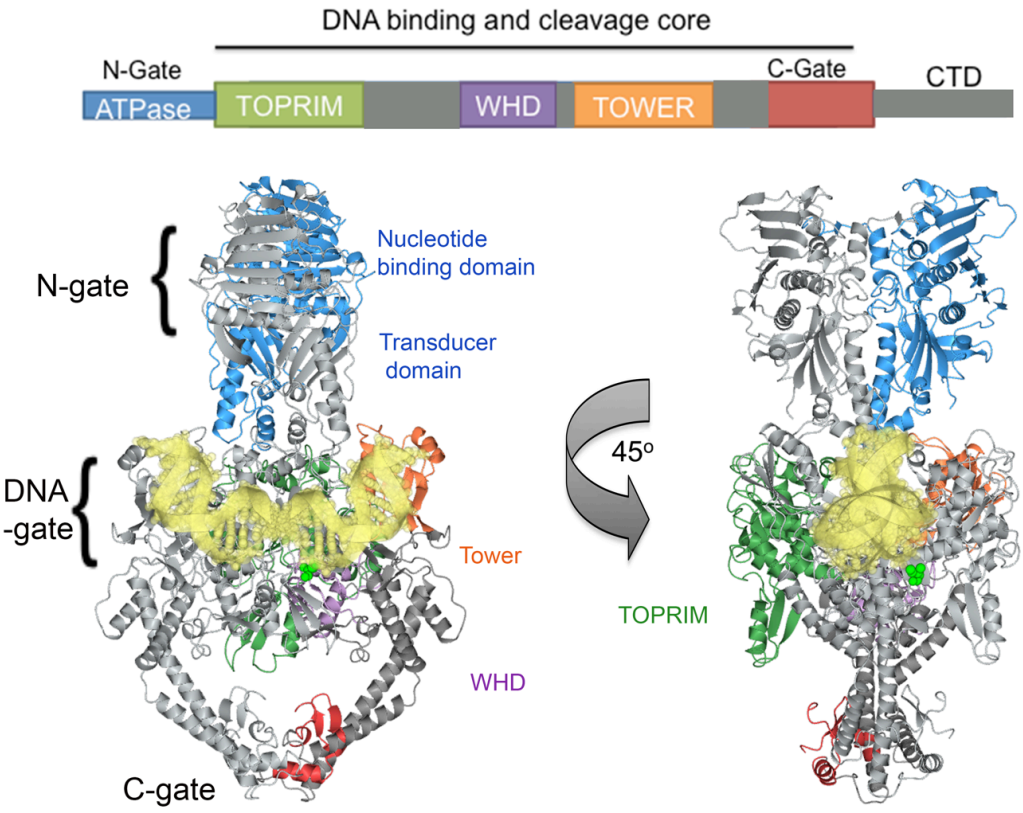


**Figure 1.3 Domain arrangement and protein structure of Saccharomyces *cerevisiae* TOP2 (PDB ID 4GFH).** One monomer of the TOP2 protein is coloured according the domain structure whilst the other monomer is coloured in grey. The DNA duplex is shown in yellow and the catalytic tyrosine is shown in green. Figure produced using CCP4MG version 2.9.0.

The DNA-gate consists of a TOpisomerase/PRIMase (TOPRIM) domain and a winged helix domain (WHD). The TOPRIM domain has a compact α/β fold of ~100 amino acids conserved from archaea, bacteria to humans. In the C-terminal region of the TOPRIM domain comprises of a catalytic $Mg^{2+}$ ion coordinated in an acidic triad (DxD motif) (Aravind *et al.*, 1998). The DxD (IMTD(Q/A)DxD) is critical and site-directed mutagenesis in this region results in an unstable protein that is rapidly degraded (West *et al.*, 2000). Also residing the TOPRIM domain is a non-catalytic tyrosine (Tyr640 for TOP2A and Tyr656 for TOP2B) is crucial for efficient TOP2 activity and mutations leads to resistance to TOP2 poisons (Kozuki *et al.*, 2017). The TOPRIM domain connects to the WHD via a three-helix bundle. The catalytic tyrosine is located in the WHD. Adjacent to the WHD is a tower domain arranged in a α/β fold (also participates in DNA binding), from the tower domain a coiled-coil domain extends to make connections with the C-gate, the site for DNA exit. Structural studies reveal the ATPase domain once dimerised, contacts the TOPRIM domain of its partner subunit. Although the significance of this is unknown, this signifies that each protomer subunit makes contacts with the neighbouring promoter serving to communicate information for strand cleavage and passage (Schmidt *et al.*, 2012).

Two separate TOP2 Saccharomyces *cerevisiae* structures revealed the dynamic nature of the TOPRIM and WHD domains as differences in the separation distance between the TOPRIM and WHD were reported by two separate studies (Berger *et al.*, 1996a; Fass *et al.*, 1999). This lead to the proposal of the TOPRIM and WHD undergo conformational changes to position the divalent $Mg^{2+}$ ion relative to tyrosine within WHD to allow DNA cleavage. Later studies showed the transition from the apo state (non DNA bound) to the DNA bound state, the TOPRIM domain would make an ~$80^{o}$ movement to contact the WHD domain. There are two main consequences for this rotation; the first is to position the $Mg^{2+}$ ion relative to the tyrosine to prime the DNA cleavage reaction and also to create a positively charged deep groove allowing channelling of the DNA into the cleavage core (breakage-reunion domain) (Dong and Berger, 2007) (see section 1.1.3).

Structural determination of the human TOP2A bound non-covalently to DNA and TOP2B stabilised in a cleavage complex with DNA and etoposide revealed similar arrangements of domains and overall quaternary structure as that of Saccharomyces *cerevisiae* (Wu *et al.*, 2011; Wendorff *et al.*, 2012) (Figure 1.4.A TOP2A bound to

DNA). By comparing previously solved TOP2 protein structures, Wendorff and colleagues suggest binding of the first segment of DNA promotes movement in the WHD domains which allow clamping of TOPRIM and tower domains around the DNA. In addition, the movement of WHD domains in each promoter is suggested to control the movement of the C-gate and therefore the coiled-coil domain that connect the DNA-gate to the C-gate controlling the movement of DNA (Wu *et al.*, 2011; Wendorff *et al.*, 2012).

Prior to solving the structure of breakage-reunion domain of TOP2, the structure of human TOP2A's dimeric ATPase domain was solved bound to ADP or AMPPNP (non-hydrolysable analogue, this locks the N-gate in the dimerised position) (Figure 1.4.B). By comparing the two bound states of the domain, authors found that in the ADP bound state, the ATPase domain displays a relaxed confirmation, in which the transducer domain extends and retracts the lysine from the QTK loop away from the γ-phosphate. This movement seems to be crucial in accommodating the second DNA segment (T-segment) into the enzyme (Wei *et al.*, 2005) (see section 1.1.3).

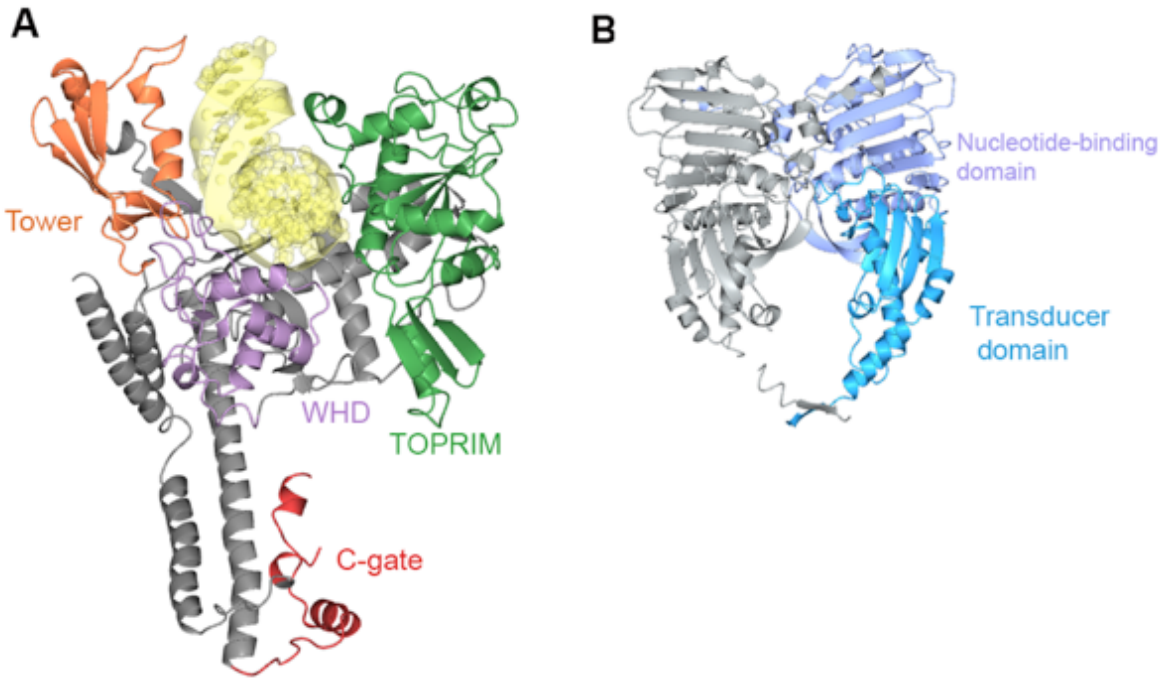


**Figure 1.4 (A) Structure of a fragment of human TOP2A bound non-covalently to DNA (residues 431-1193) (PDB ID 4FM9). (B) Structure of human TOP2A ATPase domain in ADP bound state (PDB ID 1ZXN).** DNA is coloured yellow. Figure produced using CCP4MG version 2.9.0.

However due to the structures of human TOP2A ATPase and DNA binding and cleavage core being solved separately the communication events between the two domains are not clear.

The C-terminal region (residues 1242-1531 TOP2A and 1263-1621 TOP2B) is the main but not only site for post-translational modifications, such as phosphorylation for cell-cycle control, nuclear localisation and nuclear export signals determining the cellular distribution of the enzymes (Adachi *et al.*, 1997; Cowell *et al.*, 1998; Mirski *et al.*, 1999; Mirski *et al.*, 2003; Meczes *et al.*, 2008). Studies conducted using chimeric TOP2A and TOP2B, which had exchange of C-terminal regions, showed the C-terminal region is not required for basic cleavage activity but presence of C-terminal region confers isoform specific properties of the TOP2 isoforms and allows determination of DNA's topological state (McClendon and Osheroff, 2006; McClendon *et al.*, 2008; Lindsey *et al.*, 2014).

The post-translational modifications on the C-terminal are important in controlling TOP2 activity; an example is the phosphorylation of residue Thr1342 on TOP2A. Threonine 1342 is phosphorylated throughout the cell cycle and targeting with a specific Thr1343 antibody (PT1343-reacts with TOP2A phosphoThr$^{1342}$) abolishes TOP2A activity suggesting this Thr1342 phosphorylation is key in controlling TOP2A activity (Ishida *et al.*, 1996). Similarly, phosphorylation at Ser1337 and Ser1524 during the cell cycle positively regulates TOP2A activity and defects in phosphorylation reduce TOP2A decatenation activity (Li *et al.*, 2008). Furthermore, fusion of TOP2B's C-terminal region with TOP2A resulted in a chimeric protein that was unable to support proliferation, and had lower enzymatic activity (Linka *et al.*, 2007; Meczes *et al.*, 2008). Furthermore, deletion of the C-terminal region of TOP2A but retaining the nuclear localisation signal enhances etoposide (TOP2 poison) cytotoxicity (Kozuki *et al.*, 2017). This further suggests that the C-terminal domain has an important role in controlling TOP2 activity.

### *1.1.3 Catalytic cycle of TOP2*

TOP2A and TOP2B function to alter DNA topology using an ATP dependent strand passage event to relieve DNA torsion stress (supercoiling). Both isoforms require almost identical concentrations of ATP for their catalytic activities and display similar

kinetics for ATP hydrolysis (TOP2B $k_{cat}$ 2.25$s^{-1}$ at 30$^{o}$C and for TOP2A $k_{cat}$ 2.17$s^{-1}$ at 37$^{o}$C) (West *et al.*, 2002).

However, TOP2A and TOP2B have certain differences in enzymatic properties, which are in part due the heterogeneity in the C-terminal regions. For example, TOP2B requires a higher concentration of KCl for in vitro cleavage reactions and is less thermally stable compared to TOP2A in vitro (Drake *et al.*, 1989). On the other hand, TOP2A can distinguish between different DNA geometries and can relax positively supercoiled DNA faster than negative helical twisted DNA (McClendon and Osheroff, 2006; McClendon *et al.*, 2008; Fernández *et al.*, 2014; Lindsey *et al.*, 2014). Both isoforms also display differences in DNA binding affinities, as TOP2B has a higher affinity for DNA compared to TOP2A and deletion of the C-terminal region of TOP2B greatly increases binding to DNA ($K_D$ 72.9 ± 18.6 for full length TOP2B vs 17.8± 2.72 for C-terminal truncated TOP2B) (Gilroy and Austin, 2011).

TOP2 works in a coordinated manner to alter the topological state of DNA by introducing two transient DNA nicks in one segment of DNA (G-segment) and allowing a second intact DNA molecule (T-segment) to pass unidirectionally from the N-gate to the C-gate, followed by the religation of the cleaved DNA (Cowell and Austin, 2012; Pendleton *et al.*, 2014) (Figure 1.5).

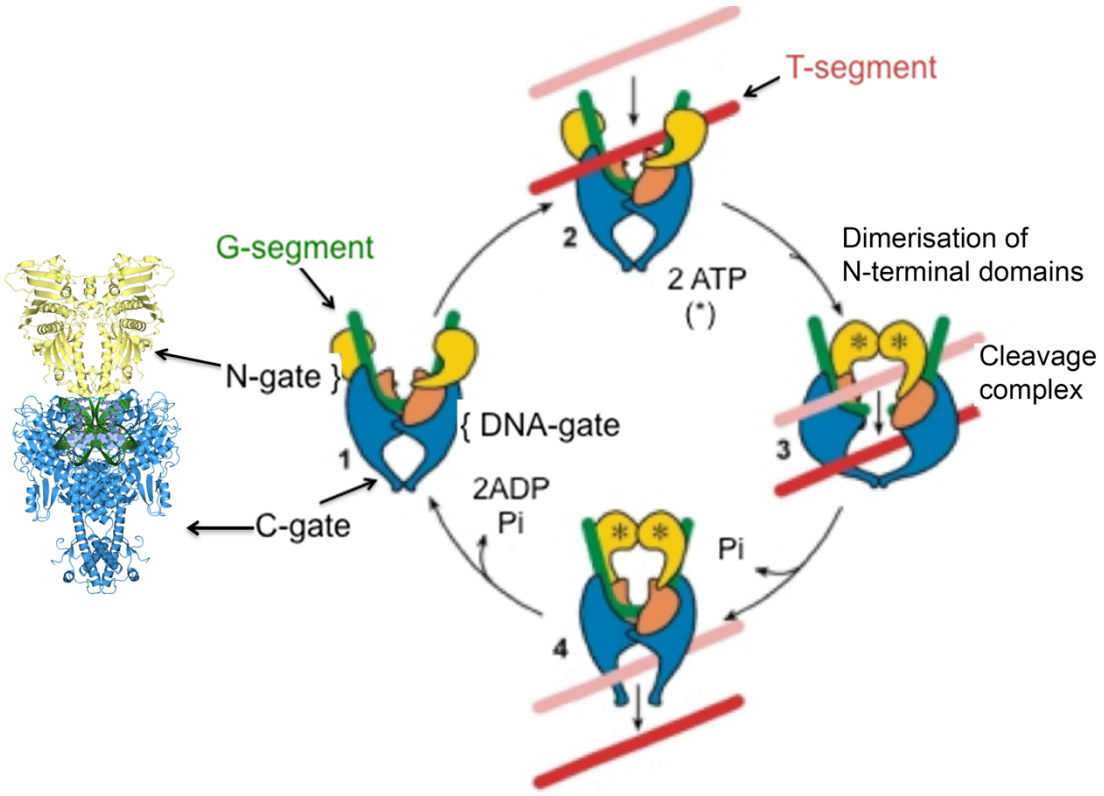


**Figure 1.5 Domain structure and catalytic cycle of TOP2.** (1) DNA duplex (G-segment) enters into the TOP2 enzyme thought the N-gate. (2) Binding of two molecules of ATP and capture of second DNA duplex (T-segment) triggers structural rearrangements causing the dimerisation and closure of the N-gate (3). The T-segment translocates through the transiently formed TOP2-DNA bridged gate and exits through the C-gate (4). Hydrolysis of a second molecule of ATP begins during the transport of the T-segment, and opens the N-gates to 'reset' TOP2 for another catalytic cycle (1). Saccharomyces *cerevisiae* TOP2 structure is shown on the left (PDB ID 4GFH) was produced using CCP4MG v2.9.0. TOP2 catalytic cycle diagram is adapted with permission from Bates *et al;* 2011.

TOP2 binds to helix-helix juxtapositions as in vitro studies showed TOP2 binds with greater affinity to four-way junction DNA compared to linear DNA (Zechiedrich and Osheroff, 1990; West and Austin, 1999). The TOP2 reaction begins with the transport of a DNA segment (G-segment) through the N-terminal gate and into the breakage-reunion core (Figure 1.5 (1)). Binding of the G-segment promotes movements of the TOPRIM, WHD and tower domains to shift into an 'engagement' conformation allowing the enzyme to clamp around the DNA segment and cause bending of the DNA duplex (Wendorff *et al.*, 2012; Laponogov *et al.*, 2013).

ATP loads onto the ATPase domain triggering structural rearrangements allowing capture of the T-segment and dimerisation of the N-terminal gate causing the closure of the gate. N-gate closure facilitates DNA deformation and enhances cleavage (Lee *et al.*, 2012b). Determination of the DNA bound structure revealed that DNA is bent

sharply by up to 150$^{o}$ (130$^{o}$ for human TOP2A) with each interface of TOP2 bending DNA by 75$^{o}$ . This deformation of DNA positions the DNA backbone near the catalytic tyrosine and $Mg^{2+}$ ion, critical to prime the DNA cleavage reaction. The bent DNA is stabilised by the positive cavity created by the rotation of TOPRIM domain relative to the WHD domain (see section 1.1.2).

Hydrolysis of one molecule of ATP allows the expansion of the upper cavity of the N-terminal gate to allow movement of T-segment towards the lower cavity (Wei *et al.*, 2005). This closure of the N-terminal gate and passage of the T-segment triggers cleavage of the G-segment to generate a TOP2-bridged DNA gate which is termed the 'cleavage complex' (Corbett *et al.*, 1992) (Figure 1.5 (2-3).

Cleavage of the G-segment is initiated by the active site nucleophilic tyrosine that resides in the WHD of the breakage-reunion domain (Figure 1.3). The tyrosine residue (Tyr805 for TOP2A and Tyr821 for TOP2B) attacks the phosphate backbone of the scissile bond resulting in the formation of a 5'phosphotyrosyl linkage between DNA and TOP2 and a 3'-hydroxyl moiety that interacts with TOP2 non-covalently (Figure. 1.6). This nucleophilic reaction is coordinated by $Mg^{2+}$ ions situated in the TOpisomerase/PRIMase (TOPRIM) domain (Deweese *et al.*, 2009a; Deweese *et al.*, 2009b) (Figure 1.3). Each protomer subunit cleaves one strand of the DNA helix generating a DNA nick that is separated 4bp apart from a second DNA nick, forming a staggered DNA break. The covalent linkage of DNA with the active site tyrosine residue and interaction of the two promoter subunits maintains genomic integrity of DNA. In addition, there are two non-catalytic $Mg^{2+}$ ions, which contact DNA bases up-stream and down-stream of the cleavage site and have a role in stabilising the transition state (Wu *et al.*, 2011; Wendorff *et al.*, 2012).

After passage of the T-segment though the C-gate, the cleaved DNA molecule is re-ligated. The 5'phosphotyrosyl linkage (TOP2-DNA linkage) is equivalent in energy to a phosphodiester bond and therefore the bond energy is preserved allowing the release of DNA from the enzyme by a nucleophilic attack from the 3'OH of the opposing strand (Figure. 1.5). Each subunit acts independently in strand re-ligation (Bromberg *et al.*, 2004). Hydrolysis of the second ATP molecule resets the enzyme to begin a new reaction cycle (Figure 1.5 (1)) (Deweese and Osheroff, 2009).

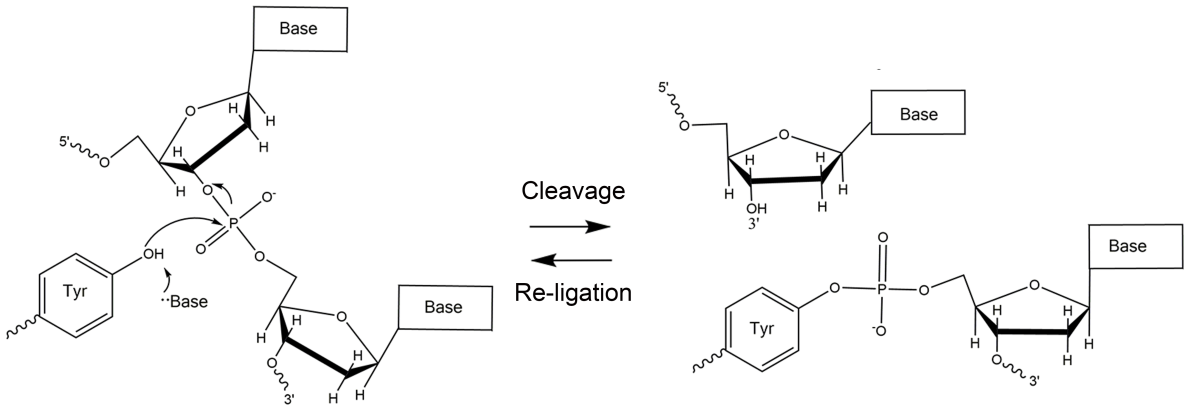


**Figure 1.6 Chemical mechanism of DNA cleavage by TOP2.** TOP2 utilises a nucleophilic tyrosine residue to attack the scissile phosphate resulting in the formation of a phosphotyrsoyl bond linking the protein to a newly generated 5' termini of DNA (cleavage complex). Ligation occurs when 3'OH of DNA is deprotonated by a general acid followed by a nucleophilic attack on the 5'phosphotyrosyl bond to release DNA from TOP2. This reaction is dependent on the coordination by $Mg^{2+}$ and DNA deformation mediated by the movements by the TOPRIM and WHD domains.

### *1.1.4. Interference of TOP2's catalytic cycle by TOP2 poisons*

There are various chemically distinct drugs available to inhibit TOP2's catalytic cycle, one such class of drugs are known as TOP2 poisons and act by stabilising the transient cleavage complex. Drugs, which inhibit other steps of TOP2's catalytic cycle are termed catalytic inhibitors and are discussed in chapter 6.

TOP2 poisons such as etoposide, mitoxantrone, doxorubicin and epirubicin act by stabilising the TOP2-DNA cleavage complex to prevent the re-ligation of DNA (Figure 1.5 and 1.7). In cells, TOP2 maintains a fine balance between enzyme-mediated DNA cleavage and re-ligation. In the presence of TOP2 poisons, this equilibrium is disrupted increasing the level of cleavage complexes within the cell, holding DNA in the cleaved state. TOP2 poisons are licensed for use in chemotherapy to treat a board spectrum of cancers (Table 1) however, TOP2 poison therapy is associated with a rare but serious side effect of the development of therapy related leukaemia. In this thesis, the focus will be on the TOP2 poisons; etoposide, mitoxantrone, doxorubicin and epirubicin and their roles as *interfacial* TOP2 poisons (Pendleton *et al.*, 2014). The other class of TOP2 poisons are *covalent* TOP2 poisons, which covalently bind at a site distinct from the active site to increase the level of cleavage complexes; an example is etoposide quinone, which is discussed in section 1.3.1.

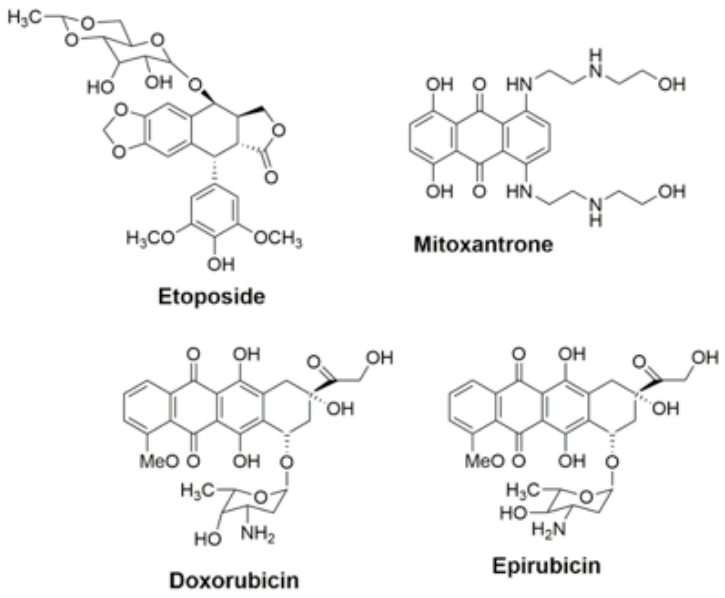


**Figure. 1.7 Chemical structures of TOP2 poisons.**

| TOP2 poison | Use in clinics (UK) |
|---|---|
| Etoposide | Lung, testicular, ovarian and stomach cancer, leukaemia and non-Hodgkin lymphoma[1,2] |
| Mitoxantrone | Metastatic breast cancer, primary liver cancer non-Hodgkin lymphoma, leukaemia [1, 2] and Multiple Sclerosis (MS) (not licensed in the UK, but is used at some specialist centers)[3] |
| Doxorubicin | Used for treatment of a range of cancers including breast, bladder, thyroid, small cell lung cancer, advanced ovarian cancer, bladder cancer, Hodgkin's disease, Ewing's sarcoma, leukaemia and advanced neuroblastoma [4] |
| Epirubicin | Breast, ovarian, stomach, lung, bowel cancer, myeloma, leukaemia and lymphoma[1] |

**Table 1: The clinical use of selected TOP2 poisons in the UK.** [1]Information obtained from Cancer Research UK; [2]Macmillan org.uk; [3]Multiple Sclerosis Trust UK; [4]electronic Medicines Compendium (eMC) UK.

### *Etoposide*

Etoposide is a semi-synthetic derivative of podophyllotoxin, synthesised in 1966 and approved for clinical use in 1983 (Hande, 1998) (Figure 1.7). Etoposide was first described to cause both DNA single and double strand breaks that quickly reversed upon drug removal. However, the mechanism of etoposide induced DNA damage was unclear (Loike and Horwitz, 1976; Wozniak and Ross, 1983). Studies later revealed that etoposide interfered with the breakage-reunion reaction of TOP2 and was termed a TOP2 poison (Chen *et al.*, 1984; Minocha and Long, 1984; Ross *et al.*,

1984). Studies conducted using cell line models specificity showed that etoposide targets both isoforms of TOP2, and upon removal of etoposide from cell medium, stabilised TOP2-DNA complexes can reverse to background levels within 120min after drug removal (Willmore *et al.*, 1998; Errington *et al.*, 2004).

A two-drug model for etoposide's TOP2 poisoning action was proposed using gel-based DNA cleavage and ligation assays. The two-drug model suggested that one molecule of etoposide intercalates into one scissile bond to physically block DNA religation (Figure 1.8 A). A second etoposide molecule independently intercalates into the neighbouring scissile bond (which is in the separate promoter unit of dimeric TOP2) stabilising the second DNA nick. Therefore, it was proposed that binding of one etoposide molecule at one active site of TOP2 does not affect the reactions occurring in the neighbouring active site and two molecules of etoposide per TOP2 enzyme are required to stabilise a DNA DSB (Bromberg *et al.*, 2003). Due to etoposide's mode of action, it is referred an *interfacial TOP2 poison*. This refers to a drug that reversibly binds at a site created by the interaction/movement of two or more components (i.e. etoposide binds at the TOP2 bridged DNA gate) (Pommier and Marchand, 2012). This two-drug model was later confirmed by structural determination of the human TOP2B-DNA-etoposide ternary complex (residues 445-1201 of TOP2B) (Wu *et al.*, 2011; Wendorff *et al.*, 2012) (Figure 1.8.B and 1.9).

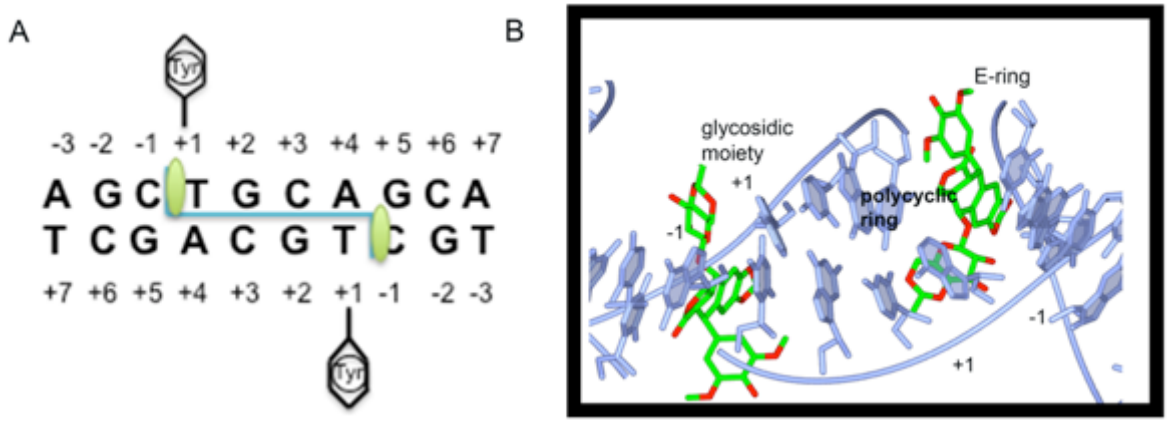


**Figure 1.8 Intercalation of etoposide into the TOP2-DNA binary complex.** (A) Etoposide (shown as green ovals) intercalates into the scissile bond using base stacking to physically block re-ligation of DNA, this is known as the two-drug model proposed by Bromberg and colleagues (Bromberg *et al.*, 2003). (B) Etoposide intercalation into the TOP2B-DNA complex. Diagram produced using CCP4MG v2.9.0 using the TOP2B-DNA-etoposide protein structure (PDB ID 3QX3).

Structural studies reveal that etoposide poisons TOP2 as predicted by the two-drug model. Etoposide intercalates into the TOP2-DNA binary complex with one molecule of etoposide per scissile bond (one etoposide at +1/+4 site and the other at -1/+5) requiring two molecules of etoposide to stabilise a DSB (Figure 1.8.B 1.9). The polycyclic ring of etoposide sits between base pairs acting as a physical block to disfavour re-ligation of DNA. This physical block induced by the presence of etoposide decouples the active site tyrosine and the catalytic $Mg^{2+}$, disrupting the $Mg^{2+}$ coordination required for re-ligation and shifts the nucleophilic 3'OH to a distance of 8.33Å away from the 5'-phosphotyrosyl bond preventing nucleophilic attack. This suggests that etoposide induces conformational changes in the TOP2B protein shifting the positions of the TOPRIM domain relative to the WHD domain resulting in displacement $Mg^{2+}$ ion relative to the cleavage site (see section 1.1.2). The E-ring of etoposide is pointed towards the minor groove-binding pocket and causes local DNA deformation. However, the DNA deformation induced by one etoposide molecule does not extend to the neighbouring active site (Wu *et al.*, 2011). This further supports the two-drug model that etoposide molecules act independently to each other (Bromberg *et al.*, 2003).

In addition to intercalating into the TOP2-DNA complex, etoposide makes hydrogen bonding and Val der Waals interactions with the TOP2 protein to stabilise its intercalation into the protein-DNA binary complex (Wu *et al.*, 2011) (1.9 right panel). Etoposide's A, B, C and D ring sit between base pairs, and rings A, B and D contact protein residues (Figure 1.9). Etoposide's glycosidic moiety makes minimal contact with DNA but is involved in making drug-protein interactions (Wendorff *et al.*, 2012).

Superimposition of the TOP2B-DNA-etoposide structure onto the TOP2A-DNA structure revealed similar interactions of etoposide with DNA and TOP2 but point towards some differences in residues (Gln778 TOP2B to Met762 in TOP2A and Ser800 of TOP2A replacing Ala816 of TOP2B) between the isoforms that could be used to develop isoform specific drugs.

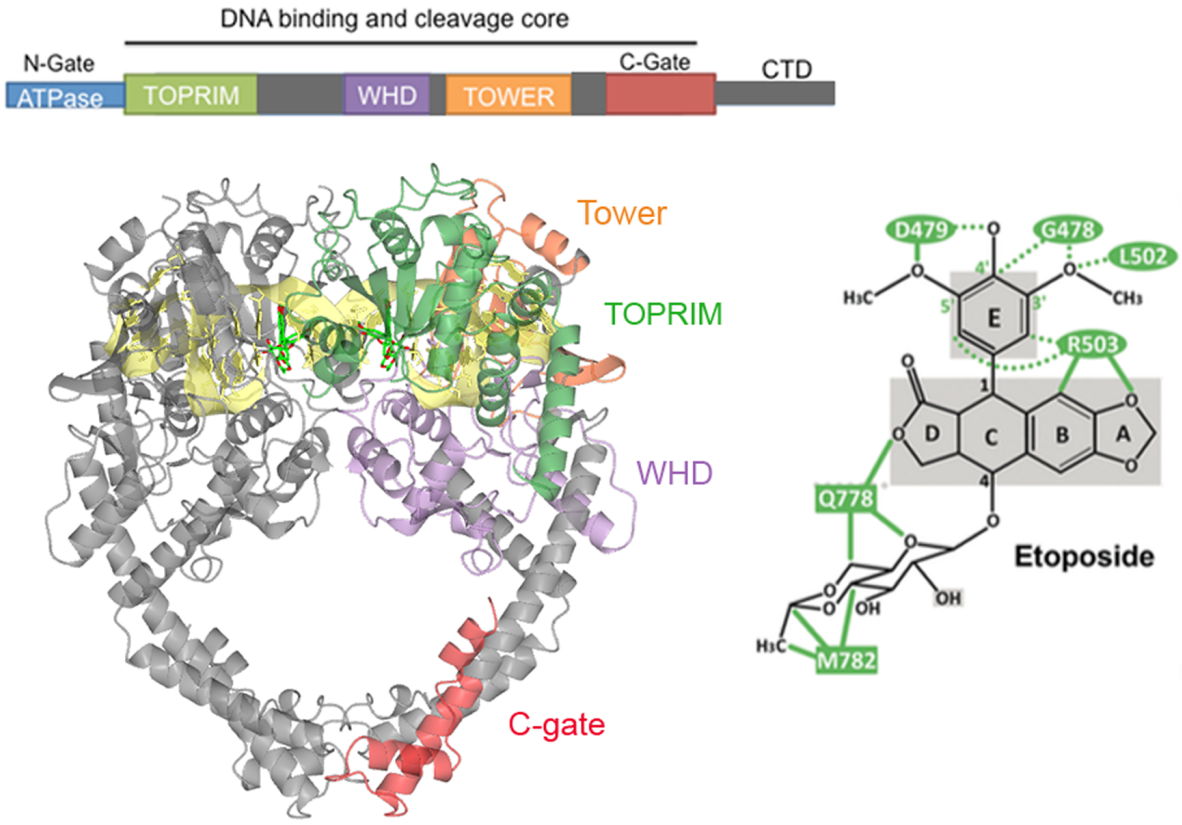


**Figure 1.9 Structure of the DNA binding and cleavage core of TOP2B-DNA (3QX3) binary complex stabilised by etoposide.** One monomer of the TOP2B dimeric structure is coloured according to the domain structure (shown above). Protein structure has been set to 0.74 opacity to show the etoposide intercalating into DNA (yellow) more clearly. Figure produced using CCP4MG 2.9.0. The right hand panel shows the key residues of the TOP2B protein that etoposide contacts, figure adapted with permission from Wu *et al.,* 2013.

Before the availability of the protein structure, it was believed etoposide or any TOP2 poison traps TOP2-DNA in the cleaved complex state in which the N- and C-gates are in the closed positions (Figure.1.3). However, the TOP2B structure revealed an open quaternary structure as opposed to closed conformation of the enzyme, which suggests that etoposide does trap the cleavage complex but is described to be a putative intermediate state between the closed pre-cleavage and open conformation (Wu *et al.*, 2011). This putative intermediate state may be a result of etoposide binding and causing conformational changes to the TOPRIM and WHD domains that results in the shifting of the $Mg^{2+}$ relative to the active site tyrosine.

***Mitoxantrone***

Mitoxantrone is a synthetic anthracenedione developed in the 1980s and approved for use in the treatment of acute myeloid leukaemia by the Food and Drug Administration (FDA) in 1987 (Faulds *et al.*, 1991). Mitoxantrone was developed to improve the therapeutic potential of anthracyclines by maintaining a planar polycyclic

aromatic ring system for DNA intercalation but substituted the sugar moiety with hydroxylalkylamino side chain to reduce cardiotoxicity (Zee-Cheng and Cheng, 1978; Evison *et al.*, 2015) (Figure 1.7). Mitoxantrone, like etoposide was predicted to intercalate into the TOP2-DNA binary complex however mitoxantrone induces more stable TOP2-DNA covalent complexes compared to that stabilised by etoposide *in cellulo* (Fox and Smith, 1990; Errington *et al.*, 2004). Recent structural determination of the mitoxantrone-TOP2B-DNA ternary complex supports the interfacial TOP2 poisoning action of mitoxantrone (Wu *et al.*, 2013).

The structure of mitoxantrone bound to TOP2B-DNA was prepared using post-crystallisation drug replacement of etoposide with mitoxantrone (Wu *et al.*, 2013). Like etoposide, mitoxantrone uses its polycyclic ring structure to intercalate between base pairs +1/+4 and -1/+5. This increases the distance between the catalytic tyrosine and $Mg^{2+}$ and the distance between the nucleophilic 3'OH and electrophilic 5'-phosphotyrosine by 8.81Å, disfavouring re-ligation (Figure 1.10 and 1.6).

A key difference to etoposide is that in the presence of mitoxantrone the attacking 3'OH nucleotide shifts position of its ribose moiety from the C3'-endo to the C2'-endo conformation (Wu *et al.*, 2013). This positions the attacking oxygen out of alignment with 5'-phosphotyrosine further suppressing religation and this arrangement is also seen in metal free TOP2 structures (Schmidt *et al.*, 2010).

To stabilise its residence within the TOP2-DNA binary complex, mitoxantrone uses both its polycyclic ring and hydroxylalkylamino arms to make hydrogen bond contacts and van der Waals interactions with the protein (Figure 1.10). One hydroxylalkylamino arm points towards the minor groove of DNA and fits into a crevice situated between the TOP2B and DNA to make contacts with residues Glu522, Asn520 and Arg503. Whereas the opposing arm points towards the major groove which is more solvent exposed and is seen to make a single hydrogen bond contact with Gln778 (Wu *et al.*, 2013).

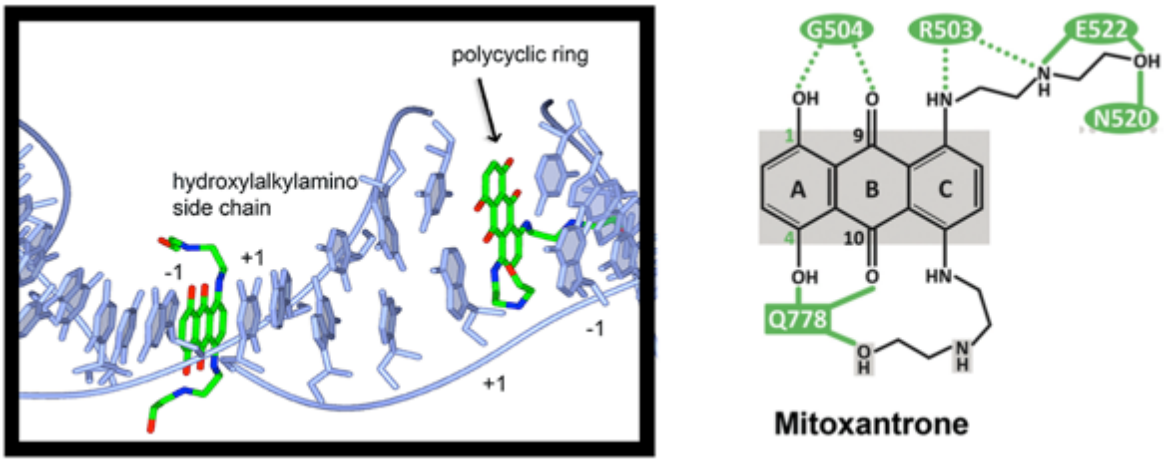


**Figure 1.10 Mitoxantrone intercalation into the TOP2B-DNA complex.** Mitoxantrone uses its polycyclic aromatic dihydroxy-anthraquinone (polycyclic ring) moiety to intercalate between DNA base pairs, the hydroxylalkylamino arms project towards the DNA major and minor grooves forming hydrogen bonding interactions with the protein stabilising the ternary complex. Diagram was produced using CCP4MG v.2.9.0 by importing the TOP2B-DNA-mitoxantrone structural coordinates from PDB ID 4G0V and for simplicity the TOP2B protein was removed to show the interactions of mitoxantrone with DNA. Right panel shows the interactions mitoxantrone makes with residues of TOP2B protein, figure adapted with permission from Wu *et al.,* 2013.

In contrast to etoposide, studies using mitoxantrone suggest that mitoxantrone can also induce DNA damage independently to its TOP2 poisoning action. However the other roles of mitoxantrone induced DNA damage are described to be minor or weak functions of mitoxantrone and that TOP2 is important in mitoxantrone induced cytotoxicity (Evison *et al.*, 2015). In support of this, studies have shown that reduction TOP2B levels or exclusion of TOP2A from nucleus leads to resistance to mitoxantrone (Harker *et al.*, 1991; Harker *et al.*, 1995a; Harker *et al.*, 1995b; Errington *et al.*, 1999).

Nevertheless, mitoxantrone can directly interfere with mitosis by preventing the formation of microtubules by directly interacting with tubule monomers and preventing their polymerisation. Failure to assemble microtubules prevents chromosome segregation and therefore cell division (Ho *et al.*, 1991). Therefore in proliferating cells mitoxantrone may utilise both the poising of TOP2A-DNA covalent complexes and binding to tubules to prevent cell division. Studies also suggest that mitoxantrone can directly bind to chromatin causing compaction and aggregation of chromatin structure which could potentially inhibit processes such as transcription and replication (Hajihassan and Rabbani-Chadegani, 2009). Additional studies showed that mitoxantrone inhibits DNA and RNA synthesis, which could be due to

mitoxantrone ability to intercalate in between base pairs or by direct binding to DNA and RNA. However a study conducted by Fox and colleagues showed the persistence of stabilised mitoxantrone TOP2-DNA complexes even after drug removable correlated with suppression of DNA synthesis (Johnson *et al.*, 1979). Therefore the block on DNA synthesis could be a function dependent on mitoxantrone's ability to poison TOP2-DNA complexes (Fox and Smith, 1990).

***Doxorubicin and epirubicin***

Doxorubicin and epirubicin belong to the anthracyclines class of drugs. The first isolated anthracyclines from *Streptomyces peucetius* were doxorubicin and dauorubicin. Epirubicin is a semi-synthetic derivate of doxorubicin that differs in the position of the C4 OH group in the daunosamine moiety (Figure 1.7). In epirubicin, the 4'OH is arranged in an equatorial configuration whereas for doxorubicin the 4'OH is arranged in an axial configuration. This epimerisation of the hydroxyl group introduces pharmacokinetic changes in drug properties whilst maintaining its cytotoxic function (Gewirtz, 1999a).

Studies reported that described doxorubicin to induced both DNA single and double strand breaks, however purified DNA fragments were found to be covalently bound to proteins, which was later deduced to be TOP2. Therefore, the role of doxorubicin as a TOP2 poison was established (Tewey *et al.*, 1984). Both doxorubicin and epirubicin induce TOP2 dependent DNA cleavage at lower drug concentrations with a preference for the nucleotide A at the -1 position relative to the cleavage site (in vitro drug concentrations 0.1-10μM) (Frederick *et al.*, 1990; Cornarotti *et al.*, 1996). At higher drug concentrations both drugs in vitro suppress TOP2-mediated DNA cleavage and inhibit the action of TOP2 poisons such as teniposide (podophyllotoxin derivative) and amsacrine (DNA intercalating TOP2 poison, drug class: acridines) (Capranico *et al.*, 1990a; Capranico *et al.*, 1990b). However, the TOP2 poisoning in cell lines has been difficult to detect (Montaudon *et al.*, 1997; Willmore *et al.*, 2002).

This suggests a different cytotoxic mode of action for anthracyclines compared to mitoxantrone or etoposide. In addition to poisoning or inhibiting TOP2, doxorubicin and epirubicin can directly intercalate between DNA base pairs causing DNA cross-linking which prevents the activity of DNA helicases and inhibits of macromolecular synthesis (Tuteja *et al.*, 1997; Gewirtz, 1999b; Minotti *et al.*, 2004). As both

doxorubicin and epirubicin can intercalate into DNA and poison TOP2 they are termed intercalative TOP2 poisons (Nitiss, 2009b).

Structural studies using post-crystallisation drug replacement show that a single doxorubicin molecule intercalates asymmetrically into sites +1/+4 and +2/+3 (between the cleavage site) of the TOP2B-DNA binary complex structure (Figure. 1.11). This intercalation is suggested to disrupt the two-fold symmetry of the cleavage site moving the attacking 3'-OH by distance of 7.83Å from the 5'-phosphotyrosine. Wu and colleagues reported that the binding of doxorubicin causes repositioning of adenine at +4 site and changes the ribose sugar orientation causing the formation of a non-canonical base pair (Wu *et al.*, 2013) (Figure 1.11). Although the consequences of this repositioning induced by doxorubicin were not fully discussed, there is a possibility that the mis-alignment of bases up-stream from the cleavage site cause distortion of the 3'-OH and

In addition, doxorubicin is reported to make only three contacts with the TOP2B protein (Lys456, Arg820 and Gln778) and relies mainly on hydrogen bonding with DNA to stabilise its interactions (Figure 1.11). However, it has been suggested that as the doxorubicin-TOP2B-DNA ternary complex structure was determined by soaking out etoposide and then subsequently soaking doxorubicin into the TOP2B-DNA complex crystals, this may not be a true representative of how doxorubicin binds into the TOP2-DNA binary complex (Wu *et al.*, 2013).

Recent in vitro experimental studies using calf thymus DNA and doxorubicin have identified the potential reason behind the preference for A-T regions outside the intercalation site. Perez-Arnaiz and colleagues propose that doxorubicin uses A-T regions to bind into the minor groove of DNA (fast step) and then slowly intercalates between CpG sites (Perez-Arnaiz *et al.*, 2014).

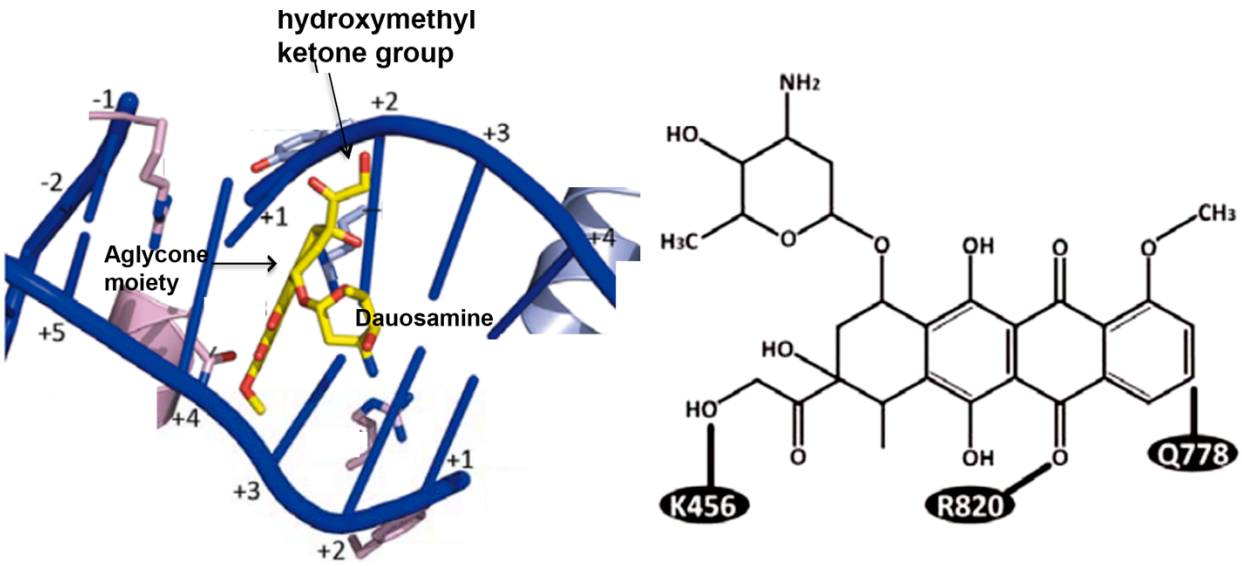


**Figure 1.11 The intercalation of doxorubicin into the TOP2B-DNA complex (left panel) and the interactions doxorubicin makes with the TOP2B protein (right panel).** Figure adapted with permission from Wu *et al.,* 2013.

## 1.2 Myeloperoxidase

Myeloperoxidase (MPO) (EC 1.11.2.2) is part of the heam peroxidase-cyclooxygenase superfamily that utilises hydrogen peroxide to catalyse the oxidation of a range of halide ions, organic and inorganic substances. Other members of this superfamily include; lactoperoxidase (LPO), eosinophil peroxidase (EPX) and thyroid peroxidase (TPO) which share 51%, 70% and 45% amino acid identify with MPO (Davies 2008). MPO is a homodimeric enzyme and has the unique ability to oxidise chloride at neutral pH generating hypochlorous acid-a strong oxidant. MPO is a key component of the azurophilic (primary) granules of neutrophils and functions in the innate immune response. In addition to MPO's role in assisting the killing of pathogenic organisms, MPO has been implicated in a growing number of inflammatory diseases, such as atherosclerosis, neurodegenerative, lung and renal diseases. Furthermore, due to MPO's strong oxidising potential, MPO can also mediate drug biotransformation leading to compounds with altered properties.

### *1.2.1 Transcription, Translation and Post-translational processing of MPO*

MPO synthesis is restricted to the promyelocytic stage of myeloid differentiation (Figure 1.12). MPO protein expression is found in the common myeloid progenitor (promyelocytic stage) (CMP), granulocyte-macrophage progenitor (GMP), monocytes and most abundantly in neutrophils (Hansson *et al.*, 2006).

The gene encoding MPO is located on chromosome 17q22. The MPO gene is transcribed and translated into a single product of 80kDa termed preproMPO that is processed through the endoplasmic reticulum (ER), Golgi and azurophilic granules to generate mature dimeric MPO of 140kDa. The stepwise processing of MPO was experimentally defined using radiolabel pulse chase and immunoprecipitation experiments predominantly conducted in HL60 cell lines. PreproMPO consists of signal peptide (45aa), pro-peptide (116aa), a heavy α subunit and light β subunit (Figure.1.13). The N-terminal signal peptide targets preproMPO to the ER, in the ER compartment preproMPO undergoes slow processing to generate enzymatically active proMPO via apoproMPO intermediate.

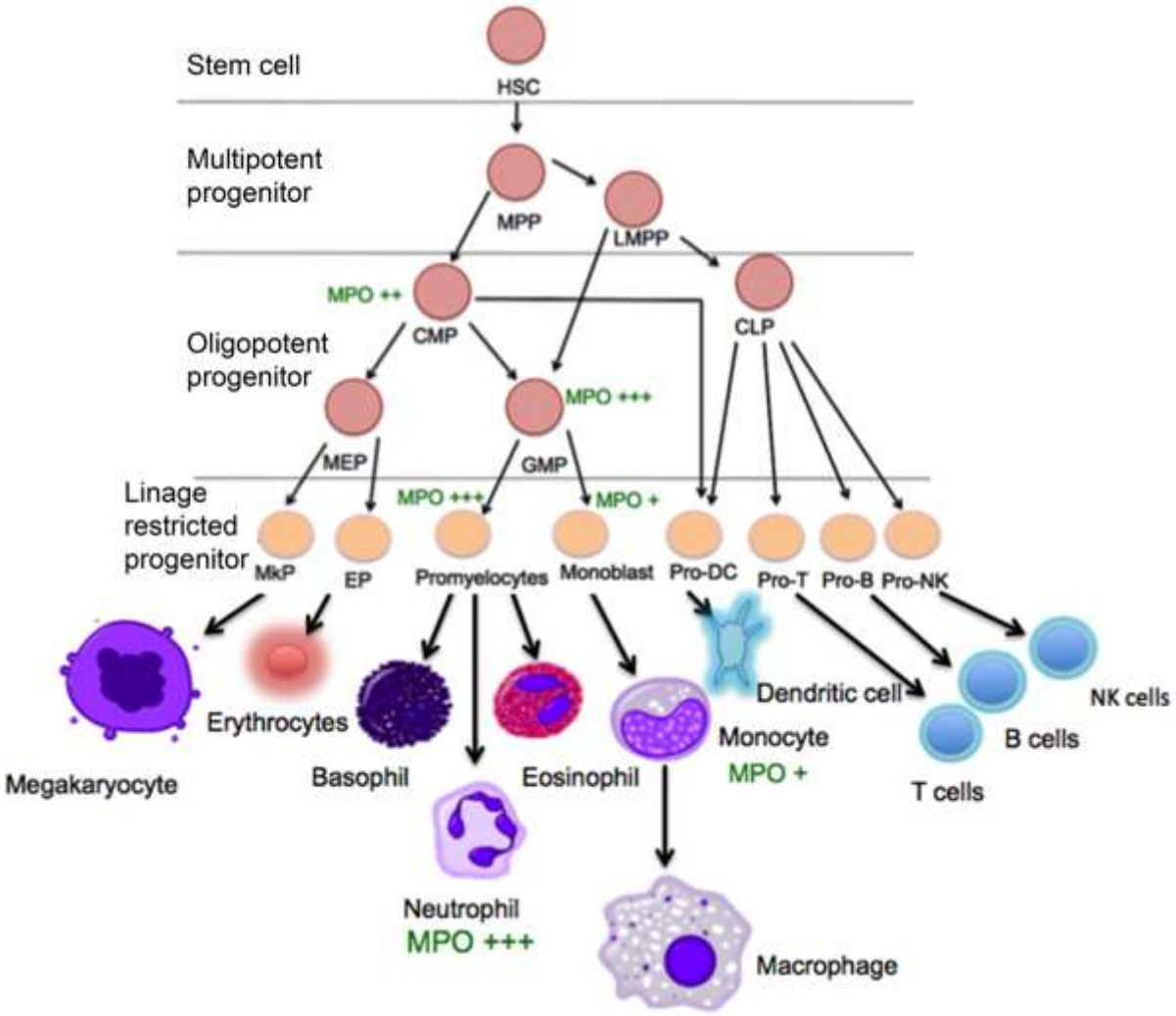


**Figure 1.12. The protein expression of MPO in hematopoietic cells**. The hematopoietic stem cell (HSC) sits at the top of hierarchy and can differentiate to over 10 distinct mature blood cells. HSC gives rise to the multipotential progenitor which has the full lineage potential but loses the capacity of self-renewal. MPP gives rise to the oligopotent progenitors; common myeloid progenitors (CMP) and common lymphoid progenitors (CLP), both, which are lineage committed (Seita and Weissman, 2010). Protein expression of MPO is shown in green. HSC and multipotential progenitors are positive for MPO expression at the RNA level. MPO protein expression in humans is restricted to the myeloid linage of cells being most abundantly expressed in neutrophils. However, in disease states such as multiples sclerosis and Alzheimer's disease MPO expression is reactivated in macrophages of the brain (Nagra *et al.*, 1997; Reynolds *et al.*, 1999). Information used to construct (Seita and Weissman 2010) (permission obtained for figure adaptions).

The first steps in the biosynthesis of mature MPO are the conversion of the 80kDa preproMPO to a glycosylated 90kDa apoproMPO. This is achieved by the co-translational cleavage of the 45aa signal peptide and *en-bloc* N-linked glycosylation consisting of two N-acetylglucosamine residues, nine mannoses and three glucoses ($GlcNAc_2Man_9Glu_3$) at five asparagine residues followed by limited deglucosylation. ApoproMPO then acquires haem by the sequential association with the ER molecular chaperon's calreticulin (CRT) and calnexin (CLN) (Nauseef *et al.*, 1995; Nauseef *et al.*, 1998).

CRT binds to apoproMPO and maintains apoproMPO in a conformation competent to allow the insertion of haem. Haem incorporation occurs at the stage of CLN binding to apoproMPO to form an enzymatically active proMPO. It is likely that limited deglucosylation also occurs after the insertion of haem to allow the release of MPO from CLN (van Leeuwen and Kearse, 1996). ProMPO then exits from the ER to undergo rapid processing in the Golgi or is constitutively secreted. The proMPO exported to the Golgi has the propeptide removed by the action of subtilisin-like proprotein convertases in the post-ER compartment to generate a 74kDa intermediate, whereas constitutively secreted proMPO retains the N-terminal propeptide (McCormick 2012). However, there is still speculation on the precise timing of the propeptide cleavage and the events that occur in the Golgi network.

Through the passage across the Trans-Golgi-network, the short-lived 74kDa intermediate MPO acquires modifications to the carbohydrate chains and exits for final processing in granules. In the granules the 74kDa intermediate is proteolytically cleaved into two subunits; a heavy α subunit (59kDa) and a light β subunit (14.5kDa) by the excision of a hexapeptide sequence (ASFVTG positions 273-278) and removal of a terminal carboxyl-terminal serine residue. The heavy α and light β subunits are held together via covalent bonds associated with the prosthetic heam group. More recently, heterogeneity in the sequence length elimination between the heavy α and light β subunits has been identified using tryptic digestion and peptide analysis (Grishkovskaya *et al.*, 2017). This study reported the excision between the two subunits can be achieved by either tetra (A273-S-F-V276), penta- (A273-S-F-V-T277) or hexapeptide (A273-S-F-V-T-G278) excisions (Grishkovskaya *et al.*, 2017). The final stage in the maturation of MPO is the dimerisation of two α heavy subunits resulting in a symmetric dimer with each half linked by a disulphide linkage at Cys319.

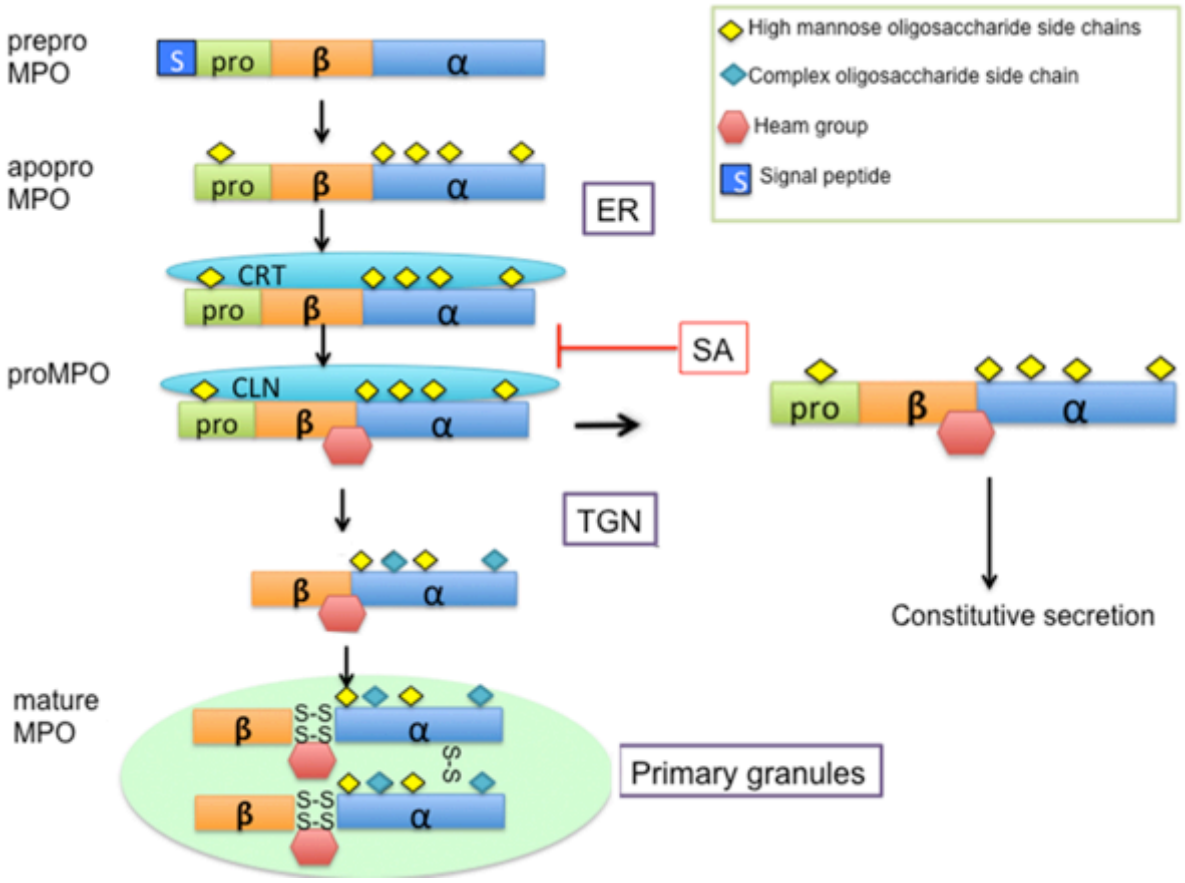


**Figure 1.13. MPO biosynthesis.** MPO is translated into an 80kDa preproMPO. In the ER, preproMPO undergoes cotranslational cleavage of the signal peptide (45 amino acids) and N-linked glycosylation ($GlcNAc_2Man_9Glu_3$) resulting in a 92kDa intermediate that is rapidly cleaved by glucosidase I to a 90kDa apoproMPO. ApoproMPO sequentially associates with the ER molecular chaperones, calreticulin (CRT) and calnexin (CLN) which assist in protein folding and insertion of haem to generate proMPO, which is enzymatically active and exits the ER. In the Trans-Golgi Network (TGN) rapid processing occurs with some complex oligosaccharide side chains being modified. Final proteolytic processing occurs in the primary granules to form mature dimeric MPO (Hansson *et al.*, 2006). Information used to construct figure obtained from Hasson *et al.,* 2006.

### *1.2.2 Structure of MPO*

The crystal structure of human MPO (PDB ID 3F9P) reveals a secondary structure consisting largely of alpha helices with very few beta sheets. The interface between the two symmetry dimers is highly glycosylated to stabilise the two-protomeric subunits (Figure 1.14). Each symmetry dimer of MPO consists of a single haem group identified as a derivative of protoporphyrin IX and a single calcium binding site arranged in pentagonal bipyramidal coordination. The haem group is crucial for the

catalytic function of MPO, whereas the $Ca^{2+}$ is important in maintaining the architecture of MPO.

The prosthetic haem group is covalently attached to the protein via a ester linkage between the methyl group of pyrrole ring C (of the haem group) to the carboxyl group of Asp94 and a sulfonium ion linkage between Met243 and the β-carbon of the vinyl group on pyrrole A (Fiedler *et al.*, 2000). A second ester linkage, previously reported to play a key role in the attachment of haem to the MPO heavy subunit forms between pyrrole ring A and $Glu^{242}$. However, a more recent study has suggested this ester linkage is not always present in MPO structure (Carpena *et al.*, 2009).

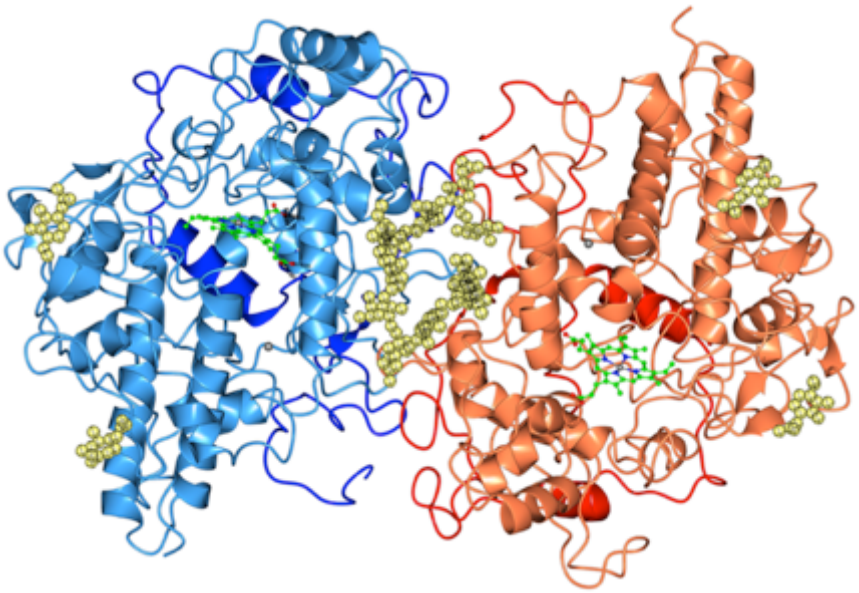

**Figure 1.14 Crystal structure of human MPO (PDB ID 3F9P).** MPO is a homodimeric enzyme with each monomer attached by a disulphide bridge at C319. Each symmetry dimer consists of a heavy α subunit (shown in light blue and orange) and light β subunit (shown in blue and red), a single calcium binding site (calcium ion shown in grey) and one haem group (shown in green). Carbohydrate chains are shown in yellow. Figure constructed using CCP4 Molecular Graphics Software version 2.9.0.

### *1.2.3 Isoforms of MPO*

Three isoforms of MPO have been purified from the azurophilic granules of neutrophils and are termed MPO form I, II and III (Yamada *et al.*, 1981). The three isoforms have identical spectral properties and have the same molecular weights for their light β subunits with differences in the molecular weight for the heavy α subunits, (form I 63kDa, form II and III 57.5kDa). The consequence for the

differences in the molecular weights of the heavy subunit is unknown however, MPO I is reported to have distinct properties from MPO forms II and III.

MPO form I is suggested to be a membrane bound protein whereas forms II and III are reported to be soluble proteins within the azurophilic granules (Pember *et al.*, 1983). In addition, MPO form I is reported to have a lower activity compared to MPO forms II and III. MPO form I has a lower content of charged amino acids compared to forms II and III (Lys+Arg residues I<II<III) and therefore a reduced surface charge and differences in amino acids sequences (Pember *et al.*, 1982; Pember *et al.*, 1983). Although additional studies have not been published to further evaluate the role of the three isoforms, differences in surface charges between the three isoforms of MPO would affect the ability of MPO (cationic protein) to bind to surfaces of red blood cells (anionic surface), leukocyte and the endothelial membranes (Adam *et al.*, 2014).

### *1.2.4 Normal function of MPO*

MPO is a key component of the neutrophils and accounts for up 5% of the total cellular protein distributed between the azurophilic granules and the nucleus (3.5µg per $10^6$ nuclei). Traditionally, it has been accepted that during the activation of neutrophils, MPO is released from the azurophilic granules to generate hypochlorous acid (HOCl), however additional roles of MPO in the innate immune response have emerged.

HOCl is a strong oxidant that causes oxidative protein unfolding and the aggregation of bacterial proteins in vitro (Winterbourn, 2002; Winter *et al.*, 2008). The ability for MPO to produce HOCl is dependent on a source of hydrogen peroxide ($H_2O_2$) which is supplied by the action of NADPH-oxidase during the neutrophil's respiratory burst (Dahlgren and Karlsson, 1999). However, the generated HOCl not only serves to kill microorganisms but can also activate intracellular pathways such as the mitogen-activated protein (MAP) kinase that promotes cell survival under oxidative stress and can modulate the activity of matrix metalloproteinases (MMPs).

MPO can also act as a autocrine and paracrine stimulator in neutrophils to up-regulate the activity of NADPH-oxidase and signalling cascades required for neutrophil degranulation (Lau *et al.*, 2005). More recently studies have suggested

that MPO has a crucial role in mediating the formation of neutrophil extracellular traps (NET) by promoting chromatin de-condensation (a function independent of MPO's ability to oxidise substances) (Papayannopoulos *et al.*, 2010; Metzler *et al.*, 2011; Metzler *et al.*, 2014). NETs are mesh like structures consisting of de-condensed chromatin and antimicrobial proteins, used to combat *Candida albicans* and patients deficient in MPO are unable to form NETs and are susceptible to *Candida* infections.

### *1.2.5 Reaction cycle*

The oxidation of halides (chloride, bromide, iodide and pseudohalide thiocyanate) begins with the reaction of ferric-MPO [Fe(III) Por] ($MPO^{3+}$) with $H_2O_2$ to generate the redox intermediate Compound I [Fe(IV)=O $Por^{\bullet+}$] (Figure 1.15) (Malle *et al.*, 2007). Compound I is two oxidising equivalents above the native enzyme and has a high two-electron reduction potential of 1.16V, this enables the oxidation of halides ions (HOX) regenerating ferric MPO. This is termed the **halogenation cycle** (Figure 1.15, reaction 1).

In the **peroxidase cycle**, compound I has an even greater reduction potential of 1.36V and can withdraw a single electron from an organic or an inorganic substrate (including drugs) (depicted as $AH_2$) (Figure 1.15, reaction 2). In the peroxidase cycle, compound I reduces to compound II [Fe(IV)=O Por]. Compound II is characterised by having a formal oxidation state of +4 with the absence of porphyrin π-cation radical and cannot react with halides (redox potential 0.97V). For Compound II to reduce to the native enzyme [Fe(III) Por] ($MPO^{3+}$) it catalyses the one-electron oxidation of a second substrate (Figure 1.15 reaction 3). In addition there a two redox intermediates of MPO termed compound III [Fe(III)-$O_2^{\bullet-}$Por] and ferrous MPO [Fe(II) Por] which do not actively participate in the catalytic cycle (Figure 1.15 reactions 4-6).

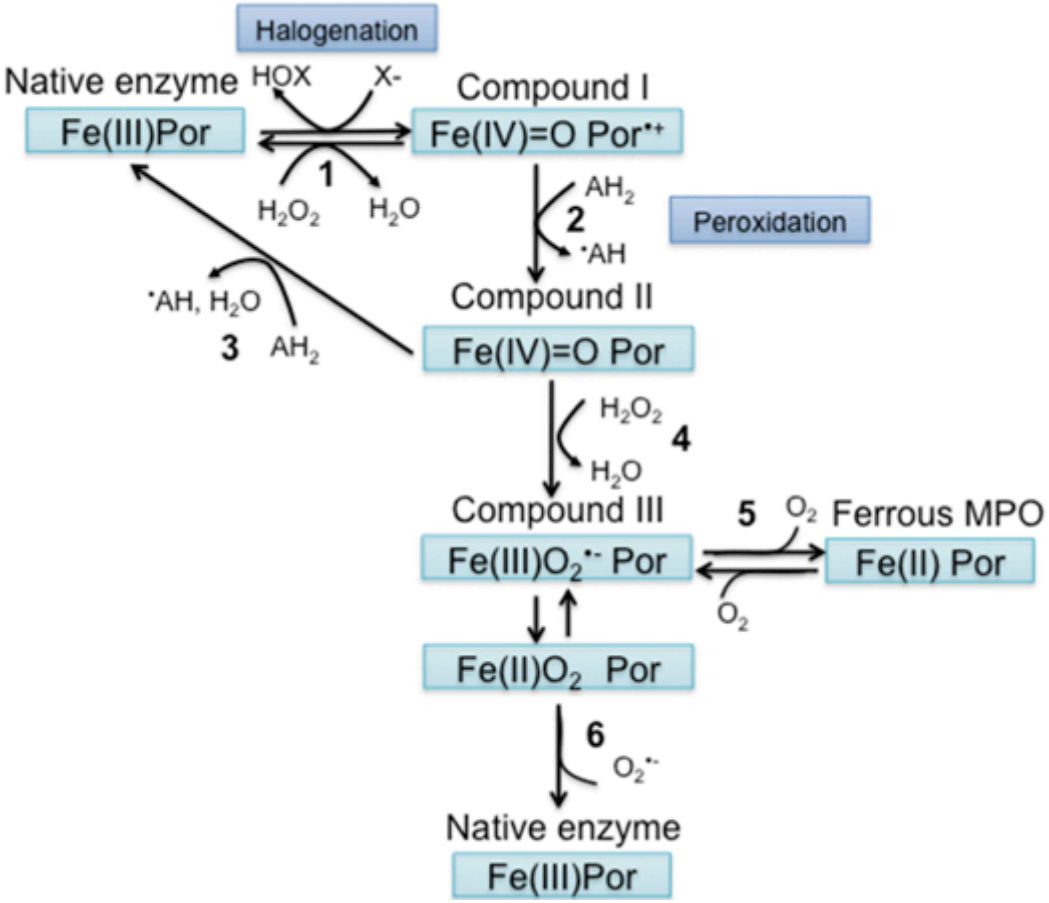


**Figure 1.15 Reaction cycle of MPO.** MPO's catalytic cycle begins with the production of compound I (halogenation cycle). Compound I is produced by the reaction of ferric MPO (native enzyme) with $H_2O_2$ (reaction 1). Compound I is characterised by oxoiron (IV) centre with a porphyrin $\pi$-cation radical. The reaction of compound I with halides regenerates native MPO. Alternatively compound I can catalyse the one-electron oxidation of a peroxidase substrate ($AH_2$) generating compound II that has a reduction potential of 0.97V (peroxidation cycle, reaction 2). Compound II can reduce to the native enzyme by a reaction with a second substrate (reaction 3). Compound III (ferrous-dioxy/ferric superoxide complex) can be formed by reaction of compound II with $H_2O_2$ (reaction 4). Compound III is unstable and can reduce to ferrous MPO with the release of oxygen or to the ferric native enzyme with the release of superoxide. Additionally, compound III can be produced by the reaction of ferric MPO (native enzyme) with superoxide or ferrous MPO with dioxygen. Diagram constructed using information from Malle *et al*., 2007 but has not been replicated from figures in this review article.

### *1.2.6 Inhibition of MPO*

MPO derived oxidants are implicated in acute and chronic inflammatory diseases, therefore MPO is an important target for the treatment of inflammatory diseases. Studies have linked the MPO 463A→G polymorphism in the incidence of Alzheimer's disease, multiple sclerosis (MS), diabetic nephropathy, AML and possibly some solid tumours such as lung, bladder, breast and pancreatic cancer (van der Veen *et al.*, 2009). The 463A/G allelic polymorphism is in the promoter region of MPO and

presence of the *G* nucleotide can up-regulate transcription of MPO by 25-fold (Piedrafita *et al.*, 1996).

Due to the prevalence of MPO activity in multiple diseases, new small direct molecular inhibitors have been developed to reduce the activity of MPO and are currently being tested in Phase I and Phase II clinical trials. The most successful MPO inhibitors to date have been the 2-thioxanthines; AZD5904 and AZD3241, and the 2-thiouracil based inhibitors PF1355 and PF-06282999 (Figure 1.16). In experimental systems 4-ABAH (a direct MPO inhibitor) and succinylacetone (SA) (a haem biosynthesis inhibitor) have been used to reduce MPO activity (Figure 1.16). The inhibitor action of MPO inhibitors used in experimental models and in phase I/II trials will be discussed below.

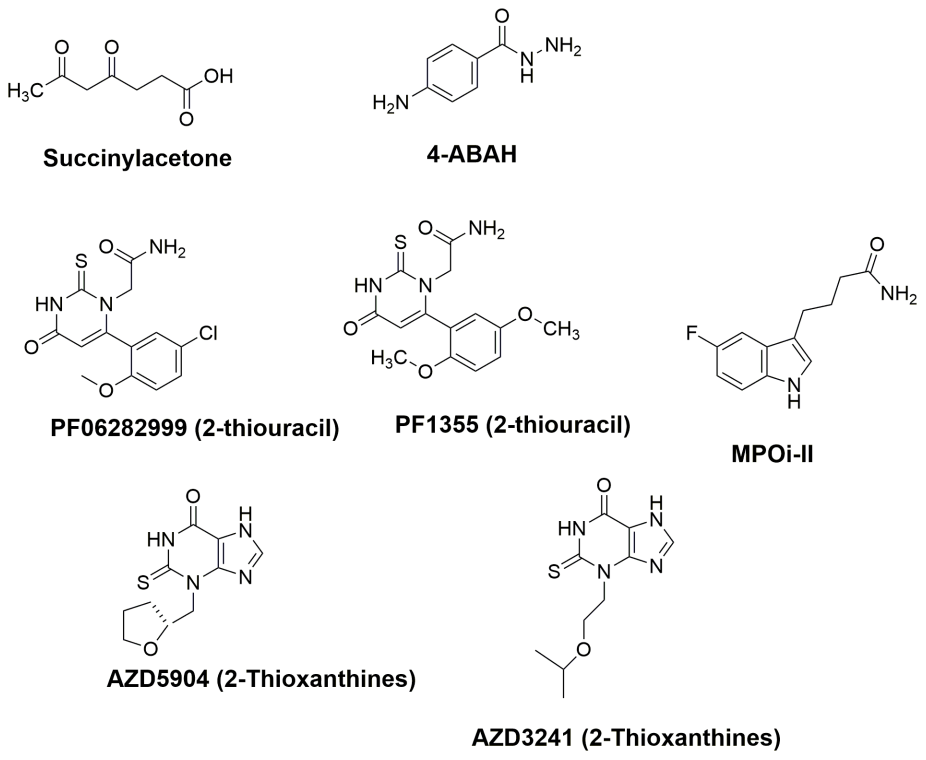


**Figure 1.16 Chemical structures of MPO inhibitors.**

### *Succinylacetone*

Succinylacetone (SA) is a potent inhibitor of haem biosynthesis, binding irreversibly to the active site of delta-aminolevulinate dehydratase (also known as porphobilinogen synthase), the second enzyme involved in haem synthesis (Tschudy et al., 1981; Giger and Meyer, 1983) (Figure 1.16). Haem is crucial for the catalytic function of MPO and the inability to incorporate haem during MPO biosynthesis, halts the processing of the protein (Figure 1.13). Experiments have shown the addition of

SA prevented the proteolytic processing of the MPO precursor, precluding its export from the ER resulting in the degradation of the preproprotein (Nauseef et al., 1992; Pinnix et al., 1994). To date SA has been a popular approach utilised to inhibit MPO in cell-based systems.

***4-ABAH***

4-aminobenzoic acid hydrazine (4-ABAH) is a specific mechanistic based inhibitor of MPO (Figure 1.16). Depending on the availability of oxygen 4-ABAH can either act as a reversible or irreversible inhibitor of MPO. The mechanism of inhibition involves the auto-catalytic oxidation of 4-ABAH to a radical intermediate (4-$ABAH_{ox}$), a process dependent on $H_2O_2$. 4-$ABAH_{ox}$ reacts with the native ferric state MPO [Fe(III) Por] ($MPO^{3+}$) reducing it to its ferrous state [Fe(II) Por] ($MPO^{2+}$) (Figure 1.17). The ferrous state of MPO does not participate in either the halogenation or peroxidase cycles (Figure 1.15). The fate of $MPO^{2+}$ is dependent on the availability of the substrates. The reaction of $MPO^{2+}$ with $H_2O_2$ leads to the destruction of the haem group (irreversible inhibition) producing an inactive ferric $MPO^{2+}$. However, in the presence of oxygen, $MPO^{2+}$ can react with oxygen to produce compound III [Fe(III)-$O_2^{\bullet-}$Por] (reversible inhibition), thus protecting the haem groups (Kettle et al., 1997; Burner et al., 1999) (Figure 1.17).

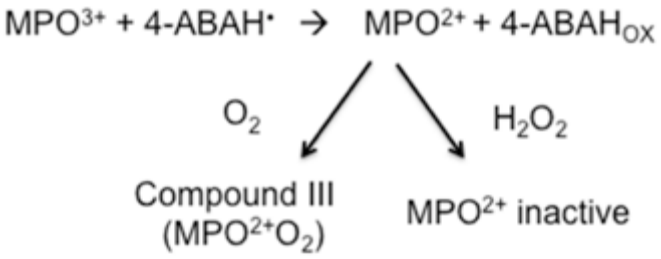


**Figure 1.17. Inhibition of MPO by 4-ABAH.** 4-ABAH oxidises to a radical intermediate (auto oxidation or MPO mediated) which reacts with ferric MPO ($MPO^{3+}$) to generate ferrous MPO ($MPO^{2+}$). Depending on the availability of oxygen, MPO can be reversibly or irreversibility inhibited. Oxygen can rapidly react with ferrous MPO producing compound III (an inactive MPO) protecting MPO's haem groups. However in the absence of oxygen, the haem group of the ferrous MPO can be destroyed leading to inactive $MPO^{2+}$. Information used to construct figure was obtained from Kettle *et al.,* 1997.

***2-Thioxanthines***

The recent development of 2-thioxanthines (2-TX) for MPO inhibition has led to clinical interest for the treatment of Multiple System Atrophy, Parkinson's disease (AZD3241) and for chronic obstructive pulmonary disease and Multiple Sclerosis (AZD5904) (Figure 1.16). The 2-TX class of compounds are mechanism-based

inactivators of MPO. 2-TX reacts with MPO's redox intermediate compound I [Fe(IV)=O Por$^{\bullet+}$], with a of rate constant 6.8 x $10^5 M^{-1}s^{-1}$, effectively competing with chloride (rate constant 2.5 x $10^5 M^{-1}s^{-1}$). The reaction of 2-TX with compound I results in the production of compound II [Fe(IV)=O Por] and a free radical species of 2-TX (2-TX$^{\bullet}$) (Figure 1.18). The free radical, 2-TX$^{\bullet}$ remains in the active site of compound II and covalently attaches to the methyl atom of the haem pyrrole D ring via a sulfonium ion linkage, causing inactivation of compound II (Tiden *et al.*, 2011; Ward *et al.*, 2013).

$$MPO^{3+} + H_2O_2 \leftrightarrow \text{Compound I} + H_2O$$

$$\text{Compound I} + \text{2-TX} \rightarrow \text{Compound II} + \text{2-TX}^{\bullet}$$

$$\text{Compound II} + \text{2-TX}^{\bullet} \rightarrow \text{Compound II-S-2-TX}^{\bullet}$$

**Figure 1.18. 2-Thioxanthines inhibition reaction equation.** 2-TX reacts with MPO compound I causing irreversible inactivation of compound II by covalent modification of the haem group. Information used to construct this figure was obtained from Tiden *et al.,* 2011 and Ward *et al.,* 2013

***PF1355 (2-thiouracil inhibitor)***

The 2-thiouracil based inhibitors have also been of clinical interest for use in the treatment of small vessel vasculitis (PF1355) and acute coronary syndrome (PF-06282999) (Figure 1.16) (Zheng *et al.*, 2015; Dong *et al.*, 2016). The biochemical mechanisms of MPO inhibition have not been clearly defined for the 2-thiouracils, however they are likely to have a similar mechanism to the 2-thioxanthines. The sulfur atom of the 2-thioxanthines is present on the 2-thiouracil substructure for both PF1355 and PF-06282999 (Figure 1.19) The MPO based inhibition for 2-thioxanthines is predicated to occur by the sulfur atom covalently attaching to the haem group of MPO compound II. It is proposed that both PF1355 and PF-06282999 react with compound I to generate a free radical that can subsequently adduct the haem group via a sulfonium ion linkage (Ruggeri *et al.*, 2015).

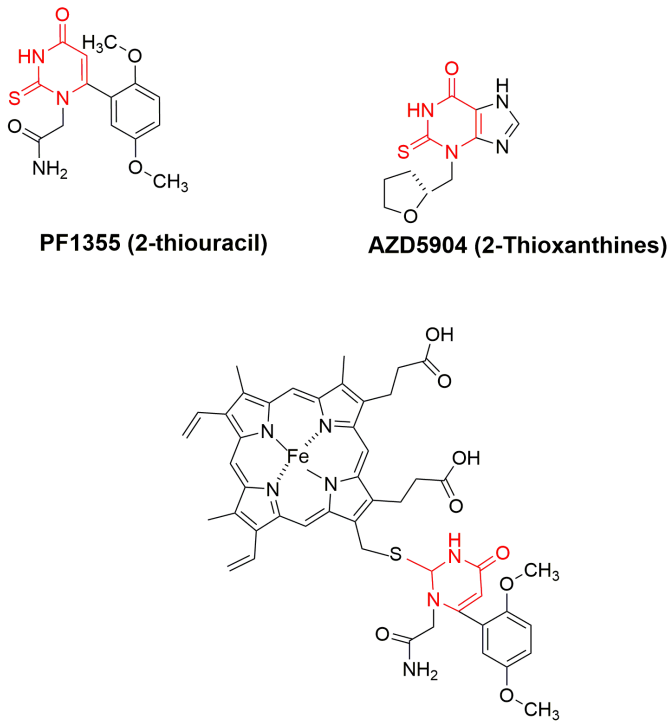


**Figure 1.19 A possible route into the inactivation of MPO haem group by PF1355.**

### *MPOi-II*

MPOi-II, is a 3-Alklindole derivative compound which is chemically distinct to the 2-thioxanthines and 2-thiouracuil based inhibitors (Figure. 1.16). MPOi-II works by reducing compound I to the compound II state, causing the accumulation of compound II. It is not known what the consequence of this accumulation is, but authors speculate that MPOi-II would have a slow dissociation from the haem cavity leading to inactivation of compound II (Soubhye *et al.*, 2010; Soubhye *et al.*, 2013). This inhibitor has not been tested in humans but MPOi-II has been tested in rats. Data reported showed that rats administered with 1mg/kg-10mg/kg of MPOi-II did not show signs of toxicity nor were changes in morphological features of organs observed therefore this compound may be of potential clinical interest (Soubhye *et al.*, 2013).

## 1.3 Oxidation of TOP2 poisons by MPO

As discussed in section 1.2.5, MPO's redox intermediate, compound I has a relatively high one-electron reduction potential (1.36V) and can catalyse the oxidation of organic compounds that subsequently have altered properties (Figure 1.15). For over

30 years, studies have been conducted to evaluate the role of MPO in the oxidation of TOP2 poisons (mainly etoposide). The MPO-mediated oxidation of TOP2 poisons generally occurs via a two-step oxidation reaction leading to metabolites that have altered DNA damaging properties compared to the parent compound.

There is still however speculation whether *in vivo* MPO directly catalyses the oxidation of TOP2 poisons or if this reaction is mediated via small species such as nitric oxide ($NO_2$) or tyrosine (Vlasova *et al.*, 2011; Sinha *et al.*, 2013). The reason for this speculation is that the active site of MPO (heam group) is buried within a narrow crevice measuring approximately 15Å in depth and 10Å in diameter with the main substrate access channel of length 20.3Å containing a bottleneck radius of 0.97Å which would restrict substrate access (Malle *et al.*, 2007; Grishkovskaya *et al.*, 2017). However, *in vitro* studies show MPO is capable of directly catalysing the oxidation of TOP2 poisons (Kagan *et al.*, 1999).

### *1.3.1 MPO mediated oxidation of etoposide.*

Etoposide can be metabolised to a redox active etoposide quinone (defined by carbonyl groups at positions 3' and 4' of the E-ring also referred as etoposide *ortho*-quinone) by MPO (Haim *et al.*, 1987b; Fan *et al.*, 2006) (Figure 1.20). The MPO catalysed reaction begins with the one-electron oxidation of etoposide to a phenoxyl radical species releasing a methyl radical. The generated methyl radical can alkylate DNA and lead to DNA strand scission (Riordan and Wei, 1994).The phenoxyl radical can then either undergo a further one-electron oxidation (by MPO) or disproportionate to form etoposide quinone.

Additionally, etoposide catechol (defined by the replacement of 3' methoxy group with hydroxyl moiety on the E-ring) can be oxidised by MPO to etoposide quinone via a two-step oxidation reaction (Figure 1.20). Etoposide catechol is an etoposide metabolite found in patient plasma, produced by the action of cytochrome P450 isoforms CYP3A4 and/or CYP3A5 (Zheng *et al.*, 2004; Zhuo *et al.*, 2004). The oxidation of etoposide catechol by MPO produces a semi-quinone intermediate releasing superoxide or $H_2O_2$. Etoposide semi-quinone can subsequently disproportionate to etoposide quinone and to etoposide (Kalyanaraman *et al.*, 1989) (Figure 1.20).

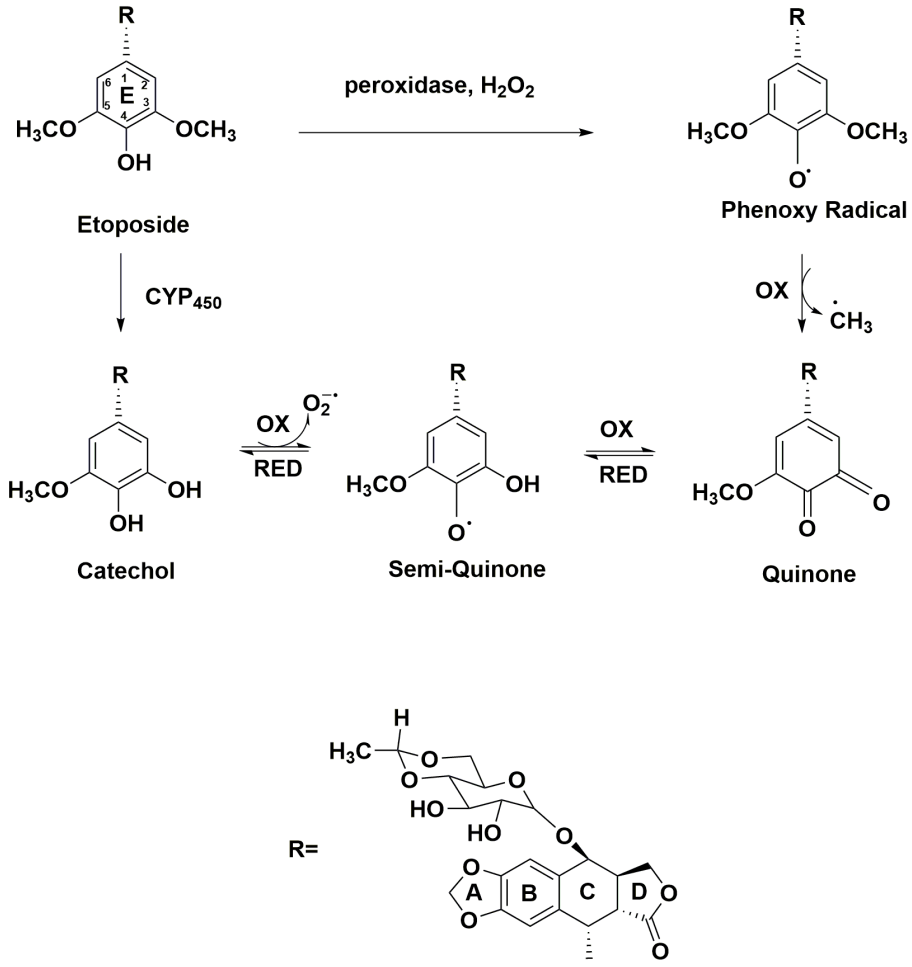


**Figure 1.20 Oxidation of etoposide by MPO.**

*In vitro* studies report etoposide catechol behaves as a interfacial TOP2 poison similar to etoposide but is 2- to 3-fold more potent at inducing TOP2-mediated DNA cleavage (Jacob *et al.*, 2013). The reason for the greater potency in TOP2 poisoning for etoposide catechol is likely due to additional hydrogen-bond interactions from the 3' hydroxyl moiety with the TOP2 protein compared to the 3' methoxy moiety of etoposide (Wu *et al.*, 2011).

Etoposide quinone is however reported to be a superior TOP2 poison compared to both etoposide and etoposide catechol with a greater activity towards TOP2B *in vitro* (Gantchev and Hunting, 1998; Jacob *et al.*, 2011; Jacob *et al.*, 2013; Smith *et al.*, 2014b). Due to the presence of the *ortho*-quinone group, etoposide quinone confers additional properties of being able to covalently bind to proteins (including TOP2) and to DNA (Haim *et al.*, 1987b; Haim *et al.*, 1987a; van Maanen *et al.*, 1988a; Mans *et al.*, 1990). In studies conducted in cellulo using MCF-7 cells (breast cancer cell line) etoposide quinone was less cytotoxic than etoposide. However, due to etoposide

quinone being more polar compared to etoposide, there was reduced cellular uptake of etoposide quinone (Sinha *et al.*, 1990).

***Dual mechanism model for etoposide quinone TOP2 targeting***

A recent study has suggested a dual-mechanism model for TOP2 poisoning by etoposide quinone *in vitro* (Gibson *et al.*, 2016). In this model, etoposide quinone has been demonstrated to behave both as an interfacial TOP2 poison (as for etoposide and etoposide catechol) and as covalent/redox-dependent TOP2 poison- a function that is distinct from etoposide and etoposide catechol. However, it is likely that etoposide quinone is not constrained to two mechanisms for targeting TOP2 but may have additional mechanisms that allow TOP2-mediated DNA damage.

The first mechanism proposed for etoposide quinone is its ability to act as a interfacial TOP2 poison due to its ability to reversibly stabilise TOP2-DNA covalent complexes and induce single strand DNA breaks (Gantchev and Hunting, 1998; Gibson *et al.*, 2016). This suggests that like etoposide; etoposide quinone can non-covalently interact with the TOP2-DNA binary complex to disrupt religation of DNA requiring one drug molecule to intercalate into each DNA break (similar to the two-drug model for etoposide) (Lindsey *et al.*, 2014) (see section 1.1.4).

The unique property of etoposide quinone from its parent compound, is its ability to act as a covalent/redox-dependent TOP2 poison, a mechanism similar to 1,4 benzoquinone (Bender *et al.*, 2007). Etoposide quinone is reported to induce higher proportion of DNA DSBs, strongly inhibit DNA religation, inhibit ATP hydrolysis and stabilise the N-terminal clamp of TOP2 (Gibson *et al.*, 2016) (see section 1.1.2 and 1.1.3). As these properties of etoposide quinone are similar to 1,4-benzoquinone, this strongly suggests that the presence of *ortho*-quinone is responsible for the additional properties.

The covalent/redox-dependent poisoning of TOP2 by etoposide quinone can occur via two or three possible routes. Firstly, studies have shown residues Cys392 and Cys405 situated on the N-terminal domain of TOP2A are important in mediating increased DNA cleavage by etoposide quinone and 1,4-benzoquinone compared to etoposide. The precise mechanism of the requirement of cysteine's residues is still not clearly defined. However, it is predicted that etoposide quinone covalently binds

to cysteine residues via the thiol group that somehow prevent DNA re-ligation (Jacob *et al.*, 2011).

The second route involves closing TOP2's N-terminal clamp by cross-linking the two protomer subunits of TOP2. This also inhibits ATP hydrolysis preventing DNA strand passage (Jacob *et al.*, 2013; Gibson *et al.*, 2016). The closing of the N-terminal clamp has two consequences, if DNA is bound to TOP2, this would trap the TOP2-DNA in a non-covalent complex. The subsequent removal of trapped TOP2 from the DNA would cause a DNA DSB. However, if etoposide quinone stabilises the N-terminal clamp prior to DNA binding, this would block the entry of DNA, leading to 'inactivation' of the enzyme (Jacob *et al.*, 2013). Interestingly, the function of blocking the N-terminal clamp does not seem to involve cysteine residues despite the cysteine residues residing in the N-terminal region of TOP2 (Bender *et al.*, 2007).

Gibson and colleagues suggest the inhibition of ATP hydrolysis by etoposide quinone is due to the stabilisation of the N-terminal clamp but earlier studies predict etoposide quinone covalently adducts charged residues (such as the amine group on arginine) on the carboxyl terminal of the $ATP_{ase}$ domain preventing hydrolysis of ATP. If this were the case then this would count for an additional mechanism of covalent poisoning by etoposide quinone (Vyas *et al.*, 1992; Gantchev and Hunting, 1998). In addition, etoposide quinone can covalently bind to DNA causing DNA damage. Moreover the presence of a covalent DNA adduct could potentially block the binding of TOP2 to DNA (Haim *et al.,* 1986, Haim *et al.,* 1987).

### *1.3.2. Biotransformation of mitoxantrone by MPO*

#### *Direct oxidation of mitoxantrone by MPO*

Mitoxantrone contains a semi-quinone and a quinone moiety in its structure (Figure 1.21), therefore given the chemical reaction between MPO and etoposide it was predicted that MPO would catalyse the oxidation of the semi-quinone moiety on mitoxantrone to a quinone, resulting in a di-quinone species. However, in vitro analysis of the MPO catalysed oxidation of mitoxantrone by high performance liquid chromatography and mass spectroscopy revealed oxidation occurs at the phenylenediamine substructure of mitoxantrone (Kolodziejczyk *et al.*, 1988; Blanz *et al.*, 1991) (Figure 1.10).

The MPO-catalysed oxidation of mitoxantrone yields a naphthoquinoxaline initial metabolite which is further oxidised to a metabolite of unknown identity (Panousis *et al.*, 1994; Panousis *et al.*, 1997) (Figure 1.21). The peroxidase catalysed reaction to naphthoquinoxaline proceeds via two consecutive one-electron oxidations where the second electron extraction is likely to be peroxidase independent. The first oxidation reactions yields quinone-diimine, a high electrophilic compound that undergoes an intramolecular nucleophilic attack to generate the cyclised naphthoquinoxaline metabolite. Studies have shown that naphthoquinoxaline can covalently adduct DNA but its role in TOP2 poisoning has not been documented (Reszka *et al.*, 1989; Panousis *et al.*, 1997).

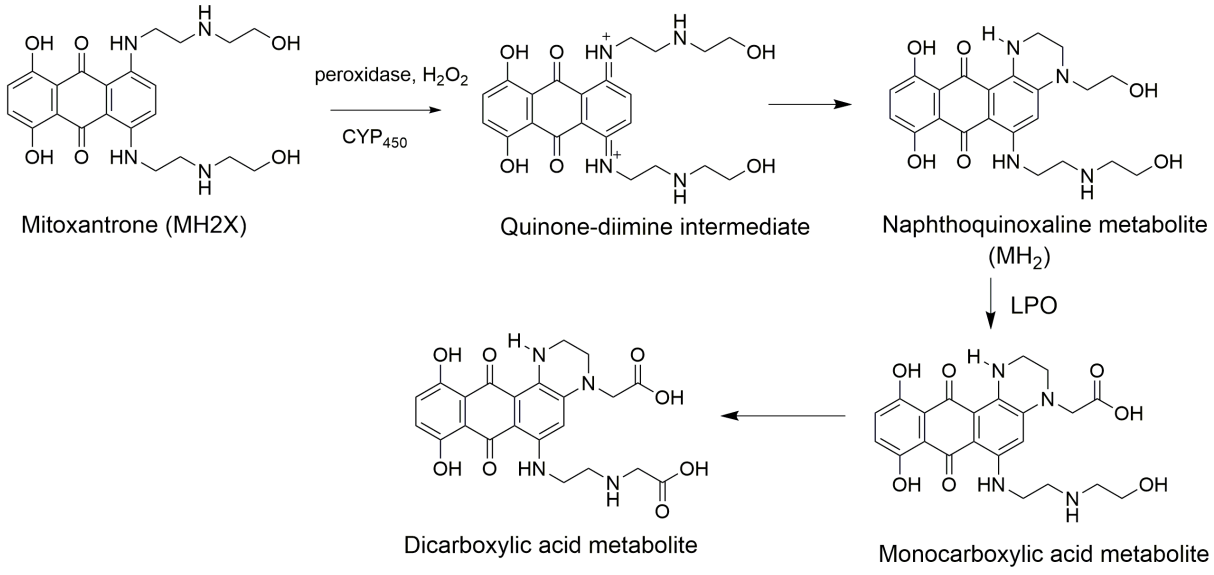


**Figure 1.21. Peroxidase-mediated biotransformation of mitoxantrone.** Information used to construct figure obtained from Blanz *et al.,* 1991, Mewes *et al.,* 1993 and Bruck and Bruck, 2011.

The peroxidase catalysed oxidation reaction of mitoxantrone to naphthoquinoxaline is identical for MPO, cytochrome P450, horseradish peroxidase, lactoperoxidase (LPO) and lignin peroxidase, however the product of the subsequent oxidation of naphthoquinoxaline is suggested to be dependent on the specific peroxidase (Reszka *et al.*, 1986; Mewes *et al.*, 1993; Bruck and Harvey, 2003; Bruck and Bruck, 2011). Whereas the final oxidation product for the MPO-catalysed oxidation of mitoxantrone has not been identified, the chemical structures for the LPO-catalysed oxidation of mitoxantrone have been characterised. As LPO shares 51% amino acid identity with MPO, it may be the case that both these peroxidases share a similar end

product in the oxidation of mitoxantrone. However, in contrast to MPO, LPO is a monomeric enzyme and LPO's redox intermediates have lower redox potentials compared to MPO (1.09V vs 1.36V for compound I) (Furtmuller *et al.*, 2003; Furtmüller *et al.*, 2006).

In the presence of LPO, naphthoquinoxaline is oxidised to monocarboxylic mitoxantrone ($MH_2Oa^*$), which is further oxidised to dicarboxylic acid mitoxantrone ($MH_2O_2^*$) metabolites via the generation of radical intermediates (Bruck and Bruck, 2011) (Figure 1.21). There are no known published studies conducted to analyse the activity and cellular functions of these two carboxylic acids mitoxantrone metabolites.

***Formation of formaldehyde activated mitoxantrone DNA adducts-an indirect role of MPO.***

Mitoxantrone can be activated by formaldehyde to form DNA adducts. These formaldehyde activated heat liable adducts occur preferentially at CpA and CpG sites and adduct formation is enhanced by DNA methylation at CpG sites (Parker *et al.*, 1999) (Figure 1.22). Formaldehyde reacts with the side chain amino group of mitoxantrone to form activated-mitoxantrone which is defined by the presence of a Schiff base at a second nitrogen of the mitoxantrone side chain (Parker *et al.*, 2004). The Schiff base can undergo a nucleophilic reaction with the exocyclic N2 of guanine generating a DNA-adduct in which mitoxantrone is covalently bound to one strand of DNA using a covalent methylene linkage and uses hydrogen bonds to interact with the opposing DNA strand forming a *virtual cross-link* (Figure 1.22). It is to be noted that the precise chemical reaction between formaldehyde and mitoxantrone has not yet been fully established (Evison *et al.*, 2015).

The consequence of the mitoxantrone-guanine adduct is to impair DNA strand separation, blocking the progression of RNA polymerase and resulting in truncated RNA transcripts (Parker *et al.*, 2000). Methylation at the CpG sites is predicted to prevent the entry of mitoxantrone into the major groove and therefore favour the entry of the activated mitoxantrone through the minor groove which positions mitoxantrone adjacent to the N2 of guanine facilitating nucleophilic attack (Parker *et al.*, 2004).

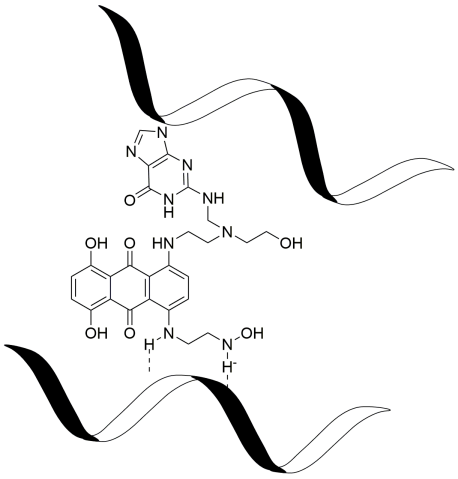

**Figure 1.22 Formaldehyde activated mitoxantrone-guanine lesion.** Mitoxantrone reacts with formaldehyde producing activated mitoxantrone -defined by the presence of an Schiff base at the second nitrogen of the amine side chain. The Schiff base is subject to nucleophilic attack by the exocyclic N2 amino group of guanine to form a covalent bond. Mitoxantrone therefore covalently links to one strand of DNA forming a mono-adduct whilst the second strand of DNA has hydrogen-bonding interactions with mitoxantrone to form a virtual cross-link (Fenick *et al.,*1997). Information to construct diagram Parker *et at.,* 1999 and Evison *et al.,* 2015.

MPO could influence the level of formaldehyde-activated mitoxantrone DNA adducts. The reason for suggesting this is, MPO catalyses the oxidation of amino acids to aldehydes via MPO-$H_2O_2$-Cl system to generate HOCl which chlorinates the free alpha amino group of amino acids generating a liable mono chloramine which decomposes to a aldehyde (Hazen *et al.*, 1998) (Zgliczynski *et al.*, 1968). Generally myeloid cells contain high concentrations of formaldehyde and this could potentially be an effect of high MPO activity within these cells (Thorndike and Beck, 1977).

### *1.3.3 Biotransformation of doxorubicin and epirubicin by MPO*

#### *Direct oxidation of doxorubicin by MPO*

Like mitoxantrone, the anthracycline doxorubicin contains a hydroquinone and quinone moiety. Given the MPO-catalysed oxidation pathway of mitoxantrone one may predict, that peroxidase oxidation of doxorubicin may occur at a distinct site from the hydro-and quinone moieties. It was first speculated that the hydroquinone of doxorubicin would be protected from oxidation by the presence of the neighbouring electrophilic quinone species. However, experimental studies using the MPO/$H_2O_2$ system showed that oxidation of doxorubicin and a structurally similar, daunorubicin occur at the hydroquinone moiety (Figure 1.23).

MPO catalyses the oxidation of the hydroquinone moiety of doxorubicin yielding a semi-quinone species and MPO compound II. Only compound I is capable of the

oxidation of doxorubicin (Reszka *et al.*, 2004). The semi-quinone disproportionates to the parent compound (reversible oxidation) and to a highly electrophilic di-quinone species (irreversible oxidation) (Reszka *et al.*, 2001; Reszka *et al.*, 2005) (Figure. 1.23A). Nitric oxide ($NO_2$) facilitates the MPO catalysed reaction of doxorubicin by two possible mechanisms. The first mechanism involves the role of nitric oxide in accelerating MPO's catalytic turnover. As the oxidation of doxorubicin to the semi-quinone species results in the formation of MPO compound II which has a lower reduction potential and therefore cannot oxidise doxorubicin, therefore nitric oxide can react with compound II reducing it back to MPO which can re-enter the catalytic cycle and oxidise more molecules of doxorubicin. Alternatively, nitric oxide is oxidised to a free radical species ($^{\bullet}NO_2$) by MPO's compound I or compound II, the free radical species can oxidise the hydroquinone moiety of doxorubicin ($QH_2$) to a semi-quinone species ($Q^{\bullet -}$) (Figure 1.23 B) (Reszka *et al.*, 2005; Wagner *et al.*, 2007).

Studies predict doxorubicin di-quinone may further undergo oxidation however no oxidation products of the di-quinone have been reported. Such di-quinone species can potentially adduct DNA and protein causing oxidative damage to cells. Attempts to purify the products of doxorubicin oxidation from cells (HL60 cells-MPO positive) have reported doxorubicin di-quinone to degrade into two inactive compounds; 3-methoxyphthalic acid (3-MePA) and 3-methoxysalicylic acid (3-MeSA). However, these degradation products have not been identified from *in vitro* reactions therefore this could suggest that doxorubicin di-quinone degrades during the process of purification from cells (Reszka *et al.*, 2001; Reszka *et al.*, 2005; Wagner *et al.*, 2007). The degradation products, 3-MePA and 3-MeSA have also been purified from cardiomyocytes. The formation of 3-MePA and 3-MeSA was reported to be dependent on the pseudo-peroxidase action of myoglobin, however it is still not clear how degradation occurs (Cartoni *et al.*, 2004; Menna *et al.*, 2007). Alternatively, as doxorubicin di-quinone is an unstable compound, failure to react quickly with protein or DNA (this would reduce the di-quinone to a quinone which is stable) may result in degradation of the tetracycline ring.

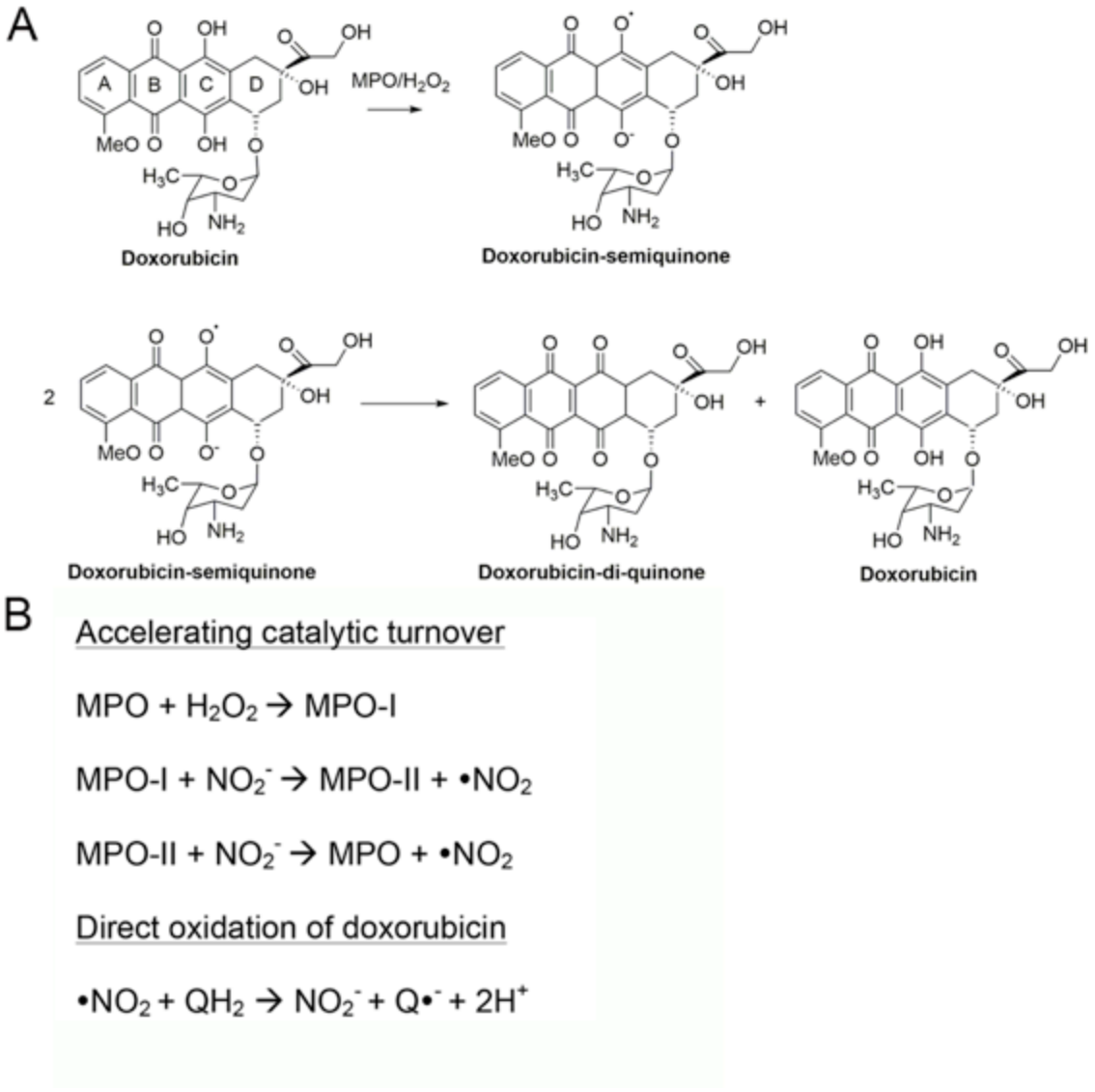


**Figure 1.23 Oxidation of doxorubicin by MPO.** (A) Reaction showing the formation of doxorubicin-di-quinone. MPO compound I catalyses the oxidation of doxorubicin to semi-quinone species that further disproportionates to doxorubicin di-quinone. (B) Nitric oxide facilitates the MPO-mediated oxidation of doxorubicin by two possible mechanisms. Information used to construct diagram obtained from Reszka *et al.,* 2001, Resezka *et al.,* 2005 and Wagner *et al.,* 2007.

***Formation of doxoform and epiform.***

As previously stated MPO can catalyse the oxidation of amino acids to form active aldehydes via the formation of HOCl. Formaldehyde can react with either doxorubicin or epirubicin to form doxoform or epiform that covalently link to the guanine base of DNA. The reaction of either doxorubicin or epirubicin results in the conjugation of two drug molecules joined to each other via a methylene group(s) resulting in doxoform or epiform (Figure 1.24) (Fenick *et al.*, 1997; Taatjes *et al.*, 1998). Interestingly the corresponding drug-formaldehyde conjugate for doxorubicin and epirubicin differ in

structure, this is perhaps surprising as epirubicin differs from doxorubicin only at the position of the 4' alcohol group on daunosamine (sugar) moiety.

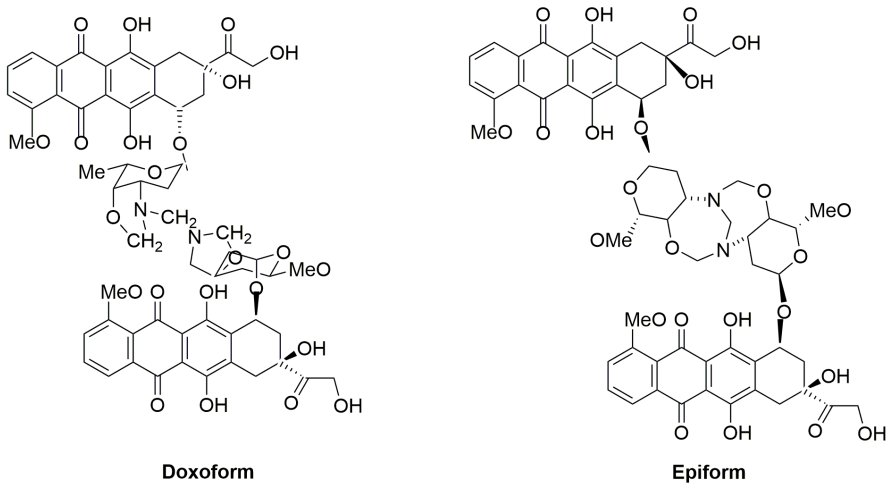


**Figure 1.24 Chemical structures of formaldehyde activated doxorubicin and epirubicin.** Chemical structure information obtained from Post *et al.,* 2005, Fenick *et al.,* 1997 and Taatjes *et al.,* 1998.

Doxoform (bis(3'-N-3'-N,4'-O-methylenedoxorubicinyl)methane is characterised by two parent molecules bound by a single methylene group (Fenick *et al.*, 1997; Post *et al.*, 2005). Whereas epiform consists of two parent molecules attached via three methylene groups in a 1,6-diaza-4,9-dioxabicyclo[4.4.1]undecane ring system (Taatjes *et al.*, 1998). However, epiform and doxoform cannot conjugate with DNA until hydrolysis occurs to form the monomeric forms of the formaldehyde conjugates. The resulting DNA adduct for the monomeric activated epiform and doxoform are identical in structure and have been confirmed using X-ray crystallography (dauo-form-DNA adduct PDB ID 1D33, 2D34) and NMR. The DNA adduct is identified to occur at the exocylic N2 amino of guanine via a single covalent bond (N-C-N) from the 3' amino of daunosamine with the central carbon derived from formaldehyde (Wang *et al.*, 1991; Kato *et al.*, 2000; Cutts *et al.*, 2005) (Figure. 1.25). The opposing DNA strand has hydrogen-bonding interactions with the drug molecule therefore the doxoform-DNA adducts are classified as a *virtual cross-link* and occur at the minor groove. A similar feature of the formaldehyde-activated drug conjugates is that they occur with the exocylic N2 amino of guanine and are hydrolytically unstable due to the formation of a *virtual cross-link*. The term *virtual cross-link* has been used to describe the linkage as a covalent bond is made to one DNA strand only whereas the interactions made with the neighbouring strand are weak hydrogen bonding

interactions (Fenick *et al.*, 1997). Despite the doxoform and epiform- DNA adducts being relatively weak in strength both doxoform and epiform are reported to be more cytotoxic than their respective parent molecules (Fenick *et al.*, 1997; Taatjes *et al.*, 1998; Kato *et al.*, 2000).

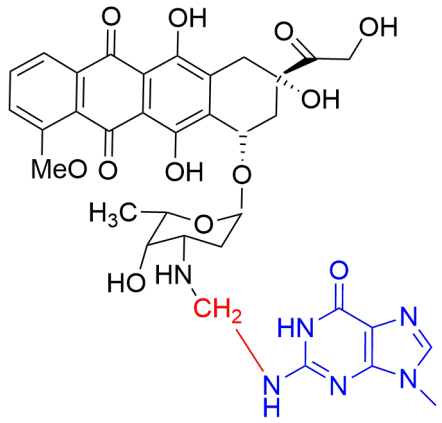


**Figure 1.25 Doxoform-DNA adduct.** Formaldehyde reacts with doxorubicin to form doxoform (Figure. 1.13) consisting of two doxorubicin molecules attached by a methylene group. At neutral pH, doxoform or epiform hydrolyse to generate monomeric and dimeric forms of doxorubicin- or epirubicin-formaldehyde conjugates that can adduct DNA in the minor groove. The DNA adduct has been characterised by X-ray crystallography and NMR and is identical for doxorubicin, dauorubicin and epirubicin. The Doxoform-DNA adduct is characterised by covalent methylene bridge (red) between the N3' of daunosamine (black) and N2 of guanine (blue). Information to construct diagram obtained from Cutts *et al.,* 2005.

## 1.4 Glutathione

Glutathione is a tri-peptide (L-γ-glutamyl-L-cysteinyl-glycine) that has multiple important functions in living organisms including protection from foreign compounds containing electrophilic sites (Habig *et al.*, 1974). Glutathione is present at high concentrations in cells ranging from 0.5mM to 10mM and is distributed in the cytoplasm, ER, nucleus and mitochondria (Lushchak, 2012).

### *1.4.1 Biosynthesis of glutathione*

The biosynthesis of glutathione requires two enzymes; glutamate cysteine ligase (EC 6.3.2.2) (γ-glutamylcysteine synthase) and glutathione synthase (EC 6.3.2.3). Both catalytic steps are dependent on ATP and magnesium (Deponte, 2013). The first step in glutathione biosynthesis is catalysed by glutamate cysteine ligase to generate a peptide bond between the γ-carboxyl of glutamate and the amino group of cysteine

to generate L-γ-glutamyl-L-cysteine (Snoke *et al.*, 1953) (Figure 1.26A). This first enzymatic step proceeds via the generation of a phosphorylated glutamate intermediate termed γ-glutamylphosphate, which undergoes a nucleophilic attack by cysteine producing L-γ-glutamyl-L-cysteine. Following this glutathione synthase catalyses the condensation of the dipeptide, L-γ-glutamyl-L-cysteine with glycine to form glutathione (Figure 1.26A) (Minnich *et al.*, 1971). The arrangement of the glutathione tripeptide protects glutathione from cleavage by common peptidases and by γ-glutamyl cyclotransferase restricting cleavage by hydrolases specific for glutathione such as γ-glutamyltransferase (E.C 2.3.2.2) (Figure 1.26B) (Lushchak, 2012).

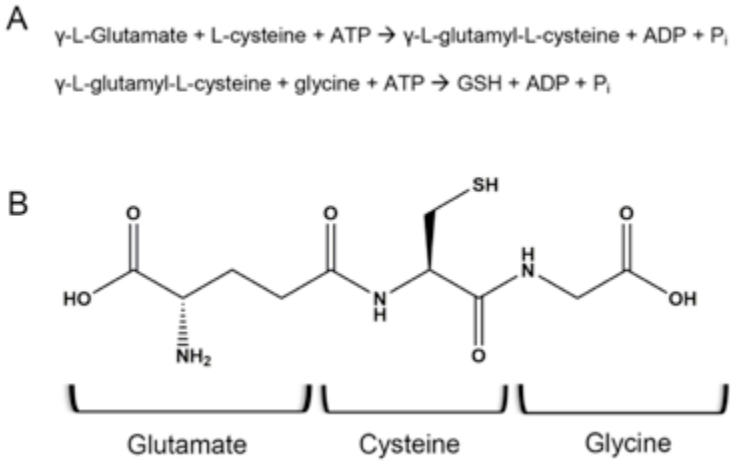


**Figure 1.26 Glutathione biosynthesis chemical equation (A) and the chemical structure of glutathione (B).** (A) Glutathione is synthesised using two enzymes the first reaction is catalysed by glutamate cysteine ligase to generate L-γ-glutamyl-L-cysteine. L-γ-glutamyl-L-cysteine is then combined with glycine by glutathione synthase to form glutathione (GSH). (B) The N-terminal glutamate is linked to cysteine via a γ-carboxyl group of glutamate; this arrangement of glutathione protects cleavage by common peptidases resulting in a relatively stable compound. Information used to construct this figure was derived from (Minnich *et al.*, 1971; Lushchak, 2012).

### *1.4.2 Inhibition by glutathione synthesis by buthionine sulfoximine (BSO)*

BSO is a mechanistic-based inhibitor of glutamate cysteine ligase, this enzyme is involved in the first step of glutathione synthesis (section 1.4.1 and Figure 1.26A). BSO has been characterised as the most potent inhibitor of glutathione (Griffith and Meister, 1979; Griffith, 1982) (Figure 1.27). BSO works by binding to the active site of glutamate cysteine ligase and is phosphorylated by an ATP/$Mg^{2+}$ dependent reaction forming a transition state analogue (similar to the attack by cysteine on the phosphorylated glutamate intermediate) (Griffith *et al.*, 1979; Biterova and Barycki,

2010). Phosphorylated BSO binds tightly to the active site occupying both the glutamate and cysteine binding sites and has a slow dissociation constant making it a successful inhibitor for glutathione synthesis and for use in the treatment of neuroblastoma to reduce glutathione mediated drug resistance (Clinical Trial ID NCT00005835) (Villablanca *et al.*, 2016).

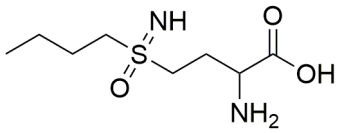


**Figure 1.27 Chemical structure of BSO.** (Information used to construct this figure was obtained from PubChem CID 2115

## 1.5 The effect of glutathione on MPO-mediated oxidation of TOP2 poisons and formaldehyde.

Metabolites generated by the MPO-mediated oxidation of etoposide, mitoxantrone, doxorubicin or epirubicin can be rendered inactive by the conjugation with glutathione. Glutathione reacts with electrophilic sites via the action of glutathione-*S*-transferase or by spontaneously to form glutathione adducts, ultimately resulting in the excretion of the metabolite (Habig *et al.*, 1974). Therefore, glutathione may play a major role in protecting cells from the effects of TOP2 poison metabolites generated by MPO.

### *1.5.1 Etoposide*

As described in section 1.4.1, MPO can catalyse the one-electron oxidation of etoposide to a phenoxyl radical, which can further oxidise to etoposide quinone (Figure 1.20). In the presence of glutathione, the formation of etoposide quinone is reduced using two mechanisms. In the first mechanism, glutathione can reduce etoposide phenoxyl radical back to etoposide releasing a glutathione thiyl radical (Figure 1.28). Studies conducted in vitro using electron paramagnetic resonance had observed a lag-phase in the production of etoposide phenoxyl radical in the MPO/$H_2O_2$/etoposide system that diminished once glutathione was titrated out (Kagan *et al.*, 1994; Kagan *et al.*, 1999).

Secondly, glutathione can conjugate with etoposide quinone or etoposide semi-quinone (reaction intermediate in etoposide catechol oxidation) producing etoposide-OH-6'-SG (major product) and/or etoposide-OH-2'-SG (minor product) (Figure 1.28) (Zheng *et al.*, 2006). The presence of etoposide-OH-6'-SG has been confirmed in HL60 cells (MPO positive cells) treated with etoposide and was shown to be dependent on MPO activity (Fan *et al.*, 2006). It is predicted that etoposide-OH-6'-SG is further modified by the cleavage of the terminal glutamate and glycine residues of glutathione followed by the acetylation to produce an N-acetylcysteine conjugate (etoposide-OH-6'-NAc-Cys) via mercapturic acid biosynthesis allowing the excretion of etoposide quinone (Hinchman *et al.*, 1991; Zheng *et al.*, 2006) (Figure 1.28). Due to this detoxification pathway by glutathione it is hypothesised that MPO-mediated oxidation of etoposide to etoposide quinone may occur at a higher efficiency in the nucleus as the etoposide quinone will be in closer proximity to DNA and the chances of conjugation with nuclear glutathione may be reduced (Murao *et al.*, 1988).

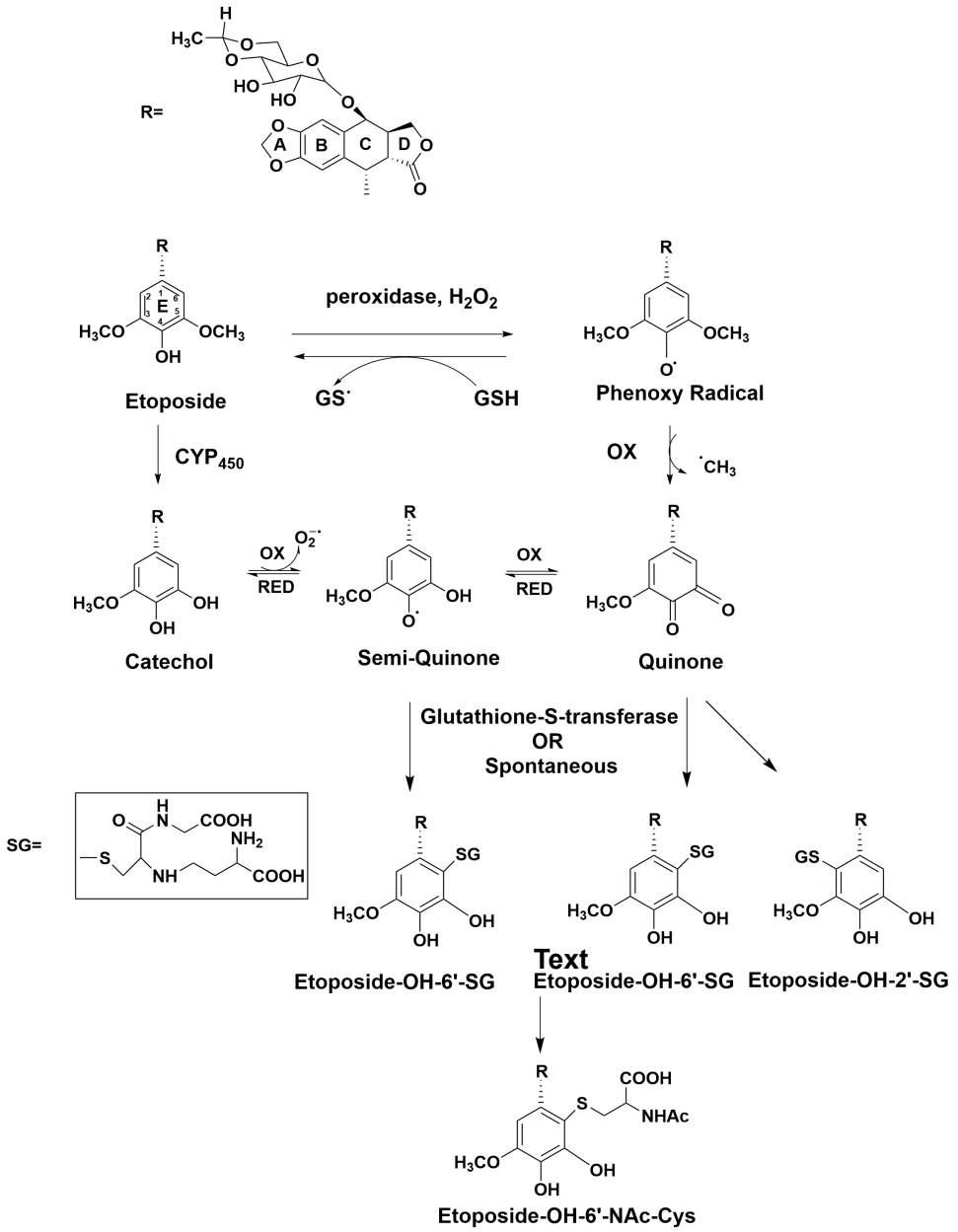


**Figure 1.28 Oxidation pathway of etoposide and formation of glutathione conjugates.** Information used to construct this diagram and numbering of the glutatathione conjuagtion sites was obtained from Zheng *et al.*, 2006.

### *1.5.2 Mitoxantrone*

The oxidation of mitoxantrone to naphthoquinoxaline involves the formation of an electrophilic quinone-diimine intermediate (Figure 1.21). Quinone-diimine is subject to conjugation with glutathione preventing completion of the peroxidase-mediated reaction. Studies had first confirmed the presence quinone-diimine glutathione conjugate using tandem mass spectrometry (MS/MS) but were not able to deduce the positioning of the glutathione conjugation and predicted the conjugation occurred at the phenylenediamine substructure (Blanz *et al.*, 1991). Later studies deduced that

glutathione conjugates at the hydroquinone moiety, but conjugation only occurs in the presence of the peroxidase/$H_2O_2$ (Mewes *et al.*, 1993) however no further published studies have confirmed this. Although the consequence of the conjugation was not stated, it is likely that the glutathione-mitoxantrone conjugate undergoes a similar process to that described for etoposide quinone by the formation of N-acetylcysteine conjugates described in section 1.6.1.

### *1.5.3 Doxorubicin*

MPO and other peroxidases (lactoperoxidase) can oxidise the hydroquinone moiety of doxorubicin to a quinone forming doxorubicin di-quinone - a highly electrophilic compound (Figure 1.23). In the presence of glutathione a rapid decline in the peroxidase-mediated oxidation of daunorubicin (structurally similar to doxorubicin) is observed and the drug is reported to largely remain unchanged (i.e. no detection of di-quinone species). This suggests that glutathione prevents the formation the di-quinone species, but perhaps not by conjugation. This may either occur via a reduction reaction of the semi-quinone species back to daunorubicin releasing a thiyl radical, a mechanism similar to the reduction of the etoposide phenoxyl radical to etoposide. However, glutathione can directly conjugate with doxorubicin and this may potentially protect doxorubicin from peroxidase-mediated oxidation (Askura *et al* ;1997).

### *1.5.4 Formaldehyde*

Formaldehyde is potentially dangerous to cells and metabolism using glutathione is a key response to effectively detoxify excess cellular generated formaldehyde. Increased formaldehyde levels have been reported in neurodegenerative diseases such as multiple sclerosis (MS) in which mitoxantrone is used as a single agent (Tulpule and Dringen, 2013). Therefore it is likely that treatment with mitoxantrone in MS may lead to higher levels of formaldehyde-activated mitoxantrone. As previously described in sections 1.4.2 and 1.4.3 formaldehyde can activate mitoxantrone, doxorubicin and epirubicin to species that form virtual cross-links with DNA (Figure 1.22, 1.24 and 1.25).

Glutathione can spontaneously react with formaldehyde via its nucleophilic thiol group to form glutathione-formaldehyde conjugates. In humans the major conjugation product is *S*-(hydroxymethyl)glutathione which is further oxidised by alcohol dehydrogenase 5 and then hydrolysed to formate releasing glutathione (Hopkinson *et al.*, 2010). Studies have reported the formation of *S*-(hydroxymethyl)glutathione could possibly be facilitated enzymatically, but no such enzymes have been identified in humans (Goenrich *et al.*, 2002; Hopkinson *et al.*, 2015) (Figure. 1.29). However more recent studies have reported addition products of the initial conjugation of glutathione with formaldehyde resulting in formation of cyclic conjugates with one of these products, $BiGF_2$ (5*R,*10*S*)-5- (carboxymethylcarbamoyl) -7-oxo-3 - thia- 1,6-diazabicylo[4.4.1] undecane-10-carboxylic acid) being observed bound to human Carbonyl Reductase I (Bateman *et al.*, 2007; Hopkinson *et al.*, 2010) (Figure. 1.29).

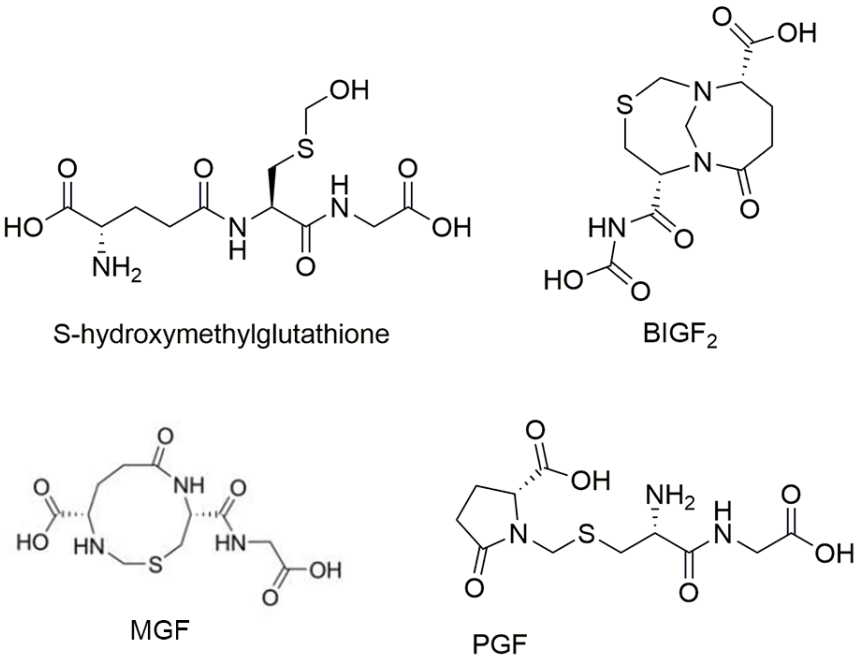


**Figure 1.29 Products of the formaldehyde-glutathione conjugation reaction.** Structure information taken from Hopkinson *et al*., 2010. Full chemical name of MGF (4S,9R)-9-(carboxymethylcarbamoyl)- 7-oxo-1,3,8-thiadiazecane-4-carboxylic acid and PGF (S)-1-(((R)-2-amino-3-(carboxymethylamino)-3- oxopropylthio)methyl)-5-oxopyrrolidine-2-carboxylic acid.

## 1.6 Development of therapy related leukaemia following TOP2 poison treatment

TOP2 poisons are effective anti-neoplastic agents used to treat a wide range of malignancies (Table 1), however a serious long-term side effect to TOP2 poison therapy is the risk of developing therapy related acute myeloid leukaemia (t-AML).

The development of t-AML is a serious complication following primary treatment for a wide range of neoplasias and is often associated with a poor prognosis especially in patients above the age of fifty (Santo *et al.*, 2016). It is estimated that up to 15% of reported AML cases are t-AML with ~70% of reported t-AMLs arising from prior therapy of solid cancers with breast cancer being the highest frequency. Haematological malignancies account for ~28% cases with Non-Hodgkin lymphoma accounting for the highest incidence (Block *et al.*, 2002; Huret, 2004). However, as survival rates improve and life expectancy following treatment of the primary cancer increases, the incidence of t-AML could potentially rise. Therefore, the understanding of how t-AML arises is crucial.

The development of t-AML or therapy related acute promyelocytic leukaemia (t-APL) following TOP2 poison exposure has a mean latency period of 1 to 3 years (Leone *et al.*, 2010; Cowell and Austin, 2012). TOP2 poison associated t-AML frequently involves chromosome translocations occurring at the *MLL (KMT2A)* gene at 11q23 with partners *AF9/MLLT3* (9q22), *AF4/AFF1* (4q21) and less frequently with other translocations partners (66 partners reported). Other recurrent translocations include *t(15,17)(PML-RARA)*, *t(8,21)(RUNX1-RUNX1T1/ETO)*, and inv*(16)(p13;q22)(CBFB-MYH11)*. Alkylating agent therapy (cyclophosphamide, melphalan and procarbazine) and antimetabolite therapy (azathioprine, fludarabine, 6-thioguanine) are also associated with the risk of developing t-AML but are characterised by chromosome deletions, particularly involving chromosome 5 and/or 7 (Leone *et al.*, 2007; Leone *et al.*, 2010). Therefore, a model of t-AML arising from TOP2 poison exposure involves the illegitimate recombination between DNA repair intermediates, resulting in leukaemogenic chromosome translocations, blocking differentiation of progenitor hematopoietic cells.

***MLL locus***

The Mixed linage leukaemia (*MLL*) gene is located on chromosome 11q23.3 and is frequently associated with etoposide related t-AML, it is estimated that 5-10% of *MLL* associated leukaemia's are therapy related (Leone 2010). In addition, mitoxantrone, epirubicin and doxorubicin therapies are also associated with *MLL* translocations (Anderson 2001 and Ng 2005).

In the non-leukaemia state, the MLL protein forms a multicomponent complex (consisting of more than 30 proteins) to regulate transcription of a number of genes involved in haematopoiesis through the induction of chromatin modifications and remodeling (Slany, 2009; Yip and So, 2013). To date, 66 translocation partners for *MLL* have been reported with 85 recurrent translocations (information obtained from http://atlasgeneticsoncology.org/Genes/MLLID13.html). The resulting translocations disrupt hematopoietic gene regulation (Slany, 2009).

*MLL* translocation breakpoints identified in acute leukaemia cases occur in a 8.3Kb region located between exons 5 and 12 (Super *et al.*, 1993). Breaks in this region for t-AML and neonatal leukaemia are clustered towards the telomeric 1Kb end (also known as SCII) of this region whereas in *de novo* leukaemia the breakpoints tend to cluster within the centromeric region (SCI) of the breakpoint cluster (bcr) (Cowell and Austin 2012) (Figure 1.30). The telomeric subcluster contains a DNAseI hypersensitive region colocalising with CTCF binding and is also reported to possess cryptic promoter activity (Scharf *et al.*, 2006; Cowell *et al.*, 2012). Furthermore, in vitro studies showed that etoposide quinone, a metabolite generated by the MPO mediated oxidation of etoposide, induces strong heat stable cleavage at the *MLL* locus (study conducted outside of hotspot region for t-AML). (Lovett *et al.*, 2001a; Lovett *et al.*, 2001b). This suggests a role of peroxidase-mediated oxidation of TOP2 poisons to reactive metabolites that may have increased potential of causing DNA damage (see section 1.1.4).

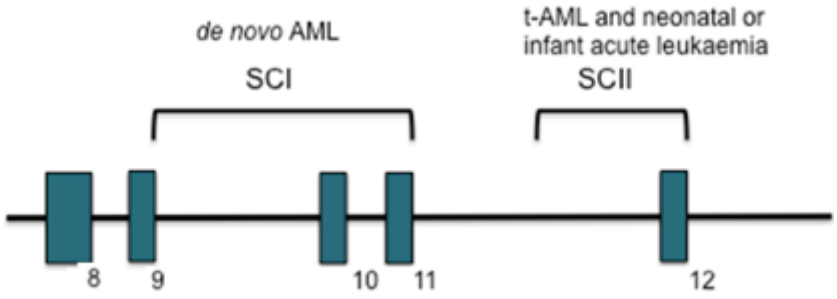


**Figure 1.30 *MLL* breakpoint cluster region.** Exons are shown as boxes and intron regions are black lines. Information used to construct diagram obtained from Cowell and Austin 2012.

### *PML/RARA*

The *PML/RARA* (t15;17)(q24;21) translocation is a hallmark of t-APL (a sub-type of t-AML). The resultant fusion protein suppresses transcription of retinoic acid regulated genes resulting in a block to myeloid differentiation. The *PML/RARA* translocation is commonly found in patients who have previously received mitoxantrone, doxorubicin or epirubicin therapy and less commonly with etoposide. Three APL-associated BCRs have been identified, and t-APL breakpoints cluster in BCR 1 (Fig 1.31). An 8bp region within intron 6 (bcr 1) is a strong site for mitoxantrone-mediated cleavage *in vitro* but not for epirubicin and is a preferred site for mitoxantrone-induced translocation breakpoints (Mistry *et al.*, 2005; Hasan *et al.*, 2008; Hasan *et al.*, 2010; Mays *et al.*, 2010). Additionally doxorubicin and etoposide induce cleavage at all breakpoint cluster sites as well as etoposide quinone (Mistry *et al.*, 2005).

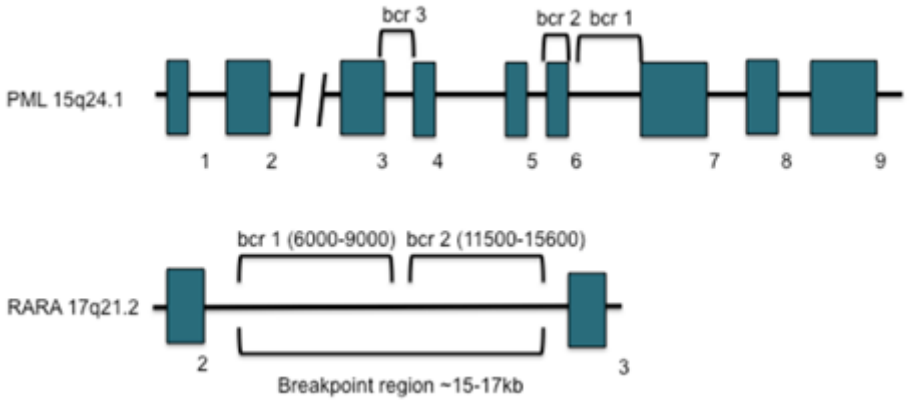


**Figure 1.31 PML and RARA breakpoint regions.** Information used to construct diagram obtained from Hasan *et al.,* 2010.

For the *RARA* the majority of breakpoint clusters are located intron 2 with high clustering of drug (mitoxantrone, doxorubicin, epirubicin and etoposide) induced TOP2 mediated cleavage at two main regions, which are breakpoint cluster 1 (nucleotide positions 6000-9800) and breakpoint cluster 2 (nucleotide positions 11500 to 15600) (Figure 1.31). However, etoposide quinone induces heat stable TOP2 mediated cleavage at bcr2 of *RARA* locus with cleavage centred at nucleotide 16089 (Mistry *et al.*, 2005). Further suggesting that peroxidase-mediated oxidation of TOP2 poisons may play a role in TOP2 poison development of t-AML.

### *TOP2B transcription and the mechanism of TOP2 poison induced chromosomal translocations*

TOP2 poisons effectively stabilise TOP2-DNA complexes for both TOP2A and TOP2B, however recent studies provide evidence for a greater role for TOP2B in TOP2 poison mediated genotoxicity. The current understanding is that TOP2B may induce DNA breaks in genes during the process of transcription which can be stabilised by TOP2 poisons such as etoposide (see section 1.1.1). However, for a translocation to occur breaks must be stabilised in different chromosome segments that are in sufficiently close proximity for erroneous repair to occur.

Studies conducted in cell lines using RNA-FISH have shown that 2-3% of actively transcribing *MLL* genes are in close proximity or overlapping with common translocations partners *AF4*, *AF9* and 4-6% of transcribing *MLL* transcripts were within a 1μm distance to either *AF4* or *AF9* (Cowell *et al.,* 2012). This was also shown to be true for *RUNX1* and its translocation partner RUNX1T1 (using DNA-FISH), (Smith *et al.*, 2014a). Additionally the frequency of this close proximity between observed between *RUNX1* and its partner gene was partly TOP2B dependent. Taken together these studies suggest a role of TOP2B in mediating TOP2 poison associated t-AML.

Despite the risk associated with TOP2 poison therapy, these drugs are central to the treatment for a wide range of adult and paediatric cancers and hematologic malignancies and to some extent for multiple sclerosis. Therefore, interventions to protect developing hematopoietic progenitors from genotoxic damage caused by TOP2 poison would be of clinical benefit. MPO expression is restricted to myeloid cells and is capable of mediating the biotransformation of TOP2 poisons to potentially more genotoxic compounds. The inhibition of MPO could potentially reduce excess DNA damage in myeloid precursors reducing the chances of t-AML.

**Aims**

The aim of the work presented is to:

- To investigate the role of MPO expression in TOP2 poison induced TOP2-DNA covalent complex stabilisation and γH2Ax (marker for DNA damage) formation
- To investigate the combined effect of glutathione depletion and MPO inhibition TOP2 poison induced DNA damage
- To test the whether anthracycline and mitoxantrone behave as TOP2 catalytic inhibitors

# Chapter 2. Materials and Methods

## 2.1 Drugs and Chemicals

All chemicals and reagents were purchased from Sigma-Aldrich (Dorset, UK) unless otherwise specified. All tissue culture plasticware was purchased from Greiner bio-one (Gloucestershire, UK) unless otherwise stated.

### *2.1.1. Preparation of drugs and chemicals*

Doxorubicin, epirubicin and mitoxantrone were dissolved in $dH_2O$ to a stock concentration of 25mM, 5mM and 10mM respectively. Etoposide was dissolved in filter sterilised DMSO to a concentration of 10mM. All prepared drug stocks were stored in small aliquots at -20$^{o}$C.

Etoposide quinone and etoposide catechol were either synthesised by (i) Caymen Chemicals (Michigan, USA) or (ii) by Angelica Mariani in Dr. Raphael Rodriguez Laboratory (Toldo *et al.*) (see Appendix Figures i-iii for data on compounds synthesised by A.Mariani). The source of etoposide quinone and catechol used to conduct each experiment are specified in the figure legends. On the day of the experiment, etoposide quinone or catechol were prepared in filter sterilised DMSO to a concentration of 10mM and used on the day of preparation.

Succinylacetone (SA) (4,6-Dioxoheptanoic acid) and DL-Buthionine sulfoximine (BSO) were prepared to 100mM in $dH_2O$ and stored in small aliquots at -20$^{o}$C.

The MPO inhibitors; PF1355 and MPOi-II (Merck-Millipore, Watford, UK) were dissolved in filter sterilised DMSO to a concentration of 5mM and 10mM respectively and stored at -20$^{o}$C in small aliquots.

## 2.2. Cell culture

Cells were cultured at 37$^{o}$C in a humidified atmosphere containing 5% $CO_2$. Cell culture was performed under aseptic conditions in BIOAIR Safe Flow 1.2 hoods.

### *2.2.1 Cell lines*

HL60 cell line (DSMZ no. ACC-3): a neutrophilic promyelocyte AML cell line that harbours the MYC gene amplification derived from a 35-year-old female (Gallagher *et al.*, 2005).

K562 cell line (ATCC CCL-243): a CML cell line derived from a 53-year-old female and is characterised by having a Philadelphia (Ph1) chromosome (Lozzio and Lozzio, 1975).

Kasumi-1 cell line (ATCC CRL-2724; kindly provided by Dr. Olaf Heidenreich, Northern Institute for Cancer Research, UK): an AML cell line containing the t(8;21) fusion gene, derived from a 7 year old male patient (Asou *et al.*, 1991).

KG1 cell line (ATCC CCL-246): were derived from a 59-year-old male whom had developed AML following erythroleukaemia (Koeffler and Golder, 1978).

NB4 cell line (DSMZ no. ACC-207): an APL cell line derived from a 23-year-old female whom had a second relapse and contains the t(15:17) *PML-RARA* fusion gene (Lanotte *et al.*, 1991).

The table shown below has the full set of chromosomal aberrations identified in each cell line (Table 2.1).

| Cell line | Primary aberration | Full set of aberrations identified |
|---|---|---|
| HL60 | amp (8)(q24) | del(1)(p31p13),del(4)(q25),del(5)(q21), del(7)(q35q36),amp(8)(q24),-9p, del(10)(p14p11),del(11)(q13),del(12)(q13), del(12)(q14.1),del(12)(q14.3),-17p, |
| K562 | t(9;22)(q34;11) | del(3)(q27),del(9)(p21),amp(9)(q34), del(18)(p11q21),gain(22)(q11) |
| Kasumi-1 | t(8;21)(q22;22) | amp(4)(q12),gain(7)(q22qter),gain(8)(q24), del(9)(p24p21),gain(10)(q21),gain(10)(q24), del(13)(q14),del(16)(p13p11),del(17)(p13) |
| KG1 | | del(1)(p31p13),del(5)(q21),del(7)(q34q36), del(8)(p22),+8(p11q11),-12,-17p,del(18)(q21) |
| NB4 | t(15;17)(q22;q11–12.1) | 1,+2,-3,-5q,+7,amp(8)(q24),gain(9)(p24p22), amp(9)(p24),del(9)(p21),+10q,gain(11)(q22qter), +12,amp(12)(p12),gain(13)(q14),del(17)(p13), amp(19)(p13),amp(19)(q13),+20 |

**Table 2.1. Cell line karyotype.** Table information obtained from (Rucker *et al.*, 2006). Abbreviations used in table amp= amplification, del=deletion.

### *2.2.2 Cell culture*

K562, Kasumi-1 and NB4 cell lines were maintained in RPMI 1640 medium supplemented with 10%(v/v) Fetal Bovine Serum (FBS) and 1%(v/v) penicillin and streptomycin (Thermo Fisher Scientific, Massachusetts, USA). The K562 derived MPO expressing cells were maintained as per K562 cells with the addition of 750

µg/mL or 500µg/mL G418 selection antibiotic. The HL60 cells were cultured as K562 and NB4 cells but the cell medium was supplemented with 15% (v/v) FBS.

KG1 cells were maintained in IDMEM medium supplemented with 20% (v/v) FBS and 1% (v/v) penicillin and streptomycin (Thermo Fisher Scientific, Massachusetts, USA).

For routine subculture, cells were grown to $1x10^6$ cells/mL and diluted 1:5-10 in fresh medium every 2-3 days.

Cells were cultured for up to 35 passages after which a fresh low passage cell stock was removed from the liquid nitrogen stores.

### *2.2.3 Cryopreservation of cell lines*

Exponentially growing cells were pelleted by centrifugation at 1000xg for 5 minutes (Harrier 15/80 MSE). Cell pellets were re-suspended in half the final volume of the appropriate pre-warmed medium, to this an equal volume of medium containing 20% of DMSO (sterile filtered through 0.2µm filter) was added and mixed. The cell suspension was transferred to a 1.5mL labelled cryogenic vial. The vials were placed in a polystyrene box at -80$^oC$ for 24 hours, for gradual freezing, after which the vials were transferred to liquid nitrogen for long term storage.

To recover cells, vials were rapidly thawed at 37$^oC$ and pelleted by centrifugation at 1000xg for 5 minutes. Pelleted cells were re-suspended in 5mL of the appropriate complete growth medium and cultured appropriately.

### *2.2.4 Cell counting*

All cell counts were performed using the TC20 automated cell counter (Bio-Rad, UK) by placing 10µL of cell suspension into the cell counting slides provided (Bio-Rad, UK). To assess the cell viability, the cell suspension was mixed with trypan blue solution in a 1:1 ratio and counted using the cell counter.

## 2.3. Whole cell extract preparation for SDS-PAGE

This method for the preparation of whole cell extracts was derived from Mirski *et al*; 1993 and is described below.

Cells were pelleted and washed in ice-cold PBS at 1000xg for 5 minutes. Pelleted cells were re-suspended in 4 pellet volumes of ice-cold extraction buffer (10mg/mL $MgCl_2$, 50mM Tris-HCl, pH 7.4, 4mM DTT, 0.05% of protease inhibitor cocktail (Melford, Suffolk, UK)). To this suspension, SDS was added to 0.25% v/v and mixed. Then, DNase I was added to the mixture at a concentration of 50µg/mL and incubated on ice for 10 to 30 minutes, until the suspension was no longer viscous. Then an equal volume of solubilisation buffer (2% SDS, 20% glycerol, 5% β-mercaptoethanol, 0.6M Tris-HCl, pH 7.2) was added to the suspension and heated at 68$^{o}$C for 10 minutes (Stuart Scientific test tube heater SHT 2D). Samples were allowed to cool down prior to protein estimation or stored in aliquots at -80$^{o}$C.

### *2.3.1 Estimation of protein concentration*

The protein concentration of the prepared WCE was estimated using the Bradford assay in 96 well plates alongside a $dH_2O$ blank. Protein samples were serially diluted 1:2 in $dH_2O$ across the plate. Bovine serum albumin (BSA) was used as the standard, this was firstly diluted 1:2 in solubilisation buffer (used to prepare WCE) and then serially diluted to a concentration ranging from 2mg/mL to 0.125mg/mL. To all wells an equal volume of Quick Start Bradford 1x Dye reagent (Bio-Rad, UK) was mixed and incubated for 10 minutes at room temperature. Absorbance readings were measured at 595nm using the Bio-Rad Microplate reader 550. The background value from $dH_2O$ blank was subtracted from all the readings obtained. A BSA standard curve of the background corrected absorbance at 595nm vs protein concentration (mg/mL) was plotted and the linear region of the curve was used to estimate the protein concentration of samples tested.

## 2.4. SDS poly-acrylamide gel electrophoresis

Protein samples (preparation stated in section 2.3) were mixed with 5x SDS loading buffer (30% Glycerol, 30% TRIS, 10% SDS; NuSep, Germany) and heated at 72$^{o}$C

for 4 minutes (Stuart Scientific test tube heater SHT 2D). Samples were resolved on precast 4-20% SDS-polyacrylamide gels (NuSep, Germany) at 100V for 1 hour (Consort BIOBLOCK E455) using 1x Tris-HEPES running buffer supplied (60% HEPES, 35% TRIS, 5% SDS). Novex pre-stained markers (Thermo Fischer Scientific, UK) or WesternSure pre-stained chemiluminescent (Li-Cor, Cambridge, UK) protein ladders were used to determine the molecular weight of the protein bands.

### 2.5 Western blotting

After electrophoresis, SDS-polyacrylamide gels were transferred onto a nitrocellulose membrane (45μM, Hybond ECL, GE healthcare, UK) surrounded by filter paper and fibre pads. Western transfer was conducted in a cooled transfer chamber at 100V for 1hour using cold western transfer buffer (25mM Tris, 192mM glycine, 20% v/v methanol). The membrane was then blocked in blocking buffer (5% w/v non-fat milk powder in Tris-buffered saline (TBS prepared using 20mM Tris-HCL pH 7.5 and 150mM NaCl) and 0.1% Tween 20 (TBS-T)) at room temperature for 1 hour. Membranes were then incubated with the desired primary antibody diluted at 1:2000 (unless otherwise stated, see table 2.2) in blocking buffer for 1 hour at room temperature. Membranes were washed using TBS-T firstly for 15 minutes and then twice for 5 minutes, followed by the incubation with the secondary antibody diluted 1:20000 for 1 hour (anti-mouse horseradish peroxidase or anti-rabbit IgG horseradish peroxidase, GE healthcare). TBS-T washes were repeated as described above.

The membrane peroxidase activity was detected using the Clarity Western ECL substrate (Bio-Rad, UK). ECL reagents were mixed in a 1:1 ratio and membranes were covered in the prepared ECL solution for 3 minutes, excess ECL solution was removed before conducting detection. Protein band detection was conducted by autoradiography in a dark room using Amersham Hyperfilm ECL film (GE healthcare) and processed using a Konica SRX-101A X-ray film developer or a C-Digit blot scanner (Li-Cor, UK).

When necessary, membranes were stripped using mild stripping conditions and re-probed with the desired antibody. For this membranes were washed with TBS-T for 15 minutes and immersed in Restore Western Blot Stripping Buffer (Thermo Fisher

Scientific, Massachusetts, USA) for 15 minutes at room temperature. TBST washes were repeated and the membrane was blocked in blocking buffer for 1 hour before re-probing.

| Antibody | Catalogue number | Host | Raised to | Supplier | Antibody dilution used in western blotting |
|---|---|---|---|---|---|
| Anti-TOP2A | 4566 | Rabbit (polyclonal) | Full CTD Human TOP2A-GST fusion (residues 1244-1531) | In house | 1:2000 |
| Anti-TOP2B | 4555 | Rabbit (polyclonal) | Full CTD Human TOP2B-GST fusion (residues 1263-1621) | In house | 1:2000 |
| Anti-β-actin | ab3280 | Mouse (monoclonal) | Human $\beta$ actin (residues 1-100) | Abcam, UK | 1:2000 |
| Anti-MPO | ab134132 | Rabbit (monoclonal) | Recognises both MPO (85-90kDa) and heavy chain (60kDa) | Abcam, UK | 1:2000 |
| Anti-MPO | Ab109116 | Rabbit (polyclonal) | Recognises both MPO (85-90kDa) and a possible cleavage fragment of the light chain (15kDa) | Abcam, UK | 1:2000 |
| Anti-MPO | P733 | Rabbit (monoclonal) | Recognises both MPO (85-90kDa) and heavy chain (60kDa) | Cell Signaling Technology, UK | 1:1000 |
| Anti-MPO | 07-496 | Rabbit (polyclonal) | Recognises both MPO (85-90kDa) and heavy chain (60kDa) | Merck Millipore, UK | 1:1000 |

**Table 2.2. List of antibodies used for Western Blotting.**

### *2.5.1 Western Quantification*

Films that were processed using autoradiography were scanned and band intensities were quantified by densitometry using Image Lab Version 5.2.1 (Bio-Rad). Membranes that had been scanned using Li-Cor were quantified using Image Studio 5.0 (Li-Cor). Band intensities were used to estimate the relative protein levels in cells.

## 2.6 siRNA knockdown

Cells were cultured in large T175 flasks to 50% confluency. The required cell density was adjusted by centrifugation at 1000xg for 5 minutes and re-suspended in the appropriate pre-warmed medium. To the electroporation cuvette (gap 4mm, Eurogentec, Belgium) 300µL of cell suspension (cell density 2.5 to 5.0 x $10^7$ cells/mL) was added with the required concentration of siRNA (300nM to 1.0µM). Electroporation was performed at 330mV, 10mS pulse using a Fischer EPI2500 electroporator. Electroporated cells were incubated at room temperature for 15 minutes before transferring cells to small T25 cell culture flasks. Mock control siRNA transfection was performed for all experiments using the ON-TARGETplus Non-targeting pool of siRNA (Thermo Fisher, catalogue number D-001810-10-20) used at an equivalent concentration to the target siRNA (target siRNA listed in Table 2.3). The control siRNA consists of four siRNAs that are stated to have minimal targeting to human, mouse or rat genes. All siRNA experiments were preformed using DNase/RNase free equipment.

| siRNA Name | Gene name | Supplier | Catalogue number | Target RNA sequence |
|---|---|---|---|---|
| Hs_MPO_2 | Myeloperoxidase (MPO) | Qiagen | SI00005425 | 5'-AGGCAUCACCACCGUGUCUAA-3' |
| ON-TARGETplus Human MPO siRNA SMARTpool | Myeloperoxidase (MPO) | Thermo Scientific | L003228-00-0020 | 5'-GAGCAGGUCAUGAGGAUUG-3'<br>5'-UCAGAUGCAUGGUGGACUU-3'<br>5'-GAUCCGGGAGCGAUUGUUU-3'<br>5'-GAACCAAGCCGACUGCAUC-3' |
| ON-TARGETplus Human TOP2B siRNA SMARTpool | Topoisomerase II Beta (TOP2B) | Thermo Scientific | L004240-00-0010 | 5'-GAAGUUGUCUGUUGAGAGA-3'<br>5'-CGAAAGACCUAAAUACACA-3'<br>5'-GAUCAUAUGGGAUGUCUGA-3'<br>5'-GGUGUAUGAUGAAGAUGUA-3' |
| ON-TARGETplus Human TOP2A siRNA SMARTpool | Topoisomerase II Alpha (TOP2A) | Thermo Scientific | L004239-00-0010 | 5'-CGAAAGGAAUGGUUAACUA-3'<br>5'-GAUGAACUCUGCAGGCUAA-3'<br>5'-GGAGAAGAUUAUACAUGUA-3'<br>5'-GGUAACUCCUUGAAAGUAA-3' |

**Table 2.3. siRNA details**

## 2.7 MPO activity assay

MPO activity was measured using a colorimetric assay purchased from Abcam, UK (ab105136). The assay was conducted according to the manufacture protocol with the following method conducted for sample preparation. Cells were pelleted and washed with ice-cold PBS at 1000xg for 5 minutes. Cell pellets were re-suspended in 4 pellet volumes of ice cold MPO assay buffer provided and lysed using sonication at conditions of 17V, pulse 5, for 2 cycles on ice (Bandelin Sonopuls HD 2070). Sonicated samples were centrifuged at 14000xg for 10 minutes at 4$^{o}$C (Sigma 1-16 microfuge) to remove insoluble material. To ensure an equal protein concentration was used for all samples in the assay, the protein concentration was estimated using the Bradford assay described in section 2.3.2. MPO activity was determined by measuring the absorbance of a TNB-2 probe at 415nm. To ensure the assay was working, a positive control supplied in the kit was used in all experiments (kit components listed in Table 2.4).

| Component | Volume supplied |
|---|---|
| DTNB Probe | 50µL |
| MPO assay buffer | 25mL |
| MPO positive control (lyophilised) | 1 vial |
| MPO substrate stock | 50µL |
| Stop Mix (lyophilised) | 20µL |
| Tris(2-carboxyethyl)phosphine hydrochloride (TCEP) (50mM) | 50µL |

**Table 2.4** MPO assay kit components (ab105136 Abcam, UK)

## 2.8 XTT assay

The Cell Proliferation Kit II (XTT) (Roche, Switzerland) was used to evaluate mitochondrial activity. The XTT assay was conducted according to the manufacturer's instructions. Briefly, NB4 cells were seeded at a cell density of 3.0 x $10^4$ cells per 100µL into 96 well plates and incubated at 37$^o$C. On the day of the XTT experiment, the XTT labelling reagent and electron coupling reagent were thawed to room temperature and mixed in a ratio of 1:50 respectively. From this mixture, 50µL (XTT concentration 0.3mg/mL) was added to the plates and incubated for 4 hours at 37$^o$C. The plates were read using the Bio-Rad Microplate reader 550, at 450nm. Absorbance values were corrected for background using medium only control values and data was analysed using GraphPad Prism 4.0.

## 2.9 Seahorse assay

Seahorse XF96 cell energy phenotype test was used to measure real-time oxygen consumption (OCR) and extracellular acidification rate (ECAR). The XF96 plate was pre-coated with poly-L-lysine onto which 2x$10^5$ cells/well NB4 cells in seahorse assay medium (DMEM without $NaHCO_3$ supplemented with 10mM glucose, 1mM pyruvate and 2mM glutamine pH 7.4) were seeded and equilibrated for 1 hour in a non-CO2 incubator. The stressor mix was composed of the mitochondrial inhibitors; oligomycin (2µM) to inhibit complex V and FCCP (1µM) to uncouple the proton gradient. The XF96 phenotype test was conducted under manufacturer guidelines. OCR and ECAR were measured under basal conditions followed by sequential additions of oligomycin and FCCP, reading were determined using the Seahorse XF96 Flux analyser on Wave Desktop 2.3 and data analysis was conducted using GraphPad Prism 7.0.

## 2.10. Stable transfection of MPO cDNA into K562 cells

K562 cells were transfected with plasmid RC216029 containing the coding sequence for full-length human MPO with a C-terminal MYC-DDK tag encoded in the pCMV6-Entry vector (Origene, Rockville USA) (Figure 2.1 and Appendix Figure iv for insert sequence). This vector also contains the gene encoding for neomycin-kanamycin

phosphortransferase type II enzyme that gives resistance to G418 to allow selection of cells which have taken up the plasmid.

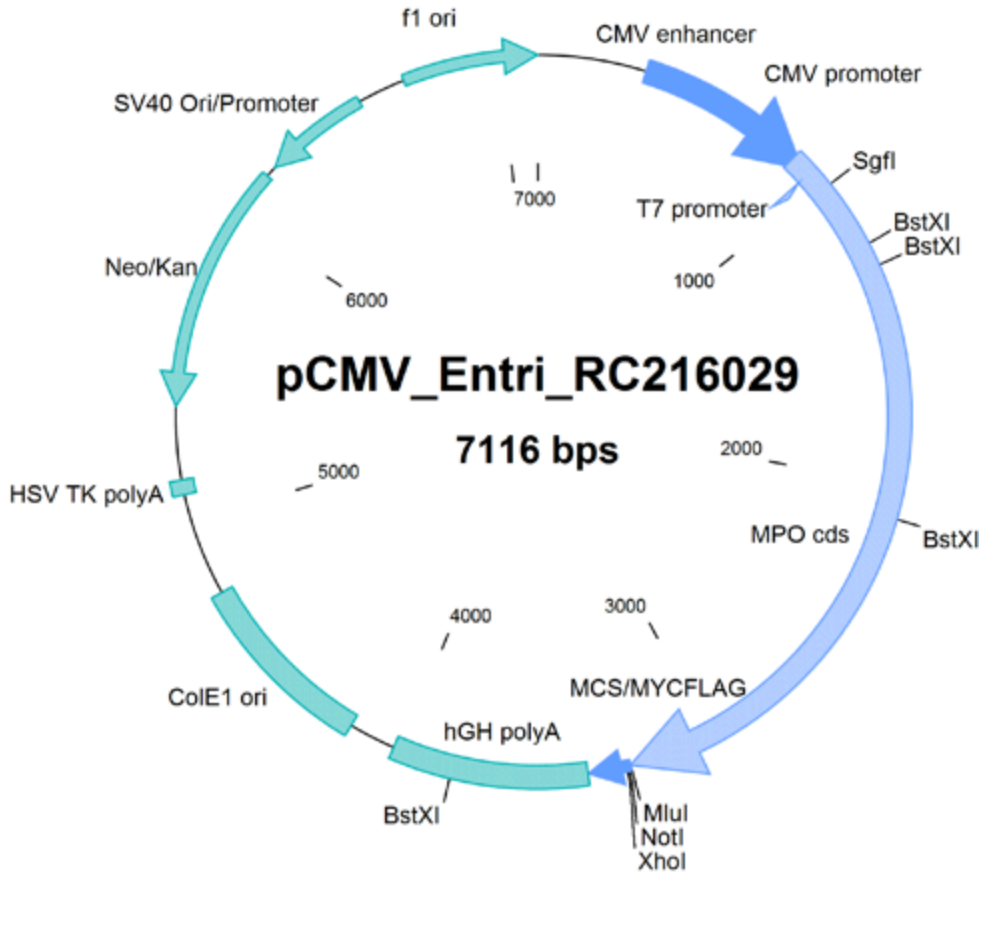


**Figure 2.1 MPO cDNA construct, diagram obtained from Origene**.

A volume of 200µL of exponentially growing K562 cells were seeded into 24 well plates at a cell density of $5x10^5$ cells/mL and incubated at 37°C for 1 hour prior to transfection. During this period the transfection mastermix was prepared (shown below), under DNase/RNase free conditions. The master mix was incubated for 20 minutes at room temperature to allow the plasmid and Dharmafect Duo (Dharmacon, UK) to form a DNA-liposomal complex, prior to transfection. To the mastermix, 200µL of antibiotic free medium (normal K562 growth medium without 1% v/v penicillin and streptomycin see section 2.2.2) was mixed and added drop-wise to K562 cells. For a non-transfected control, 300µL of antibiotic free medium was added to separate K562 cells.

| Component | Volume (µL) |
|---|---|
| Serum free RPMI 1640 medium | 80 |
| Expression plasmid (stock 100µg/mL) | 10 (MPO stock 1µg/mL) |
| Dharmafect Duo (stock 200µg/mL in serum free medium) | 10 |

**Mastermix preparation for K562 cell transfection**

Transfected cells were incubated overnight at 37$^{o}$C. The following day cell viability was assessed using trypan blue (2.2.4) and for selection, 750µg/mL of G418 was added. When cells became confluent in 24 well plates, cells were transferred to 6 well plates and grown in the presence of 500µg/mL of G418 and tested for MPO expression by immunofluorescence (section 2.11). In all cases the population of K562 cells with positive MPO expression was low and to achieve a single colony of MPO expressing K562 cell line, cells were isolated by limited dilution.

### *2.10.1 Cloning by limited dilution*

To isolate single colonies of MPO expressing cells the 'Cell Cloning by Serial Dilution in 96 Well Plates Protocol' method by John A Ryan (Corning Incorporated, New York) was used. Briefly, all wells of a 96 well plate expect well A1 were filled with 100µL of K562 cell medium and 500µg/mL of G418 (Figure. 2.2). In well A1, 200µL of 2.0x10$^{4}$ cells/mL of transfected K562 cells were seeded. Then 100µL of cell suspension from well A1 was transferred to well B1 and mixed gently, this series of 1:2 dilutions was repeated down the entire column (C1-H1). An additional 100µL of medium was added to columns A1-H1. Then 100µL of cell suspension was transferred from the first columns (A1-H1) to the second columns (A2-H2), these 1:2 dilutions were repeated across the entire plate. The final volume of each well was brought to 200µL with the addition of 100µL of K562 cell medium and 500µg/mL G418. Single clones in the well were visible down a light microscope after 3 weeks of plating. When clones became sufficiently confluent, they were pipetted from the selected well and transferred into 24 well plates and tested for MPO expression by immunofluorescence (see section 2.11).

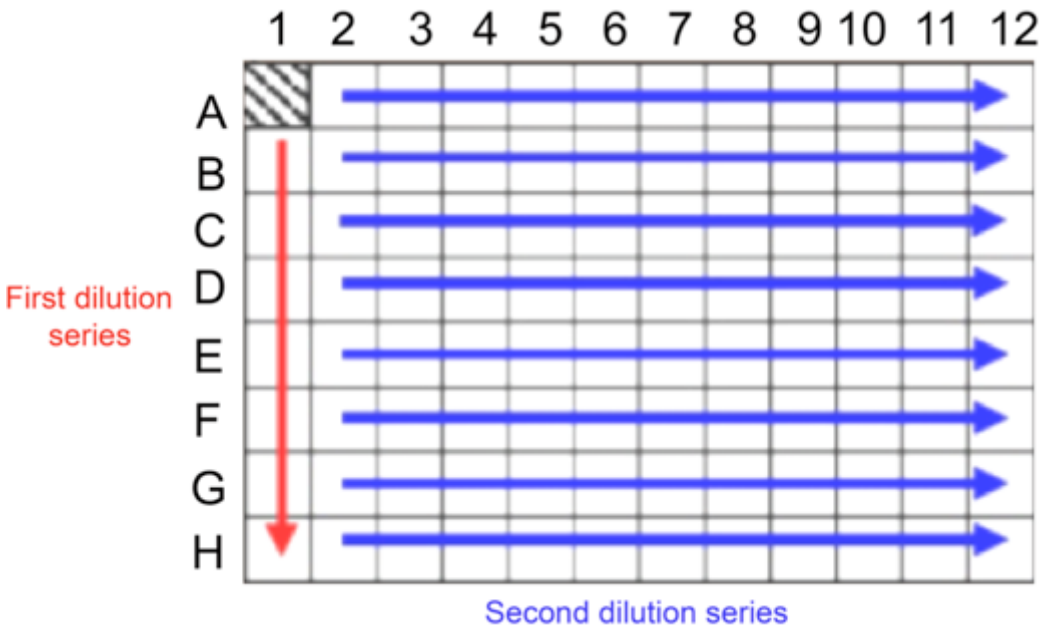


**Figure 2.2 Limited dilution method.**

## 2.11 Immunofluorescence analysis of γH2Ax and MPO

### *2.11.1 Fixation and permeabilisation of cells*

Cells were pelleted at 1000xg for 5 minutes and re-suspended in 50μL PBS. This suspension was applied onto pre-coated poly-L-lysine slides and cells were allowed to adhere onto slides for 10 minutes. Cells were fixed in 4% paraformaldehyde in PBS for 10 minutes and permeabilised using KCM+T buffer (120mM KCl, 20mM NaCl, 10mM Tris-HCl pH 8.0, 1mM EDTA, 0.1% Triton-X-100) for 15 minutes at room temperature. Slides were blocked in blocking buffer (2% (w/v) BSA, 10% (w/v) non-fat milk powder in KCM+T) for 1 hour at room temperature.

### *2.11.2 Staining*

The desired primary antibody (see Table 2.5) was incubated onto the slides at a concentration of 1:100 or 1:400 diluted in blocking buffer for 1.5 hours at room temperature. To remove the unbound antibody, slides were washed thrice in KCM+T buffer, each wash for 10 minutes, and then incubated with the appropriate fluorescent secondary antibody diluted 1:250 in blocking buffer (Alexa-488 anti rabbit

λex = 490 nm, λem = 525 nm or Alexa-594 anti-mouse λex = 590 nm, λem = 617 nm) for 1.5 hours, protected from light. KCM+T washes were then repeated.

Slides were mounted using mounting medium containing DAPI (Vector Labs, CA) and secured with sealant. Slides were either immediately viewed under the microscope or stored at 4$^{o}$C for a maximum of three days before viewing.

| Antibody | Catalogue number | Host | Raised to | Supplier | Application | Dilution |
|---|---|---|---|---|---|---|
| Anti-TOP2 | 4882 | Rabbit (polyclonal) | N-terminal 40kDa calf thymus | In house | TARDIS | 1:100 |
| Anti-TOP2A | 4566 | Rabbit (polyclonal) | Full CTD Human TOP2A-GST fusion (residues 1244-1531) | In house | TARDIS and IF | 1:400 |
| Anti-TOP2B | 4555 | Rabbit (polyclonal) | Full CTD Human TOP2B-GST fusion (residues 1263-1621) | In house | TARDIS and IF | 1:400 |
| Anti-MPO | ab9535 | Rabbit (polyclonal) | Raised to MPO isolated from human granulocytes. | Abcam, UK | IF | 1:100 |
| γH2Ax | 05-636 | Mouse (monoclonal) | Recognises Histone H2A.X phosphorylated at Ser139. | Merck Millipore, UK | IF | 1:400 |

**Table 2.5** List of primary antibodies used for immunofluorescence (IF).

### *2.11.3 Microscopy*

Images of blue (Hoechst-stained DNA) fluorescence (λex = 361nm, λem =497 nm) and green (FITC 488 fluorescence) (λex = 490nm, λem = 525nm) or red (Texas Red 594) (λex = 590nm, λem = 617nm) were captured separately using an epifluorescence microscope (Olympus IX-81, 10x objective) fitted with an Orca-AG camera (Hamamatsu) and suitable narrow band filter sets. Images were taken to give at least 2000 cells per treatment. For background correction, images were taken

using a blank slide (dark shade correction) and a fluorescence green slide (for FITC) or an orange slide (for Texas Red) for bright shade correction.
Image analysis was conducted using Volocity 6.3 (PerkinElmer Inc.). For quantitative immunofluorescence (for γH2Ax), the integrated fluorescence obtained for 594 background-subtracted values per cell, per treatment was used to conduct analysis.

### 2.12 Glutathione colorimetric assay

The glutathione assay separately measures the concentration of total and reduced glutathione in cells. The principle of the assay is based on the glutathione recycling system, in which reduced glutathione (GSH) can react with a DTNB probe (colourless) to generate glutathione disulfide (GSSG) and TNB (yellow). The level of TNB produced can be assayed spectrophotometrically. Therefore, the level of TNB produced is dependent on the amount of GSH present in cells. The generated GSSG can be reduced back to GSH by the action of glutathione reductase (provided in assay kit) that in turn generates more molecules of GSH to react with DTNB, improving the sensitivity of the assay. To measure the levels of reduced glutathione the enzyme glutathione reductase is omitted from the reaction (see Table 2.6), separating the levels of reduced glutathione and oxidised forms of glutathione in the mixture.
The assay was conducted using the manufacturer's guidelines (KA0797, Abnova, Taiwan). The following method was used for sample preparation. NB4 cells (cell density 2 x $10^6$ cells/mL) were treated with various concentrations of BSO for 4.5 hours, after this cells were pelleted (1000xg, 5 min) and washed in ice cold PBS. Cells were lysed in 4 pellet volumes of ice-cold glutathione assay buffer provided. Levels of total glutathione (GSH and GSSG) were determined by measuring the absorbance of the TNB chromophore at 490nm. To measure the levels of reduced glutathione, the enzyme glutathione reductase (see Table 2.6) was omitted from the reaction mixture and the absorbance of the TNB chromophore was measured at 405nm. The level of TNB absorbance measured from this reaction (glutathione reductase omitted) is the measure of the level of reduced glutathione in the cell sample and not a contribution of the oxidised glutathione (GSSG) being reduced in the system to generate glutathione. The levels of total and reduced glutathione were calculated from a glutathione standard curve, prepared using glutathione standards provided (kit components listed in Table 2.6).

| Component | Volume |
|---|---|
| Glutathione Reaction Buffer | 100mL |
| Glutathione Substrate DTNB (lyophilised) | 2 vials |
| NADPH Generation Mix (lyophilised) | 2 vials |
| Glutathione Reductase (lyophilised) | 50µL |
| 5-Sulfosalicylic acid (SSA) | 1 gram |
| GSH Standard (lypohilised, MW 307) | 2mg |

**Table 2.6.** Components supplied in glutathione colorimetric assay kit (KA0797, Abnova, Taiwan)

## 2.13 Trapped in agarose DNA immunostaining (TARDIS) assay

The TARDIS assay enables the detection and quantification of TOP2 enzyme covalently bound to nuclear DNA, *in situ*, for an individual cell (Figure.2.3). This method is described in Willmore *et al;* (1998).

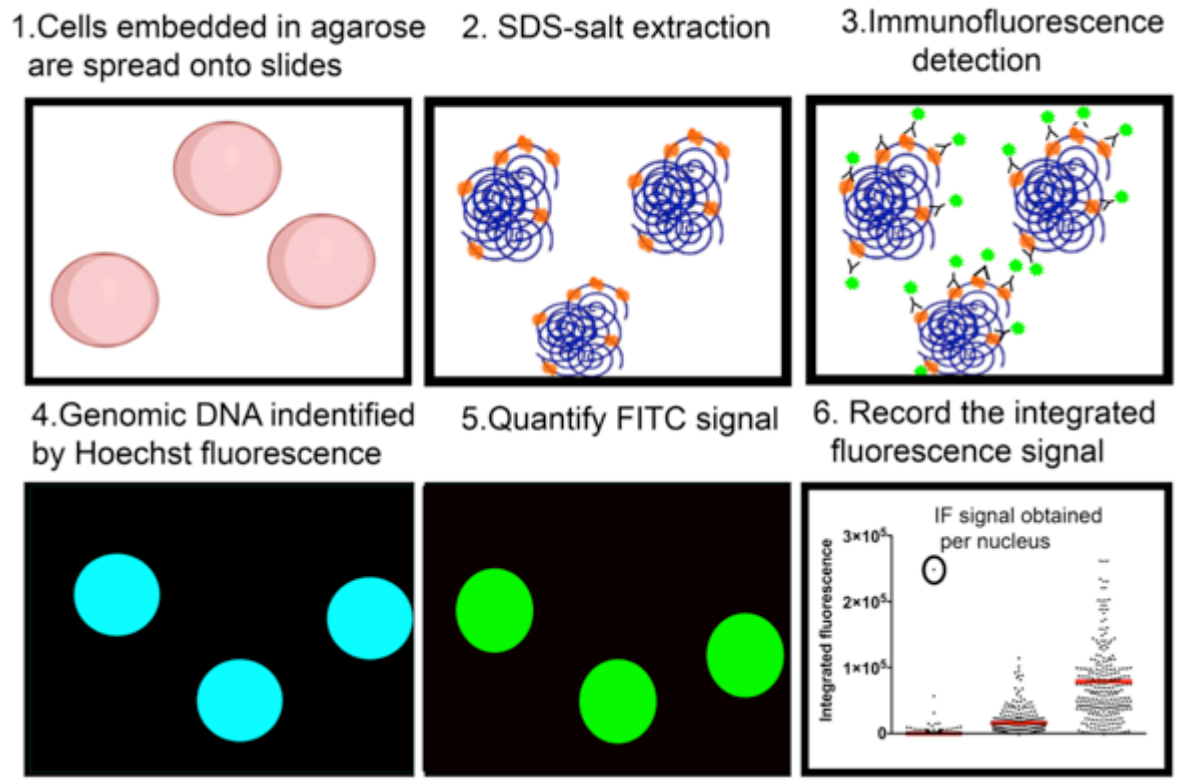


**Figure 2.3** Schematic representation of the TARDIS assay.

### *2.13.1 Drug incubations*

Exponentially growing cells (2-5 x $10^5$ cells/mL) were seeded into 6 well plates and treated with the desired drug or a solvent control for 1 hour, unless otherwise specified. Cells were pelleted by centrifugation (1000xg, 5mins) and washed in ice-cold PBS at 1000xg for 5 minutes. The supernatant was removed and cell pellets were re-suspended in 50µL PBS.

### *2.13.2 Slide preparation and SDS-salt extraction*

The suspension consisting of cell pellet mixed with 50µL PBS was warmed at 37$^o$C for 30 seconds and mixed with an equal volume of low melting point 2% agarose (Seaprep ultra-low gelling, FMC Bioproducts, Rockland, USA, prepared in PBS and pre-warmed to 37$^o$C prior to use). This mixture was spread evenly onto 0.5% agarose coated microscope slides and placed onto ice to allow rapid solidification of agarose.

Agarose-embedded cells were placed in lysis buffer (1% (w/v) sodium dodecyl sulfate, 20mM sodium phosphate (pH 6.5), 10mM EDTA plus 0.25% v/v of protease inhibitor cocktail, (Melford, Suffolk, UK)) for 30 minutes at room temperature. This disrupted the cell membrane and allowed the release of soluble proteins. Following this, slides were placed in 1M NaCl plus 0.1% v/v of protease inhibitor cocktail for 30 minutes at room temperature. This procedure removed non-covalently nuclear proteins bound to cellular DNA. After this slides were washed three times with PBS for 5 minutes, the last wash of PBS had the addition of 0.05% of protease inhibitor cocktail.

### *2.13.3 Staining of slides*

Following lysis, TOP2 covalent complexes were detected by immunofluorescence. Anti-topo II rabbit polyclonal antibodies (4566 for TOP2A, 4555 for TOP2B or 4882 for TOP2 only see Table 2.5) were used at a 1:400 or 1:100 dilution in PBS containing 0.1% (v/v) Tween 20 (PBST) and 1% (w/v) bovine serum albumin (1% BSA-PBST) unless otherwise specified. The slides were incubated with the primary antibody for 1.5 hours at room temperature and then washed three times in PBST containing 0.05% protease inhibitor cocktail. From this point onwards all procedures were conducted in subdued light. Slides were incubated with Alexa488-conjugated secondary antibody (A11008 Alexa Fluor 488 goat anti-rabbit IgG, Life Technologies,

1:250 diluted in 1% BSA-PBST) for 1.5 hours at room temperature. Washes were performed twice with PBST for 5 minutes and then with PBS for 20 minutes at room temperature. At this point, slides could be stored in PBS plus 0.05% protease inhibitor cocktail overnight at 4$^{o}$C or processed immediately.

Slides were counterstained with Hoechst 33258 (Invitrogen, diluted 2µg/ml in PBS) for 5 minutes to allow detection of DNA and mounted using Vectashield (Vector Laboratories, Peterborough, UK), coverslips were applied and secured with a sealant. At this stage slides were ready for viewing under the microscope or alternatively slides could be stored at 4$^{o}$C for up to 3 days before conducting microscopy.

### *2.13.4 Microscopy*

Images of blue (Hoechst-stained DNA) fluorescence (λex = 361 nm, λem = 497 nm) and green (FITC-stained drug-stabilised TOP2) fluorescence (λex = 490 nm, λem = 525 nm) were captured separately using an epifluorescence microscope (Olympus IX-81, 10x objective) fitted with an Orca-AG camera (Hamamatsu) and suitable narrow band filter sets. Minimum of five images were taken per slide to give at least 300 cells per treatment. In addition, background correction images were taken. A dark correction image was taken using a slide prepared in an analogous way as the sample slides but containing no cells. The bright correction slides were taken using a fluorescence green slide.

Fluorescence images were processed as described in Cowell *et al*., 2011. Background correction and analysis of images was conducted using Volocity 6.3 (PerkinElmer Inc.) The integrated fluorescence FITC background subtracted value per cell, per treatment was used to conduct analysis.

Part of the microscopy used to generate the results in chapter 6 was conducted using a DMLB microscope (Leica, 10x objective) fitted with a Coolsnap HQ2 camera V1.0.0 (Photometrics). Images were captured for both blue (Hoechst-stained DNA) and green (FITC-stained drug-stabilised TOP2) and background correction was conducted as previously stated. Images taken were manually imported into Volocity 6.3 (PerkinElmer Inc.) for image analysis.

### *2.13.5 Variations to the standard TARDIS assay*

The TARDIS assay can be modified at the stage of drug incubations (2.13.1) to determine (i) the longevity of drug-stabilised complexes after the removal of the drug from cell medium, this is known as the TARDIS Reversal assay, (ii) if a certain drug/compound behaves as an inhibitor of TOP2, this is termed as the TARDIS inhibitor assay. The assays are described in detail below.

### *2.13.6 TARDIS Reversal assay*

Exponentially growing cells (2-5 x $10^5$ cells/mL) were seeded into 6 well plates and treated with the desired drug or a solvent control for 1 hour, unless otherwise stated. Cells were pelleted by centrifugation at 1000xg for 5 minutes to remove the drug containing medium. The supernatant was removed and cell pellets were re-suspended in drug free cell medium and then returned to the incubator for the desired length of time. At the specified time points (e.g. 30, 60, 120min) the cells were removed from the incubator and pelleted (1000xg for 5 minutes). The supernatant was removed and cell pellets are mixed with ice-cold 50µL PBS. From this the point onwards the procedure stated in sections 2.13.2 to 2.13.5 were followed.

### *2.13.7 TARDIS inhibitor assay*

Exponentially growing cells (2-5 x $10^5$ cells/mL) were seeded into 6 well plates and treated with the proposed catalytic inhibitor for 1 hour. Following this a TOP2 poison, such as etoposide, was added for 1 hour. Cells were then pelleted (1000xg, 5mins) and mixed with ice-cold 50µL PBS and procedures stated in sections 2.13.3 to 2.13.5 were followed. If a particular drug behaves as catalytic inhibitor of TOP2, then a decline in the level of etoposide (or any TOP2 poison) stabilised TOP2-DNA complexes is seen compared to etoposide only treated cells.

### 2.14. Normalisation to combine biological replicates

Data obtained from individual quantitative immunofluorescence experiments (including TARDIS) were combined using the following method described below (Figure 2.4).

1. For each individual experiment the median values obtained for the highest drug treatment were taken and averaged out e.g. an example this normalisation step is shown below. For 100μM etoposide in each experiment the average median value for n=1 was 14800; n=2 13870 and n=3 14560 these are referred to as the experimental average
2. An average value of the all the experimental averages is then calculated i.e. for the example above the average value is 14410
3. The average value is then divided by the experimental average i.e. for n=1 14800/14410 =1.027, this value is referred to the normalisation factor and is specific to each experiment (normalisation factor for n=2 0.963 and n=3 1.010)
4. All values in one individual experiment were divided by the normalisation factor (values in experiment n=1 will be divided by 1.027) to give a normalised values for each experiment
5. The normalised values for each experiment were all combined together into one data set
6. The normalised values were then calculated as a percentage of the positive control (e.g. 100μM etoposide) and expressed as histogram to conduct statistical analysis.

### 2.15 Statistical analysis

Data were organised and analysed using Microsoft Excel 2011 and GraphPad Prism 4.0. Data were plotted using mean ± standard error of means (SEM) unless otherwise stated. For statistical analysis an unpaired Students t-test was used to compare differences between two sample means; or a one-way ANOVA with post analysis conducted using the Tukey test was used for multiple comparisons. The two-way ANOVA was used to analyse the interaction of two independent variables on one dependent variable with multiple comparisons conducted using the Bonferroni multiple comparison test; p-values of $<0.05$ were considered statistically significant.

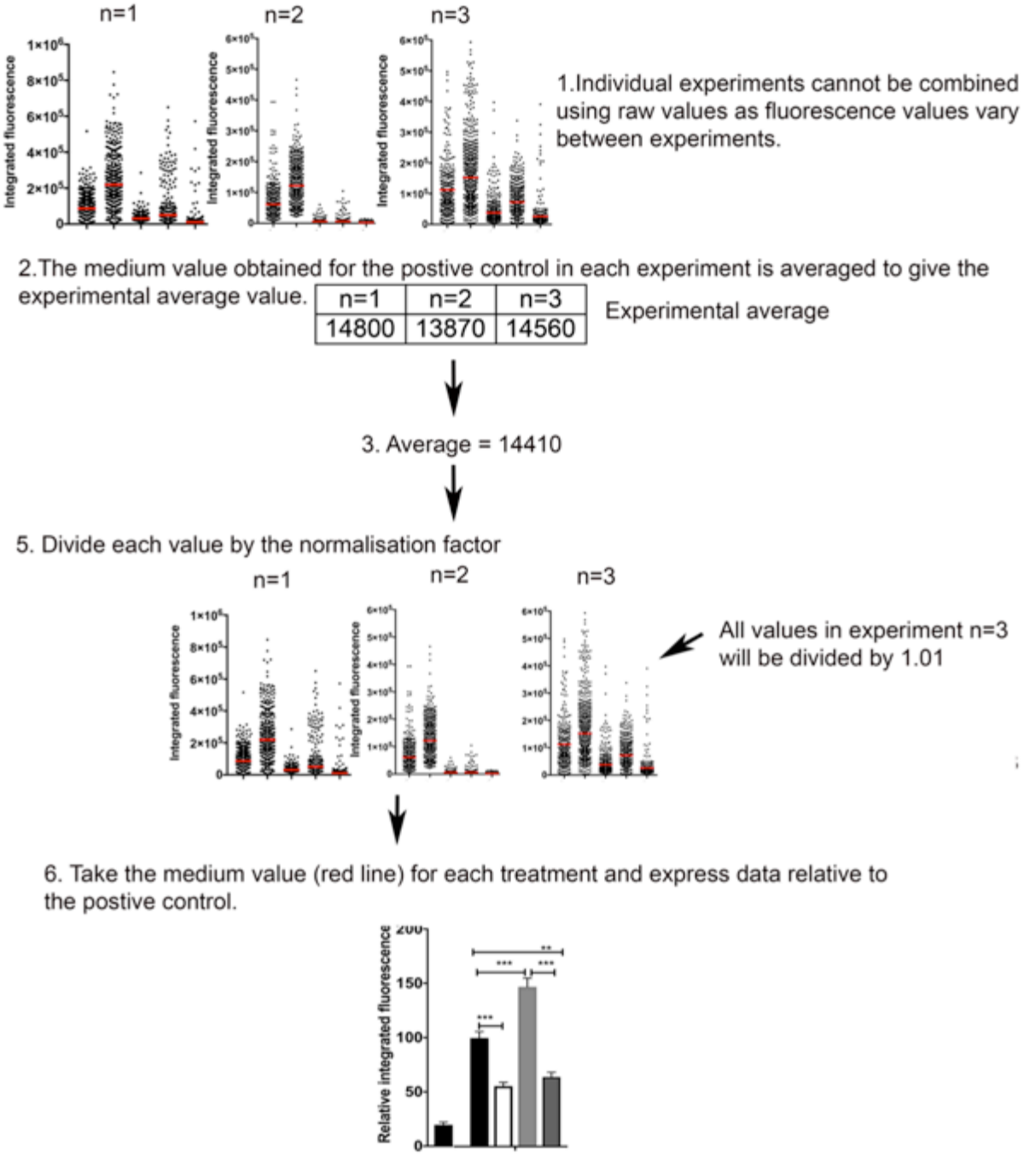


**Figure 2.4. Normalisation of data.**

# Chapter 3. Quantification and manipulation of TOP2 and MPO expression in myeloid cells and depletion of glutathione.

## 3.1 Introduction

This chapter aims to demonstrate how the tools required to answer the questions addressed in this thesis have been generated. Throughout this study, myeloid leukaemia cell lines have been used to study the effects of MPO. The selected cell lines are likely to have originated from the early myeloid precursor/progenitor cells (MacLeod and Drexler, 2008; Inoue *et al.*, 2014; Jensen *et al.*, 2015). A characteristic of myeloid progenitor cells is their potential to express MPO. The cell lines NB4, HL60 and Kasumi-1 express MPO protein whereas K562 and KG1 do not express MPO protein. The K562 cell line is a chronic myelogenous leukaemia (CML)-derived erythroleukaemia cell line. They originate from the erythroid lineage, which is MPO negative (Psaila *et al.*, 2016). However, K562 cells can be engineered to successfully produce functional MPO protein when transfected with an MPO expression construct (Nauseef *et al.*, 1996). KG1 cells are an acute myeloid leukaemia (Lee *et al.*) myoblast cell line that are reported to be positive for MPO at the RNA level but do not synthesise the MPO protein (Hu *et al.*, 1993).

The key aim for the work presented in this chapter, was to establish a cell-based system in which MPO can be effectively down regulated. This will allow the determination whether MPO has a role in TOP2 poison induced DNA damage. A literature search was conducted to determine the methods that have been employed to inhibit MPO activity or protein production in cell-based systems. The most common method to inhibit MPO activity was to use succinylacetone (SA), a heam biosynthesis inhibitor (Figure. 3.1) (Kagan *et al.*, 1999; Kagan *et al.*, 2001; Fan *et al.*, 2006; Nakazato *et al.*, 2007; Vlasova *et al.*, 2011). SA indirectly inhibits MPO by preventing mature protein synthesis via the depletion of heam pools but SA does not alter cell morphology or proliferation (Giger and Meyer, 1983).

The effectiveness of SA to supress MPO activity in NB4 cells was determined. Three direct MPO inhibitors; 4-ABAH and the recent commercially available inhibitors, PF1355 and MPOi-II were also used (Figure.3.1). The three direct inhibitors act as suicide substrates for MPO causing the inactivation of different MPO redox

intermediates (Kettle *et al.*, 1997; Soubhye *et al.*, 2010; Zheng *et al.*, 2015) (see section 1.2.5). In addition to chemical inhibitors, the conditions for MPO targeted knockdown using siRNA and the transfection of a MPO expression construct into K562 cells were also tested.

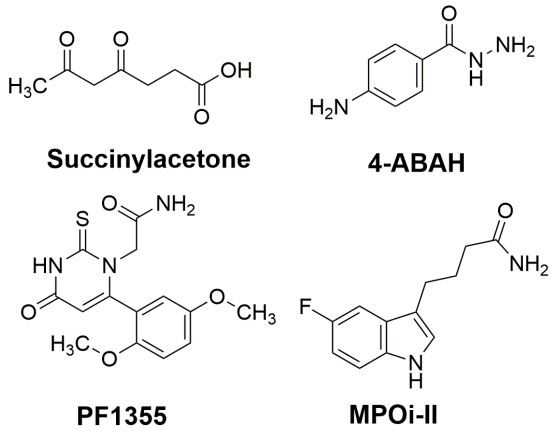


**Figure 3.1.Chemical structure of MPO inhibitors.**

The effects of MPO mediated oxidation of TOP2 poisons can be limited by glutathione (Kagan *et al.*, 1999; Kagan *et al.*, 2001; Vlasova *et al.*, 2011) (see section 1.4). Therefore, to allow the determination of glutathione depletion and MPO inhibition on TOP2 poison induced DNA damage; the conditions to reduce cellular levels of glutathione were also established.

## 3.2 Aims:

- To quantify the relative levels of TOP2 protein in the myeloid cell lines; HL60, K562, KG1 and NB4.
- To determine the conditions required to knockdown TOP2 and MPO using siRNA and whether siRNA knockdown of MPO was a suitable approach for these studies.
- To optimise inhibitor concentrations required to chemically inhibit the enzymatic activity of MPO.
- To test the conditions required to reduce cellular glutathione levels using buthionine sulfoximine (BSO).

## 3.3. Results

### *3.3.1 Level of TOP2 protein in selected myeloid cell lines*

The expression of TOP2A and TOP2B were determined at the protein level in K562, KG1, HL60 and NB4 cell lines using western blotting (method described in section 2.3. to 2.5). Whole cell extracts were prepared from cells growing in mid-log phase and western blots were probed using rabbit polyclonal antibodies specific to TOP2A (4566 anti-sera) or TOP2B (4555 anti-sera) (antibody details listed in Table 2.2). Protein band intensities were quantified and compared relative to K562 cells. Western blot analysis indicated all cell lines tested contain similar levels of both TOP2A and TOP2B protein (Figure.3.2.A-D).

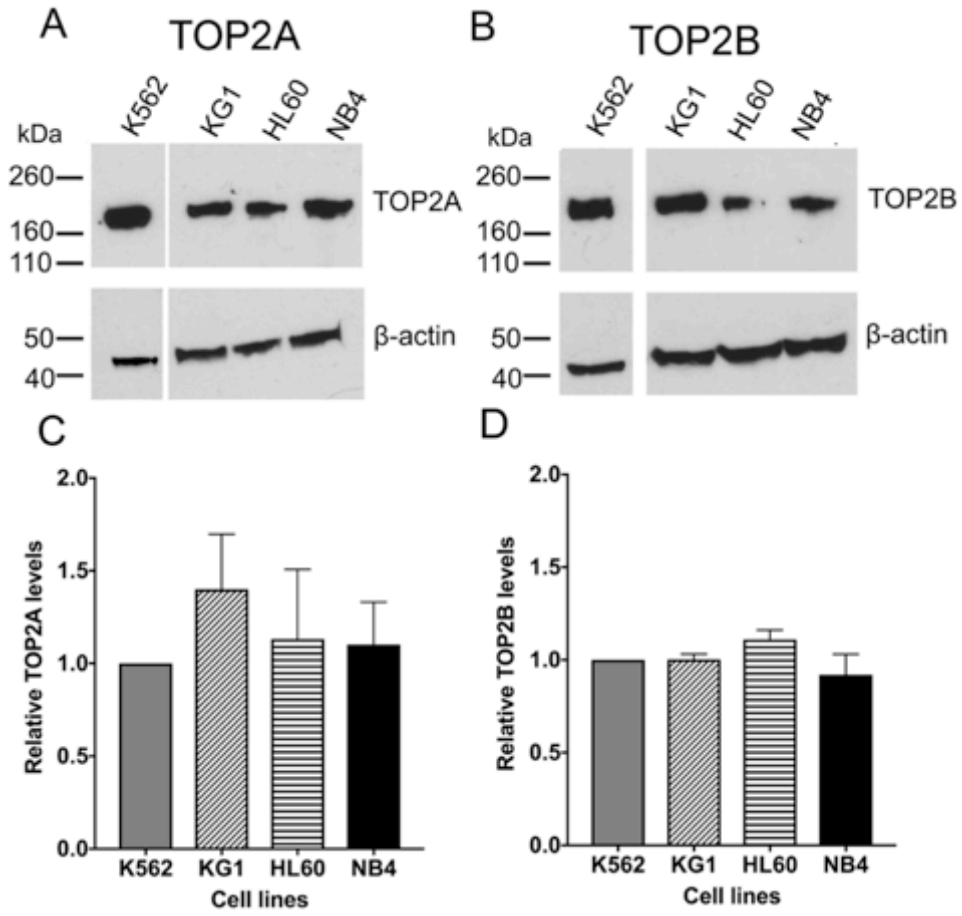


**Figure 3.2. TOP2A and TOP2B protein expression levels in K562, KG1, HL60 and NB4 cell lines.** Representative blots show the level of TOP2A (A) and TOP2B (B) protein in the specified cell lines with β-actin used as a loading control. Protein band intensities were quantified using densitometry for TOP2A (C) and TOP2B (D) and levels were compared to the mean value obtained for K562 cells. Band intensities were quantified for two separate protein loadings per blot to avoid band saturation. Data are expressed as mean ± S.E.M for four separate experiments (C-D).

### *3.3.2 Knockdown of TOP2 using siRNA.*

Conditions for TOP2 knockdown were characterised in K562, NB4 and HL60 cells using siRNA to individually target each isoform of TOP2. The targeting siRNA consisted of a pool of four individual siRNAs each targeted towards a different mRNA sequence for human TOP2A or TOP2B (Thermo Fisher Scientific, Leicestershire, UK) (siRNA target RNA sequences listed in Table 2.3). Each siRNA nucleotide sequence was analysed using Blast. Analysis of sequences using Blast confirmed the targeting sequence was specific to one isoform of TOP2. For each siRNA knockdown experiment, cells were electroporated separately with either TOP2A or TOP2B targeting siRNA and tested for the reduction in TOP2 protein levels compared to cells electroporated with a control siRNA (see section 2.6). The control siRNA consists of a four non-targeting siRNAs designed with patent modifications which are validated to have minimal targeting to human, mouse or rat genes (Thermo Fischer Scientific, Leicestershire, UK).

***K562***

In K562 cells, levels of both TOP2A and TOP2B were reduced more than two-fold compared to control siRNA cells up to 72hr post-electroporation (Figure.3.3.A-C). The greatest reduction in TOP2A was visualised at 72hr with 18.7% of TOP2A protein remaining compared to control cells (Figure. 3.3.A&C). TOP2B levels were the lowest at 72hr and 96hr time-points as less than 10% of TOP2B protein was detectable in comparison to control siRNA cells (Figure. 3.3.B-C). Electroporation with TOP2B siRNA gave a cell viability that was comparable to control siRNA cells (Figure.3.3.D). However, TOP2A siRNA electroporation initially reduced the cell viability at 24hr and 48hr time-points compared to control cells (Figure.3.3.D). But recovery in cell viability was detected at 72hr time-point with 100% viability at 96hr, this was accompanied by some recovery in TOP2A protein levels (Figure. 3.3.C-D).

To check whether the reduction in protein levels of one TOP2 isoform would affect the other isoform. K562 cells electroporated with the TOP2A siRNA were probed for TOP2B by western blotting whilst cells electroporated TOP2B siRNA were probed for TOP2A (Figure. 3.4.A-B). Quantification of protein bands at the 72hr time-point revealed no detectable difference in protein band intensities between control and TOP2 siRNA targeted cells.

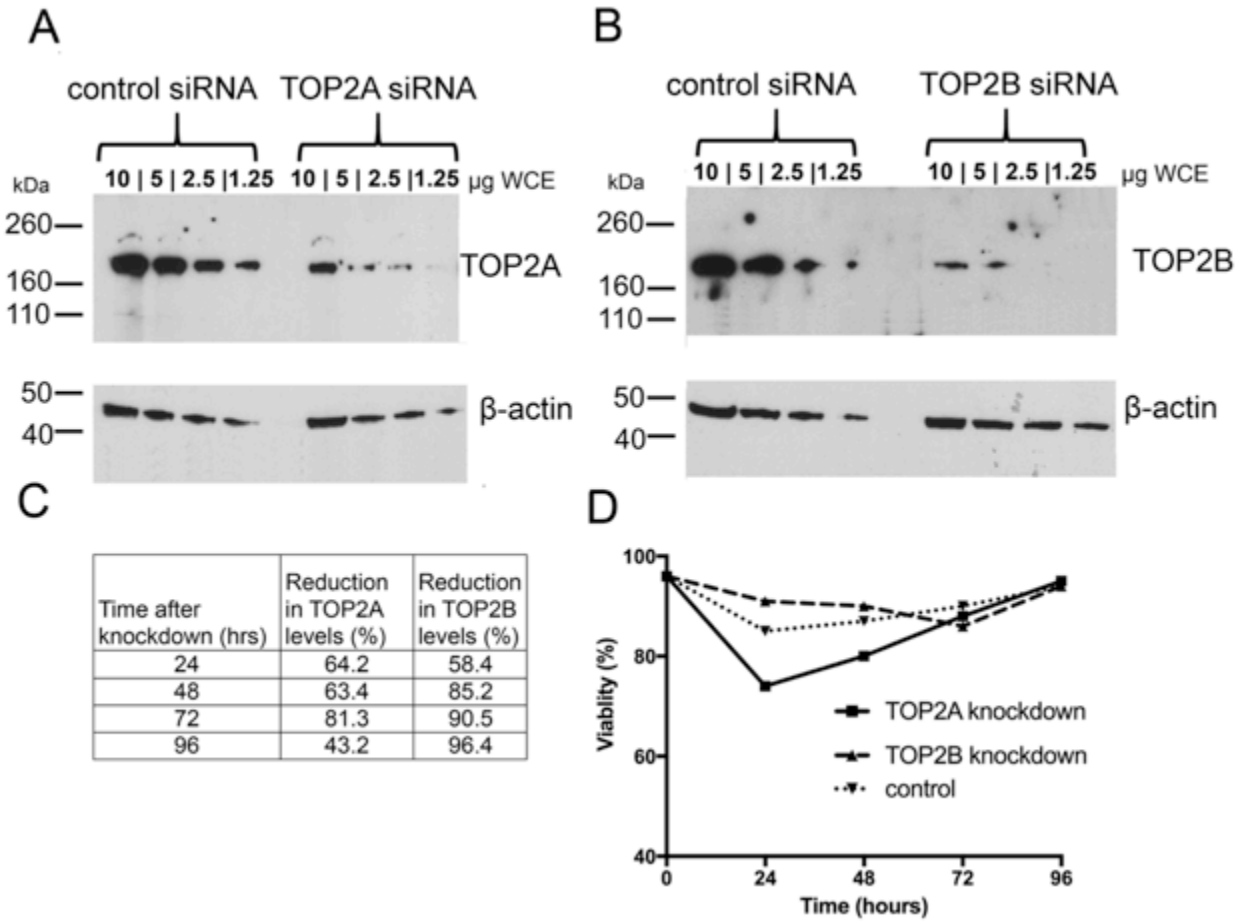


| Time after knockdown (hrs) | Reduction in TOP2A levels (%) | Reduction in TOP2B levels (%) |
|---|---|---|
| 24 | 64.2 | 58.4 |
| 48 | 63.4 | 85.2 |
| 72 | 81.3 | 90.5 |
| 96 | 43.2 | 96.4 |

**Figure 3.3. Down-regulation of TOP2A or TOP2B protein expression in K562 cells using siRNA.** K562 cells were electroporated with 400nM (330mV and 10ms pulse) siRNA targeted against TOP2A or TOP2B. Representative blots for cells 72hr after electroporation are shown for TOP2A (A) and TOP2B (B), β-actin was used as a loading control. (C) The percentage reduction of TOP2 was quantified using densitometry for each loading at the specified time-point after electroporation and compared to cells electroporated with a control siRNA for the respective loading. Values are shown as an average of the percentage reduction for each loading quantified. (D) Cell viability of electroporated cells were assessed using trypan blue exclusion counts after electroporation. Data shown in this figure were obtained from a single experiment.

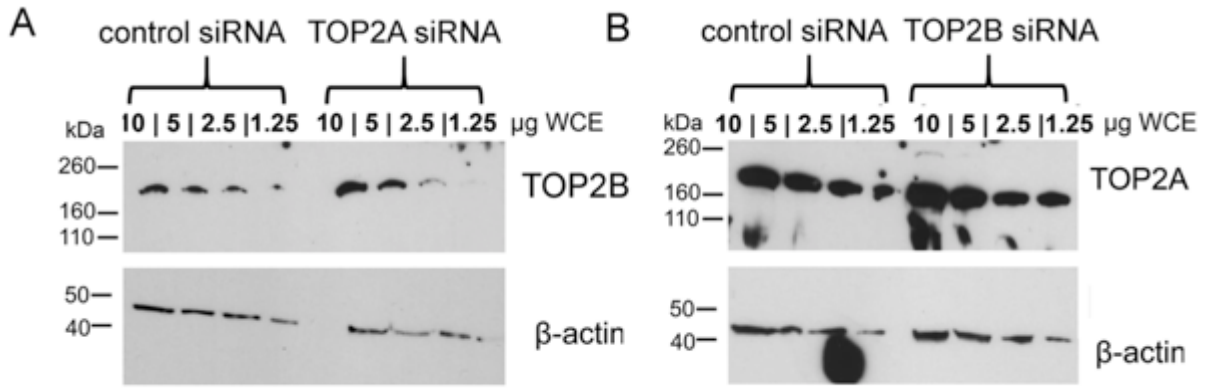


**Figure 3.4. TOP2 siRNA specificity.** K562 TOP2 siRNA extracts electroporated with siRNA targeted against one isoform of TOP2 were probed for the other isoform, to verify the isoform specificity of the siRNAs and to check whether the reduction in one isoform affects the protein levels of the other isoform. Blots 72hr after electroporation for one isoform of TOP2 were stripped using western stripping buffer and TOP2A siRNA extracts were probed using anti-TOP2B (4555 anti-sera) (A); TOP2B siRNA extracts were probed using anti-TOP2A (4566 anti-sera) (B).

***NB4 & HL60***

Electroporation of TOP2A or TOP2B targeted siRNA into NB4 cells resulted in 63% and 70% reduction in TOP2A and TOP2B protein levels 48hr post-electroporation (Figure. 3.5.A-C). NB4 cells before electroporation had cell viability of 70%, this is normal for NB4 cells growing in cell culture. Following electroporation with siRNA, the cell viability of cells targeted with TOP2B siRNA was similar to that of control siRNA cells (Figure.3.5.D). However, as observed in K562 cells, TOP2A siRNA electroporation reduced the cell viability at 24hr with recovery in cell viability observed at 48hr (Figure.3.5.D).

TOP2 targeted knockdown in HL60 cells reduced the protein levels of both TOP2A and TOP2B by 55% and 63% respectively (Figure.3.6.A-C). The cell viability, as assessed using trypan blue (see section 2.2.4) post-electroporation, showed all siRNA-targeted cells had reduced viability, suggesting conditions used for electroporation require optimisation (Figure.3.6D). However at the 48hr time-point HL60 cells targeted using siRNA against either TOP2A or TOP2B had a recovery in cell viability but cells targeted with the control siRNA had a continual decline in cell viability up to 72hr post-electroporation (Figure.3.6D).

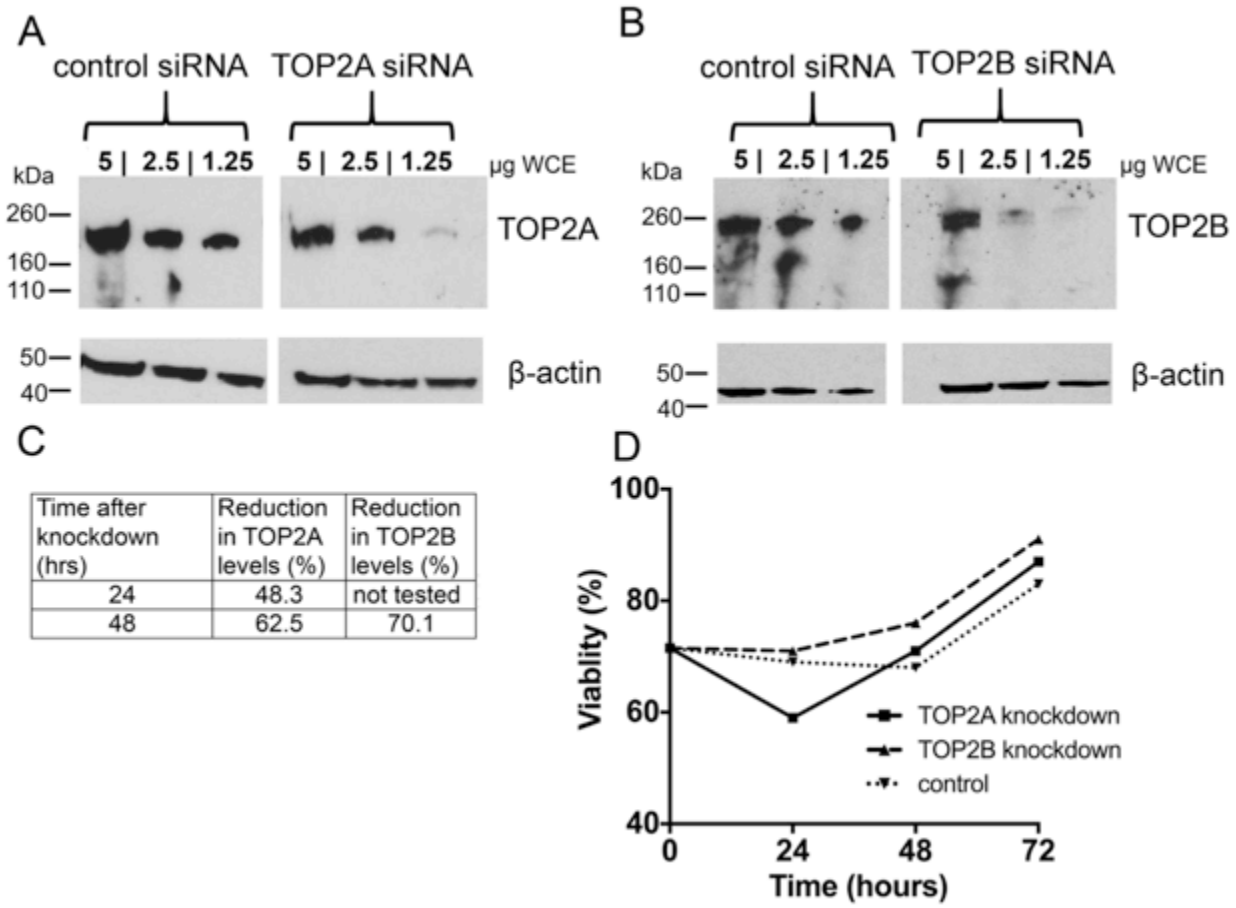


| Time after knockdown (hrs) | Reduction in TOP2A levels (%) | Reduction in TOP2B levels (%) |
|---|---|---|
| 24 | 48.3 | not tested |
| 48 | 62.5 | 70.1 |

**Figure 3.5. The siRNA targeted knockdown of TOP2A or TOP2B in NB4 cells.** Cells were electroporated with 400nM siRNA targeted towards TOP2A (A) or TOP2B (B). Representative blots are shown for cells 48hr after electroporation. (C) The level of TOP2 knockdown was estimated using densitometry and the percentage reduction was calculated relative to cells electroporated with a control siRNA. (D) NB4 cells were assessed for cell viability using trypan blue for up to 72hr after electroporation. Data shown in this figure were obtained for a single experiment.

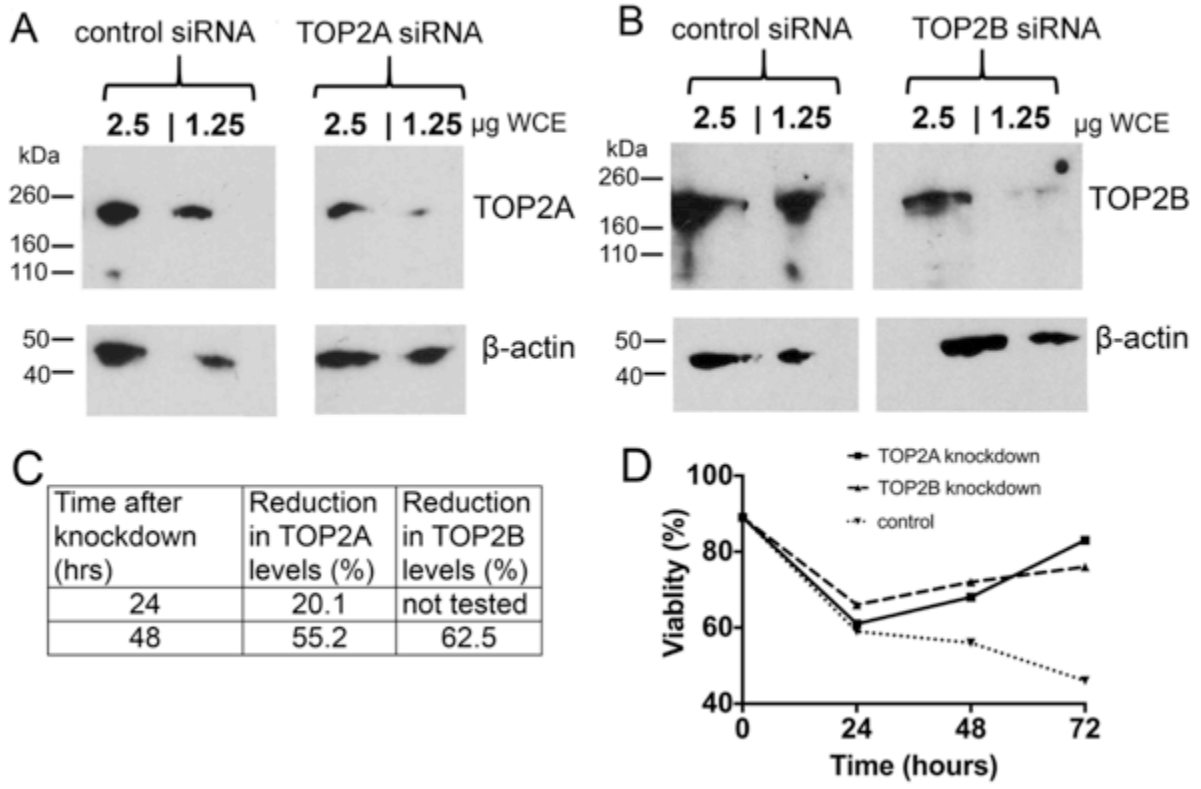


| Time after knockdown (hrs) | Reduction in TOP2A levels (%) | Reduction in TOP2B levels (%) |
|---|---|---|
| 24 | 20.1 | not tested |
| 48 | 55.2 | 62.5 |

**Figure 3.6. The knockdown of TOP2A or TOP2B in HL60 cells using siRNA.** Representative blots are shown for cells 48hr after electroporation with TOP2A siRNA (A) or TOP2B siRNA (B), β-actin was used as a loading control. (C) Quantification for the percentage reduction in TOP2 levels after electroporation were compared to cells electroporated with the control siRNA using densitometry. (D) Viability counts of cells were conducted using trypan blue for up to 72hr after electroporation. Data shown in this figure were obtained from a single experiment.

### *3.3.3 MPO protein expression and activity in cell lines*

#### *MPO protein expression*

The expression level of MPO protein expressed in normal cell culture conditions was examined in Kasumi-1, NB4, HL60, KG1 and K562 cells using western blotting with four separate commercial antibodies (Figure. 3.7.A-E) (see Table 2.2 for antibody details and section 2.3 to 2.5 for method). Band intensities were quantified to deduce the levels of precursor MPO and mature MPO (indicated by the level of heavy subunit) present in each cell line tested. Results were consistent with published data showing that Kasumi-1, NB4 and HL60 are positive for MPO protein expression, with Kasumi-1 having the highest level of MPO protein whilst K562 and KG1 cells are negative for MPO (Figure.3.7.B) (Hu *et al.*, 1993; Kim *et al.*, 2010).

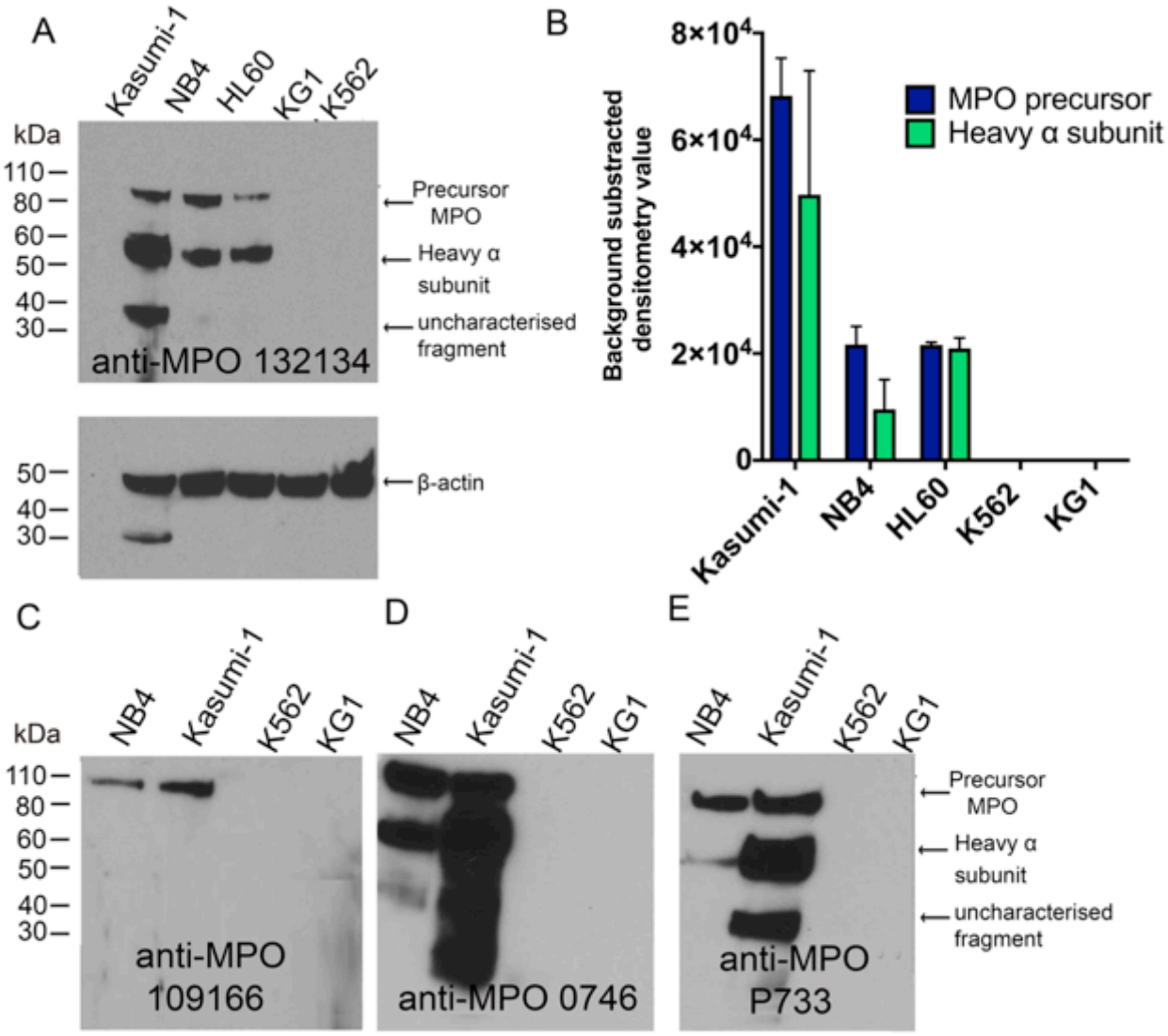


**Figure 3.7. Evaluation of the MPO protein expression levels in five myeloid cell lines and validation of anti-MPO antibodies.** (A) Cell lines were tested for the presence of MPO protein using anti-MPO 132134. (B) Levels of precursor and heavy subunit of MPO were quantified using densitometry for whole cell extracts tested using anti-MPO 132134 (n=3). (C-E) Western blot data obtained for MPO protein expression were validated using an additional three different MPO targeting antibodies; names of antibodies are specified within each blot (n=2 for each antibody).

### *MPO activity levels*

MPO activity levels were analysed in the above cell lines using a commercial colorimetric activity assay kit (see section 2.7). The principle of the assay is based on the unique ability of MPO to oxidise chloride ($Cl^-$) to hypochlorous acid (HOCl) at physiological pH. In this reaction, the hypochlorous acid generated can be effectively trapped by taurine ($TauNH_2$) generating taurine chloramine (TauNHCl), a stable oxidant (Figure. 3.8.A). The generated taurine chloramine can react with 5-thio-2-

nitrobenzoic acid (TNB $\lambda$ =412nm) producing disulphide,5,5'-dithiobis(2-nitrobenzoic acid) (DTNB), a colourless compound (Weiss *et al.*, 1982). MPO activity is calculated by measuring the reduction in TNB absorbance. The activity assay data showed NB4 cells have considerably higher MPO activity (203.02 nmol TNB consumed/min/mL) compared to HL60 (48.42 nmol TNB consumed/min/mL) and Kasumi-1 cells (53.03 nmol TNB consumed/min/mL) (Figure.3.8.B). This suggests that a considerable proportion of MPO in HL60 and Kasumi-1 is in the inactive form. For further studies NB4 cells were employed as the main cell line used to study the effects of MPO on TOP2 poison activity.

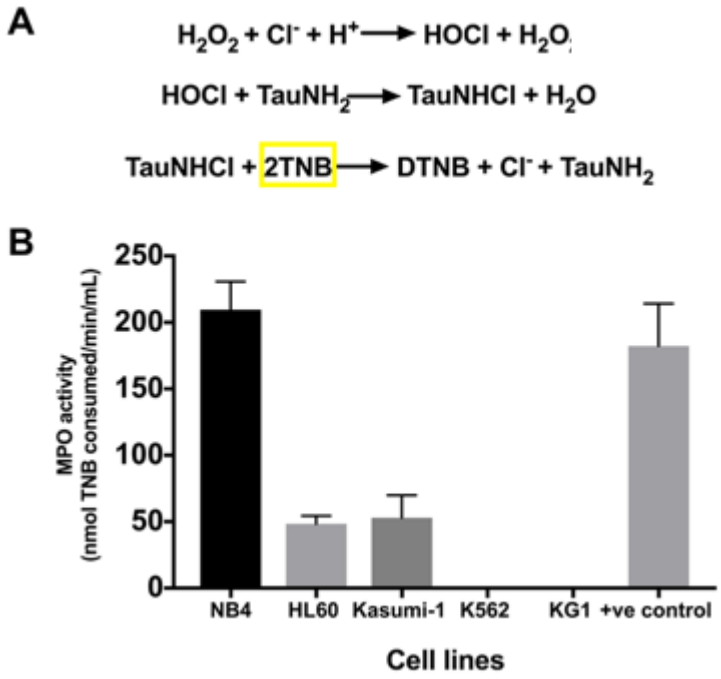


**Figure 3.8. NB4 cells contain the highest level of MPO activity.** (A) Principle of the MPO activity assay. (B) MPO activity levels were deduced by measuring the intensity of TNB probe at 415nm. Data are expressed as mean ± S.E.M from four separate experiments. The positive control supplied was used to ensure all assay components were working correctly (ab105135, Abcam UK).

### *3.3.4 Modulation of MPO protein and activity levels*

#### *Down regulation of MPO using siRNA*

Conditions for MPO knockdown in NB4, HL60 and Kasumi-1 were tested using two different commercially available siRNAs (Table 2.3 for siRNA information and target sequences). The first tested siRNA consisted of a single siRNA purchased from Qiagen, the second siRNA purchased from Thermo Scientific consisted of four different sequence specific siRNAs for MPO. All siRNA sequences were tested using Blast, analysis confirmed the targeting siRNA were specific to MPO RNA sequences. All cells were electroporated under the same conditions (330mV and 10ms pulse)

with different concentrations of siRNA. Published data were initially used to deduce a suitable siRNA concentration of 200nM (Qiagen) to use in NB4 cells (Kim *et al.*, 2010) however under these conditions there was no quantifiable difference in MPO band intensities between cells electroporated with MPO siRNA compared to control siRNA by western blotting (Table 3.1). Therefore, the concentration of siRNA used (Qiagen) was increased to 400nM, which resulted in a 32.9% decrease in MPO levels at 72hr (Table 3.1). A sequential electroporation of MPO siRNA was also tested, for this cells were electroporated with 400nM siRNA (Qiagen) followed by a second electroporation of 400nM siRNA 24hr after the initial electroporation. However this only resulted in a 37.5% decrease in MPO protein levels, a similar level of reduction compared to single electroporation with 400nM of siRNA (Table 3.1).

| **siRNA supplier and catalogue number** | **Cell line** | **siRNA concentration used for electroporation (nM)** | **% of total protein remaining from control at 72hrs** |
|---|---|---|---|
| Qiagen SI00005425 | NB4 | 200 | 100 |
| Qiagen SI00005425 | Kasumi-1 | 200 | 100 |
| Qiagen SI00005425 | NB4 | 400 | 67.1 |
| Thermo Scientific L003228-00-0020 | NB4 | 400 | 97.1 |
| Thermo Scientific L003228-00-0020 | NB4 | 500 | 36.1 |
| Thermo Scientific L003228-00-0020 | NB4 | 400 (double electroporation) | 62.5 |
| Thermo Scientific L003228-00-0020 | NB4 | 1000 (1μM) | 50.9 |
| Thermo Scientific L003228-00-0020 | HL60 | 400 | 100 |
| Thermo Scientific L003228-00-0020 | HL60 | 500 | 60.7 |
| Thermo Scientific L003228-00-0020 | HL60 | 1000 (1μM) | 53.2 |

**Table 3.1. Testing the conditions required to knockdown MPO protein in three MPO positive cell lines using siRNA.** Cells were electroporated (conditions 330mV and 10mS pulse) with the specified concentration of siRNA. The 400nM double electroporation was conducted by firstly electroporating NB4 cells with 400nM MPO siRNA followed by a second electroporation of 400nM siRNA 24hr after the initial electroporation. For each condition specified, extracts were prepared and tested using western blot analysis. Each siRNA condition listed was tested once for the level of MPO protein reduction.

The siRNA purchased from Qiagen consisted of a single siRNA sequence. To increase the chances of protein knockdown a pool consisting of four-siRNAs targeted towards MPO were obtained (Thermo Scientific) and tested for MPO knockdown efficiency. The conditions that resulted in the greatest reduction in total MPO protein

were tested for MPO activity (Table 3.1 & Figure. 3.9.A-C). Electroporation of NB4 cells with 500nM of the four MPO siRNAs (Thermo Scientific) resulted in an average reduction of 70.4% ± 3.6 in MPO activity and a 64% reduction in protein levels compared to cells electroporated with a control siRNA (Figure. 3.9.A and Table 3.1). Replicate conditions in HL60 cells resulted in a reduction of 64.8% ± 5.3 in MPO activity and a 39% reduction in MPO protein (Figure. 3.9.B and Table 1). However, doubling the siRNA concentration to 1μM in NB4 cells did not further reduce MPO activity (65% ± 20 reduction) or protein levels (51% reduction) (Figure. 3.9.C & Table 3.1). As MPO is stored in granules once synthesised, the lack of reduction in MPO levels after increasing the siRNA concentration was perhaps not surprising. As the siRNA would target the destruction of MPO mRNA, reducing the level of newly synthesised MPO without affecting the protein already packaged into granules.

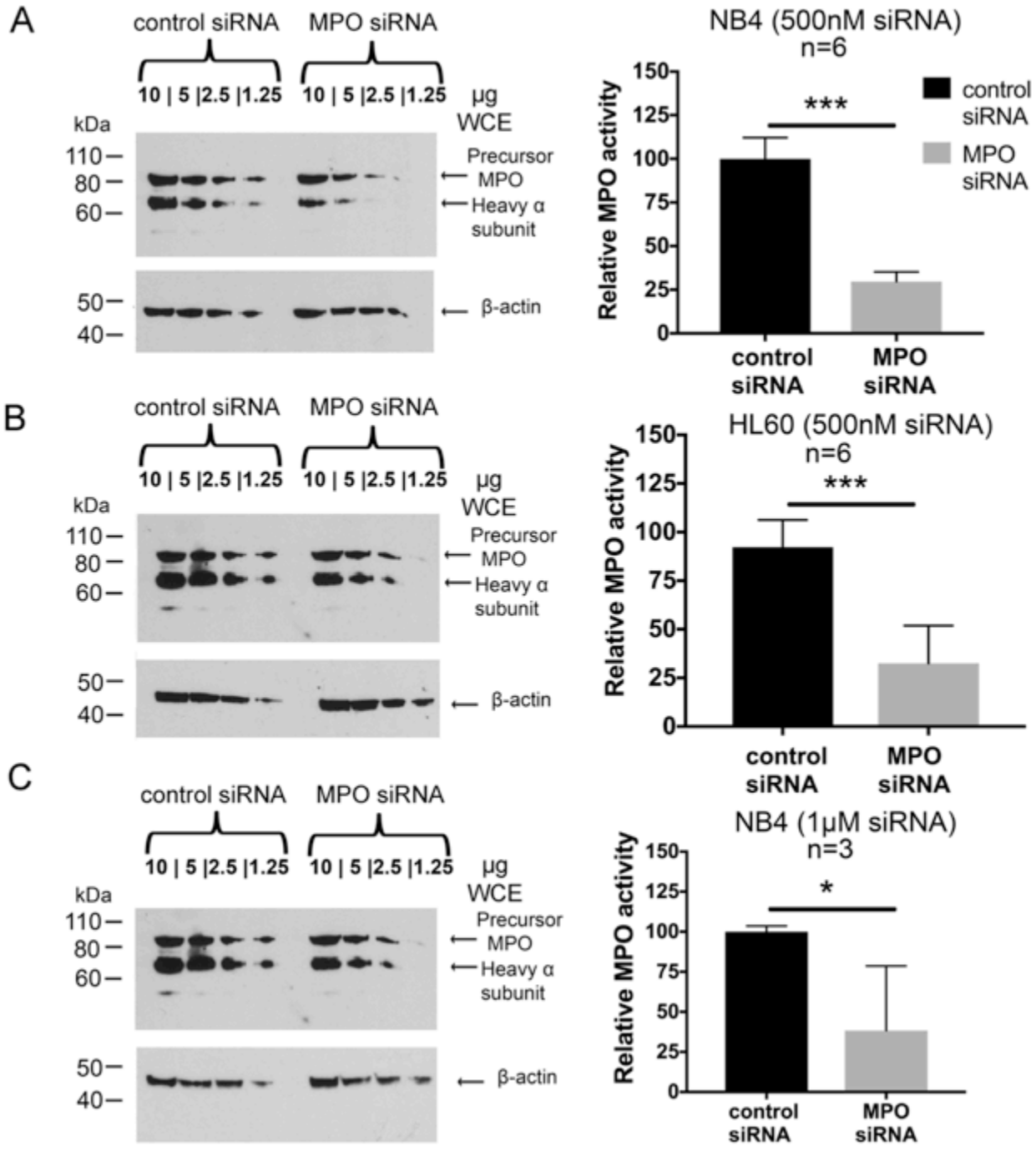


**Figure 3.9. The siRNA targeted down regulation of MPO significantly reduces MPO activity.** Both NB4 and HL60 cells were electroporated with siRNA targeted towards MPO or a control. Samples were probed for both MPO protein (anti-MPO ab132134) (left panel) and activity levels (right panel) 72hr post-electroporation. Activity assay data are expressed relative to the respective control siRNA and data are represented as mean ± S.E.M. (A) NB4 cells were electroporated with 500nM siRNA, (B) HL60 cells electroporated with 500nM siRNA and (C) NB4 cells electroporated with 1µM. The siRNA used in these experiments were purchased from Thermo Scientific (L003228-00-0020). Statistical analysis was conducted using the Students t-test, * $P<0.05$ and *** $P<0.001$ are considered statistically significant.

### *3.3.5 Inhibition of MPO activity using chemical inhibitors*

Two chemical inhibitors, SA and 4-ABAH were chosen to test their effect on MPO activity (Figure. 3.1). NB4 and HL60 cells were individually treated with either SA (200μM for 48hr) or 4-ABAH (100μM for 3hr) using previous published data and measured for MPO activity as previously described in section 3.3.3 and 2.7 (Kagan *et al.*, 2001; Miyamoto *et al.*, 2003; Knaapen *et al.*, 2005; Vlasova *et al.*, 2011). In both cell lines SA effectively abolished MPO activity to below the level of detection (assay sensitivity 0.05nmol TNB consumed/min/mL) (Figure. 3.10.A-B). Whereas the concentration selected for 4-ABAH reduced MPO activity in NB4 cells to 13.7% ± 4.2 (Figure. 3.10.A) but substantial MPO activity remained in HL60 cells (83.3% ± 29.1 activity remaining) under conditions tested (Figure. 3.10.B), suggesting a higher dose of 4-ABAH is required to inhibit MPO activity in HL60 cells.

As SA reduces heam synthesis in cells, the lowering of MPO activity is likely due to reduction in mature protein synthesis. Western blotting analysis confirmed that SA treatment dramatically reduced the level of the heavy subunit of MPO, which indicates defective processing from the precursor MPO to the mature protein (Figure.3.11.A). Quantification data obtained from three separate experiments at 48hr showed the heavy chain was reduced by 77.6% ± 6.1 compared to untreated NB4 cells (Figure. 3.11.B, right panel) (see section 2.3 to 2.5 for method). As indicated by quantification of the precursor MPO, this also reduced the overall pool of MPO protein in cells by 29.5% ± 4.6 (Figure. 3.11.B, left panel). Thus SA can effectively reduce both MPO activity and protein in cells and therefore, was employed as the main MPO inhibitor for further studies presented in this thesis.

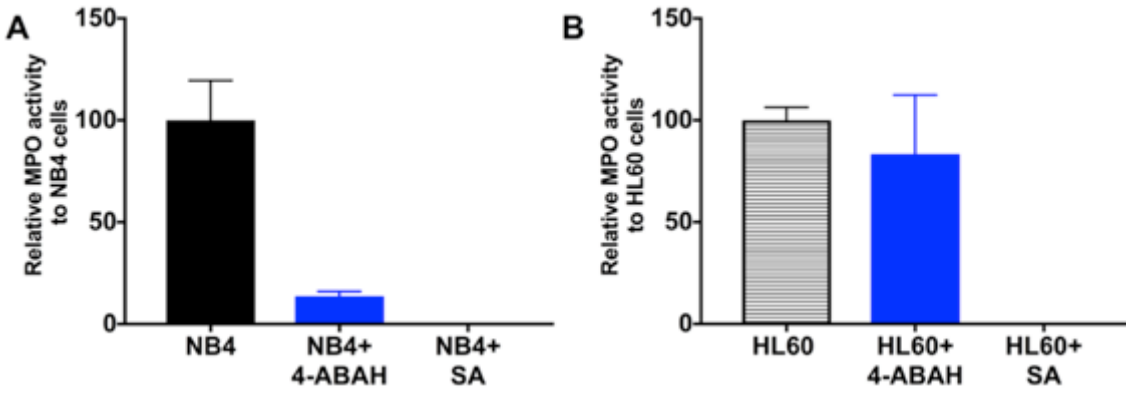


**Figure 3.10. Inhibition of MPO activity in NB4 and HL60 cells using 4-ABAH (a specific MPO inhibitor) or SA (a heam biosynthesis inhibitor).** NB4 cells (A) and HL60 cells (B) were treated either with 150μM 4-ABAH for 3hr; or 200μM SA for 48hr and assayed for MPO activity. The percentage of activity remaining is shown compared to untreated cells. The untreated control level is set at 100% MPO activity. Data are expressed as mean ± S.E.M for three separate experiments.

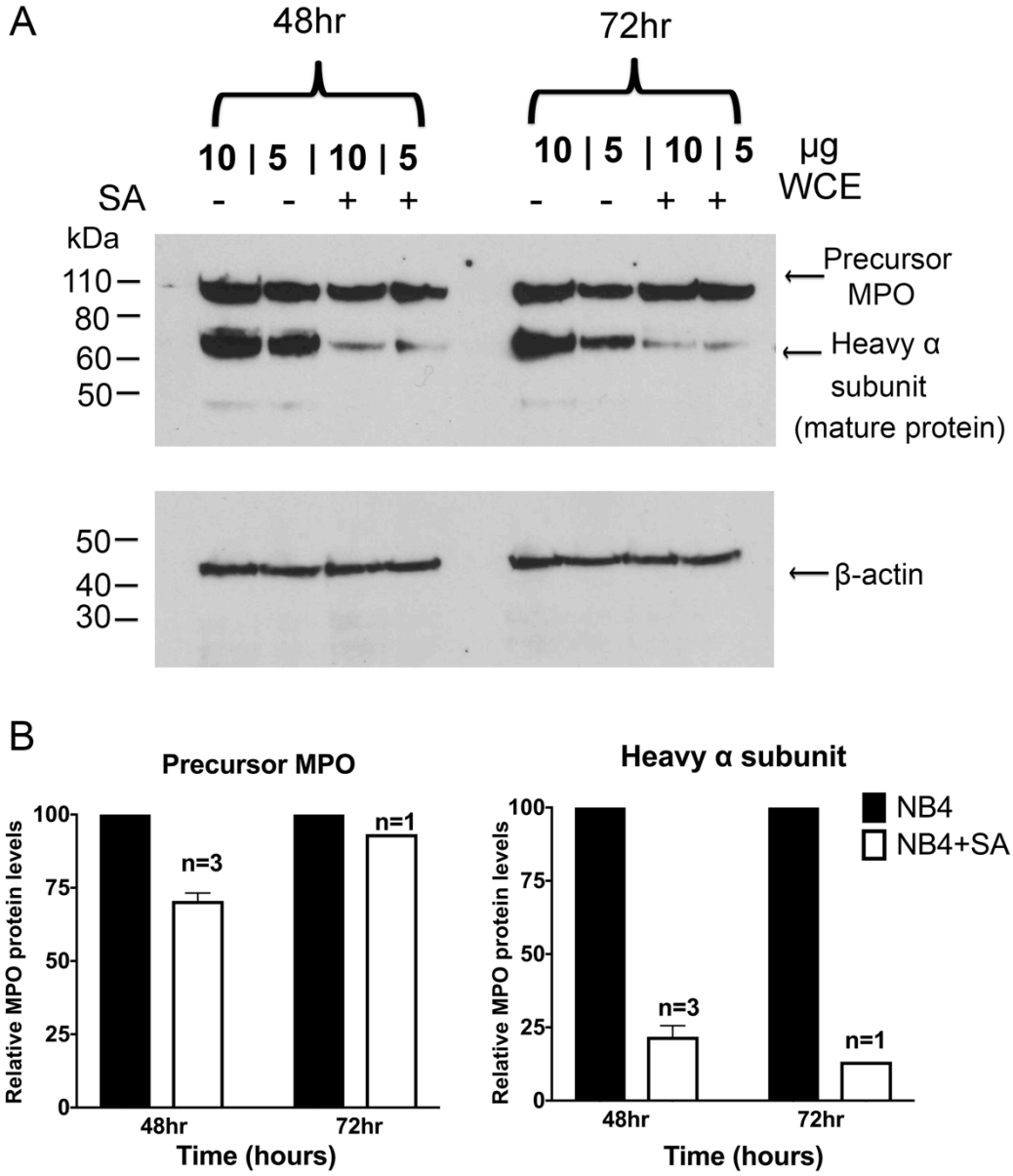


**Figure 3.11. Succinylacetone (SA) reduces the level of mature MPO protein in NB4 cells.** Following SA pretreatment (200µM for 48hr or 72hr) NB4 cells were probed for the level of MPO protein (ab132134) by western blotting (A). (B) Band intensities were quantified to deduce the relative levels of precursor MPO (lower left panel) and heavy subunit (lower right panel) remaining compared to untreated NB4 cells. Data are expressed as mean ± S.E.M. relative to untreated NB4 cells, numbers of replicates are indicated within each figure.

### *3.3.6 Testing the effect of SA on mitochondrial activity and TOP2 protein levels.*

SA inhibits total heam biosynthesis in cells, therefore it is feasible that under conditions used above, the cells energy sources may be comprised affecting mitochondrial function, an organelle where heam is synthesised and is a component of respiratory complex proteins (Kim *et al.*, 2012). It is important to know this and whether SA alters cell viability or proliferation as this could affect the interpretation of the TARDIS and DNA damage assays performed later in this study. For this reason, the effect of SA on mitochondrial function, cell viability and growth of NB4 cells were assessed. Two assays were used to analyse the potential effect of SA on the mitochondrial activity of NB4 cells.

The first assay (XTT Cell proliferation assay) involves measuring the reduction of a tetrazolium salt (XTT) to a water-soluble orange formazan salt, which is dependent on a functioning citric acid cycle and electron transport chain (Figure.3.12.A) (method described in 2.8). The XTT cell proliferation kit was used as a surrogate to measure mitochondrial function. The XTT salt is regularly used to assess cell growth and also to measure the activity of succinate dehydrogenase - a component of both the citric acid cycle and electron transport chain (Kregiel *et al.*, 2008). NB4 cells were treated in the presence or absence of SA. At each 24hr timepoint, the XTT reagent supplemented with PMS (an electron carrier, helping to drive the reduction of the XTT salt) was added to the cells. Data generated showed that a 96hr incubation with SA does significantly increase the generation of the XTT formazan salt (*P=0.0001*) (Figure. 3.12B). SA pre-treatment did not affect cell growth (*P=0.706*) or cell viability compared to untreated NB4 cells, measured using trypan blue cell counts (Figure.3.13.A-B) (Pinnix et al., 1994).

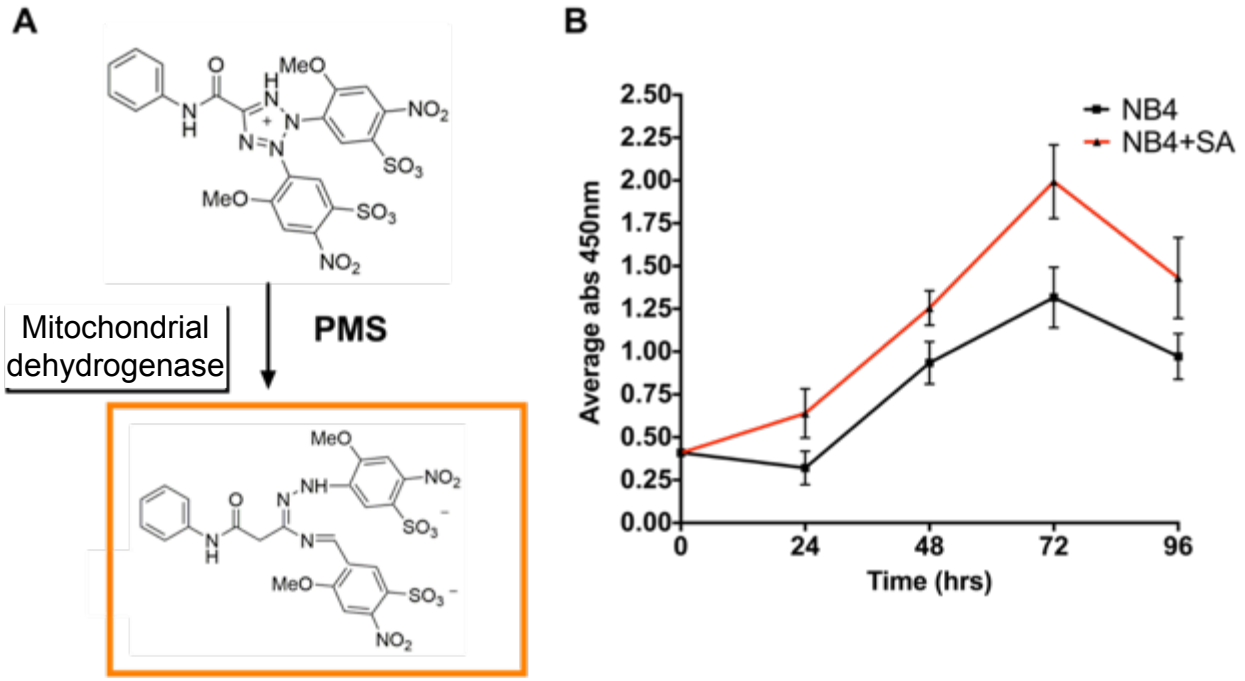


**Figure 3.12. SA increases formazan salt formation in NB4 cells.** (A) Principle of the XTT assay. (B) NB4 cells were treated with 200μM of SA (red) and were measured for the level of salt cleavage using the XTT assay (Roche, Switzerland) compared to untreated NB4 cells (black) for up to 96hr of treatment. Data are expressed as mean ± S.E.M for four separate experiments each comprising of six technical replicates. Statistical analyses were performed using the two-way ANOVA *P=0.0001*.

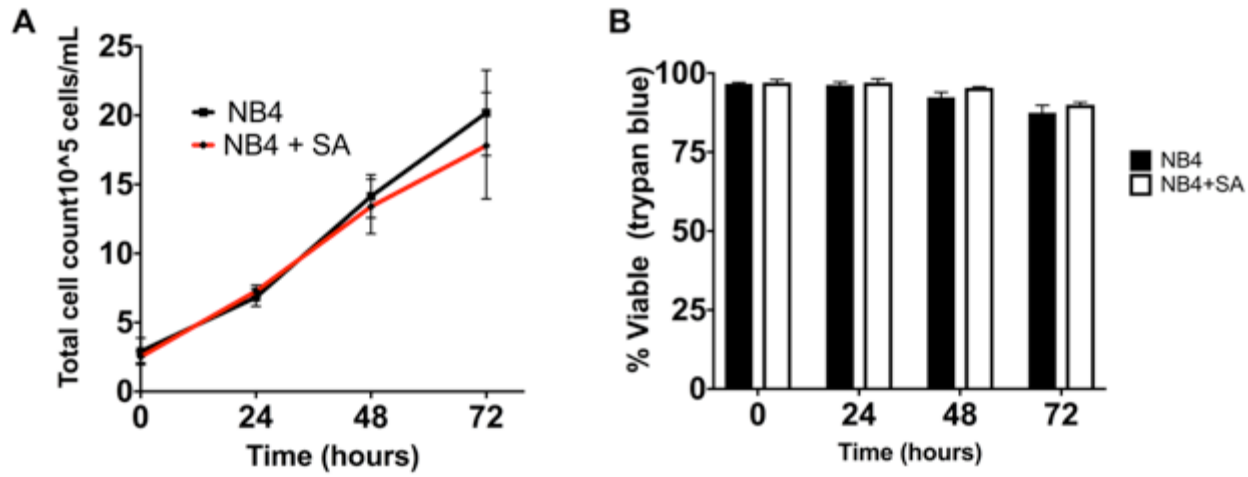


**Figure 3.13. Treatment with SA does not affect cell growth (A) or viability (B) up to 72hr in NB4 cells.** Data are expressed as mean ± S.E.M for three separate experiments, statistical analysis was performed for (A) using the two-way ANOVA with Bonferroni's multiple comparison test, *P=0.706*.

In addition to the XTT assay, the seahorse phenotype assay (section 2.9) was utilised to analyse the effects of SA on oxidative phosphorylation and glycolysis. In the Seahorse assay, to determine if certain parameters/conditions affect the cells energy phenotype it is important to 'stress' the mitochondria. In the assay two stressors were used; oligomycin, to inhibit ATP synthase and FCCP to uncouple the electron transport from oxidative phosphorylation. Once the mitochondria are stressed it is feasible to analyse if a condition affects the cells energy phenotype. NB4 cells were incubated with 200μM SA for 48hr, under these conditions SA did not affect the oxygen consumption level (OCR) or extracellular acidification rate (ECAR), either under baseline conditions or stressed conditions (Figure. 3.14.A-B). Taking the OCR and ECAR data together it can be concluded that SA does not impact the cells metabolic potential under baseline or stressed conditions (Figure. 3.14.C). In addition, the effect of SA on the rate of acidification of cell growth medium was evaluated and the results obtained show SA does not accelerate acidification of the cell culture media (*P=0.317*) (Figure. 3.15.).

Additionally, whether SA affected TOP2 protein levels in NB4 cells was investigated. This was an important factor to examine, as this study has a central focus on TOP2-DNA covalent complexes and if SA induced changes in overall TOP2 protein levels then this would need to be taken into account when conducting analyses. SA was added to NB4 cells and western blots were probed for TOP2A and TOP2B after 48hr and 72hr of treatment (Figure. 3.16.A). Quantification of replicate blots revealed SA did not affect TOP2A or TOP2B protein levels for up to 72hr of incubation (Figure. 3.16.B). In addition 200μM SA treatment did not affect the *in vitro* activity TOP2 (experiment conducted by C.A.Austin published in (Atwal *et al.*, 2017)).

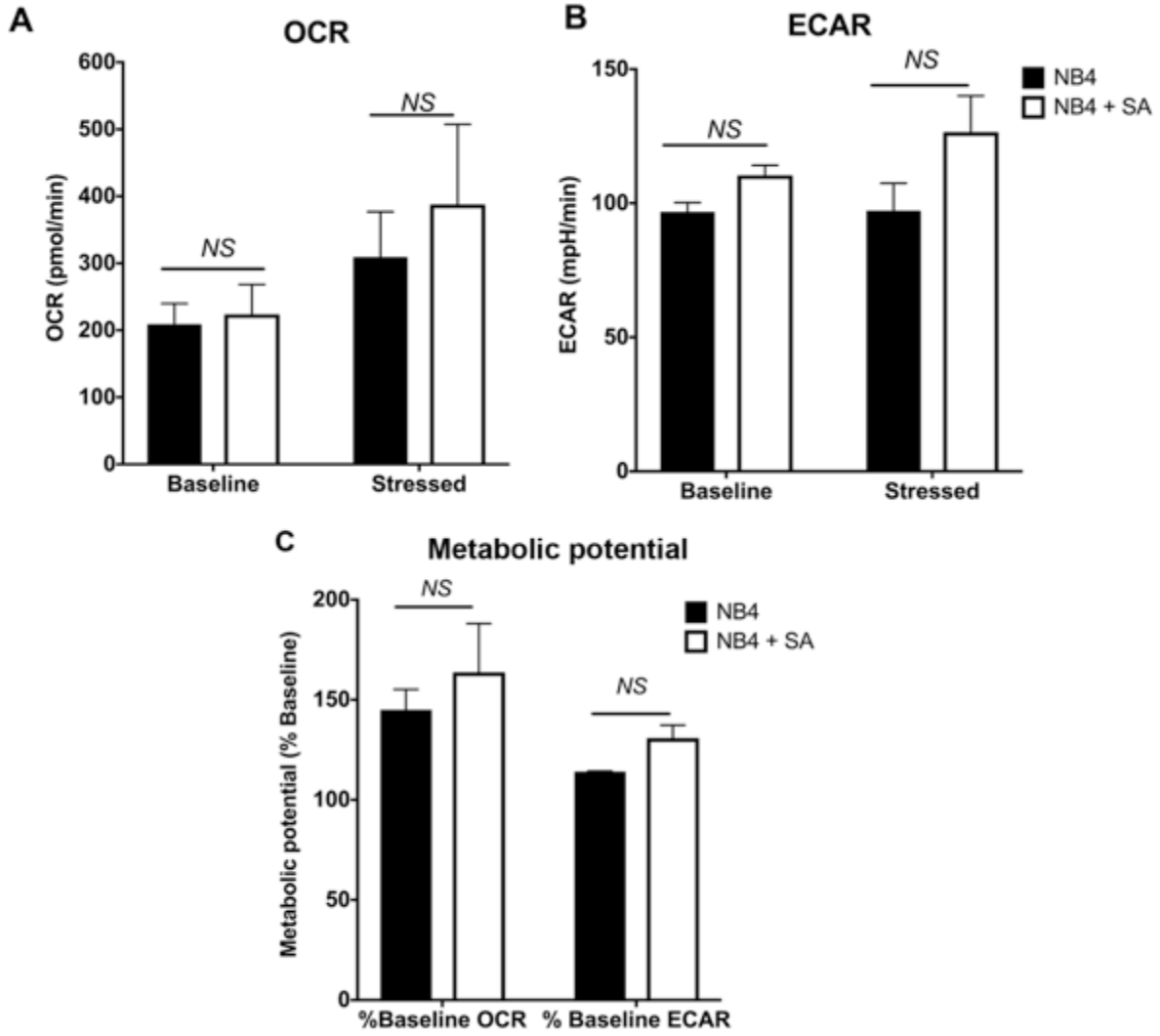


**Figure 3.14. SA treatment does not alter the oxygen consumption rate (OCR) (A) or extracellular acidification rate (ECAR) (B) or the metabolic potential (C) of NB4 cells.** Seahorse Bioscience XF96 extracellular flux analyzer was used to assess the effect of SA (200μM for 48hr) on the cell energy phenotype. Measurements were performed at the baseline time point and under stressed conditions (2μM oligomycin and 1μM FCCP). (C) Metabolic potential rates were calculated from the difference between the stressed and baseline values obtained from A&B and are expressed as a percentage from the baseline. Data are expressed as mean ± S.E.M from three experiments; statistical analysis was performed using the Student's t-test.

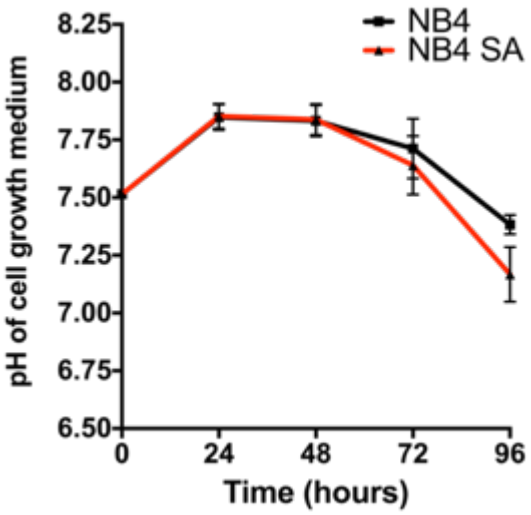


**Figure 3.15. SA does not alter extracellular pH levels of NB4 cells.** Cells were treated with 200μM SA for up to 96hr and pH measures were performed at the specified time-points. Data are represented as mean ± S.E.M for four separate experiments; statistical analysis were performed using the two-way ANOVA with Bonferroni's multiple comparison test, *P=0.317*.

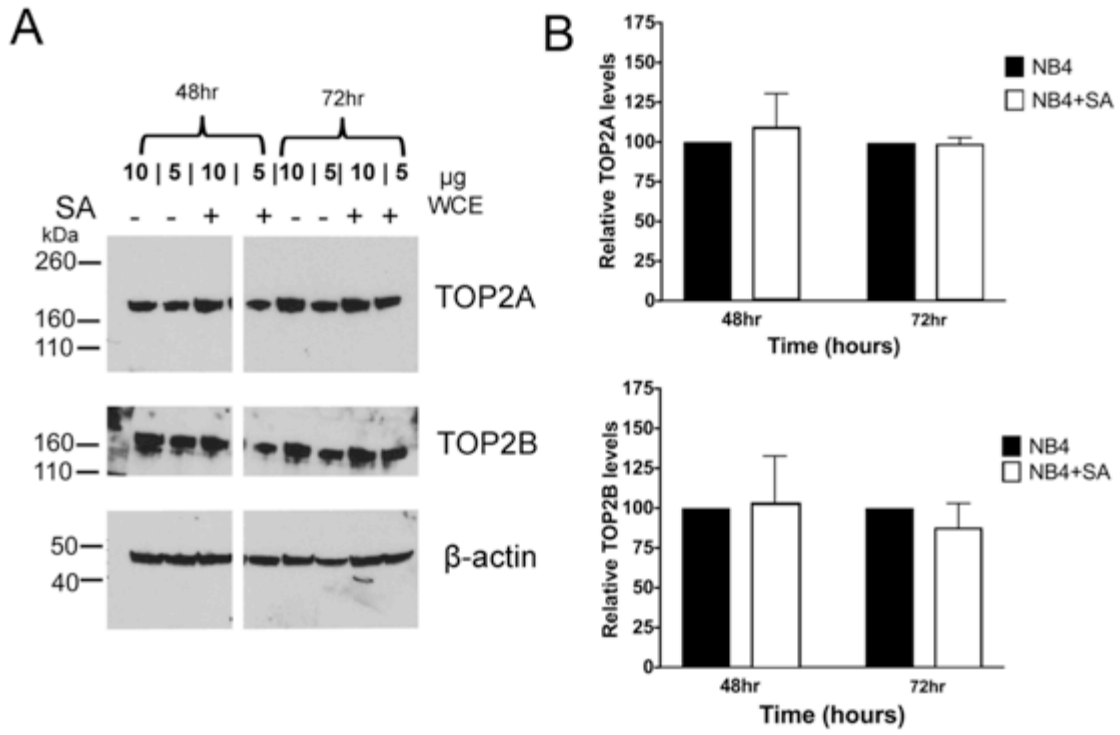


**Figure 3.16. SA treatment does not alter TOP2A or TOP2B protein levels in NB4 cells.** (A) Representative blots of NB4 cell extracts probed with anti-TOP2A (4566) or anti-TOP2B (4555) anti-sera after treatment with 200μM SA for 48hr or 72hr, blots were cut in half to probe for TOP2A and β-actin (loading control), the TOP2A blot was stripped (Thermo Restore stripping buffer) and probed for TOP2B. (B) Protein bands were quantified from three separate experiments and compared to untreated NB4 cells for the relative levels of TOP2A (upper right panel) and TOP2B (lower right panel) protein. Data are expressed as mean ± S.E.M relative to untreated NB4 cells (black bars).

### *3.3.7 Chemical inhibition of MPO using recently developed small molecule inhibitors.*

Two recently developed MPO inhibitors; PF1355 and MPOi-II were also tested (Figure. 3.1). PF1355 has previously been tested in neutrophils (Zheng *et al.*, 2015), but MPOi-II has not been previously tested in cell-based systems. Therefore, a series of doses of the two inhibitors were tested to establish suitable concentrations to reduce MPO activity in NB4 cells for use in further experiments. Figure 3.17A-B shows both PF1355 and MPOi-II are effective at reducing MPO activity as both inhibitors produced a dose dependent decrease in MPO activity. For PF1355 all doses tested were effective at reducing MPO activity to below 10%, resulting in undetectable levels of MPO activity at 10μM after a 4hr incubation (assay sensitivity 0.05 nmol TNB consumed/min/mL) (Figure. 3.17.A). For later experiments a dose of 10μM PF1355 for 4hr was used. At doses greater than 30μM, PF1355 becomes non-specific and targets thyroid peroxidase (Zheng *et al.*, 2015). For MPOi-II a dose of 5μM for 4hr was selected, this dose reduced MPO activity by 92.8% ± 5.7 (Figure 3.17.B).

The effects of both PF1355 and MPOi-II on TOP2 protein levels were analysed at 96hr using western blot analysis. Levels of TOP2A and TOP2B protein were analysed in NB4 cells treated with PF1355 (Figure.3.18.A-B). Quantification of protein bands showed PF1355 had minimal effect on the level of TOP2 protein (Figure. 3.18.C). Furthermore, PF1355 did not affect proliferation of NB4 cells under the concentrations tested (Figure. 3.18.D). A similar trend for TOP2 protein levels was seen for MPOi-II (Figure.3.19.A-C), however doses of 0.1μM to 5μM gave a growth advantage to cells (Figure. 3.19.D). The reason for this effect is unknown but this may have clinical implications.

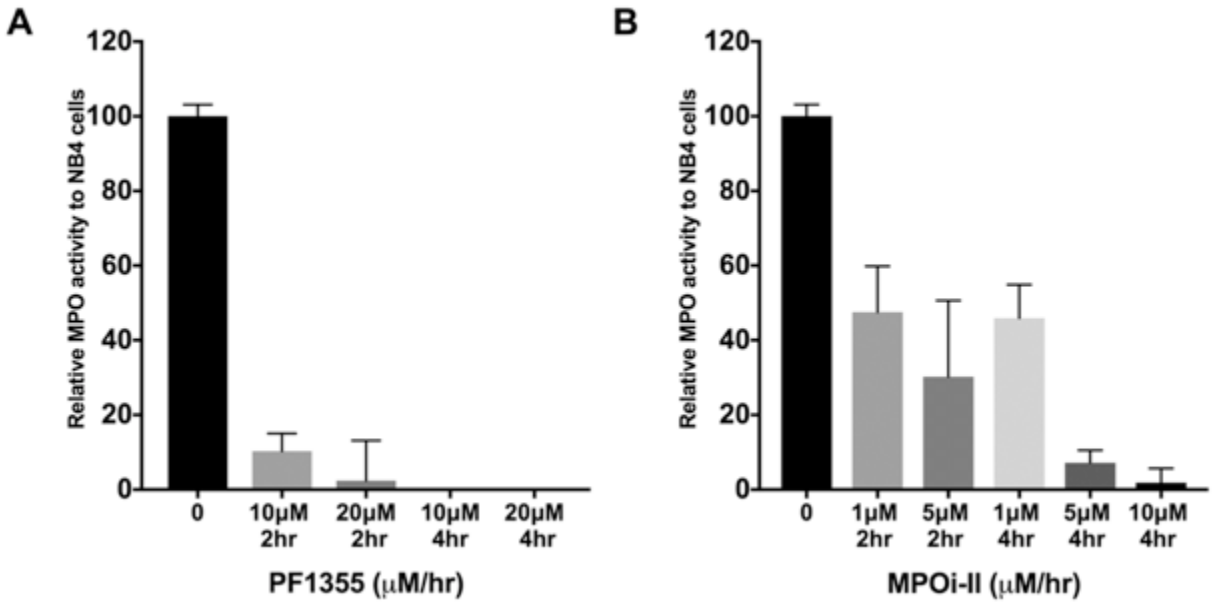


**Figure 3.17. PF1355 and MPOi-II inhibit MPO activity in NB4 cells.** Two direct irreversible inhibitors of MPO; PF1355 (A) and MPOi-II (B) were used at the times and doses specified to test for the reduction in MPO activity using the MPO colorimetric activity assay (ab105136, Abcam UK). Data are expressed relative to the mean value obtained for DMSO treated (vehicle control) NB4 cells ± S.E.M for three separate experiments. (Experiment conducted partly by Emma L. Lishman)

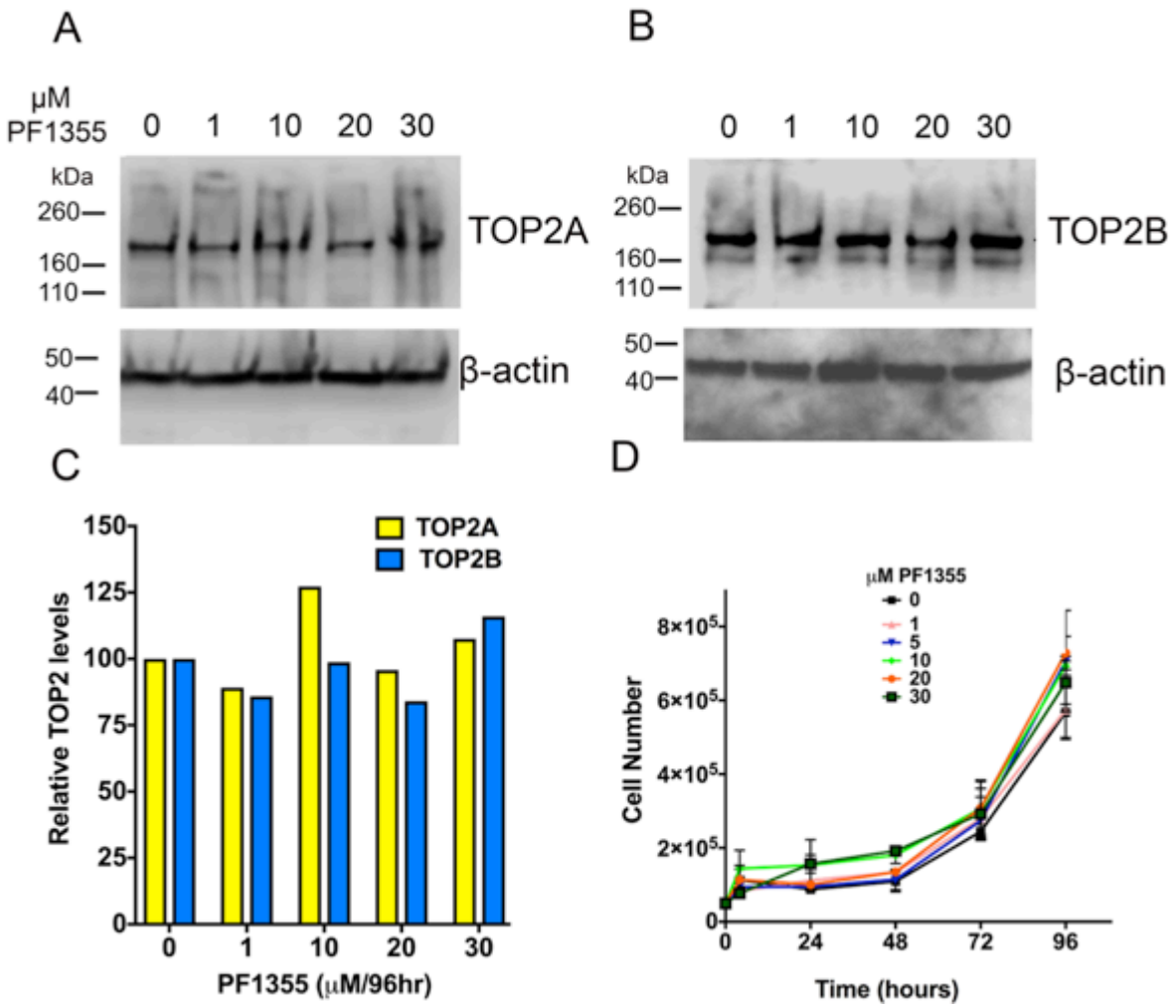


**Figure 3.18. Effect of PF1355 treatment on TOP2 levels.** NB4 cells were treated with PF1355 (0-30μM) for 96hr and probed for TOP2A (A) and TOP2B (B) protein levels. Protein band intensities were quantified electronically (C-digit) and compared relative to the vehicle control (DMSO) treated NB4 cells (C) (n=1 for each inhibitor concentration). (D) PF1355 did not affect cell growth, using cell counts n=3, data are expressed as mean ± S.E.M. (Experiments conducted by Emma L. Lishman).

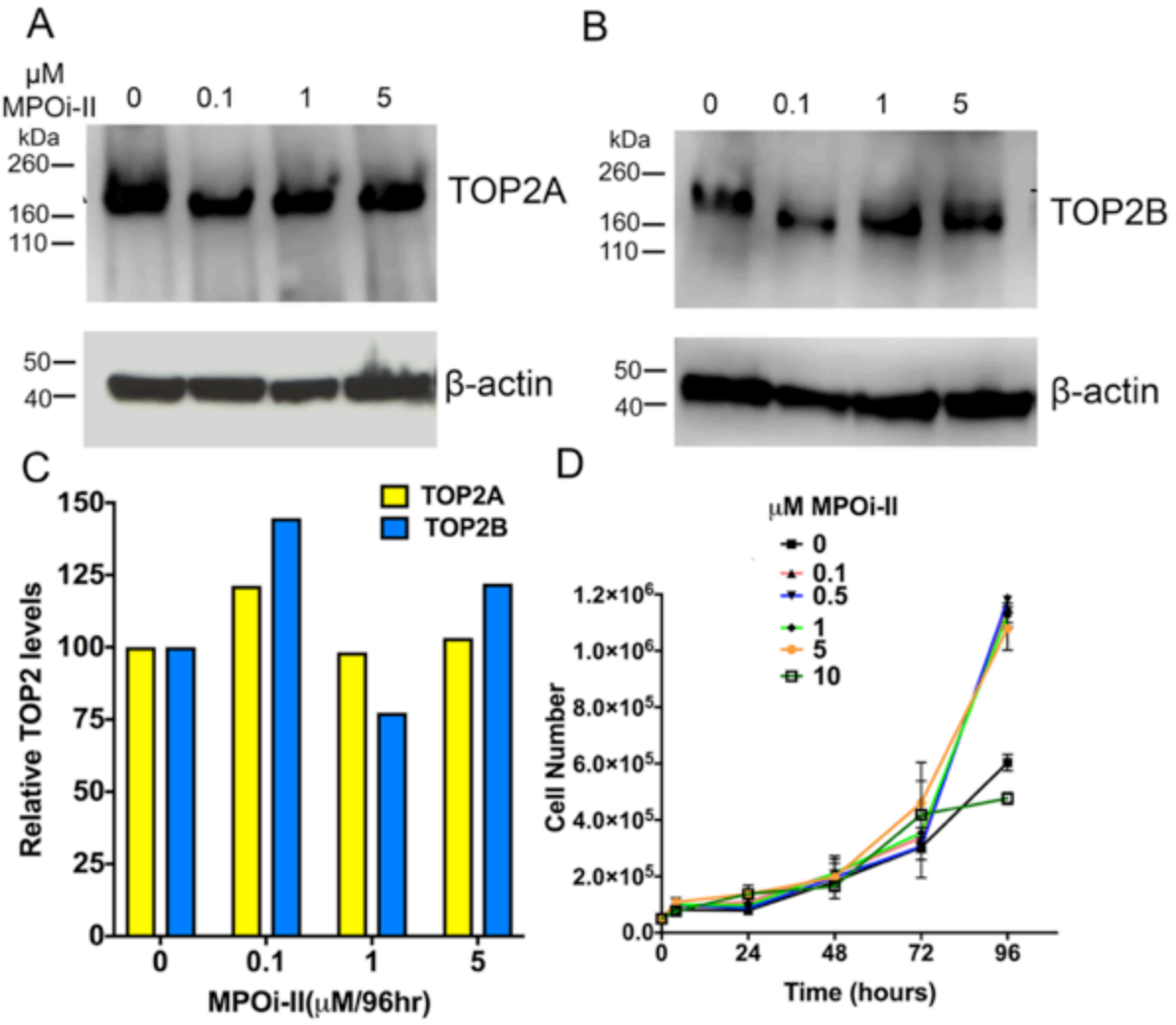


**Figure 3.19. MPOi-II treatment and the effect on the TOP2 protein levels in NB4 cells.** MPOi-II (0-5μM) was added to NB4 cells and assayed for TOP2A (A) and TOP2B (B) protein levels after 96hr of inhibitor treatment, protein bands were quantified electronically (C-digit) (C) and compared relative to NB4 cells treated with DMSO (solvent control) n=1 for each concentration tested. (D) Cell counts were preformed up to 96hr of MPOi-II treatment with and data are expressed as mean ± S.E.M (n=3). (Experiments conducted by Emma L. Lishman).

### *3.3.8 Transfection of an MPO expression construct into K562 cells*

In order to confirm conclusions drawn from studies using MPO inhibition in NB4 cells, K562 cells that do not express MPO, were transfected with a human MPO expression construct to generate MPO positive K562 clones. A plasmid construct consisting of the full-length human MPO gene with a C-terminal Myc-DDK tag expressed under the CMV promoter was transfected using a liposomal transfection method (Figure.3.20.A-B) (full details of the plasmid construct are given in section 2.10 and appendix Figure. iv). To allow selection the vector encodes the gene which

gives rise to resistance to geneticin (G148). To determine the dose of G418 required for selection a series of G418 doses (0- 1mg/mL) were tested in K562 cells. A dose of 750µg/mL was selected for initial selection of clones, after which clones were cultured in medium containing 500µg/mL of G418, this was the lowest dose which inhibited cell proliferation of K562 cells (Figure.3.21).

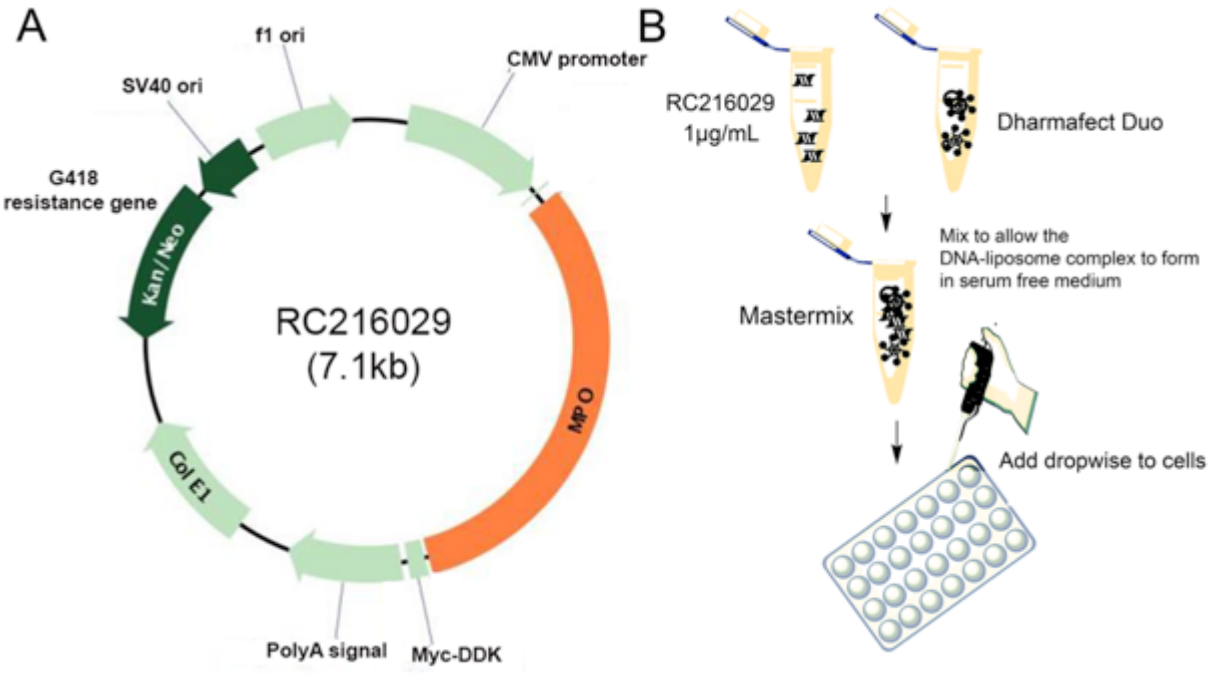


**Figure 3.20. (A) MPO expression construct, taken from Orgiene. (B) Diagrammatic representation of the transfection procedure.** (A) K562 cells were transfected with the expression construct RC216029 that encodes the human full-length MPO gene and G418 resistance gene. (B) K562 cells were transfected with the expression construct using a liposomal transfection method, in this method the expression construct and Dharmafect Duo are mixed prior to transfection allowing a DNA-liposome complex to form. Cells are transfected with the expression construct-Dharmafect duo mixture and incubated overnight at 37$^{o}$C. The following day 750µg/mL of G418 is added to allow selection, when cells become sufficiently dense they are tested for MPO expression by immunofluorescence.

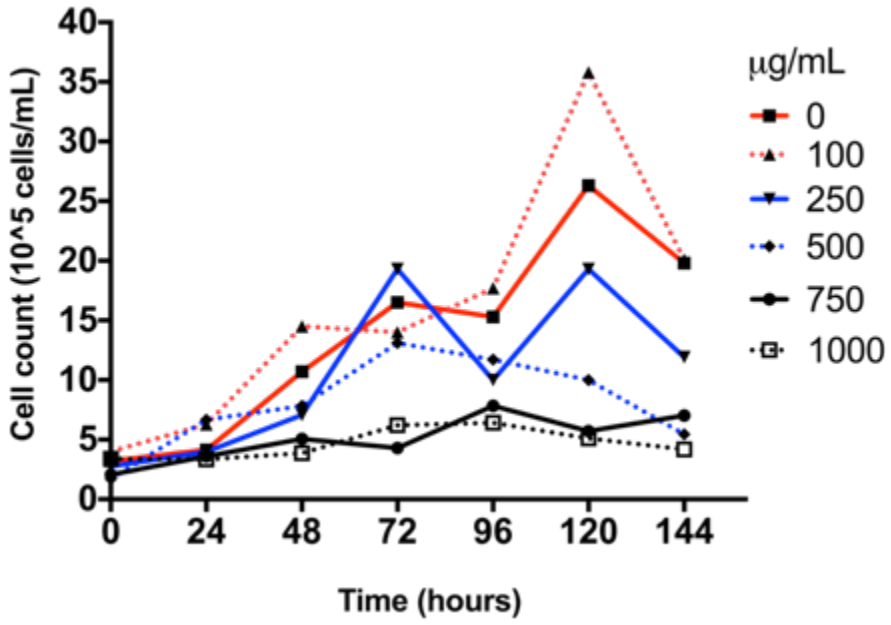


**Figure 3.21. Testing G418 doses, a selection antibiotic, in K562 cells.** K562 cells were treated with G418 (0-1mg/mL) for up to 6 days and assessed for cell growth at each 24hr timepoint.

The transfection efficiency of K562 cells was 18%, determined from the number of cells remaining after addition of G418, which is in line with published data (Schakowski *et al.*, 2004). Due to the low transfection efficiency, the K562 expressing MPO cells were isolated using a serial dilution method (method described in section. 2.10.1). In this method K562 cells were seeded in one well of a 96-well plate and were serially diluted 1:2 across the entire plate. The aim is to dilute cells down to a single cell which after cycles of cell doubling will form discrete colonies containing a monoclonal cell population. Five clones were selected that were positive for both MPO activity and positive for MPO protein expression across the whole cell population (Figure. 3.22.) (see section 2.10.1 and 2.11). None of the five $K562^{MPO}$ cell clones had MPO activity above 40% of that in NB4 cells, however the activity of $K562^{MPO}$ cell lines 4 and 5 were comparable to HL60 and Kasumi-1 cells (Figure. 3.8.B). Additionaly, K562 cells were transfected with a empty vector and clones were selected as a non-MPO expressing control. The selected K562 MPO expressing clones were probed using quantitative immunofluorescence for the level of TOP2 protein (method described in section 2.11). This was important to investigate as if introduction of an MPO expression construct into K562 cells causes changes in overall TOP2 levels then this would effect data interpretation in latter experiments.

Results indicated the level of TOP2A or TOP2B did not differ between K562 and K562-derived MPO cell lines (Figure. 3.23).

A limitation of the transfection of an MPO cDNA into K562 cells was the gradual silencing of the expression construct. MPO positive K562 cells that had been cultured for three weeks were probed for MPO expression. The tested cell lines had reduced MPO positive immunofluorescence compared to cells tested immediately after initial selection (Figure. 3.24). This limited the time available to conduct experiments on the K562-dervived MPO lines.

### *3.3.9 Use of buthionine sulphoximine (BSO) to reduce glutathione levels.*

The metabolites of TOP2 poisons generated by MPO-mediated oxidation can be reduced by glutathione, limiting the level of DNA damage (Kagan *et al.*, 1999; Kagan *et al.*, 2001; Vlasova *et al.*, 2011). Patients undergoing chemotherapy regimens generally have reduced levels of glutathione (Mukundan *et al.*, 1999; Charushila and Subodhini, 2013; Kadam and Abhang, 2015). Therefore, glutathione levels were reduced using BSO, to investigate the effects of glutathione on TOP2 poison mediated DNA damage in Chapter 5. BSO is an irreversible inhibitor of glutamate cysteine ligase (γ-glutamylcysteine synthetase), inhibiting glutathione synthesis (Drew and Miners, 1984). The level of total and reduced glutathione remaining was analysed spectrophotometrically after the addition of BSO to NB4 cells (method described in 2.12). This assay relies on the glutathione recycling system in which glutathione reacts with exogenously added DTNB to produce TNB ($\lambda$=412nm), a substrate yellow in colour, allowing the determination of total and reduced glutathione (by omitting glutathione reductase) (Figure. 3.25.A). The addition of BSO in NB4 cells leads to a dose dependent decrease in both total and reduced levels of glutathione. A dose of 150μM gave the highest reduction in total glutathione (74.3% ± 8.4) and reduced glutathione (79.3% ± 8.57) (Figure. 3.25.B) and did not affect the *in vitro* TOP2 activity (experiment conducted by C.A. Austin published in Atwal *et al.,* 2017).

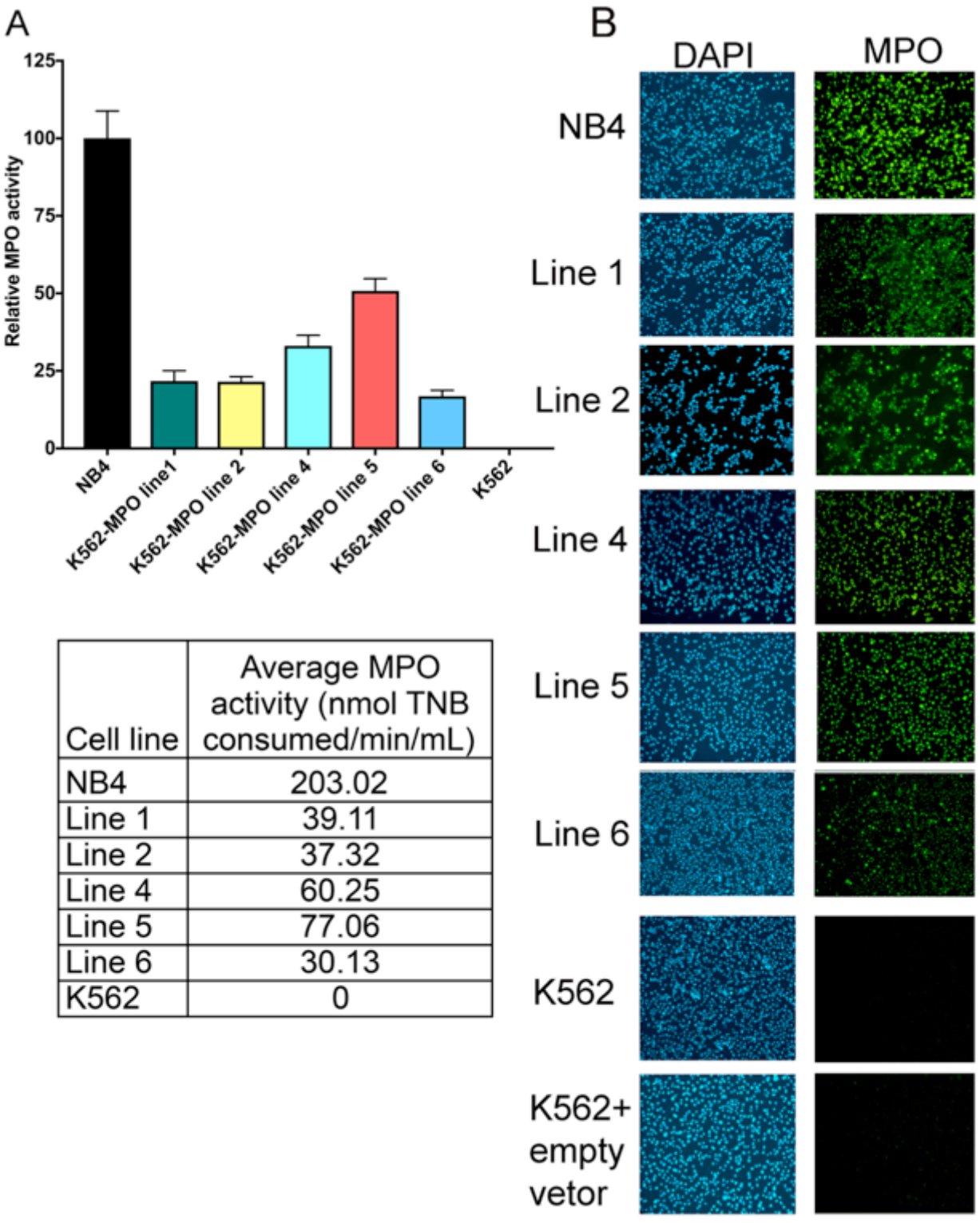


| Cell line | Average MPO activity (nmol TNB consumed/min/mL) |
|---|---|
| NB4 | 203.02 |
| Line 1 | 39.11 |
| Line 2 | 37.32 |
| Line 4 | 60.25 |
| Line 5 | 77.06 |
| Line 6 | 30.13 |
| K562 | 0 |

**Figure 3.22. Determination of MPO activity in five K562-dervived MPO expressing cells lines.** (A) K562 derived MPO expressing cell lines were tested for the level of MPO activity colourimetrically and compared to NB4 cells (ab105135, Abcam UK). (B) K562 derived MPO expressing cell lines were tested for protein expression using immunofluorescence. All cells in the K562 MPO cell population were 100% positive for MPO expression. DAPI stains for DNA and MPO was probed using anti-MPO ab9535 (Abcam, UK).

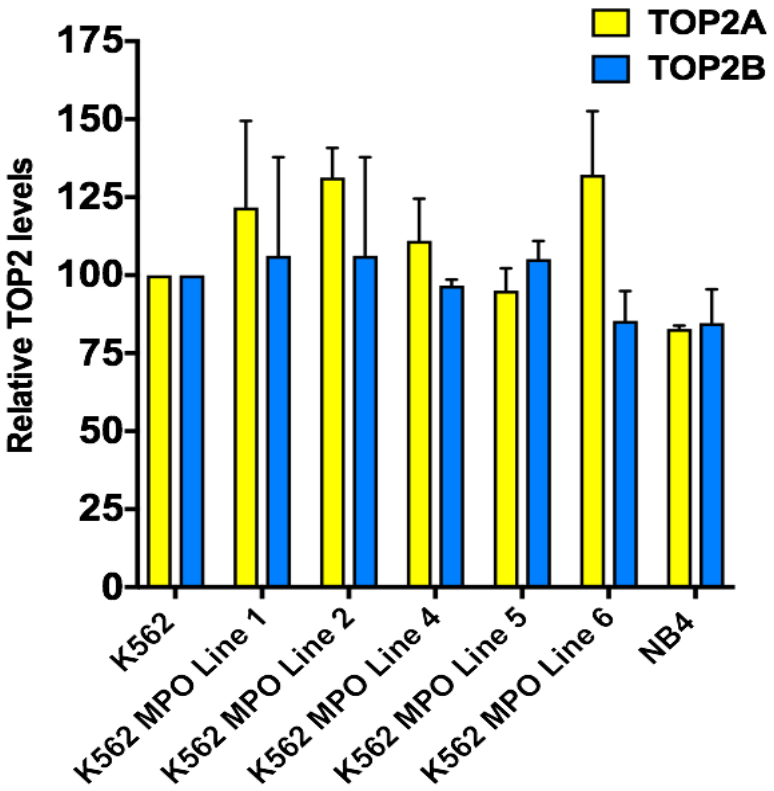


**Figure 3.23. Relative levels of TOP2A and TOP2B protein in K562 MPO expressing cell lines.** TOP2 levels were quantified by immunofluorescence using antibodies specific to TOP2A (4566) or TOP2B (4555). Integrated fluorescence (IF) values were obtained per nucleus, data were combined from three separate experiments and expressed as a percentage relative to the mean of TOP2 IF levels in K562 cells ± S.E.M.

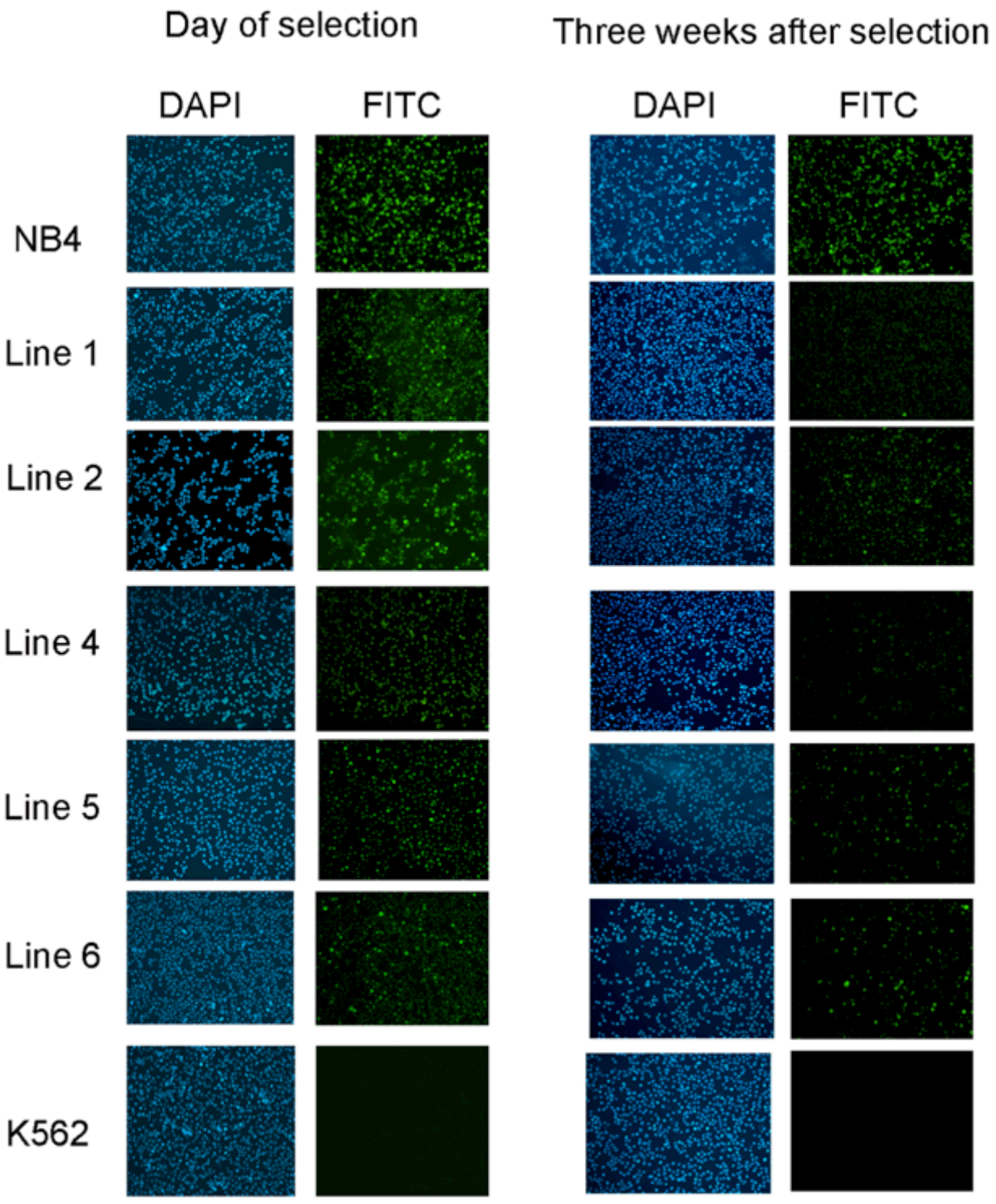


**Figure 3.24. Silencing of MPO expression in K562-derived MPO cell lines.** Cell lines were tested for MPO expression by immunofluorescence. DAPI stains for DNA and MPO was probed using anti-MPO ab9535 (Abcam, UK).

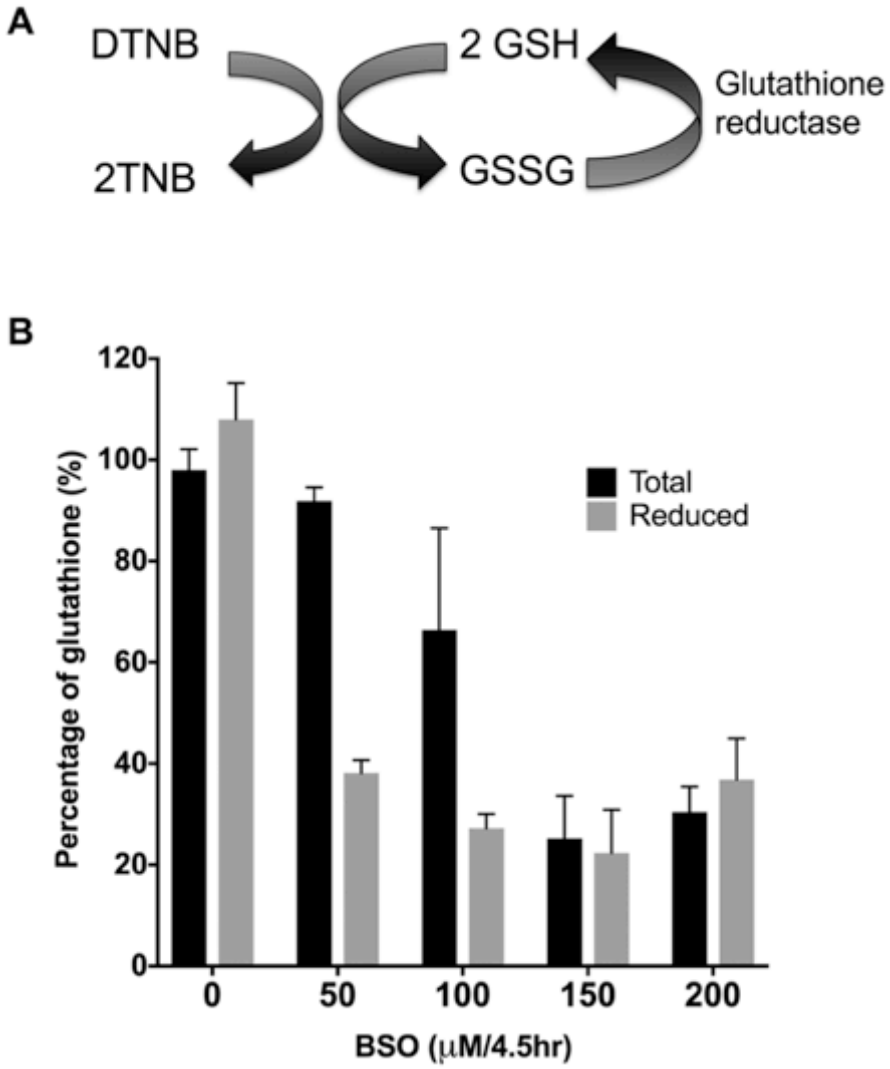


**Figure 3.25. Reduction of glutathione levels in NB4 cells upon BSO treatment.** (A) Principle of colorimetric glutathione assay (KA0797, Abnova, Taiwan). (B) NB4 cells were treated with BSO (0-200μM for 4.5hr) and assayed for the level of total (black) and reduced (grey) glutathione remaining following treatment. Data are expressed as mean ± S.E.M, n=3 except 0μM and 150μM measurements were conducted to n=6.

## 3.4 Discussion

This chapter describes how the various 'tools' required to address the question posed in this thesis were generated. The aim was to have a robust system in which MPO activity could be modulated. The siRNA knockdown approach specifically reduced the level of MPO protein and activity, but 25% or more activity remained after knockdown (Figure. 3.9 and Table 3.1). It was judged that this degree of residual MPO activity would make it difficult to determine any effect of MPO on TOP2

poison-mediated DNA damage. Therefore, a chemical inhibition strategy was pursued initially focussing on SA. Despite SA being a heam biosynthesis inhibitor rather than a direct inhibitor of MPO, SA has been extensively used as the main-line inhibitor for MPO inhibition *in cellulo* studies (Kagan *et al.*, 1999; Kagan *et al.*, 2001; Fan *et al.*, 2006; Nakazato *et al.*, 2007; Vlasova *et al.*, 2011). SA behaves as a dual inhibitor of MPO as it reduces both protein and activity levels (Figure. 3.10-3.11). Previous studies have shown that the addition of SA does not disrupt cellular morphology (Pinnix *et al.*, 1994). However, to our knowledge published studies lacked appropriate controls to analyse whether SA, under the conditions used in this work (200μM, 48hr) would affect the cell growth, viability or cellular respiration. On the basis of the control experiments conducted in this work, SA treated cells behave similarly to untreated NB4 cells in terms of cell respiration and proliferation (Figures. 3.13-3.15). Treatment with SA for up to 96hr did induce an increase in the reduction of the XTT tetrazolium salt (Figure 3.12B). But experiments conducted using the Seahorse assay confirm that mitochondrial respiration and glycolytic activity remain unaffected with a 48hr pre-incubation of SA, which is the incubation time used to conduct further experiments (Figure.3.14).

In addition, direct inhibitors of MPO became available during this work and two of these inhibitors; PF1355 and MPOi-II were also used to confirm the effects seen with SA. PF1355 and MPOi-II are chemically different in structure to each other (Figure.3.1). To allow confirmation of the data generated using inhibitors in NB4 cells, MPO expressing K562-dervived cell lines were established in which five cells lines were shown to be positive for MPO activity at a level comparable to HL60 and Kasumi-1 cells (Figure.3.22).

With the conditions to modulate MPO expression and to reduce glutathione levels, the effect of TOP2 poison activity in relation to MPO and glutathione were investigated.

# Chapter 4. Effect of MPO expression on TOP2 poison mediated DNA damage.

## 4.1 Introduction

Myeloperoxidase (MPO) expression is restricted to developing myeloid progenitor cells and neutrophils (Klebanoff, 2005; Malle *et al.*, 2007). In neutrophils, MPO aids in the killing of pathogenic microorganisms by generating hypochlorous acid and is involved in the formation of neutrophil extracellular traps (NETs) (Harrison and Schultz, 1976; Metzler *et al.*, 2011). MPO is also capable of the biotransformation of both etoposide and mitoxantrone resulting in metabolites that have altered DNA damaging properties (Haim *et al.*, 1986; Haim *et al.*, 1987b; Kagan *et al.*, 1994; Panousis *et al.*, 1994; Panousis *et al.*, 1997; Kagan *et al.*, 1999; Kagan *et al.*, 2001; Vlasova *et al.*, 2011; Gibson *et al.*, 2016) (Details in section 1.2 and 1.3).

The mechanism of MPO-mediated oxidation of etoposide has been well documented. However, less is known about the mechanisms of mitoxantrone oxidation. MPO can catalyse the sequential one-electron oxidation of etoposide generating etoposide quinone via a phenoxyl radical intermediate (Fan *et al.*, 2006) (Figure. 4.1). Additionally MPO can oxidise etoposide catechol to etoposide quinone. Etoposide catechol is a metabolite generated from the action of CYP3A4 and/or CYP3A5, and can poison TOP2 with a two-fold greater potency compared to etoposide *in vitro* (Figure. 4.1) (Zhuo *et al.*, 2004; Jacob *et al.*, 2013; Zheng *et al.*, 2015). However, etoposide quinone is reported to be several fold more potent at poisoning TOP2 *in vitro* and can also covalently interact with the N-terminal clamp of TOP2 acting as a covalent TOP2 poison (Vlasova *et al.*, 2011; Jacob *et al.*, 2013; Gibson *et al.*, 2016) (described in section 1.3.1).

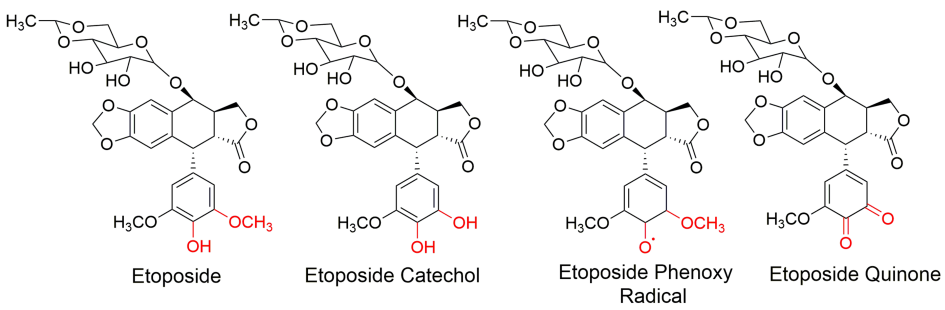


**Figure. 4.1. Chemical structure of etoposide metabolites.**

Mitoxantrone undergoes biotransformation at its phenylenediamine substructure resulting in the formation of a reactive quinone-diimine intermediate, which further undergoes intramolecular cyclisation to a naphthoquinoxaline metabolite (Figure. 4.2) (Blanz *et al.*, 1991). Naphthoquinoxaline is the intermediate product of the MPO catalysed reaction and is further oxidised to an additional two metabolites of unknown identity (Panousis *et al.*, 1994).

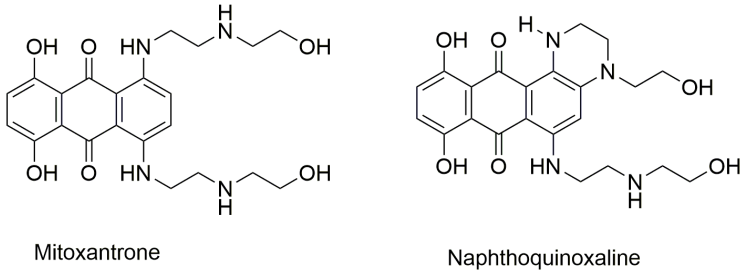


**Figure 4.2. Chemical structures of mitoxantrone and naphthoquinoxaline metabolite.**

The presence of active MPO expression has been shown to increase the level of etoposide mediated DNA damage in CD34+ cells (multipotent hematopoietic stem cells) and may also increase the level of drug stabilised TOP2-DNA complexes in the absence of glutathione in myeloid cell lines (Kagan *et al.*, 2001; Vlasova *et al.*, 2011). However, the studies reported used the SDS-KCl precipitation assay which allows the detection of all covalent proteins bound to DNA, but is not specific for TOP2 and neither does it identify which isoform of TOP2 is bound to DNA (Zhitkovich and Costa, 1992). The identity the TOP2 isoform is of interest, as TOP2B appears to be required for etoposide mediated carcinogenesis in mice and for etoposide-mediated chromosomal breaks at *MLL* and *RUNX1* loci (Azarova *et al.*, 2007; Cowell *et al.*, 2012; Smith *et al.*, 2014a). Therefore it is of interest to investigate whether the inhibition of MPO affects the level of TOP2 poison stabilised TOP2-DNA complexes differentially between the two TOP2 isoforms.

## 4.2 Aims

The aims of this chapter are to investigate the effects of MPO expression on the level of etoposide- and mitoxantrone-induced TOP2-mediated DNA damage. To address this, two separate cell based systems were employed to deduce the effects of MPO. Firstly, MPO activity was inhibited in the MPO expressing cell line, NB4 and secondly MPO was exogenously expressed in the MPO non-expressing cell line, K562. MPO

inhibition was achieved using succinylacetone (SA) and when they became available, new direct MPO inhibitors, PF1355 and MPOi-II. Using these systems, the effects of MPO activity on the accumulation of TOP2 poison induced TOP2-DNA complexes and DNA DSB, as measured by γH2Ax phosphorylation at Ser139 was investigated.

## 4.3 Results

### *4.3.1 Stabilisation of TOP2-DNA covalent complexes by etoposide and mitoxantrone*

To quantify the level of TOP2 poison-stabilised TOP2-DNA covalent complexes the TARDIS assay was employed (Willmore *et al.*, 1998; Cowell *et al.*, 2011). Previous work from the Austin lab has determined the range of etoposide and mitoxantrone concentrations for which the TARDIS assay can reliably quantify TOP2-DNA complexes. For etoposide, the dose range was determined to be 1μM to 100μM for detecting stabilised TOP2A-DNA complexes and 10μM to 100μM etoposide for TOP2B-DNA complexes (Willmore *et al.*, 1998; Errington *et al.*, 1999). For mitoxantrone, 0.5μM and 1μM were the optimal doses to detect both stabilised TOP2A and TOP2B complexes. However, these concentrations were determined in human lymphoblast cell lines, K562 cells and in mouse embryonic fibroblasts (MEFs). To ascertain whether these doses are also suitable in NB4 cells, NB4 cells were exposed to a range of concentrations of either etoposide (1μM to 100μM) or mitoxantrone (0.1μM to 20μM) for 1 hour. Following this the drug was removed from the cell medium and cells were embedded in agarose on slides, lysed, and probed using quantitative immunofluorescence to detect TOP2 protein covalently bound to DNA, using the TARDIS assay. This assay allows the quantification of TOP2 protein bound to DNA after removal of cellular constituents and non-covalently bound proteins from nuclear DNA by SDS-salt extraction (see section 2.13).

Consistent with previous data, etoposide produced a dose-dependent increase in TOP2A- and TOP2B-DNA covalent complex stabilisation (Figure. 4.3.A-D). (Willmore *et al.*, 1998). In Figures 4.3.A and B data are represented as scatter-grams where each data-point represents the integrated fluorescence signal obtained from a single nucleus, a minimum of 300 nuclei were analysed per treatment. The intensity of integrated fluorescence is distributed heterogeneously in the cell population, which

may be due to the differences in cell-cycle phases of each individual cell (Figure. 4.3A-B). For this reason when conducting analysis of replicate experiments, the median value, indicated by the red line (Figure. 4.3A-B), is selected to combine data from biological replicates (normalisation details described in section. 2.14). Figure. 4.3.A and B represent data obtained from a single biological replicate, data from four additional experiments were combined using the median values, to produce the data shown in Figure. 4.3.C and D. The intensity of the integrated fluorescence was lower for TOP2B than TOP2A, an observation that is consistent with previous data and is seen with different anti-TOP2 antibodies (Willmore *et al.*, 1998). As a result 1μM etoposide gave a fluorescence signal reproducibly above background for TOP2A ($P$=0.016), however for TOP2B 10μM etoposide was required to obtain a signal that was significantly above background ($P$=0.045). Therefore, for subsequent TARDIS experiments, a higher dose of 100μM and a lower dose of 10μM of etoposide were chosen. The chosen etoposide dose range can robustly allow the quantification of TOP2-DNA complexes by the TARDIS assay in NB4 cells. These doses are comparable with previous observations reported data in CCRF-CEM (human lymphoblast cell line) and MEFs (Willmore *et al.*, 1998; Errington *et al.*, 1999).

Similar dose range experiments were performed for mitoxantrone using doses ranging from 0.1μM to 20μM. In contrast to the results obtained for etoposide, mitoxantrone reached a peak in fluorescence intensity at 1μM and higher doses of 10μM and 20μM resulted in a lower signal (Figure. 4.4.A-D). Notably this phenomenon was observed previously in MEFs cells (Errington *et al.*, 1999). The reason for the decline could be that in addition to poisoning TOP2, mitoxantrone can behave as a catalytic inhibitor of TOP2 (see chapter 6 section 6.3.5). The mechanism of catalytic inhibition is likely to be indirect, through either mitoxantrone oxidation leading to mitoxantrone-DNA adducts or through chromatin compaction, hence preventing TOP2 from binding to DNA (Parker *et al.*, 1999; Parker *et al.*, 2000; Hajihassan and Rabbani-Chadegani, 2009). In addition, the relative intensity of integrated fluorescence for mitoxantrone was lower than that obtained with etoposide suggesting mitoxantrone is a less potent TOP2 poison compared to etoposide (Figure. 4.3A-B & 4.4A-B). For subsequent experiments, a dose of 1μM of mitoxantrone was selected as the higher dose and a lower dose of 0.5μM was also chosen. The effect of mitoxantrone at 20μM is presented in chapter 6 section 6.3.5.

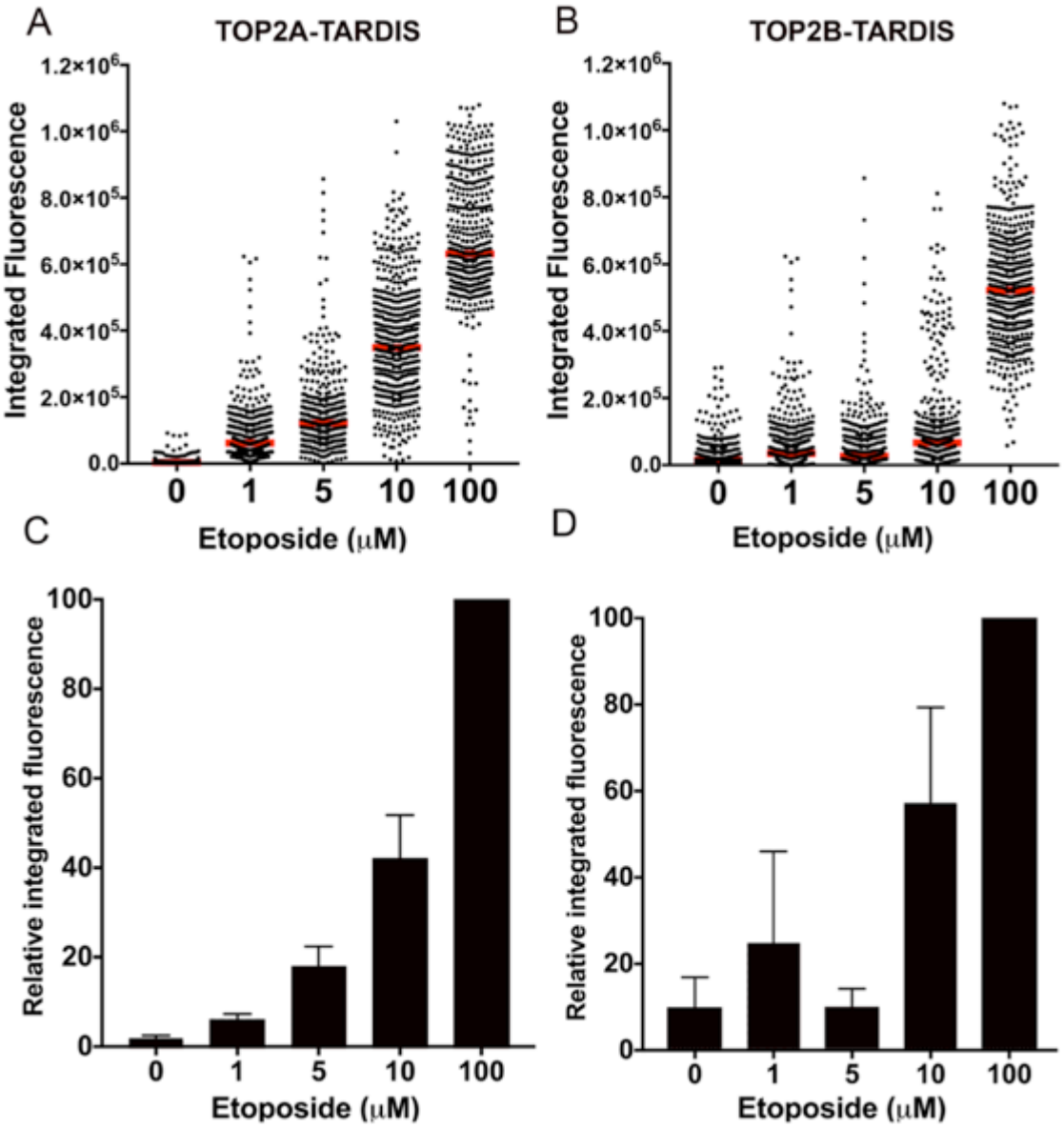


**Figure 4.3. Dose response for etoposide mediated TOP2A and TOP2B-DNA covalent complex stabilisation.** NB4 cells were treated with the specified doses of etoposide or a vehicle control (DMSO 0.02%(v/v)), for 1hr. TOP2-DNA covalent complexes were quantified by TARDIS analysis using antibodies specific to TOP2A (A) or TOP2B (B) n=1. Integrated fluorescence values were determined per nucleus (at least 300 nuclei per treatment), data are depicted as scatterplots, and each point corresponds to the integrated fluorescence value obtained for a single nucleus. From these experiments the median values (red line) were obtained and the mean of medians were calculated for replicate experiments (n=5). Data are expressed relative to 100μM etoposide (n=5) for stabilised TOP2A (C) and TOP2B (D) DNA complexes ± S.E.M.

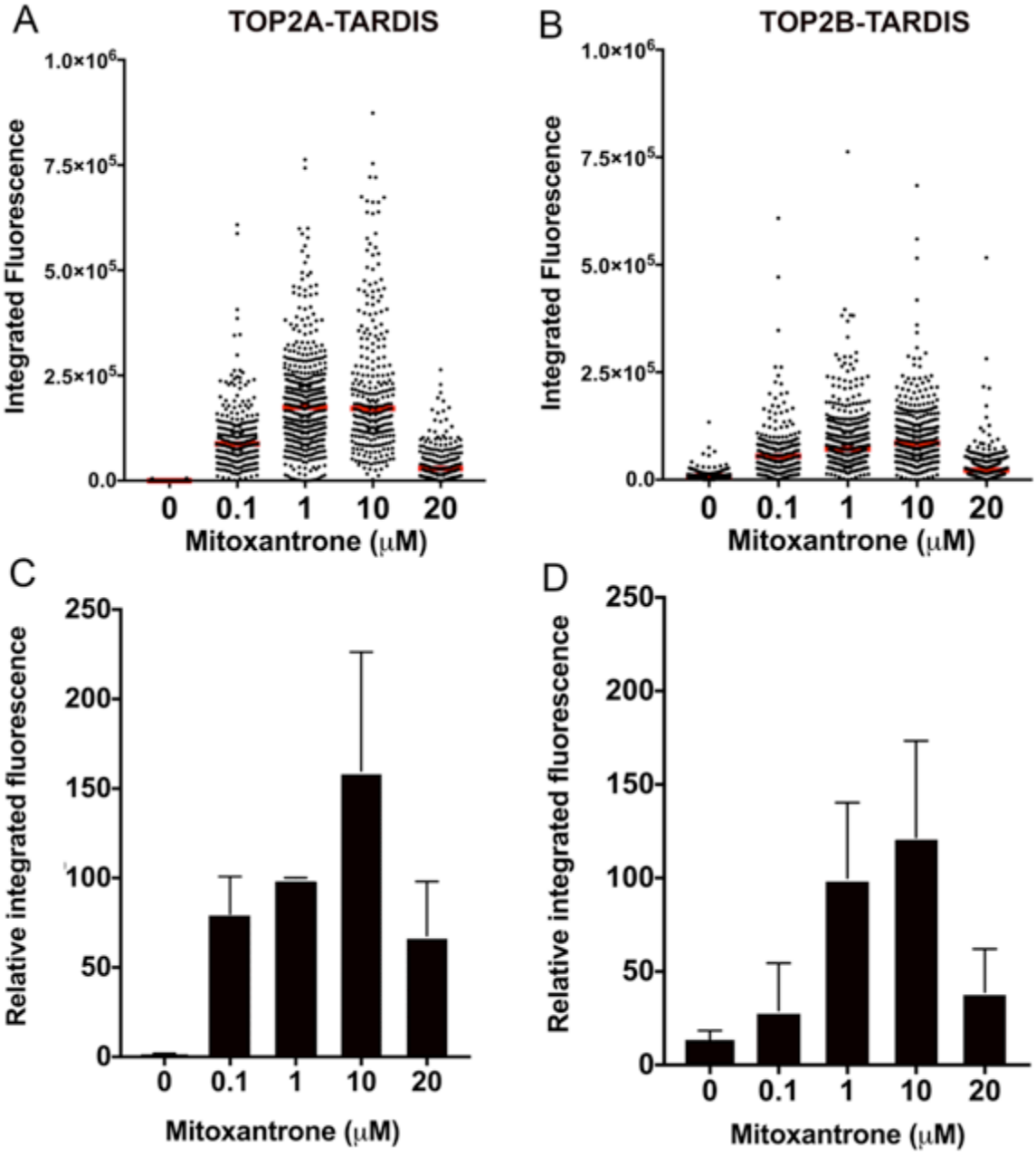


**Figure 4.4. Mitoxantrone stabilises TOP2A and TOP2B-DNA covalent complexes.** NB4 cells were treated with the specified doses of mitoxantrone for 1 hr. Mitoxantrone stabilised TOP2-DNA covalent complexes were quantified using the TARDIS assay for either TOP2A (A) or TOP2B (B) (n=1). Data in (A) and (B) are depicted as scatterplots, each point represents the integrated fluorescence value obtained for a single nucleus, the red line indicates the median value. The means of medians were calculated from replicate experiments (n=5). Data are expressed as a percentage from the mean value obtained with 1μM mitoxantrone for TOP2A (C) and TOP2B (D) stabilised DNA complexes ± S.E.M.

### *4.3.2 Active MPO expression enhances etoposide-mediated TOP2-DNA covalent complex stabilisation.*

MPO activity can be effectively reduced in the MPO-expressing cell line NB4 using the heam biosynthesis inhibitor, SA. A 48hr pre-incubation of NB4 cells with 200μM SA resulted in complete loss of detectable MPO activity accompanied by the reduction in mature MPO protein with no effect on TOP2 protein levels or activity (see sections 3.3.4, 3.3.6 and (Atwal *et al.*, 2017). This system was employed to determine the affect of MPO activity on the accumulation of TOP2A and TOP2B enzyme-DNA complexes measured by the TARDIS assay. Inhibition of MPO using SA pre-treatment in NB4 cells reduced the level of etoposide stabilised TOP2A- and TOP2B-DNA complexes at both 10μM and 100μM etoposide for all cells within the population (Figure.4.5A-B). Notably the magnitude of complex reduction after etoposide treatment was greater for TOP2B than TOP2A (Figure.4.5.C-D). At 10μM etoposide, there was a 55% (*P=0.013*) reduction in the level of TOP2B-DNA complexes whereas for TOP2A, levels reduced by 18% (*P=0.033*) (Figure 4.5.E). A similar trend was observed at 100μM etoposide treatment, the level of complex reduction for SA pre-treated cells was 38% for TOP2B (*P=0.019*) and 12% for TOP2A (*P=0.025*) (Figure.4.5.C-E). To confirm the reduced TARDIS signal in SA-pretreated cells was due to suppression of MPO activity, similar experiments were performed in K562 cells, a cell line that does not express MPO (Ch3.3.3). As expected, SA pretreatment did not affect the level of etoposide stabilised TOP2 complexes in K562 cells (Figure.4.6.A-C).

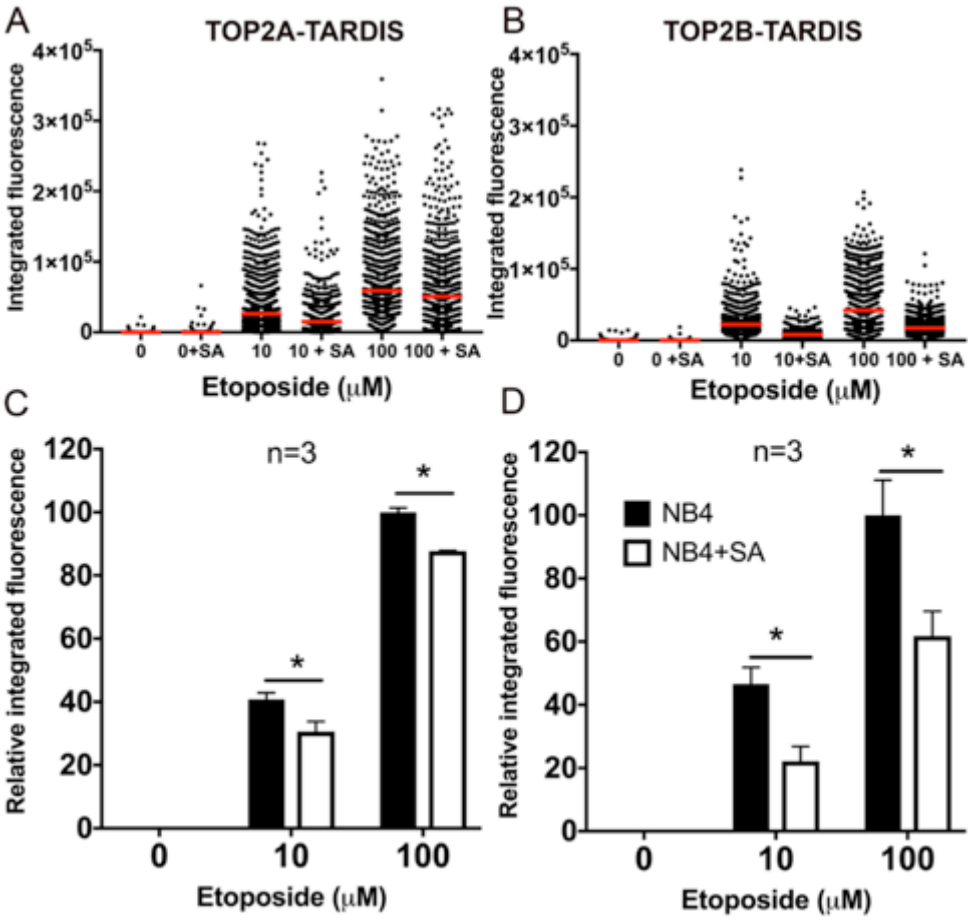


E

| Cell line | TARDIS Assay | Pre-treatment | Etoposide/ μM | %+ve control | SEM | Sig (*P*-value) | % reduction by SA |
|---|---|---|---|---|---|---|---|
| NB4 | TOP2A | None | 10 | 39.4 | 2.3 | | |
| NB4 | TOP2A | SA | 10 | 32.3 | 3.9 | 0.033 | 18.1 |
| NB4 | TOP2A | None | 100 | 100 | 1.4 | | |
| NB4 | TOP2A | SA | 100 | 87.7 | 0.2 | 0.025 | 12.4 |
| NB4 | TOP2B | None | 10 | 50.5 | 4.9 | | |
| NB4 | TOP2B | SA | 10 | 22.6 | 6.7 | 0.013 | 55.3 |
| NB4 | TOP2B | None | 100 | 100 | 11.1 | | |
| NB4 | TOP2B | SA | 100 | 59.6 | 7.9 | 0.019 | 38.3 |

**Figure 4.5. Inhibition of MPO reduces etoposide stabilised TOP2-DNA covalent complexes.** NB4 cells were pre-incubated with 200μM SA for 48hr followed by 1hr incubation with etoposide (10μM or 100μM), or a vehicle control. Cells were processed and analysed for the level of etoposide stabilised TOP2-DNA covalent complexes for TOP2A (A) or TOP2B (B). Data in A-B are represented as the integrated fluorescence obtained per nucleus for a single biological replicate (a minimum of 600 nuclei were analysed per treatment). Data obtained from an additional two experiments were combined and expressed as histograms shown in C and D for TOP2A and TOP2B respectively and are expressed relative to the mean value obtained with 100μM etoposide in the absence of SA. (E) Percentage values are expressed relative to the mean value obtained with 100μM etoposide in the absence of SA and significance (Sig) values are shown for the difference between control and SA pretreatment. Statistical analysis was performed by the one-way ANOVA with post hoc Tukey's multiple comparison test. * $P$ <0.05.

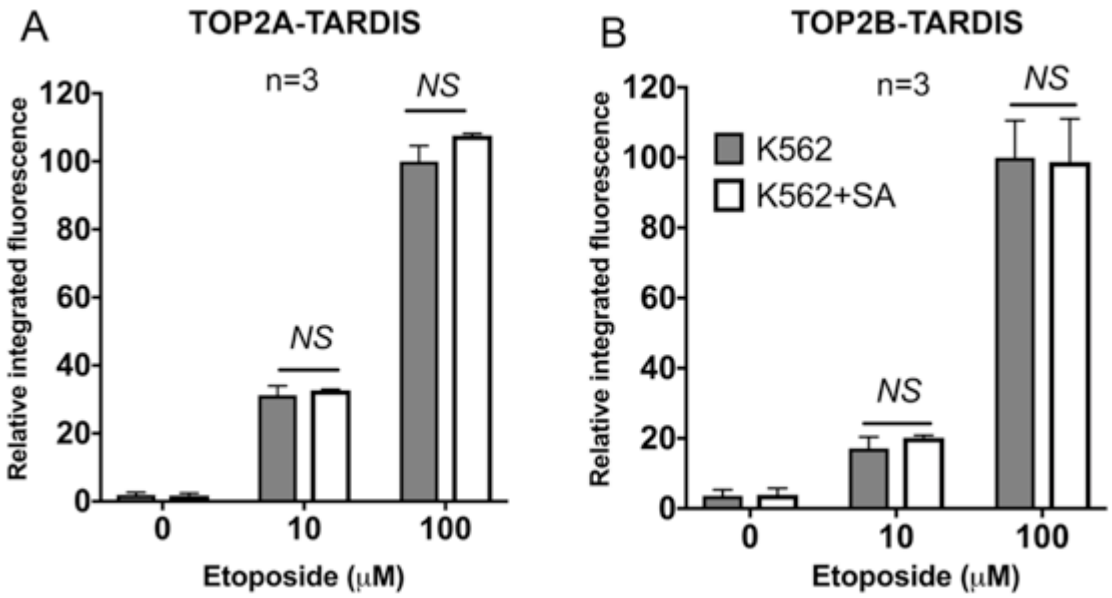


C

| Cell line | TARDIS Assay | Pre-treatment | Etoposide/ μM | %+ve control | SEM | Sig (*P*-value) |
|---|---|---|---|---|---|---|
| K562 | TOP2A | None | 10 | 31.2 | 2.8 | |
| K562 | TOP2A | SA | 10 | 32.7 | 0.3 | 0.979 |
| K562 | TOP2A | None | 100 | 100 | 4.6 | |
| K562 | TOP2A | SA | 100 | 107.6 | 1.9 | 0.271 |
| K562 | TOP2B | None | 10 | 17.1 | 3.3 | |
| K562 | TOP2B | SA | 10 | 20.2 | 1.2 | 0.993 |
| K562 | TOP2B | None | 100 | 100 | 10.6 | |
| K562 | TOP2B-TOP2B | SA | 100 | 98.8 | 12.3 | >0.999 |

**Figure 4.6. SA does not affect etoposide TOP2 poisoning ability in cells that do not express MPO.** K562 cells were incubated with 200μM of SA for 48hr followed by the treatment with etoposide or a vehicle control and evaluated for the level of stabilised TOP2A (A) and TOP2B (B) DNA complexes. Data are expressed relative to 100μM etoposide in the absence of SA ±S.E.M. (C) Percentage values are expressed relative to the mean value obtained with 100μM etoposide in the absence of SA and significance (Sig) values are shown for the difference between control and SA pretreatment for each drug dose tested. Statistical analysis was performed by the one-way ANOVA with post hoc Tukey's multiple comparison test.

To further verify the role of MPO in elevating the level of TOP2-DNA complexes induced by etoposide, MPO expressing K562 clones were produced by the stable transfection of a human full-length MPO expression construct using a liposomal transfection method (see section 3.3.8). Using this method, five K562-dervived MPO expressing cell lines were obtained, all cells were positive for MPO expression by immunofluorescence. Results from the MPO colorimetric activity assay showed the $K562^{MPO}$ cells have MPO activity ranging from 15% to 40% of that compared to NB4 cells, with lines 4 and 5 having more MPO activity compared to HL60 and Kasumi-1

cells (Table 4.1). Additionally, the K562$^{MPO}$ cell lines were tested for TOP2A and TOP2B expression levels using quantitative immunofluorescence. This was important to examine, as variations in TOP2 protein levels between the K562$^{MPO}$ cell lines and parental K562 cells would affect the data obtained from the TARDIS and γH2Ax assays. Data obtained for TOP2 protein expression showed both the K562$^{MPO}$ cell lines and parental K562 cells express TOP2A and TOP2B at similar levels (Table 4.2).

| Cell line | Average MPO activity (nmol TNB consumed/min/mL) | % MPO activity compared to NB4 cells |
|---|---|---|
| NB4 | 203.02 | 100.0±8.8 |
| HL60 | 48.42 | 23.8±5.9 |
| Kasumi-1 | 53.03 | 26.1±10.2 |
| K562MPO Line 1 | 39.11 | 19.3±3.3 |
| K562MPO Line 2 | 37.32 | 18.4±1.6 |
| K562MPO Line 4 | 60.25 | 29.7±3.5 |
| K562MPO Line 5 | 77.06 | 38.0±2.5 |
| K562MPO Line 6 | 30.13 | 14.8±1.9 |

**Table 4.1** MPO activity in cells lines, assayed using the MPO colorimetric activity assay (ab105136, Abcam) (for further details see 3.3.3 and 3.3.8).

| Cell line | Relative levels of TOP2A | Relative levels of TOP2B |
|---|---|---|
| K562 | 100 | 100 |
| K562MPO Line 1 | 121.7±27.8 | 106.3±31.5 |
| K562MPO Line 2 | 131.3±9.42 | 99.7±21.3 |
| K562MPO Line 4 | 111±13.4 | 96.7±2.0 |
| K562MPO Line 5 | 95.1±7.1 | 95.2±4.2 |
| K562MPO Line 6 | 132.2±20.3 | 85.4±9.6 |

**Table 4.2** Protein expression levels of TOP2A and TOP2B determined by quantitative immunofluorescence (for further details see 3.3.8)

The K562$^{MPO}$ cell lines were treated with either 10μM or 100μM etoposide and assayed for the level of drug-stabilised complexes by the TARDIS assay. The K562$^{MPO}$ cell lines displayed greater levels of etoposide-stabilised complexes for both TOP2A and TOP2B compared to parental K562 cells, the level of increase in complex stabilisation correlated with MPO activity (Figure.4.7.A-C). K562$^{MPO}$ line 5 expresses 77.06 nmol TNB consumed/min/mL MPO activity which is 38% of that observed in NB4 cells (Table 4.1). Etoposide (10μM) treatment in line 5 induced 58%

(*P<0.001*) and 46% (*P=0.042*) more stabilised TOP2A and TOP2B complexes compared to parental K562 cells (Figure. 4.7B-D). For 100μM etoposide, the figures were 39% (*P<0.001*) and 48% (*P=0.002*) for TOP2A and TOP2B respectively (Figure. 4.7B-C). Whereas, $K562^{MPO}$ line 1, which has 39 nmol TNB consumed/min/mL MPO activity (Figure. 4.7A) displayed an increase in TOP2A stabilised complexes with 10μM and 100μM etoposide, but no difference in TOP2B stabilised complexes were observed compared to parental K562 cells (Figure. 4.7B-C). The results generated in the $K562^{MPO}$ cell lines show greater level of etoposide-stabilised complexes compared to parental K562 cells that do not contain MPO expression. The level of increase in etoposide-stabilised complexes is dependent on the level of MPO activity present within a cell.

K562 cells were transfected with an empty plasmid vector using the equivalent transfection conditions used to produce the $K562^{MPO}$ cell lines. K562 cells transfected with the empty plasmid vector were tested for the level of etoposide stabilised TOP2-DNA complexes. The empty vector did not affect the level of etoposide-stabilised complexes for either TOP2A or TOP2B compared to non-transfected K562 cells, further confirming the effect observed in the $K562^{MPO}$ cells was due to the expression of active MPO (Figure. 4.8A-B).

If the elevated level of etoposide-induced TOP2A and TOP2B TARDIS signal is due to the exogenous expression of MPO in K562 cells, then it should be abolished by the inhibition of MPO. The effect of SA pretreatment in $K562^{MPO}$ cell line 2 was analysed for the level of TOP2 covalent complex stabilisation at 100μM etoposide. As shown in Figure 4.9, pretreatment with SA reduced the level of etoposide stabilised TOP2 complexes in comparison to non-SA pretreated $K562^{MPO}$ cell line 2. For TOP2A, SA pretreatment resulted in a 52% (*P<0.001*) reduction in TOP2A complexes and for TOP2B the reduction was 46% (*P<0.001*) (Figure 4.9.A-C). Notably, SA reduced the level of etoposide-stabilised complexes in the $K562^{MPO}$ cell line 2 to a level that was no longer significantly different to parental K562 cells (*P>0.999* for TOP2A and *P= 0.830* for TOP2B) (Figure.4.9 A-B). The effect of SA pre-treatment could not be tested in the remaining $K562^{MPO}$ cells lines due to silencing of the MPO expression construct, which limited the time available to conduct experiments.

A

| Cell line | Average MPO activity (nmol TNB consumed/min/mL) |
|---|---|
| NB4 | 203.02 |
| Line 1 | 39.11 |
| Line 2 | 37.32 |
| Line 4 | 60.25 |
| Line 5 | 77.06 |
| Line 6 | 30.13 |
| K562 | 0 |

B

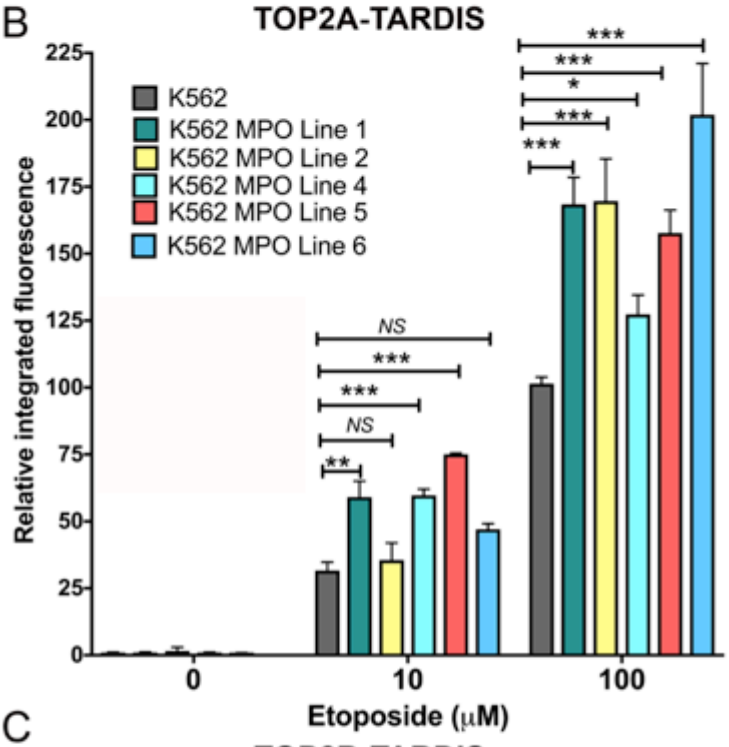


C

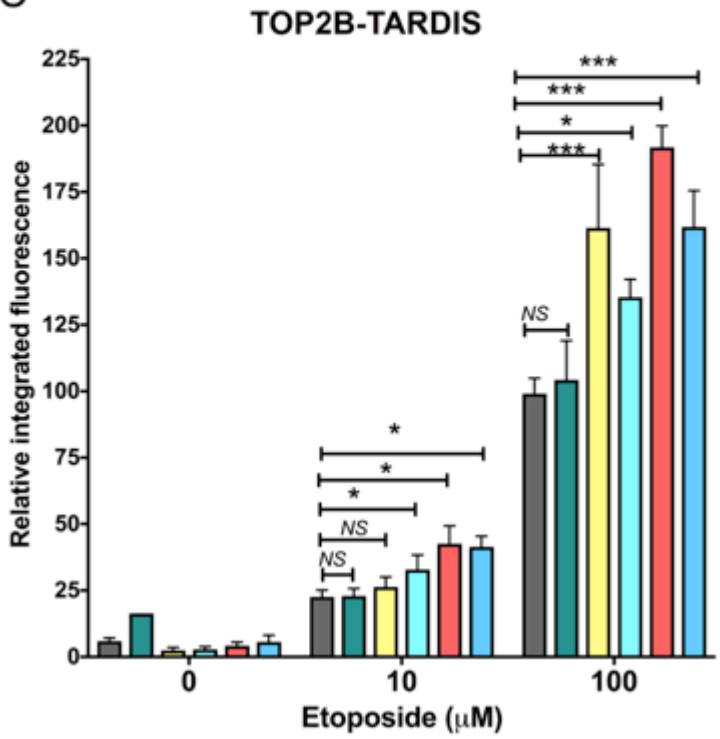

D

| Cell line | TARDIS Assay | Etoposide /μM | %+ve control | SEM | Sig (*P*-value) | % increase compared to K562 |
|---|---|---|---|---|---|---|
| K562 | TOP2A | 10 | 31.2 | 3.2 | | |
| K562-line 1 | TOP2A | 10 | 59.1 | 6 | 0.003 | 47.2 |
| K562-line 2 | TOP2A | 10 | 35.6 | 6.4 | 0.988 | - |
| K562-line 4 | TOP2A | 10 | 59.8 | 2.4 | <0.001 | 47.7 |
| K562-line 5 | TOP2A | 10 | 75.2 | 0.5 | <0.001 | 58.4 |
| K562-line 6 | TOP2A | 10 | 47.1 | 2.1 | 0.160 | - |
| K562 | TOP2A | 100 | 100 | 2.7 | | |
| K562-line 1 | TOP2A | 100 | 168.4 | 10.1 | <0.001 | 40.1 |
| K562-line 2 | TOP2A | 100 | 169.6 | 15.8 | <0.001 | 41 |
| K562-line 4 | TOP2A | 100 | 134.5 | 7.2 | 0.027 | 25.6 |
| K562-line 5 | TOP2A | 100 | 163.9 | 8.5 | <0.001 | 39.0 |
| K562-line 6 | TOP2A | 100 | 201.9 | 19.2 | <0.001 | 50.4 |
| K562 | TOP2B | 10 | 22.6 | 2.6 | | |
| K562-line 1 | TOP2B | 10 | 23 | 2.7 | >0.99 | - |
| K562-line 2 | TOP2B | 10 | 26.3 | 3.7 | >0.99 | 12.7 |
| K562-line 4 | TOP2B | 10 | 32.9 | 5.5 | 0.030 | 30.1 |
| K562-line 5 | TOP2B | 10 | 42.6 | 6.7 | 0.042 | 45.6 |
| K562-line 6 | TOP2B | 10 | 41.4 | 4 | 0.026 | 43.8 |
| K562 | TOP2B | 100 | 100 | 5.4 | | |
| K562-line 1 | TOP2B | 100 | 104.2 | 14.8 | >0.99 | - |
| K562-line 2 | TOP2B | 100 | 161.4 | 23.9 | <0.001 | 37.9 |
| K562-line 4 | TOP2B | 100 | 135.4 | 6.7 | 0.046 | 26 |
| K562-line 5 | TOP2B | 100 | 191.8 | 8 | 0.002 | 48 |
| K562-line 6 | TOP2B | 100 | 161.8 | 13.7 | <0.001 | 37.9 |

**Figure 4.7. Expression of active MPO potentiates the level of etoposide-stabilised TOP2-DNA covalent complexes.** (A) MPO activity of $K562^{MPO}$ cell lines. Parental K562 and five MPO expressing K562-derived cell lines were treated with etoposide (10μM or 100μM), or a vehicle control for 1hr**.** TOP2-DNA complexes were quantified using the TARDIS assay for TOP2A (B) or TOP2B (C). (D) Supporting percentage values expressed relative 100μM etoposide and p values obtained for the significance between parental K562 cells and $K562^{MPO}$ cell lines following each treatment. Data are expressed relative to the mean value obtained for parental K562 cells treated with 100μM etoposide ±S.E.M. Statistical analysis was performed by the one-way ANOVA with post hoc Tukey's multiple comparison test. **P*<0.05; ***P*<0.01; and ****P*<0.001.

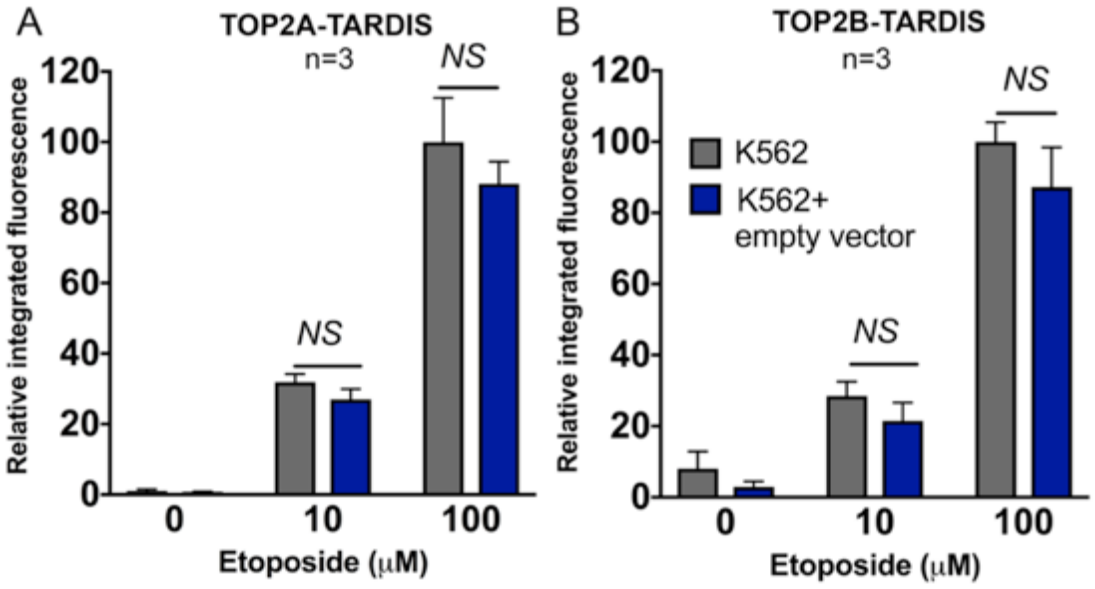


C

| Cell line | TARDIS Assay | Etoposide /μM | %+ve control | SEM | Sig (*P*-value) |
|---|---|---|---|---|---|
| K562 | TOP2A | 10 | 31.9 | 2.3 | |
| Empty vector | TOP2A | 10 | 27.0 | 2.9 | 0.960 |
| K562 | TOP2A | 100 | 100.0 | 15.5 | |
| Empty vector | TOP2A | 100 | 88.2 | 6.3 | 0.670 |
| K562 | TOP2B | 10 | 28.5 | 4.0 | |
| Empty vector | TOP2B | 10 | 21.5 | 5.2 | 0.890 |
| K562 | TOP2B | 100 | 100.0 | 5.5 | |
| Empty vector | TOP2B | 100 | 87.2 | 11.1 | 0.600 |

**Figure 4.8. K562 cells transfected with an empty plasmid vector does not alter etoposide-stabilised TOP2-DNA complexes.** K562 cells were transfected with a p-CMV-6 empty plasmid vector. Parental K562 cells and K562 transfected cells were treated with etoposide (10μM or 100μM), or a vehicle control for 1hr. TOP2-DNA covalent complexes were quantified using antibodies specific to TOP2A (A) or TOP2B (B). (C) Supporting table to show the percentage values relative to the mean value obtained with 100μM etoposide and significance values obtained for the difference between the control and empty vector drug treatments. Data are expressed relative to the mean value obtained for parental K562 cells treated with 100μM etoposide ±S.E.M. Statistical analysis was performed by the one-way ANOVA with post hoc Tukey's multiple comparison test.

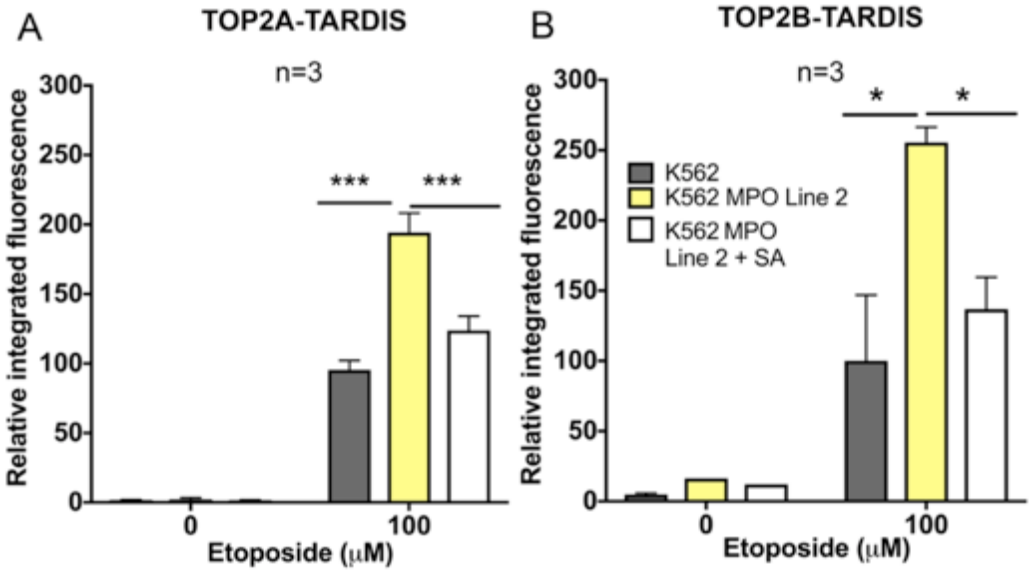


C

| Cell line | Pre-treatment | TARDIS Assay | Etoposide /μM | %+ve control | SEM | Sig (*P*-value) | % reduction by SA |
|---|---|---|---|---|---|---|---|
| K562 | None | TOP2A | 100 | 100 | 3.2 | | |
| K562-line 2 | None | TOP2A | 100 | 191.8 | 16.0 | <0.001 | 51.6 |
| K562-line 2 | SA | TOP2A | 100 | 93.3 | 2.6 | <0.001 | |
| K562 | None | TOP2B | 100 | 100 | 46.8 | | |
| K562-line 2 | None | TOP2B | 100 | 255.5 | 10.9 | <0.001 | 46.4 |
| K562-line 2 | SA | TOP2B | 100 | 136.9 | 22.8 | <0.001 | |

**Figure 4.9. SA reduces the level of etoposide stabilised TOP2-DNA covalent complexes in K562$^{MPO}$ cell line 2.** K562 $^{MPO}$ cell line 2 was pre-incubated in the presence or absence of SA (200μM 48hr) followed by the treatment with 100μM etoposide, or a vehicle control for 1hr. TOP2-DNA complex levels were analysed using the TARDIS assay for (A) TOP2A or (B) TOP2B. (C) Percentage values relative to the mean value obtained for 100μM etoposide in the absence of SA and significance of the difference between the control (non SA treated K562 $^{MPO}$ cell line 2) and SA treated K562 $^{MPO}$ cell line 2. Data are expressed relative to the mean of parental K562 treated with 100μM etoposide ±S.E.M. Statistical analysis was performed by the one-way ANOVA with post hoc Tukey's multiple comparison test. *$P$<0.05; ***$P$<0.001.

A limitation in the stable transfection of MPO expression into K562 cells was the silencing of the expression construct. Figure. 4.10.A-B shows cells three weeks after the selection of K562$^{MPO}$ cell line 6, this clone displayed a reduction in MPO expression and activity (*P=0.023*) compared to immediately after selection. The MPO silenced Line 6 was tested in the TARDIS assay and the silenced Line 6 did not differ in the level of etoposide stabilised complexes compared to parental K562 cells for either TOP2A or TOP2B (Figure. 4.10.C-E). Taken together, the data generated in the K562 derived MPO expressing cell lines and NB4 cells supports the hypothesis

that active MPO protein has a role in enhancing etoposide stabilised TOP2-DNA complexes.

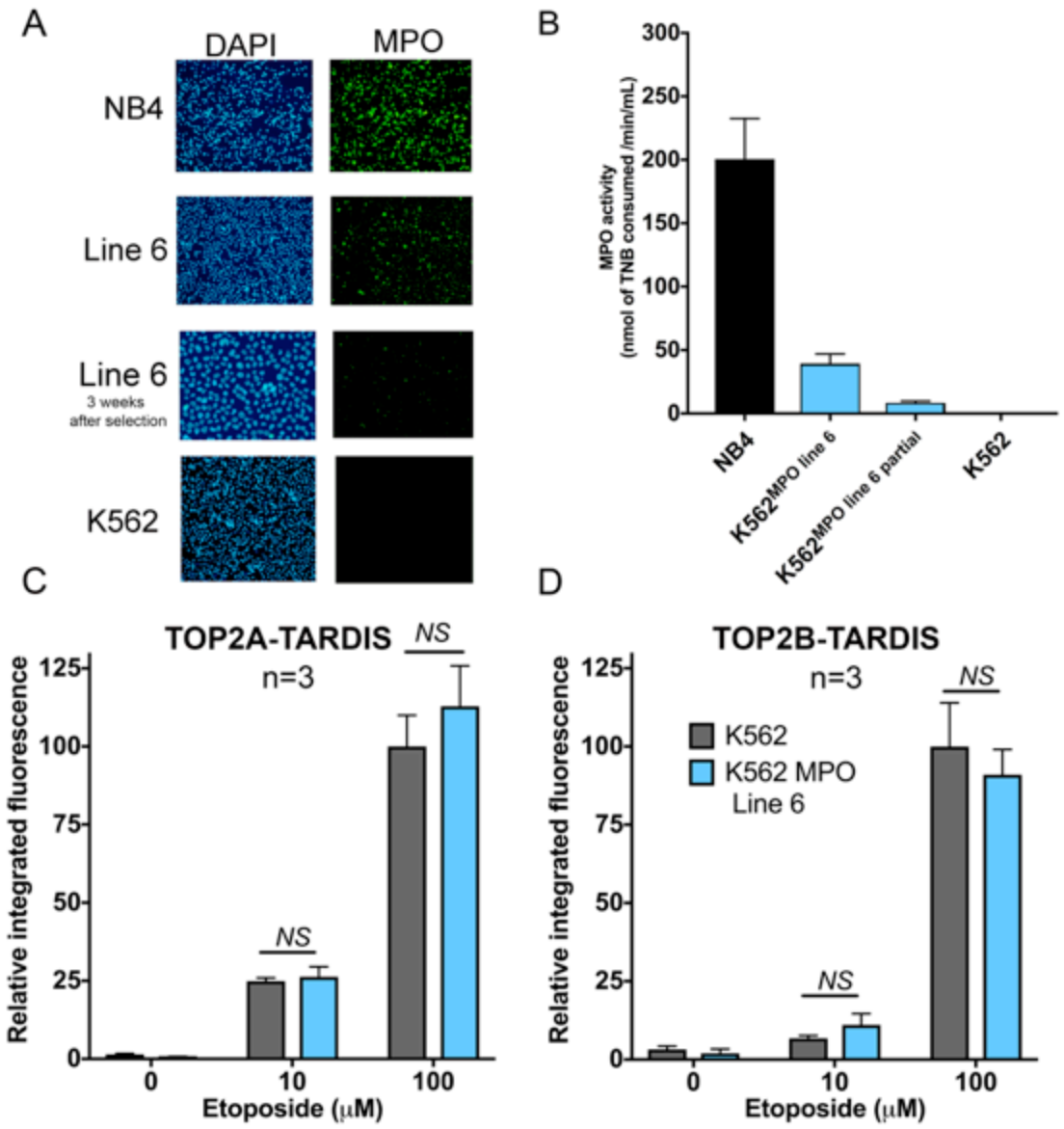


E

| Cell line | TARDIS Assay | Etoposide/ μM | %+ve control | SEM | Sig (*P*-value) |
|---|---|---|---|---|---|
| K562 | TOP2A | 10 | 24.9 | 1 | |
| K562-line 6 | TOP2A | 10 | 26.2 | 3.3 | 0.999 |
| K562 | TOP2A | 100 | 100 | 10 | |
| K562-line 6 | TOP2A | 100 | 113 | 13 | 0.747 |
| K562 | TOP2B | 10 | 6.7 | 0.9 | |
| K562-line 6 | TOP2B | 10 | 11 | 3.6 | 0.982 |
| K562 | TOP2B | 100 | 100 | 14 | |
| K562-line 6 | TOP2B | 100 | 91 | 8.1 | 0.865 |

**Figure 4.10. Silencing of the MPO expression construct in K562 cells results in a comparable level of etoposide stabilised TOP2-DNA complexes to parental K562 cells.** Comparison of (A) MPO immunofluorescence and (B) MPO activity in NB4, K562 $^{MPO}$ cell line 6 and K562 cell line 6 three weeks after selection. (C-D) K562 and K562$^{MPO}$ cell line 6 (three week after selection) were treated with etoposide or vehicle control for 1hr and processed for the level of TOP2A (C) and TOP2B (D) complexes. (E) Supporting table to show mean percentage values of integrated fluorescence obtained relative to the mean value of 100μM etoposide in K562 cells and the significance values between parental K562 and K562 cell line 6 three weeks after selection. Data are expressed relative to the mean value obtained for parental K562 cells treated with 100μM etoposide ±S.E.M. Statistical analysis was performed by the one-way ANOVA with post hoc Tukey's multiple comparison test.

### *4.3.3 MPO expression enhances mitoxantrone stabilised TOP2 covalent complexes*

The previous section demonstrated MPO-dependent stimulation of etoposide induced TOP2-DNA covalent complex accumulation. Next, the effect of MPO on TOP2 DNA complex formation by the anthracenedione, mitoxantrone was studied using the TARDIS assay. NB4 cells were pre-treated with 200μM SA for 48hr to inhibit MPO activity. SA pre-treatment in NB4 cells substantially reduced the level of mitoxantrone-stabilised complexes compared to control cells (Figure.4.11.A-D), reducing the level of complexes across the cell population (Figure.4.11A-B). At 0.5μM mitoxantrone, SA pre-treatment reduced TOP2A complexes by 49% (*P<0.001*) and by 50% (*P=0.020*) for TOP2B, for 1μM the figures were 31% (*P<0.001*) and 46% (*P<0.001*) respectively (Figure.4.11.E) This supports the hypothesis that active MPO protein enhances mitoxantrone stabilisation of TOP2-DNA complexes.

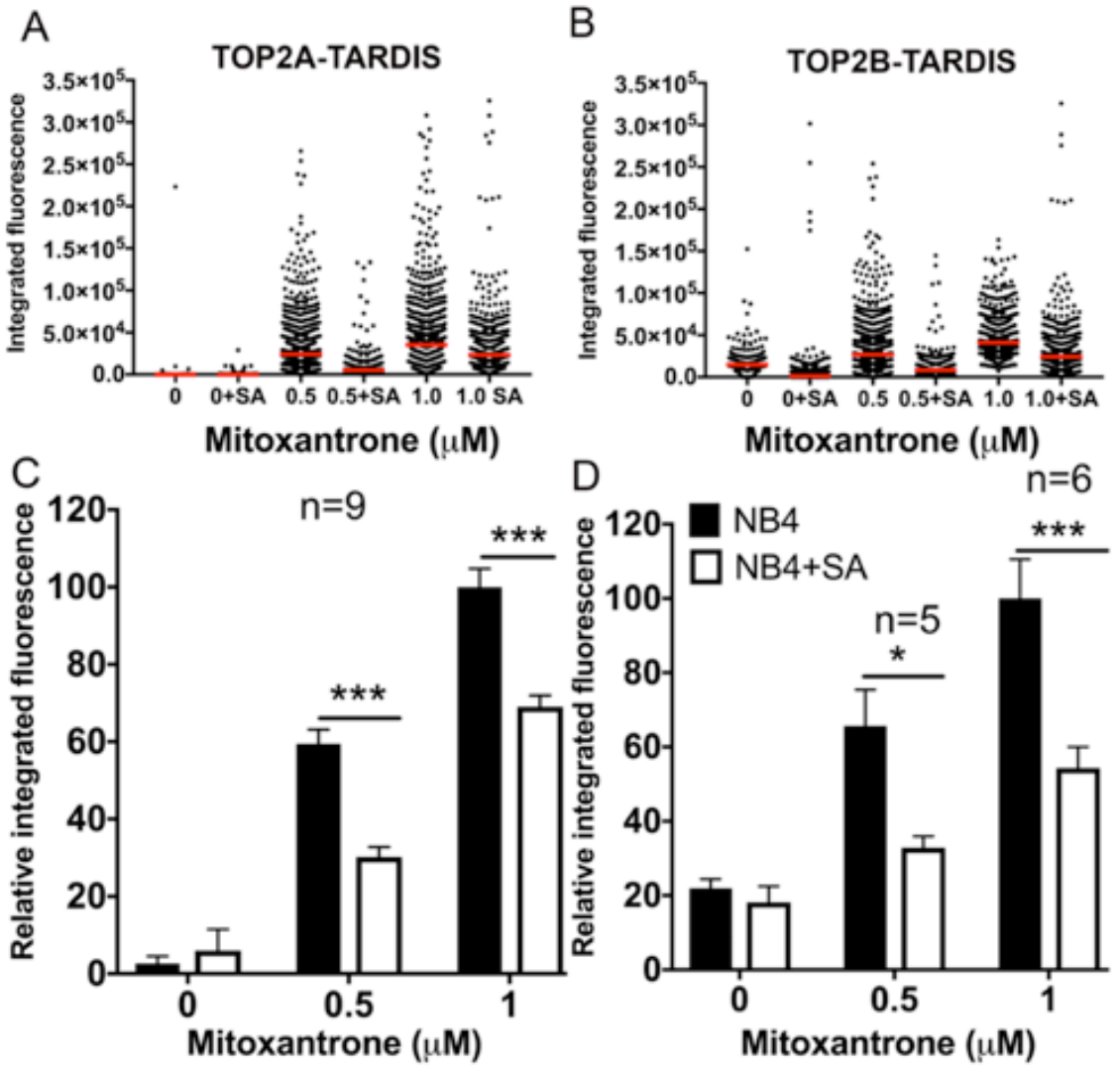


E

| Cell line | TARDIS Assay | Pre-treatment | Mitoxantrone /μM | %+ve control | SEM | Sig (*P*-value) | % reduction by SA |
|---|---|---|---|---|---|---|---|
| NB4 | TOP2A | None | 0.5 | 59.43 | 3.7 | | |
| NB4 | TOP2A | SA | 0.5 | 30.21 | 2.6 | <0.001 | 49.2 |
| NB4 | TOP2A | None | 1 | 100 | 4.8 | | |
| NB4 | TOP2A | SA | 1 | 69.1 | 2.9 | <0.001 | 31 |
| NB4 | TOP2B | None | 0.5 | 65.6 | 9.8 | | |
| NB4 | TOP2B | SA | 0.5 | 32.8 | 3.1 | 0.020 | 50 |
| NB4 | TOP2B | None | 1 | 100 | 10.5 | | |
| NB4 | TOP2B | SA | 1 | 54.3 | 5.7 | <0.001 | 45.7 |

**Figure 4.11. MPO inhibition reduces the level of mitoxantrone stabilised TOP2A and TOP2B-DNA complexes.** NB4 cells were pre-incubated in presence or absence of 200μM SA for 48hrs followed by a 1hr treatment with mitoxantrone (0.5 or 1μM). TOP2-DNA covalent complexes were quantified for (A&C) TOP2A or (B&D) TOP2B. A-B represents data obtained from a single experiment with at least 600 nuclei analysed per treatment. Data from additional experiments were combined using median values (red line) and represented in figures C-D for TOP2A or TOP2B respectively and expressed relative to the mean value obtained with 1μM mitoxantrone in the absence of SA ± S.E.M.. (E) Percentage values are expressed relative to the mean value obtained with 1μM mitoxantrone in the absence of SA and significance (Sig) values are shown for the difference between control and SA pretreatment. Statistical analysis was performed by the one-way ANOVA with post hoc Tukey's multiple comparison test. **P*<0.05 and ****P*<0.001.

TOP2B gives a noticeable TARDIS signal in non-drug treated cells. Therefore, the non-drug treated levels were subtracted from the mitoxantrone treated values for both TOP2A and TOP2B. The data processed in this way is shown in Figure 4.12. After subtraction of the signal obtained in untreated cells, TOP2A and TOP2B complexes reduced by 59% (*P<0.001*) and 67% (*P=0.043*) with 0.5μM mitoxantrone in SA treated cells, and with 1μM mitoxantrone complexes reduce by 37% (*P<0.001*) and 64% (*P=0.003*) (Figure.4.12 A-C). Additionally, the level of stabilised complexes with 1μM mitoxantrone in SA pre-treated cells were comparable to the level of complexes stabilised at 0.5μM mitoxantrone in non-SA treated cells for both TOP2A (*P=0.253*) and TOP2B (*P=0.695*).

As expected, SA pre-treatment in K562 cells did not alter the level of mitoxantrone-stabilised complexes (Figure.4.13.A-B). The effect of mitoxantrone-stabilised complexes in the $K562^{MPO}$ cell line 2 was tested. Line 2 exhibits MPO activity of 37.3 nmol TNB/consumed/min/mL which is 18% compared to NB4 cells (Table.4.1) Treatment with 1μM mitoxantrone induced a 54% (*P<0.001*) and 60% (*P=0.021*) increase in TOP2A and TOP2B complexes in $K562^{MPO}$ cell line 2 compared to parental K562 cells (Figure. 4.14.A-C). This further supports the idea that MPO increases mitoxantrone stabilised TOP2-DNA complexes.

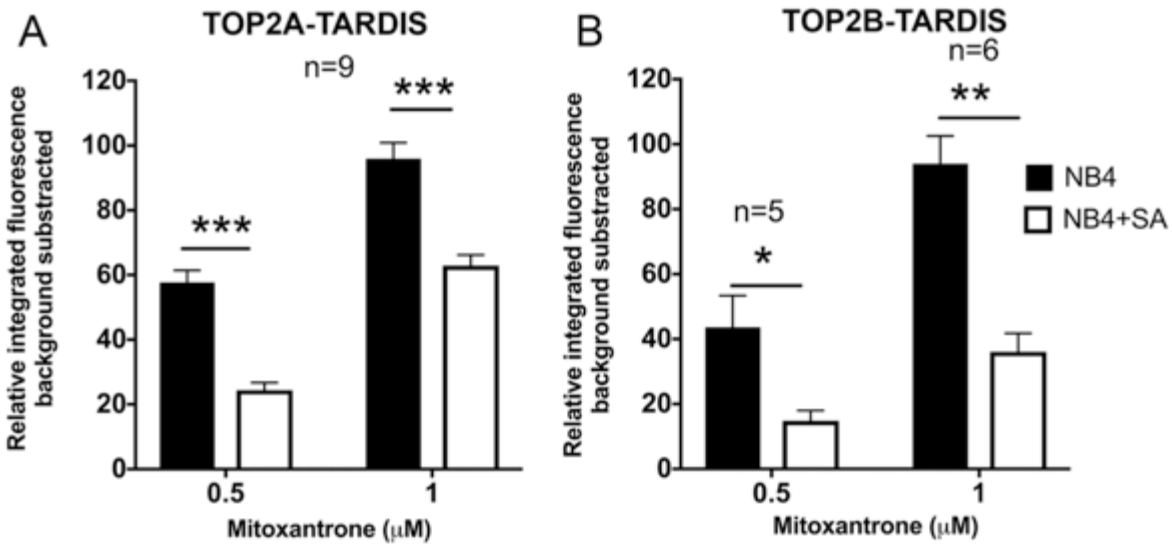


C

| Cell line | TARDIS Assay | Pre-treatment | Mitoxantrone /μM | %+ve control | SEM | Sig (*P*-value) | % reduction by SA |
|---|---|---|---|---|---|---|---|
| NB4 | TOP2A | None | 0.5 | 57.44 | 4.3 | | |
| NB4 | TOP2A | SA | 0.5 | 24.41 | 2.3 | <0.001 | 57.5 |
| NB4 | TOP2A | None | 1 | 100 | 4.9 | | |
| NB4 | TOP2A | SA | 1 | 62.89 | 3.3 | <0.001 | 37.1 |
| NB4 | TOP2B | None | 0.5 | 43.63 | 9.8 | | |
| NB4 | TOP2B | SA | 0.5 | 14.84 | 3.1 | 0.043 | 67 |
| NB4 | TOP2B | None | 1 | 100 | 10.5 | | |
| NB4 | TOP2B | SA | 1 | 36.08 | 5.7 | 0.003 | 64 |

**Figure 4.12. Subtraction of non-drug treated levels: MPO inhibition reduces the level of mitoxantrone stabilised TOP2A and TOP2B-DNA complexes.** NB4 cells were pre-incubated in presence or absence of 200μM SA for 48hr followed by a 1hr treatment with mitoxantrone (0.5 or 1μM) and analysed for the level of drug-stabilised TOP2A- (A) or TOP2B- (B) DNA complexes. (C) Supporting table to show percentage values expressed relative to the mean value obtained with 1μM mitoxantrone in the absence of SA and significance (Sig) values are shown for the difference between control and SA pretreatment. Data are expressed relative to the mean value obtained with 1μM mitoxantrone after subtraction of non-drug treated integrated fluorescence values, in the absence of SA ± S.E.M. Statistical analysis was performed by the one-way ANOVA with post hoc Tukey's multiple comparison test. **P*<0.05; ***P*<0.01; and ****P*<0.001.

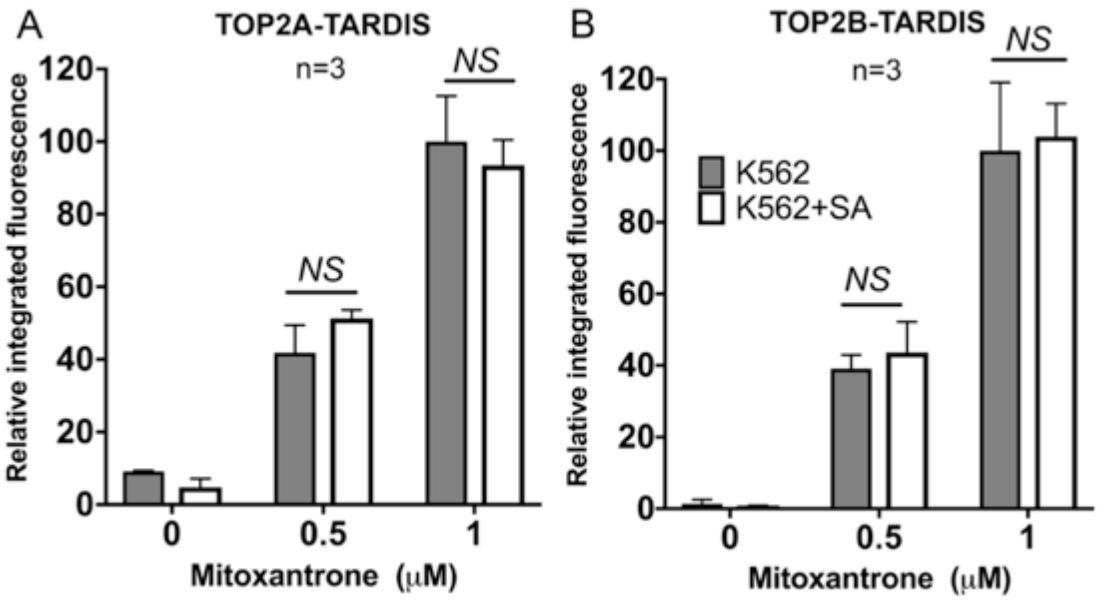


C

| Cell line | TARDIS Assay | Pre-treatment | Mitoxantrone /μM | %+ve control | SEM | Sig (*P*-value) |
|---|---|---|---|---|---|---|
| K562 | TOP2A | None | 0.5 | 41.8 | 7.6 | |
| K562 | TOP2A | SA | 0.5 | 51.3 | 2.3 | 0.888 |
| K562 | TOP2A | None | 1 | 100.0 | 12.6 | |
| K562 | TOP2A | SA | 1 | 93.5 | 7 | 0.967 |
| K562 | TOP2B | None | 0.5 | 39.1 | 3.9 | |
| K562 | TOP2B | SA | 0.5 | 43.6 | 8.6 | 0.998 |
| K562 | TOP2B | None | 1 | 100.0 | 19.1 | |
| K562 | TOP2B | SA | 1 | 104.0 | 9.2 | 0.999 |

**Figure 4.13. SA does not alter the level of mitoxantrone stabilised TOP2-DNA complexes in K562 cells (a non-MPO expressing cell line).** Cells were pre-incubated with 200μM SA for 48hr followed by 1hr incubation with mitoxantrone (0.5μM or 1.0μM), or a vehicle control. TOP2A (A) or TOP2B (B)-DNA covalent complexes were quantified as specified using the TARDIS assay. (C) Supporting table to show percentage values are expressed relative to the mean value obtained with 1μM mitoxantrone in the absence of SA and significance (Sig) values are shown for the difference between control and SA pretreatment. Data are expressed relative to the mean value obtained with 1μM mitoxantrone in the absence of SA ± S.E.M. Statistical analysis was performed by the one-way ANOVA with post hoc Tukey's multiple comparison test.

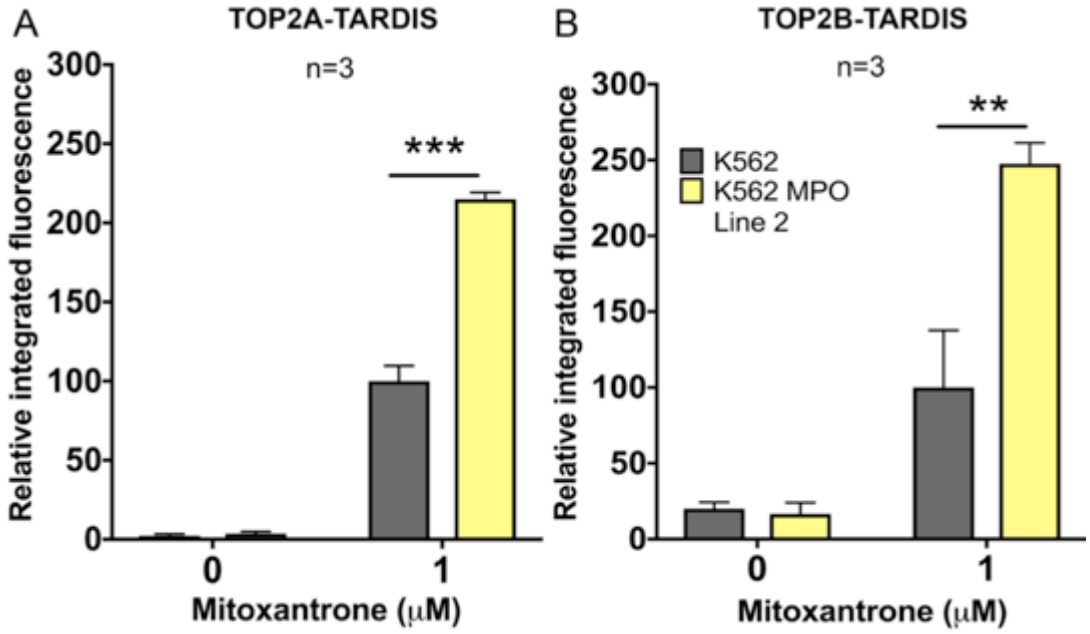


C

| Cell line | TARDIS Assay | Mitoxantrone /μM | %+ve control | SEM | Sig (*P*-value) | % increase compared to K562 |
|---|---|---|---|---|---|---|
| K562 | TOP2A | 1 | 100 | 9.8 | | |
| K562-line 2 | TOP2A | 1 | 214.9 | 4.3 | <0.001 | 53.5 |
| K562 | TOP2B | 1 | 100 | 37.8 | | |
| K562-line 2 | TOP2B | 1 | 247.6 | 13.8 | 0.021 | 60 |

**Figure 4.14. Active MPO expression in K562 cells enhances mitoxantrone stabilised TOP2-DNA covalent complexes.** Parental K562 cells and K562$^{MPO}$ line 2 were treated with 1μM mitoxantrone or a vehicle control for 1hr. TOP2A (A) and TOP2B (B) DNA covalent complexes were quantified using the TARDIS assay. (C) Percentage values relative to the mean value obtained for parental K562 cells treated with 1μM mitoxantrone and significance values show the difference between K562 and K562$^{MPO}$ line. Data are expressed relative to the mean value obtained for 1μM mitoxantrone in parental K562 cells ±S.E.M. Statistical analysis was performed by the Students t-test.***P*<0.01; ****P*<0.001

### *4.3.4 MPO increases the level of etoposide induced DNA double strand breaks.*

Etoposide elicits the induction of γH2Ax formation in cells, which indicates the processing of stabilised TOP2-DNA complexes to DNA double strand breaks (DSB) (Soubeyrand *et al.*, 2010; Sunter *et al.*, 2010; Cowell *et al.*, 2011; Cowell *et al.*, 2012; Álvarez-Quilón *et al.*, 2014). The γH2Ax assay is commonly used as a surrogate for DNA DSB formation and was employed here to quantify DSB formation following TOP2 poison addition (method described in section 2.11).

For each experiment, the γH2Ax integrated fluorescence values were determined per nucleus. Data were then calculated for the mean of the median values (red line)

obtained from at least three biological replicates using this assay (Figure.4.15.A). Etoposide exposure induces a dose-dependent increase in γH2Ax (Figure.4.15.A-B). Pre-treatment of NB4 cells with SA reduced the level of etoposide induced γH2Ax formation by 51% at 100μM etoposide (*P<0.001*), but had no significant effect at lower etoposide doses (Figure.4.15.B-C). The γH2Ax signal after SA pre-treatment at 100μM etoposide was equivalent to the γH2Ax signal obtained at 10μM etoposide in the absence of SA (*P>0.999*). SA treatment alone did not alter the level of basal γH2Ax signal obtained in cells (Figure.4.15.B). The basal level of γH2Ax signal is thought to be due to DSBs caused during normal cell cellular progresses (McManus and Hendzel, 2005; An *et al.*, 2010). The addition of SA to K562 cells did not affect the level of etoposide-induced γH2Ax at either 10μM (*P>0.999*) or 100μM (*P=0.992*) etoposide treatment, suggesting the effect seen with SA pre-treatment is due to the inhibition of MPO activity (Figure. 4.16. A-B).

To further support the finding obtained in NB4 cells, the $K562^{MPO}$ cell lines 4, 5 and 6 were treated with 10μM or 100μM etoposide and processed for the detection of γH2Ax formation (Figure. 4.17). At 10μM etoposide, all three $K562^{MPO}$ cell lines had significantly higher levels of γH2Ax signal compared to parental K562 cells with $K562^{MPO}$ cell lines 5 and 6 producing more than 50% higher γH2Ax signal than parental cells (*P<0.001* and *P=0.005* respectively). At 100μM etoposide, only line 5 produced a significant increase of 19% in γH2Ax signal intensity (*P=0.020*) (Figure. 4.17A-B). However, it was observed the level γH2Ax signal reaches saturation by 100μM etoposide treatment in K562 cells (Figure.4.18). Therefore, it was not surprising that lines 4 and 6 did not show an elevated signal with 100μM etoposide as the γH2Ax signal had reached saturation.

The empty vector K562 control line was also tested for γH2Ax formation after treatment with 10μM or 100μM etoposide. This cell line had a level of γH2Ax fluorescence comparable to non-transfected K562 cells at both 10μM (*P>0.999*) and 100μM etoposide (*P=0.930*) (Figure.4.19.A-B). The data generated supports the idea that active MPO expression increases the DNA damage caused by etoposide in cells.

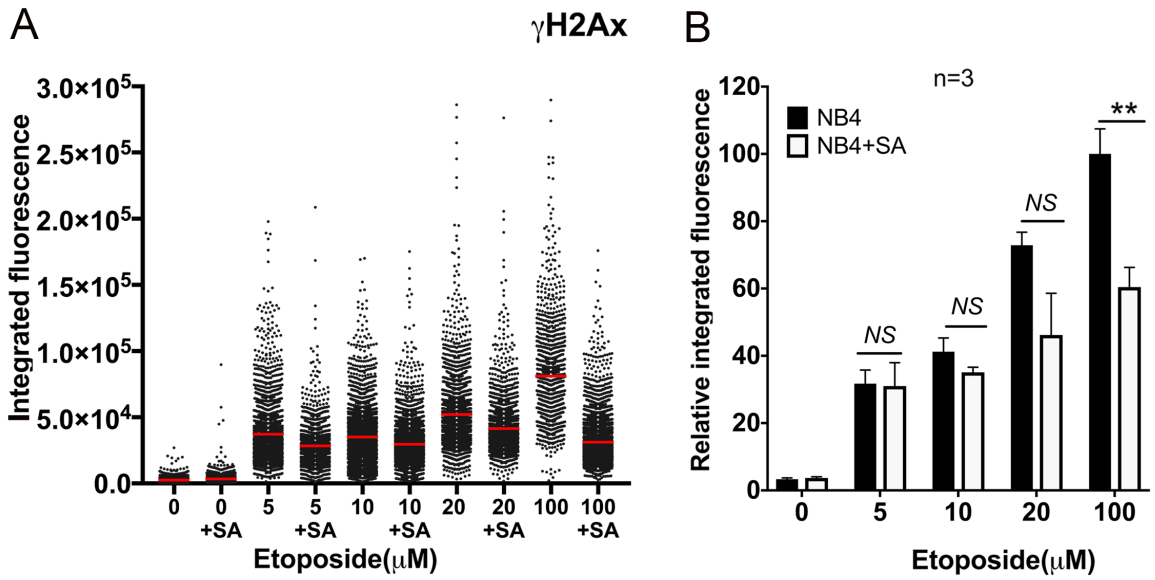


C

| Cell line | Assay | Pre-treatment | Etoposide /μM | %+ve control | SEM | Sig (*P*-value) | % reduction by SA |
|---|---|---|---|---|---|---|---|
| NB4 | γH2Ax | None | 5 | 31.7 | 4.1 | | |
| NB4 | γH2Ax | SA | 5 | 31 | 6.9 | >0.999 | 2.2 |
| NB4 | γH2Ax | None | 10 | 45.6 | 3 | | |
| NB4 | γH2Ax | SA | 10 | 35.1 | 1.5 | 0.880 | 23 |
| NB4 | γH2Ax | None | 20 | 69.4 | 5 | | |
| NB4 | γH2Ax | SA | 20 | 49.7 | 15 | 0.453 | 28.3 |
| NB4 | γH2Ax | None | 100 | 100 | 7.5 | | |
| NB4 | γH2Ax | SA | 100 | 48.2 | 4.7 | <0.001 | 51.2 |

**Figure 4.15. Inhibition of MPO reduces the level of etoposide induced global H2Ax phosphorylation at 100μM etoposide.** NB4 cells were pre-treated with SA (200 μM for 48hrs) followed by the treatment with etoposide (0-100μM) or a vehicle control and processed by immunofluorescence to quantify the level of H2Ax phosphorylation. (A) A single biological replicate experiment is shown for the γH2Ax phosphorylation obtained per nucleus (a minimum of 2000 cells were analysed per treatment), data from additional biological experiments were combined using median values (red line) obtained (see section 2.14). (B) Data are expressed relative to the mean value of NB4 cells treated with 100μM etoposide ±S.E.M in the absence of SA. (C) Supporting table to show percentage values expressed relative to the mean value obtained with 100μM etoposide in the absence of SA and significance (Sig) values are shown for the difference between control and SA pretreatment. Statistical analysis was performed by the one-way ANOVA with post hoc Tukey's multiple comparison test. ****P*<0.001.

A

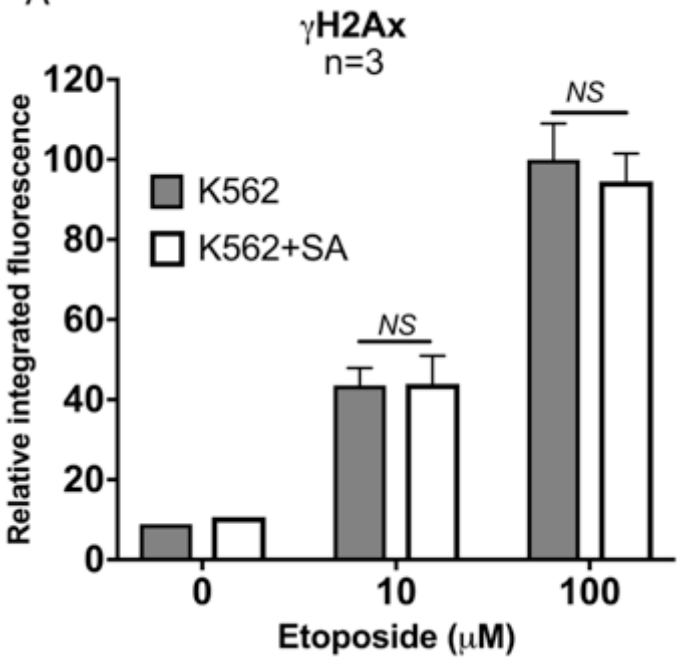


B

| Cell line | Assay | Pre-treatment | Etoposide/ μM | %+ve control | SEM | Sig (*P*-value) |
|---|---|---|---|---|---|---|
| K562 | γH2Ax | None | 10 | 43.6 | 4.4 | |
| K562 | γH2Ax | SA | 10 | 43.9 | 7.0 | >0.999 |
| K562 | γH2Ax | None | 100 | 100.0 | 9.0 | |
| K562 | γH2Ax | SA | 100 | 94.5 | 7.0 | 0.992 |

**Figure 4.16. SA does not alter the level of etoposide induced H2Ax phosphorylation in non-MPO expressing cells.** K562 cells were incubated with 200μM of SA for 48hr followed by the treatment with etoposide or a solvent control (DMSO 0.02%(v/v)). Cells were processed as previously described to detect the level H2Ax phosphorylation.(B) Supporting table to show percentage values expressed relative to the mean value obtained with 100μM etoposide in the absence of SA and significance (Sig) values are shown for the difference between control and SA pretreatment. Data are expressed relative to the mean value obtained with 100μM etoposide in non-SA treated K562 cells ±S.E.M. Statistical analysis was performed by the one-way ANOVA with post hoc Tukey's multiple comparison test.

A

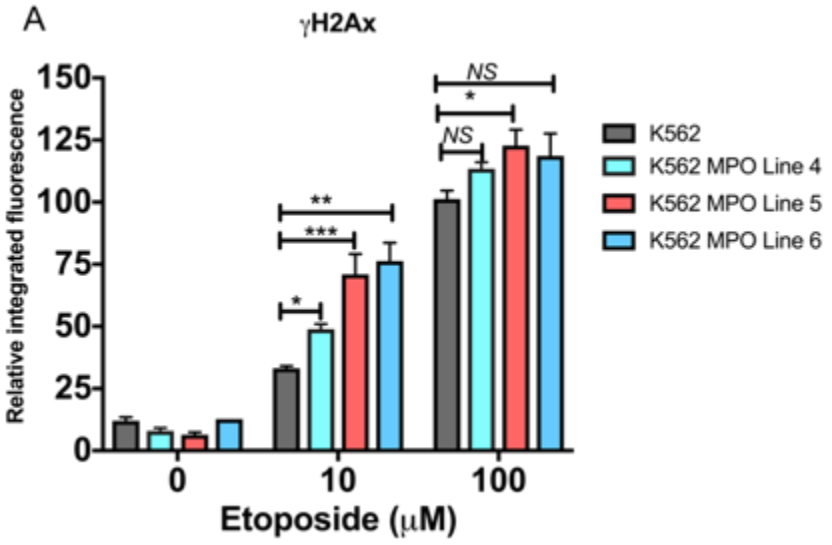


B

| Cell line | Assay | Etoposide /μM | %+ve control | SEM | Sig (*P*-value) | %increase compared to K562 |
|---|---|---|---|---|---|---|
| K562 | γH2Ax | 10 | 33.2 | 0.9 | | |
| K562-line 4 | γH2Ax | 10 | 48.8 | 2.1 | 0.035 | 31.9 |
| K562-line 5 | γH2Ax | 10 | 71.0 | 20.0 | <0.001 | 53.2 |
| K562-line 6 | γH2Ax | 10 | 76.4 | 7.3 | 0.005 | 56.6 |
| K562 | γH2Ax | 100 | 100.0 | 3.4 | | |
| K562-line 4 | γH2Ax | 100 | 113.4 | 2.7 | 0.970 | 11.8 |
| K562-line 5 | γH2Ax | 100 | 122.8 | 6.3 | 0.020 | 18.6 |
| K562-line 6 | γH2Ax | 100 | 118.6 | 9.0 | 0.650 | 15.7 |

**Figure 4.17. Active MPO Expression increases etoposide-induced global H2Ax phosphorylation.** K562 and K562$^{MPO}$ cell lines 4,5 and 6 were treated with etoposide (10μM or 100μM), or a vehicle control for 1hr. Etoposide-induced H2Ax phosphorylation was quantified by immunofluorescence. (B) Table shows the percentage values relative to 100μM etoposide obtained for parental K562 cells and significance values compare between parental K562 cells to K562$^{MPO}$ cell lines. Data are expressed relative to the mean value obtained with 100μM etoposide for parental K562 cells ±S.E.M. Statistical analysis was performed by the one-way ANOVA with post hoc Tukey's multiple comparison test. **P*<0.05; ***P*<0.01; and ****P*<0.001.

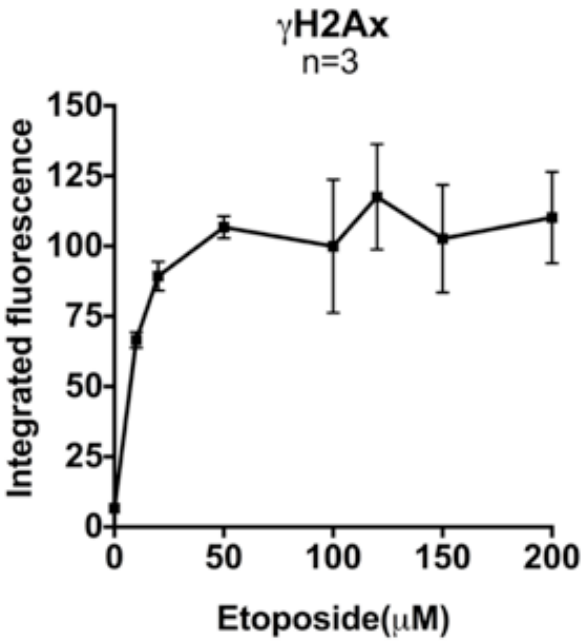


**Figure 4.18. Etoposide-induced H2Ax phosphorylation plateaus at 50μM.** K562 cells were treated with etoposide (0,10,20,50,100 and 200μM) or a vehicle control for 1hr. Cells were quantified for the level of H2Ax fluorescence. Data are expressed as mean value obtained for 100μM etoposide ±S.E.M.

A

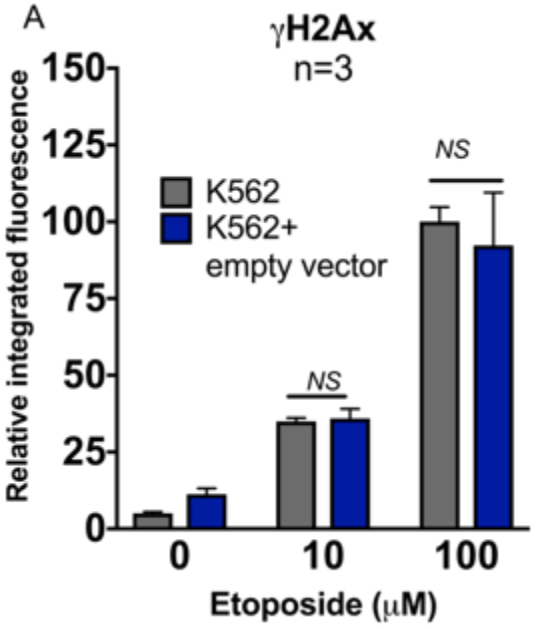


B

| Cell line | Assay | Etoposide /μM | %+ve control | SEM | Sig (*P*-value) |
|---|---|---|---|---|---|
| K562 | γH2Ax | 10 | 34.9 | 1.1 | |
| Empty vector | γH2Ax | 10 | 36.0 | 3.1 | >0.999 |
| K562 | γH2Ax | 100 | 100.0 | 4.7 | |
| Empty vector | γH2Ax | 100 | 92.3 | 17.3 | 0.930 |

**Figure 4.19. K562 cells transfected with an empty vector have comparable level of H2Ax phosphorylation to parental cells.** K562 and K562 cells transfected with an empty plasmid vector (K562+empty vector) were treated with etoposide (10μM or 100μM), or a vehicle control for 1hr. Etoposide-induced γH2Ax phosphorylation was quantified. (B) Supporting table shows the percentage values relative to 100μM etoposide obtained for parental K562 cells, significance values are shown for the difference between K562 cells and K562+empty vector. Data are expressed relative to the mean value obtained with 100μM etoposide for parental K562 cells ±S.E.M. Statistical analysis was performed by the one-way ANOVA with post hoc Tukey's multiple comparison test.

### *4.3.5 MPO increases mitoxantrone induced γH2Ax formation.*

Mitoxantrone mediated DNA damage initiates γH2Ax formation (Huang *et al.*, 2003). Analogous experiments to those performed etoposide were carried out for mitoxantrone to detect γH2Ax phosphorylation in NB4 cells. Mitoxantrone produced a dose dependent increase in γH2Ax formation up to 1μM mitoxantrone (Figure 4.20), with a decrease in signal intensity observed from 10μM, mirroring the trend observed for TOP2-DNA complex stabilisation (Figure. 4.4.A-D).

H2Ax phosphorylation was quantified in cells exposed to 0.5μM or 1μM mitoxantrone in the presence or absence of SA (to inhibit MPO). Pretreatment with SA in NB4 cells reduced the mitoxantrone induced γH2Ax formation by 40% at 1μM (*P<0.001*), resulting in a γH2Ax signal which is comparable to 0.5μM mitoxantrone treatment in non-pretreated NB4 cells (*P=0.673*) (Figure.4.21.A-B). In addition, SA pre-treatment did not alter the mitoxantrone induced γH2Ax formation in K562 cells (Figure.4.22). This data supports the idea that MPO has a role in mitoxantrone mediated DNA damage.

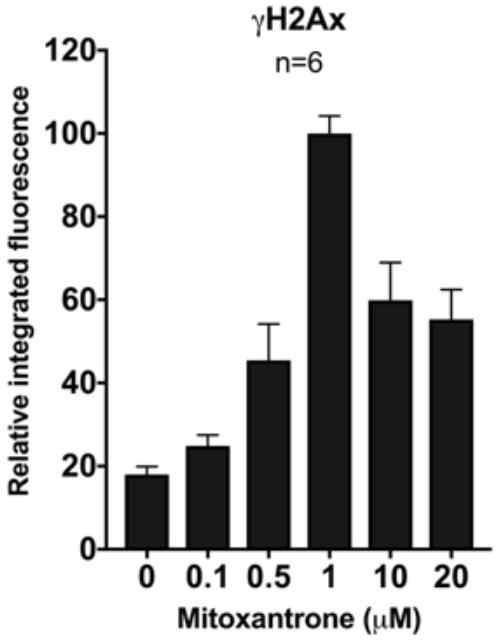


**Figure 4.20. Mitoxantrone induces H2Ax phosphorylation in NB4 cells.** Cells were treated with mitoxantrone (dose specified) or a vehicle control for 1hr. Cells were then analysed for the level of H2Ax phosphorylation by quantitative immunofluorescence (a surrogate measure for DNA double strand breaks). Data are expressed relative to 1μM mitoxantrone ±S.E.M.

A

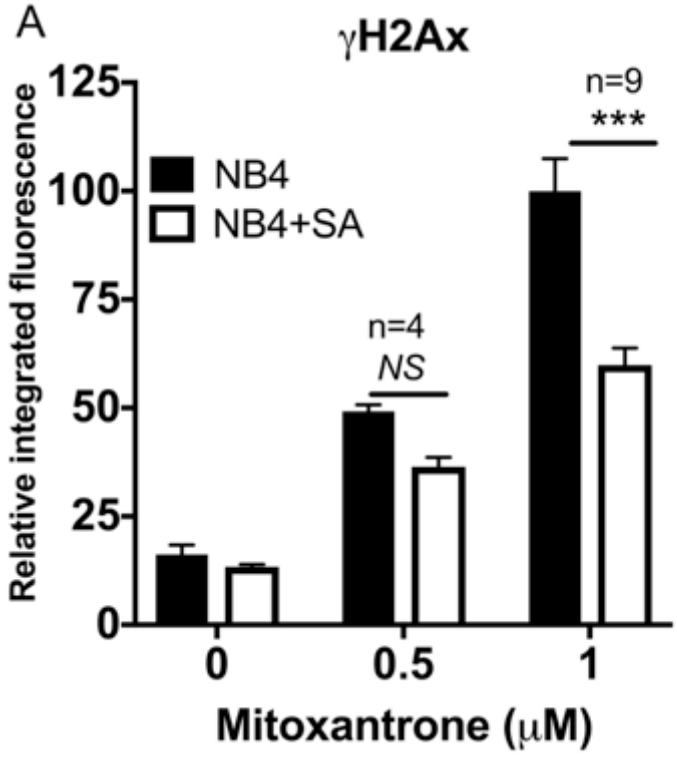


B

| Cell line | Assay | Pre-treatment | Mitoxantrone /μM | %+ve control | SEM | Sig (*P*-value) | % reduction by SA |
|---|---|---|---|---|---|---|---|
| NB4 | γH2Ax | None | 0.5 | 49.3 | 1.5 | | |
| NB4 | γH2Ax | SA | 0.5 | 36.4 | 2.2 | 0.692 | 26.2 |
| NB4 | γH2Ax | None | 1 | 100.0 | 7.5 | | |
| NB4 | γH2Ax | SA | 1 | 59.9 | 3.9 | <0.001 | 40.1 |

**Figure 4.21. Inhibition of MPO reduces H2Ax phosphorylation at a higher dose of mitoxantrone.** NB4 cells were pre-incubated with 200μM SA for 48hr followed by the treatment with mitoxantrone (0.5μM or 1.0μM) or a vehicle control for 1hr. Mitoxantrone induced H2Ax phosphorylation was quantified by immunofluorescence. (B) Percentage values are expressed relative to the mean value obtained with 1μM mitoxantrone in the absence of SA and significance (Sig) values are shown for the difference between control and SA pretreatment. Data are expressed relative to 1μM mitoxantrone in the absence of SA ±S.E.M. Statistical analysis was performed by the one-way ANOVA with post hoc Tukey's multiple comparison test. ****P*<0.001.

A

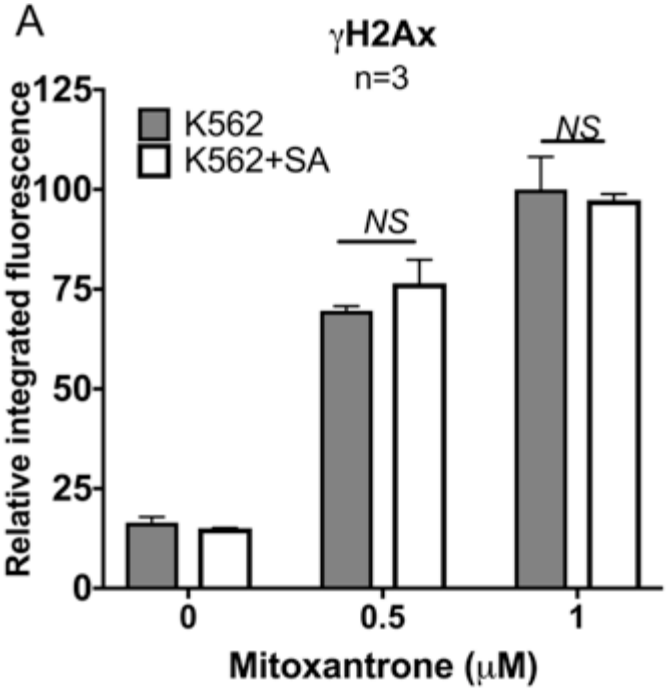


B

| Cell line | Assay | Pre-treatment | Mitoxantrone/ μM | %+ve control | SEM | Sig (*P*-value) |
|---|---|---|---|---|---|---|
| K562 | γH2Ax | None | 0.5 | 69.6 | 1.3 | |
| K562 | γH2Ax | SA | 0.5 | 76.4 | 5.9 | 0.780 |
| K562 | γH2Ax | None | 1 | 100.0 | 8.2 | |
| K562 | γH2Ax | SA | 1 | 97.3 | 1.5 | 0.980 |

**Figure 4.22. SA does not alter mitoxantrone induced H2Ax phosphorylation in non-MPO expressing cells.** K562 cells were pre-incubated with 200μM of SA for 48hr followed by the treatment with mitoxantrone (0.5μM or 1μM), or vehicle controls for 1hr. γH2Ax signals were quantified by immunofluorescence. (B) Percentage values are expressed relative to the mean value obtained with 100μM etoposide in the absence of SA and significance (Sig) values are shown for the difference between control and SA pretreatment. Data are expressed relative to the mean obtained with 1μM mitoxantrone in the absence of SA ±S.E.M. Statistical analysis was performed by the one-way ANOVA with post hoc Tukey's multiple comparison test.

### *4.3.6 Direct inhibition of MPO significantly reduces mitoxantrone and etoposide mediated TOP2 DNA damage.*

The data presented above in this chapter has shown the impact of active MPO expression on TOP2 poison induced TOP2-DNA complex and γH2Ax formation. However, the work conducted in NB4 cells employed the heam biosynthesis inhibitor SA to modulate MPO activity. Recently two specific MPO inhibitors; PF1355 and MPOi-II have become commercially available. PF1355 and MPOi-II were used in NB4 cells to test whether direct inhibition of MPO could reduce TOP2-DNA complex stabilisation and γH2Ax formation following exposure with etoposide or mitoxantrone. Optimal concentrations of PF1355 and MPOi-II to inhibit MPO in NB4 cells were determined as shown in section 3.3.7. To inhibit MPO either 10μM PF1355 or 5μM MPOi-II were added to NB4 cells for 4 hours prior to TOP2 poison addition. These doses of inhibitors were shown to significantly reduce MPO enzymatic activity whilst having minimal effect on cell growth or TOP2 levels (see section 3.3.7). Following drug removal, analysis of stabilised TOP2-DNA complexes using the TARDIS assay or DSB formation using γH2Ax detection by quantitative immunofluorescence were conducted.

The addition of MPO inhibitors suppresses etoposide induced TOP2A- and TOP2B-DNA complex formation, the magnitude of reduction being more prominent for TOP2B (Figure.4.23.A-B), following a similar trend to that observed with SA (Figure.4.5.A-D). At 100μM etoposide treatment, TOP2B-DNA complexes reduced by 47% in PF1355 treated cells (*P<0.001*) and by 58% with MPOi-II (*P<0.001*) (Figure.4.23.E). Notably the level of stabilised TOP2B complexes at 100μM etoposide in the presence of MPO inhibitors were comparable to the TARDIS signal obtained with 10μM etoposide in the absence of inhibitors (*P=0.144* and *P=0.797* for PF1355 and MPOi-II respectively). For TOP2A the reduction in stabilised complexes was 21% with PF1355 (*P<0.001*) and 18% with MPOi-II (*P<0.001*) in the presence of 100μM etoposide. Prior treatment with PF1355 or MPOi-II reduced the level of mitoxantrone stabilised TOP2-DNA complexes (Figure.4.23.C-D). With 1μM mitoxantrone, the addition of PF1355 reduced the level of TOP2A-DNA complexes by 46% (*P=0.005*), for MPOi-II the reduction was 52% (*P<0.001*) (Figure.4.23.C-D). For TOP2B the addition of PF1355 or MPOi-II reduced the level of complexes by 50% (*P<0.001*) and 53% (*P<0.001*) respectively with 1μM mitoxantrone treatment.

With 0.5μM mitoxantrone the level of TOP2B complexes reduced by 39% for both PF1355 and MPOi-II (Figure.4.23C-F).

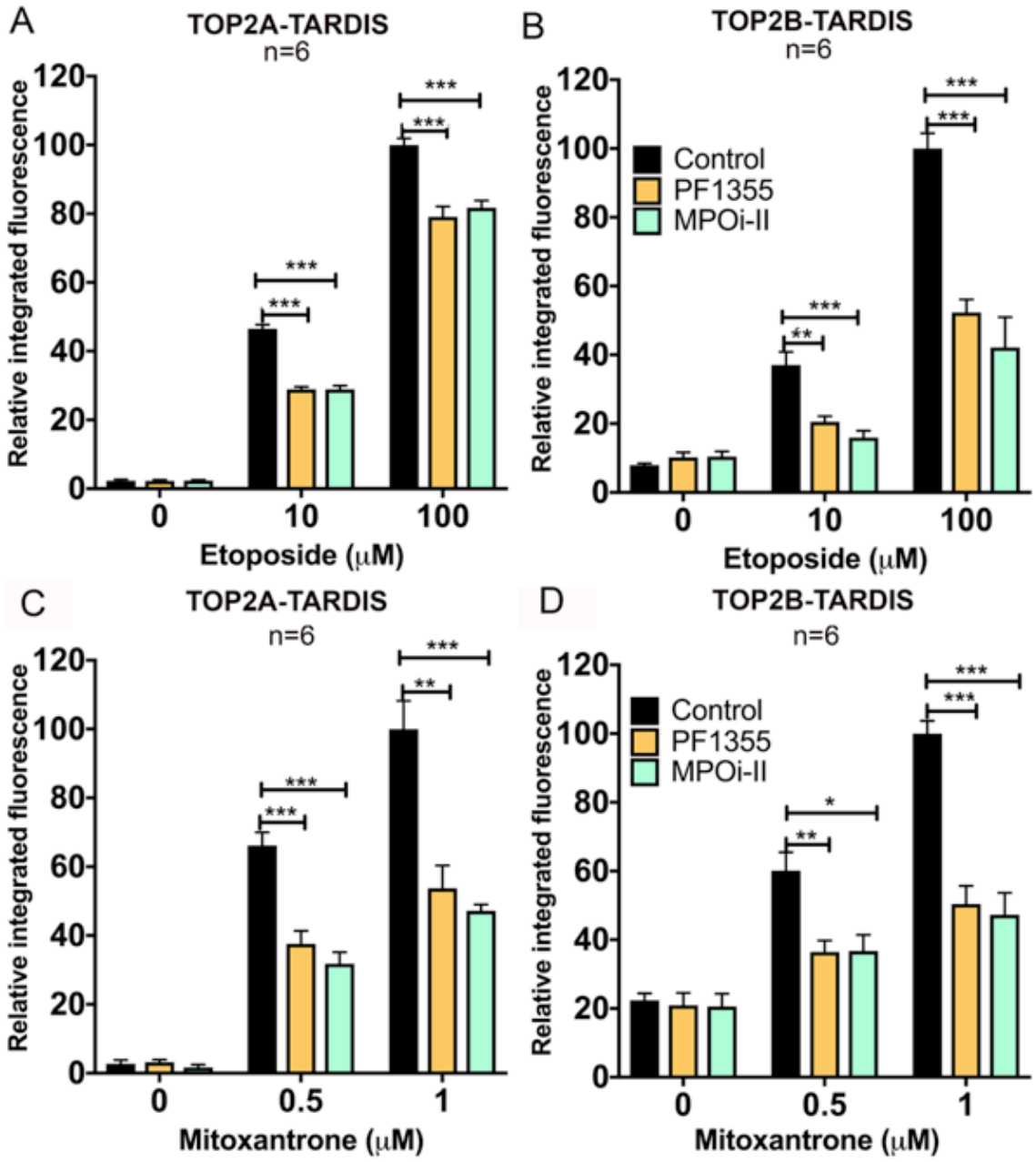


**Figure 4.23. Direct MPO inhibition reduces etoposide or mitoxantrone (C-D) stabilised TOP2-DNA complexes.** NB4 cells were pre-treated with MPO inhibitors PF1355 (10μM 4hr) or MPOi-II (5μM 4hr) or neither before adding etoposide (10μM or 100μM) (A,B) or mitoxantrone (0.5μM or 1μM) for 1hr or a vehicle control. TOP2 poison stabilised TOP2-DNA complexes were quantified by TARDIS for TOP2A (A&C) or TOP2B (B&D). Data are expressed relative to the mean of 100μM etoposide obtained from untreated NB4 cells (black bars) ±S.E.M. Statistical analysis was performed by the one-way ANOVA with post hoc Tukey's multiple comparison test. *$P$<0.05; **$P$<0.01; ***$P$<0.001. (E-F) Supporting tables on next page to show the percentage values expressed relative the mean value obtained for 100μM etoposide (E) or 1μM mitoxantrone (F) in non-pretreated NB4 cells and significance values compare non-pretreated NB4 cells to inhibitor treated cells for each specified drug dose.

E

| Cell line | TARDIS Assay | Pre-treatment | Etoposide /μM | %+ve control | SEM | Sig (*P*-value) | % decrease with MPO inhibitors |
|---|---|---|---|---|---|---|---|
| NB4 | TOP2A | None | 10 | 46.5 | 1.2 | | |
| NB4 | TOP2A | PF1355 | 10 | 28.9 | 0.8 | <0.001 | 37.8 |
| NB4 | TOP2A | MPOi-II | 10 | 28.8 | 1.0 | <0.001 | 38.1 |
| NB4 | TOP2A | None | 100 | 100.0 | 1.9 | | |
| NB4 | TOP2A | PF1355 | 100 | 79.1 | 3.0 | <0.001 | 20.9 |
| NB4 | TOP2A | MPOi-II | 100 | 81.7 | 2.1 | <0.001 | 18.3 |
| NB4 | TOP2B | None | 10 | 37.0 | 3.9 | | |
| NB4 | TOP2B | PF1355 | 10 | 20.5 | 1.6 | <0.01 | 44.6 |
| NB4 | TOP2B | MPOi-II | 10 | 15.9 | 2.0 | <0.001 | 57 |
| NB4 | TOP2B | None | 100 | 100.0 | 4.5 | | |
| NB4 | TOP2B | PF1355 | 100 | 52.3 | 3.8 | <0.001 | 46.8 |
| NB4 | TOP2B | MPOi-II | 100 | 42.2 | 8.8 | <0.001 | 57.8 |

F

| Cell line | TARDIS Assay | Pre-treatment | Mitoxantrone /μM | %+ve control | SEM | Sig (*P*-value) | % decrease with MPO inhibitors |
|---|---|---|---|---|---|---|---|
| NB4 | TOP2A | None | 0.5 | 66.1 | 3.9 | | |
| NB4 | TOP2A | PF1355 | 0.5 | 37.6 | 3.9 | <0.001 | 43.1 |
| NB4 | TOP2A | MPOi-II | 0.5 | 31.8 | 3.3 | <0.001 | 51.9 |
| NB4 | TOP2A | None | 1 | 100.0 | 8.2 | | |
| NB4 | TOP2A | PF1355 | 1 | 53.7 | 6.6 | 0.005 | 46.3 |
| NB4 | TOP2A | MPOi-II | 1 | 47.2 | 1.8 | <0.001 | 52.8 |
| NB4 | TOP2B | None | 0.5 | 60.1 | 5.4 | | |
| NB4 | TOP2B | PF1355 | 0.5 | 36.5 | 3.3 | 0.005 | 39.3 |
| NB4 | TOP2B | MPOi-II | 0.5 | 36.7 | 4.7 | 0.042 | 38.9 |
| NB4 | TOP2B | None | 1 | 100.0 | 3.7 | | |
| NB4 | TOP2B | PF1355 | 1 | 50.4 | 5.3 | <0.001 | 50 |
| NB4 | TOP2B | MPOi-II | 1 | 47.3 | 6.4 | <0.001 | 52.7 |

As previously mentioned, TOP2B gives a noticeable TARDIS signal in non-drug treated cells therefore the non-drug treated levels were subtracted for TOP2B and TOP2A. After subtraction of the signal detected in non-drug treated cells, PF1355 treatment reduced TOP2A and TOP2B complexes by 45% (*P=0.005*) and 64% (*P=0.037*) at 0.5μM mitoxantrone and by 49% (*P<0.001*) and 76% (*P<0.001*) at 1μM mitoxantrone (Figure.4.24A-B). Similarly, in MPOi-II treated cells the figures were 54% (*P<0.001*) and 70% (*P=0.019*) at 0.5μM mitoxantrone for TOP2A and for

TOP2B and a reduction of 78% (*P<0.001*) and 77% (*P<0.001*) was observed for 1μM mitoxantrone (Figure.4.24A-C).

As seen with SA (Figure.4.15), the level of etoposide induced γH2Ax formation at 100μM was reduced by 45% (*P<0.001*) in PF1355 and 51% (*P<0.001*) in MPOi-II treated cells yet no significant difference was observed at 10μM etoposide (Figure 4.25.A and C). In contrast, MPO inhibition by PF1355 or MPOi-II reduced the levels of γH2Ax formation at 0.5μM and 1μM mitoxantrone (Figure.4.25B and D), whilst SA treatment only showed a significant reduction at 1μM mitoxantrone (Figure 4.21). PF1355 and MPOi-II had no effect on either etoposide or mitoxantrone induced TOP2 complex stabilisation or γH2Ax formation in the MPO non-expressing K562 cells (Figures. 4.26-27). Taken together the results generated using the MPO inhibitors, PF1355 and MPOi-II support the conclusions obtained using SA and $K562^{MPO}$ cell lines, that MPO enhances etoposide and mitoxantrone mediated damage.

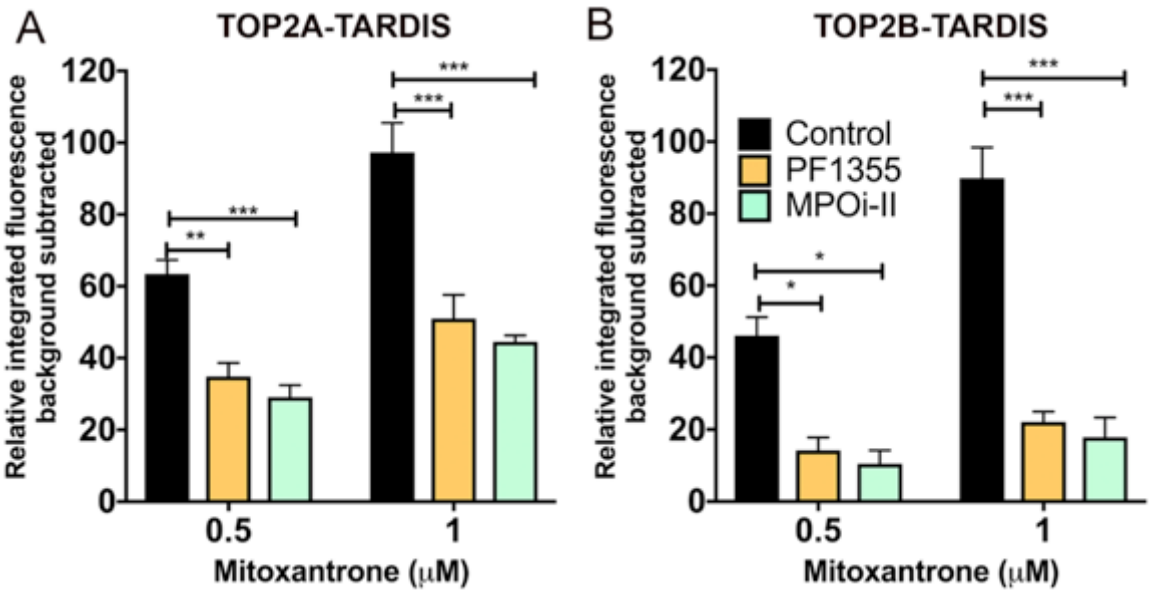


C

| Cell line | TARDIS Assay | Pre-treatment | Mitoxantrone /μM | %+ve control | SEM | Sig (*P*-value) | % decrease with MPO inhibitors |
|---|---|---|---|---|---|---|---|
| NB4 | TOP2A | None | 0.5 | 63.44 | 3.9 | | |
| NB4 | TOP2A | PF1355 | 0.5 | 34.88 | 3.9 | 0.005 | 45 |
| NB4 | TOP2A | MPOi-II | 0.5 | 29.12 | 3.3 | <0.001 | 54.1 |
| NB4 | TOP2A | None | 1 | 100 | 8.2 | | |
| NB4 | TOP2A | PF1355 | 1 | 51 | 6.6 | <0.001 | 49 |
| NB4 | TOP2A | MPOi-II | 1 | 22.51 | 1.8 | <0.001 | 77.5 |
| NB4 | TOP2B | None | 0.5 | 40.09 | 5.4 | | |
| NB4 | TOP2B | PF1355 | 0.5 | 14.59 | 4.9 | 0.037 | 63.6 |
| NB4 | TOP2B | MPOi-II | 0.5 | 12.05 | 4.7 | 0.019 | 70 |
| NB4 | TOP2B | None | 1 | 95.39 | 4.7 | | |
| NB4 | TOP2B | PF1355 | 1 | 23.22 | 4.1 | <0.001 | 75.7 |
| NB4 | TOP2B | MPOi-II | 1 | 22 | 7.4 | <0.001 | 77 |

**Figure 4.24. Non-drug treated levels subtracted: Direct inhibition of MPO reduces the level of mitoxantrone stabilised TOP2A and TOP2B-DNA complexes.** NB4 cells were pre-treated with MPO inhibitors PF1355 (10μM 4hr) or MPOi-II (5μM 4hr) or neither before the adding mitoxantrone (0.5μM or 1μM) for 1 hr. TOP2 poison stabilised TOP2-DNA complexes were quantified by TARDIS for TOP2A (A) and TOP2B (B). (C) Supporting tables to show the percentage values expressed relative the mean value obtained for 1μM mitoxantrone non-pretreated NB4 cells and significance values compare non-pretreated NB4 cells to inhibitor treated cells for each specified drug dose. Data are expressed relative to the mean of 1μM mitoxantrone after non-drug treated levels were subtracted ±S.E.M. Statistical analysis was performed by the one-way ANOVA with post hoc Tukey's multiple comparison test. **P*<0.05; ***P*<0.01; ****P*<0.001.

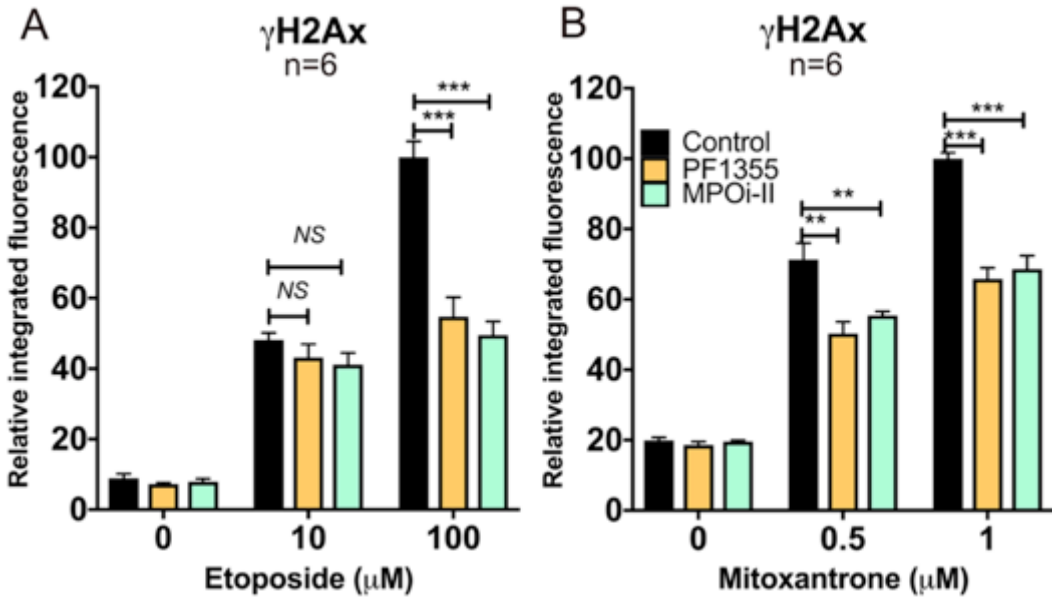


C

| Cell line | Assay | Pre-treatment | Etoposide /μM | %+ve control | SEM | Sig (*P*-value) | % decrease with MPO inhibitors |
|---|---|---|---|---|---|---|---|
| NB4 | γH2Ax | None | 10 | 48.1 | 2 | | |
| NB4 | γH2Ax | PF1355 | 10 | 43.2 | 3.7 | >0.999 | 10.2 |
| NB4 | γH2Ax | MPOi-II | 10 | 41.1 | 3.3 | >0.999 | 14.6 |
| NB4 | γH2Ax | None | 100 | 100 | 4.5 | | |
| NB4 | γH2Ax | PF1355 | 100 | 54.7 | 5.6 | <0.001 | 45.3 |
| NB4 | γH2Ax | MPOi-II | 100 | 49.5 | 3.9 | <0.001 | 50.5 |

D

| Cell line | Assay | Pre-treatment | Mitoxantrone /μM | %+ve control | SEM | Sig (*P*-value) | % decrease with MPO inhibitors |
|---|---|---|---|---|---|---|---|
| NB4 | γH2Ax | None | 0.5 | 71.3 | 4.7 | | |
| NB4 | γH2Ax | PF1355 | 0.5 | 50.3 | 3.4 | 0.010 | 29.5 |
| NB4 | γH2Ax | MPOi-II | 0.5 | 55.4 | 1.2 | 0.009 | 15.9 |
| NB4 | γH2Ax | None | 1 | 100 | 1.7 | | |
| NB4 | γH2Ax | PF1355 | 1 | 65.8 | 3.2 | <0.001 | 34.2 |
| NB4 | γH2Ax | MPOi-II | 1 | 68.7 | 3.8 | <0.001 | 31.3 |

**Figure 4.25. PF1355 and MPOi-II protect against etoposide and mitoxantrone induced H2Ax phosphorylation**. Cells were pre-treated with either PF1355 (10μM 4hr) or MPOi-II (5μM 4hr) followed by the treatment with etoposide (10μM or 100μM) (A) or mitoxantrone (0.5μM or 1μM) (B) for 1hr or a vehicle control and processed for detection of H2Ax phosphorylation. Data are expressed relative to the mean of 100μM etoposide (black bars) (A) or 1μM mitoxantrone (B) ±S.E.M. Statistical analysis was performed by the one-way ANOVA with post hoc Tukey's multiple comparison test. ***P*<0.01, ****P*<0.001. (C-D) Supporting tables to show the percentage values expressed relative the mean value obtained for 100μM etoposide (C) or 1μM mitoxantrone (D) in non-pretreated NB4 cells and significance values compare non-pretreated NB4 cells to inhibitor treated cells for each specified drug dose.

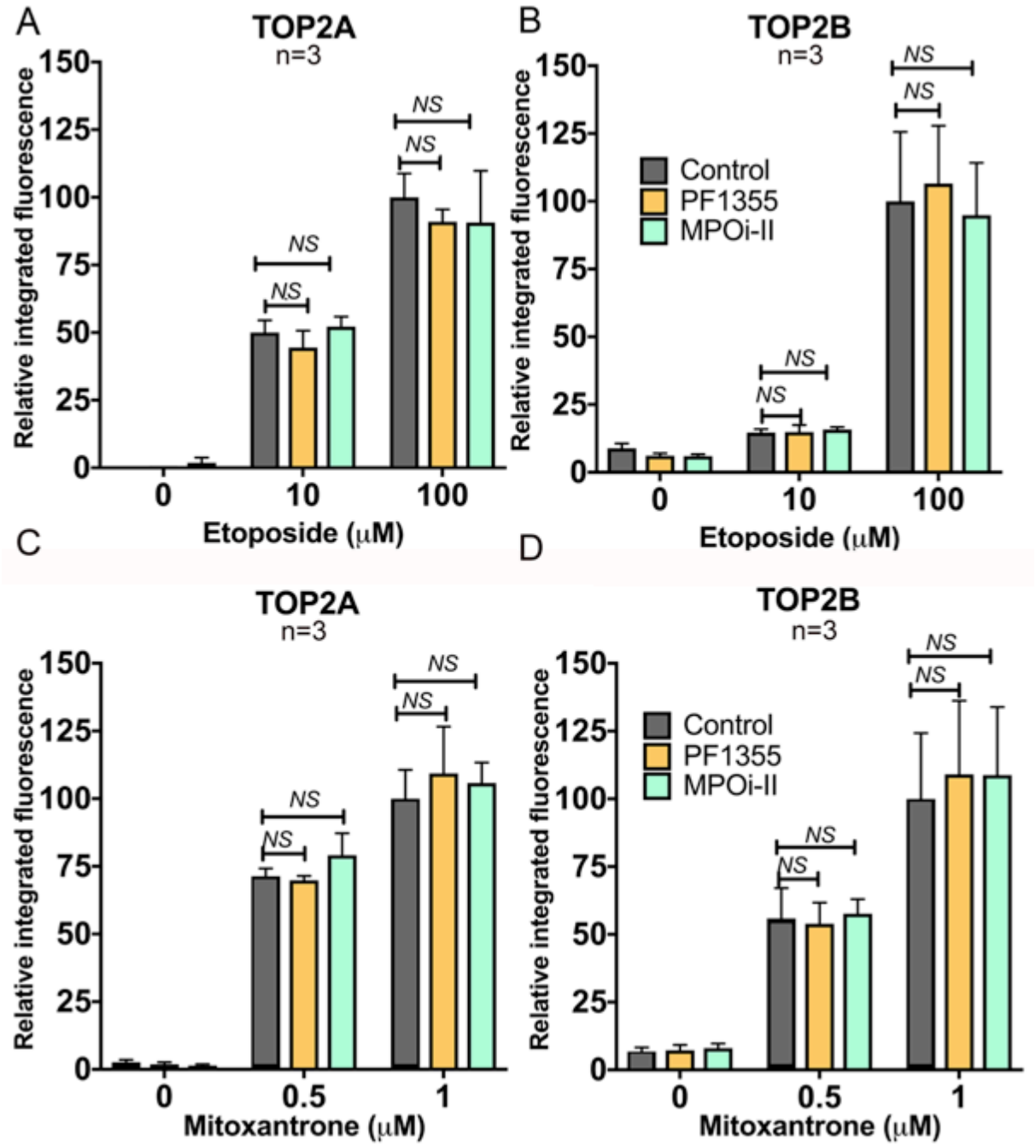
A
TOP2A
n=3
Relative integrated fluorescence
150
125
100
75
50
25
0
NS
NS
NS
NS
0
10
100
Etoposide (μM)
B
TOP2B
n=3
Relative integrated fluorescence
Control
PF1355
MPOi-II
NS
NS
NS
NS
0
10
100
Etoposide (μM)
C
TOP2A
n=3
Relative integrated fluorescence
NS
NS
NS
NS
0
0.5
1
Mitoxantrone (μM)
D
TOP2B
n=3
Relative integrated fluorescence
Control
PF1355
MPOi-II
NS
NS
NS
NS
0
0.5
1
Mitoxantrone (μM)

E

| Cell line | TARDIS Assay | Pre-treatment | Etoposide /μM | %+ve control | SEM | Sig (*P*-value) |
|---|---|---|---|---|---|---|
| K562 | TOP2A | None | 10 | 50 | 4.5 | |
| K562 | TOP2A | PF1355 | 10 | 44.4 | 6.3 | >0.999 |
| K562 | TOP2A | MPOi-II | 10 | 52.2 | 3.7 | >0.999 |
| K562 | TOP2A | None | 100 | 100 | 8.8 | |
| K562 | TOP2A | PF1355 | 100 | 91 | 4.7 | >0.999 |
| K562 | TOP2A | MPOi-II | 100 | 90.7 | 19.1 | >0.999 |
| K562 | TOP2B | None | 10 | 14.7 | 1.3 | |
| K562 | TOP2B | PF1355 | 10 | 14.8 | 2.6 | >0.999 |
| K562 | TOP2B | MPOi-II | 10 | 15.8 | 0.9 | >0.999 |
| K562 | TOP2B | None | 100 | 100 | 25.6 | |
| K562 | TOP2B | PF1355 | 100 | 106.6 | 213 | >0.999 |
| K562 | TOP2B | MPOi-II | 100 | 94.8 | 19.4 | >0.999 |

F

| Cell line | TARDIS Assay | Pre-treatment | Mitoxantrone / μM | %+ve control | SEM | Sig (*P*-value) |
|---|---|---|---|---|---|---|
| K562 | TOP2A | None | 0.5 | 71.3 | 2.9 | |
| K562 | TOP2A | PF1355 | 0.5 | 69.9 | 1.6 | >0.999 |
| K562 | TOP2A | MPOi-II | 0.5 | 79.07 | 8.1 | >0.999 |
| K562 | TOP2A | None | 1 | 100 | 10.7 | |
| K562 | TOP2A | PF1355 | 1 | 105.8 | 7.5 | >0.999 |
| K562 | TOP2A | MPOi-II | 1 | 109.3 | 17.3 | >0.999 |
| K562 | TOP2B | None | 0.5 | 55.9 | 11.2 | |
| K562 | TOP2B | PF1355 | 0.5 | 53.9 | 7.8 | >0.999 |
| K562 | TOP2B | MPOi-II | 0.5 | 57.6 | 5.4 | >0.999 |
| K562 | TOP2B | None | 1 | 100 | 25.3 | |
| K562 | TOP2B | PF1355 | 1 | 110.5 | 27.2 | >0.999 |
| K562 | TOP2B | MPOi-II | 1 | 105.3 | 25.1 | >0.999 |

**Figure 4.26. PF1355 and MPOi-II do not affect etoposide (A&B) or mitoxantrone (C&D) stabilised TOP2-DNA complexes in non-MPO expressing cells.** K562 cells were pre-treated with MPO inhibitors PF1355 (10μM 4hr) or MPOi-II (5μM 4hr) or neither before the adding etoposide (10μM or 100μM) or mitoxantrone (0.5μM or 1μM) for 1 hr or a vehicle control. TOP2 poison stabilised TOP2-DNA complexes were quantified by TARDIS for TOP2A (A) and TOP2B (B). Data are expressed relative to the mean of 100μM etoposide (A&B) or 1μM mitoxantrone (C&D) for non-treated K562 cells (grey bars) ±S.E.M. Statistical analysis was performed by the one-way ANOVA with post hoc Tukey's multiple comparison test. (E-F) Supporting tables to show the percentage values expressed relative the mean value obtained for 100μM etoposide (E) or 1μM mitoxantrone (F) in non-pretreated NB4 cells and significance values compare non-pretreated NB4 cells to inhibitor treated cells for each specified drug dose.

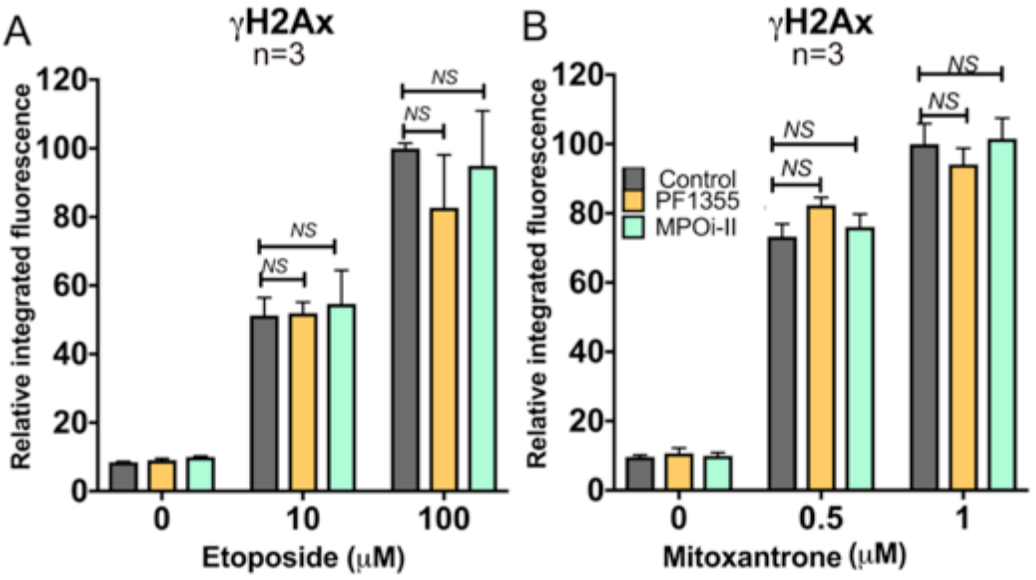


C

| Cell line | Assay | Pre-treatment | Etoposide/ μM | %+ve control | SEM | Sig (*P*-value) |
|---|---|---|---|---|---|---|
| K562 | γH2Ax | None | 10 | 55.3 | 4.3 | |
| K562 | γH2Ax | PF1355 | 10 | 54.1 | 2.3 | >0.999 |
| K562 | γH2Ax | MPOi-II | 10 | 57.4 | 10.2 | >0.999 |
| K562 | γH2Ax | None | 100 | 100 | 2.1 | |
| K562 | γH2Ax | PF1355 | 100 | 80.3 | 15.4 | >0.999 |
| K562 | γH2Ax | MPOi-II | 100 | 95.3 | 14.6 | >0.999 |

D

| Cell line | Assay | Pre-treatment | Mitoxantrone/ μM | %+ve control | SEM | Sig (*P*-value) |
|---|---|---|---|---|---|---|
| K562 | γH2Ax | None | 0.5 | 73.2 | 3.7 | |
| K562 | γH2Ax | PF1355 | 0.5 | 82.4 | 2.2 | >0.999 |
| K562 | γH2Ax | MPOi-II | 0.5 | 76 | 3.7 | >0.999 |
| K562 | γH2Ax | None | 1 | 100 | 5.9 | |
| K562 | γH2Ax | PF1355 | 1 | 94.2 | 4.6 | >0.999 |
| K562 | γH2Ax | MPOi-II | 1 | 101.6 | 5.9 | >0.999 |

**Figure 4.27. Direct MPO inhibitors do not effect TOP2 poison induced H2Ax phosphorylation in non-MPO expressing cells.** K562 were pre-treated with either PF1355 (10μM 4hr) or MPOi-II (5μM 4hr) or neither followed by the treatment with etoposide (10μM or 100μM) (A) or mitoxantrone (0.5μM or 1μM) (B) for 1hr or a vehicle control and processed for the detection the of H2Ax phosphorylation. Data are expressed relative to the mean of 100μM etoposide (A) or 1μM mitoxantrone (B) ±S.E.M in non-pretreated cells. Statistical analysis was performed by the one-way ANOVA with post hoc Tukey's multiple comparison test. (C-D) Supporting tables to show the percentage values expressed relative the mean value obtained for 100μM etoposide (E) or 1μM mitoxantrone (F) in non-pretreated NB4 cells and significance values compare non-pretreated NB4 cells to inhibitor treated cells for each specified drug dose.

## 4.4 Discussion

In this study, the role of myeloperoxidase in enhancing etoposide and mitoxantrone-mediated DNA damage was investigated using three different cell-based systems. The first system employed SA to inhibit MPO activity in the MPO expressing cell-line NB4. In the second system, K562 cells that do not express MPO were engineered to express MPO. Thirdly, new chemical inhibitors of MPO were used to reduce MPO activity in NB4 cells to further confirm the results generated using SA and in the MPO expressing K562 cell line. Two key assays were used, one to quantify TOP2-DNA complex levels (TARDIS assay) and one to measure the formation of DSB (γH2Ax assay) following exposure to etoposide or mitoxantrone in NB4 or K562 cells.

Myeloperoxidase can mediate the one or two-electron oxidation of etoposide to generate etoposide quinone via a phenoxyl-radical intermediate (Gantchev and Hunting, 1998). Previous studies have shown that etoposide quinone is a more effective TOP2 poison compared to etoposide, with greater potency towards the TOP2B isoform *in vitro* (Jacob *et al.*, 2011; Smith *et al.*, 2014b; Gibson *et al.*, 2016). In the cell line based work described here, the presence of active MPO increased the level of etoposide-stabilised complexes for both TOP2A and TOP2B (Figure.4.7A-B) and the inhibition of MPO resulted in a greater decrease in TOP2B complexes compared to TOP2A (Figure. 4.5A-D and Figure.4.23A-B). These results suggest the effect of MPO-dependent enhancement in etoposide-stabilised complexes formed in cellulo is due the production of etoposide quinone. To our knowledge, this is first time that the effect of MPO on etoposide-stabilised complexes has been investigated at a TOP2 isoform specific level. The results generated from the γH2Ax assay complemented the TARDIS data, showing MPO contributes to etoposide mediated γH2Ax formation in cells, an indication of the level of DSB in cells. In the presence of MPO, etoposide induced γH2Ax formation is likely to be due the contribution of DSB induced by etoposide, etoposide phenoxyl radical and etoposide quinone which stabilise the TOP2-DNA complexes that are subsequently processed to DSB using proteolytic and nucleolytic pathways. In addition, the methyl radical produced from the oxidation of etoposide to the phenoxyl radical, can directly lead to DNA strand breaks (Haim *et al.*, 1986; Augusto *et al.*, 1990).

While the results with etoposide can be explained by the MPO mediated biotransformation of etoposide to etoposide quinone, the situation is less clear for mitoxantrone. MPO mediates the oxidation of mitoxantrone to a naphthoquinoxaline metabolite, which is the intermediate species generated in the reaction (Panousis *et al.*, 1994; Panousis *et al.*, 1997). Naphthoquinoxaline can react covalently with DNA both in cell-free systems and in cells. The end reaction product of the MPO mediated reaction has not been determined which is partly due to instability of the unknown compound. Additionally, MPO can oxidise amino acids to produce reactive aldehydes, including formaldehyde. Mitoxantrone can be activated by formaldehyde to generate DNA adducts which can covalently adduct to the N2 exocyclic amino group of guanine (Anderson *et al.*, 1997; Hazen *et al.*, 1998; Parker *et al.*, 2004) (see section 1.3.2). However, it is unclear whether these mitoxantrone metabolites interact directly with TOP2. The data generated in this study shows the inhibition of MPO in NB4 cells significantly reduces mitoxantrone stabilised TOP2A and TOP2B complexes (Figure.4.11, 4.12 and 4.23C-D). Whereas exogenous expression of MPO in K562 cells resulted in a two-fold increase in mitoxantrone stabilised TOP2A and TOP2B complexes (Figure.4.14). Suggesting MPO mediates the biotransformation of mitoxantrone to metabolites that poison the catalytic cycle of TOP2, although the mechanism may be as result of DNA adducts or repair intermediates that can also result in TOP2 poisoning and the results presented here do not distinguish between these possibilities (Kingma *et al.*, 1995; Sabourin and Osheroff, 2000).

The use of the recently developed chemically distinct MPO inhibitors; PF1355 (Phase I clinical trials) and MPOi-II have further supported the conclusions drawn using SA and induction of exogenous expression of MPO into K562 cells. Pre-treatment with PF1355 or MPOi-II in NB4 cells resulted in a significant reduction in both TOP2-DNA complex stabilisation and γH2Ax formation upon exposure to etoposide or mitoxantrone (Figure 4.23A-D, 4.24A-B and 4.25A-B). This shows the potential of such compounds to be tailored into primary chemotherapy regimes to reduce genetic damage in myeloid progenitors.

The effect of MPO enhancement in TOP2 poison mediated DNA damage reported above, is likely due the presence of MPO in the nucleus (Murao *et al.*, 1988) as metabolites produced from the oxidation of etoposide and mitoxantrone are prone to be conjugated with glutathione (Blanz *et al.*, 1991; Mewes *et al.*, 1993; Kagan *et al.*,

1999; Zheng *et al.*, 2006). The effects of glutathione on TOP2 poison mediated damage are discussed in chapter 5.

# Chapter 5. The role of glutathione in TOP2 poison mediated DNA damage

## 5.1 Introduction

The peroxidase-mediated oxidation of etoposide or mitoxantrone leads to metabolites that contain high electrophilic centers (reactive quinone and quinone-diimine moieties) these can effectively react with thiol containing peptides/proteins and adduct DNA (Kolodziejczyk *et al.*, 1988; Blanz *et al.*, 1991; Gantchev and Hunting, 1997; Fan *et al.*, 2006; Vlasova *et al.*, 2011). However, in cells the effect of these reactive metabolites can be effectively dampened down by conjugation with reduced glutathione, thereby reducing intracellular damage including DNA damage (Mewes *et al.*, 1993; Kagan *et al.*, 1994; Gantchev and Hunting, 1997). Glutathione (L-γ-glutamyl-L-cysteinyl-glycine) is a major intracellular non-protein thiol present in cells at milli-molar concentrations serving to protect cells from oxidative damage and to detoxify xenobiotics (Chatterjee, 2013) (see section 1.4). Conjugation with glutathione occurs via the active thiol group (in the form of a cysteine residue), this reaction either occurs spontaneously or is catalysed by glutathione-*S*-transferase.

The MPO-mediated oxidation of etoposide yields etoposide quinone (Fan *et al.*, 2006; Zheng *et al.*, 2006) (Figure 5.1). Etoposide quinone may either intercalate into the TOP2-DNA binary complex (TOP2 poison) or interact with N-terminal clamp of TOP2 by adducting sulfhydryl residues and block the entry of DNA (TOP2 covalent poison) (Jacob *et al.*, 2011; Jacob *et al.*, 2013; Smith *et al.*, 2014b; Gibson *et al.*, 2016) (see section 1.3.1). Due to the presence of the 3' and 4' carbonyl groups on the E-ring, etoposide quinone can potentially react with any protein that contains a free sulfhydryl group modifying protein function. To overcome this, glutathione can conjugate with etoposide quinone producing etoposide-OH-6'-SG and/or etoposide-OH-2'-SG reducing the carbonyl groups of the E-ring to hydroxyls (Fan *et al.*, 2006; Zheng *et al.*, 2006) (Figure 5.1).

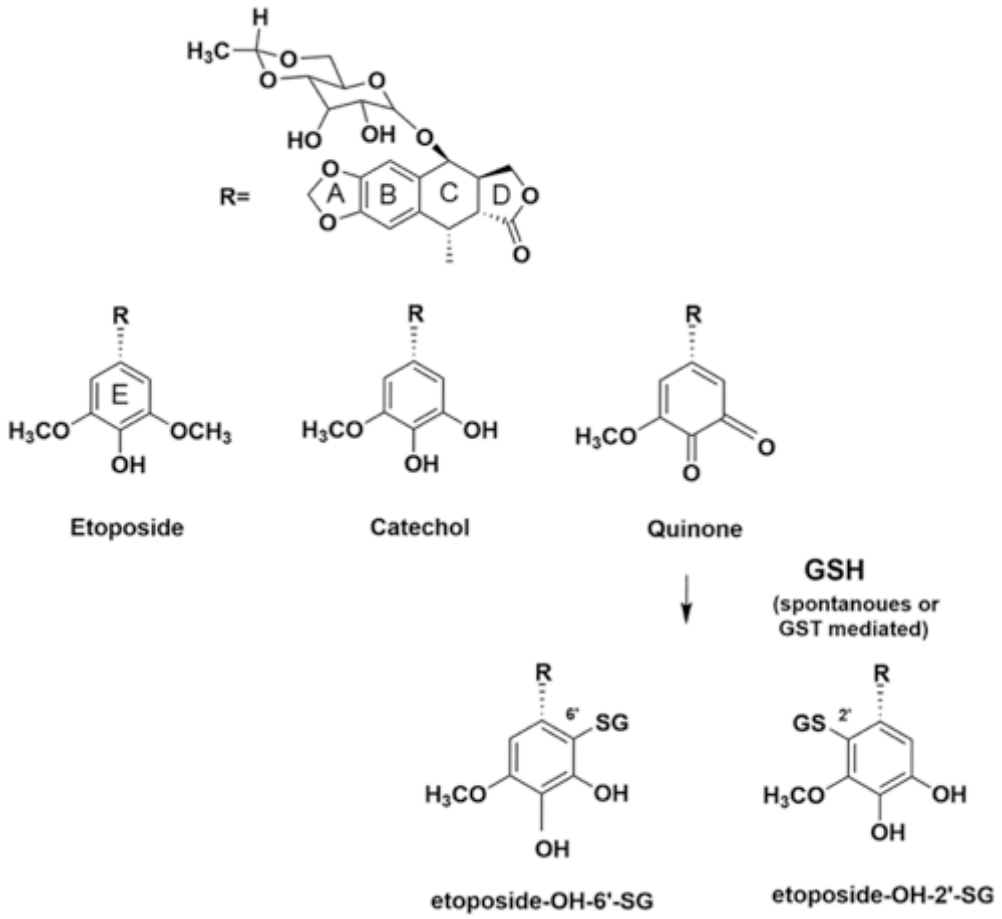


**Figure 5.1. Conjugation of reduced glutathione with etoposide quinone.** Etoposide can undergo a sequential two-electron oxidation yielding reactive etoposide quinone, however in cells etoposide quinone can be rendered ineffective by the conjugation with reduced glutathione. The reaction with glutathione reduces etoposide quinone to etoposide-OH-6'-SG and/or etoposide-OH-2'-SG. (The 2' and 6' numbering of the E-ring shown in this figure were used from Zheng, 2006).

The oxidation of mitoxantrone to a naphthoquinoxaline metabolite proceeds via the generation of a reactive quinone-diimine that is able to covalently modify DNA and proteins (Figure 5.2) (Kolodziejczyk *et al.*, 1988; Reszka *et al.*, 1989; Blanz *et al.*, 1991). Whilst mitoxantrone and naphthoquinoxaline do not seem to react with glutathione, the quinone-diimine intermediate effectively conjugates with glutathione and prevents the formation of the naphthoquinoxaline metabolite (Blanz *et al.*, 1991; Mewes *et al.*, 1993). However the structure of the glutathione- quinone-diimine have not been confirmed.

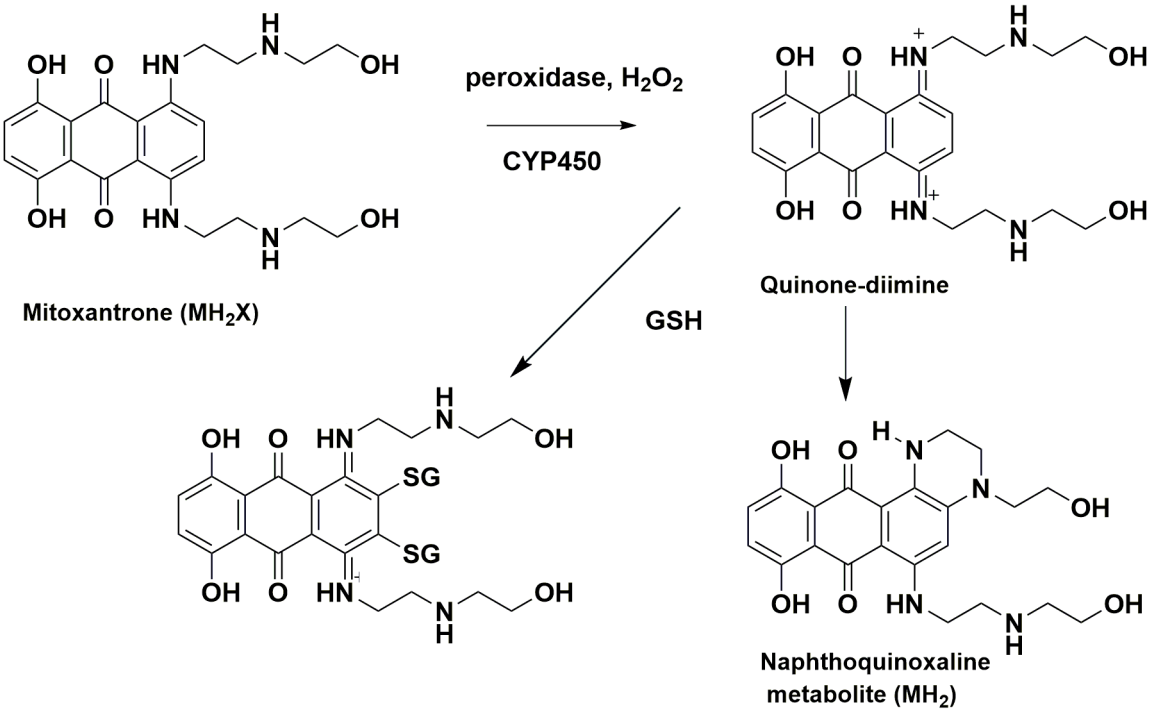


**Figure 5.2. Conjugation of glutathione with mitoxantrone-quinone-diimine.** The peroxidase-mediated biotransformation of mitoxantrone proceeds via a quinone-diimine intermediate, which further undergoes intramolecular cyclisation to generate the naphthoquinoxaline metabolite. Glutathione reacts with quinone-diimine via a nucleophilic 1,4 addition detoxifying the peroxidase mediated reaction (predicted structure obtained from Blanz *et al*., 1991).

In the previous chapter, data generated showed the presence of active MPO increases TOP2 poison induced damage, this is suggested to be mediated via the MPO-mediated oxidation of etoposide or mitoxantrone. If this were the case then the presence of glutathione in cells would limit the damage caused by MPO-mediated oxidation of TOP2 poisons. Therefore, in this chapter, the effects of depletion of glutathione on TOP2 poison induced TOP2-DNA covalent complex stabilisation and γH2Ax formation were analysed in MPO positive cells.

## 5.2 Aims:

- To investigate the effect of glutathione depletion and MPO inhibition on the level of etoposide or mitoxantrone-induced TOP2-DNA covalent complex and γH2Ax formation.
- To test for the level of TOP2-DNA covalent complex stabilisation and γH2Ax formation induced by the etoposide metabolites; etoposide catechol or etoposide quinone in NB4 cells (structures shown in Figure 5.1).

- To compare the stability of etoposide or etoposide quinone stabilised TOP2-DNA covalent complexes after depletion of glutathione in NB4 cells.

## 5.3. Results

### *5.3.1 Glutathione depletion increases etoposide-mediated TOP2 DNA damage.*

Etoposide quinone can be reduced by the conjugation with glutathione rendering etoposide quinone inactive (Figure 5.1). As etoposide quinone is the product of the MPO-mediated oxidation of etoposide, it follows that in the presence of glutathione the effects of high MPO expression may be limited. To investigate the effect of glutathione on the level of etoposide induced damage in MPO positive cells (NB4 cells), cellular glutathione levels were reduced using buthionine sulfoximine (BSO). BSO inhibits glutathione synthesis by irreversibly inhibiting glutamate cysteine ligase (γ-glutamylcysteine synthetase) (Griffith and Meister, 1979; Biterova and Barycki, 2010). Incubation with 150μM BSO for 4.5hr in NB4 cells reduced the levels of total glutathione by 74.3% ± 8.4, and levels of reduced glutathione by 79.3% ± 8.57 compared to untreated cells (see section 3.3.9 and 2.12). In addition, 150μM BSO did not affect TOP2 activity *in vitro* (conducted by C.A. Austin published in (Atwal *et al.*, 2017). Following the depletion of glutathione, NB4 cells were treated with 10μM or 100μM etoposide for 1hr whilst retaining BSO in the cell medium during the time of drug incubation. Cells were then processed to quantify the level of etoposide-stabilised TOP2A and TOP2B-DNA covalent complexes using the TARDIS assay (see section 2.13 and 4.3.1).

BSO-treated NB4 cells displayed greater levels of stabilised TOP2A- and TOP2B-DNA complexes with 10μM etoposide (44% and 63% more, respectively) (Figure 5.3.A-C). With 100μM etoposide, BSO treatment increased the level of TOP2B-DNA complexes by 32% but no increase was observed for TOP2A (*P=0.460*). Next, the effect of MPO inhibition combined with the depletion of glutathione on etoposide induced TOP2-DNA complex stabilisation was investigated. To test this, NB4 cells were firstly treated with SA (200μM for 48hr) to reduce mature MPO protein synthesis (Ch3.3.5), followed by the incubation with BSO (150μM for 4.5hr) to deplete glutathione. As shown in Figures 5.3.A-B the reduction in MPO activity and glutathione levels significantly decreases the level of etoposide stabilised TOP2A- and TOP2B-DNA covalent complexes (Figure. 5.3.A-B). With 10μM etoposide the

level of stabilised TOP2A complexes reduced by 31% (*P=0.031*) in SA+BSO pre-treated cells and for TOP2B the reduction was 34% (*P=0.024*) compared to non-pre-treated NB4 cells (10μM etoposide, black bars) (Figure. 5.3.A-B). For 100μM etoposide, TOP2A complexes reduce by 25% (*P=0.024*) whereas no reduction in TOP2B complexes (*P=0.900*) is observed with 100μM etoposide compared to non-pre-treated NB4 cells (Figure. 5.3.A-B). Notably, the level of stabilised complexes observed with the combined treatment of SA and BSO were not significantly different to that observed with SA pre-treatment at 10μM (*P=0.714)* and 100μM (*P>0.999)* etoposide for TOP2A and at 10μM etoposide (*P>0.999)* for TOP2B (Figure. 5.3.A-B). The data generated shows the observed increase in etoposide-stabilised TOP2-DNA complexes in gluatathione-depleted cells is dependent on active MPO protein expression

In addition, the effect of glutathione on etoposide induced γH2Ax formation (a marker for DSB) was analysed using quantitative immunofluorescence (see section 2.11 and 4.3.4). γH2Ax foci appear within 20 minutes upon etoposide treatment (Sunter *et al.*, 2010). This indicates the processing of drug-stabilised TOP2-DNA complexes to DSBs, a process that involves the proteolytic and/or nucleolytic removal of TOP2 from DNA and conversion of the DNA strand break to a DSB (Nitiss, 2009a; Lee *et al.*, 2012a; Povirk, 2012; Lee *et al.*, 2016).

NB4 cells were treated with BSO (150μM, 4.5hr) followed by the incubation with 10μM or 100μM etoposide. Cells were then fixed onto slides, permeabilised and probed for the level of γH2Ax formation. BSO treated cells exhibited significantly higher levels of γH2Ax signal after etoposide addition (Figure 5.4). At 10μM etoposide, BSO treated cells had a 54% (*P<0.001*) increase in γH2Ax formation, a level which was no longer significantly different from 100μM etoposide treatment (*P=0.494*) (Figure 5.4). At 100μM etoposide an even greater increase of 70% (*P<0.001*) in γH2Ax formation was observed in BSO treated cells (Figure 5.4). BSO alone (0μM) did not increase the basal level of γH2Ax compared to non-BSO treated cells (*p=0.761*) (Figure 5.4). In addition to the depletion of glutathione, cells were also pre-treated with SA to inhibit MPO. The combination of MPO inhibition and glutathione depletion reduced the level of etoposide-induced γH2Ax formation at 100μM etoposide (41%) but not with 10μM etoposide treatment (*P=0.964*) compared to non-pretreated NB4 cells (Figure 5.4). However as observed in the TARDIS assay,

BSO did not affect the level of γH2Ax formation in SA treated cells (Figure 5.3. and 5.4). These results indicate the observed increase in etoposide γH2Ax formation following the depletion of glutathione is due to MPO-mediated oxidation of etoposide to reactive metabolites that poison TOP2.

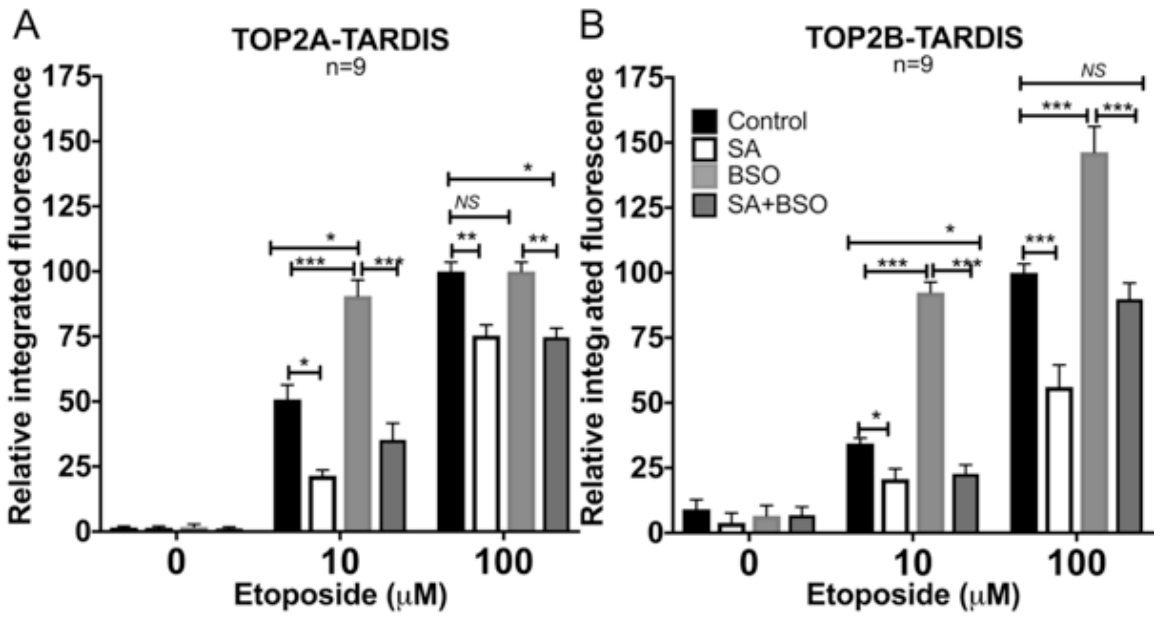


C

| Cell line | TARDIS Assay | Pre-treatment | Etoposide/ μM | %+ve control | SEM | Sig (*P*-value) | % decrease with SA | % increase with BSO | % decrease with SA+BSO |
|---|---|---|---|---|---|---|---|---|---|
| NB4 | TOP2A | None | 10 | 50.8 | 5.6 | | | | |
| NB4 | TOP2A | SA | 10 | 21.5 | 2.2 | 0.019 | 57.1 | | |
| NB4 | TOP2A | BSO | 10 | 90.6 | 6.1 | <0.001 | | 43.9 | |
| NB4 | TOP2A | SA+BSO | 10 | 35.3 | 6.4 | 0.031 | | | 30.5 |
| NB4 | TOP2A | None | 100 | 100.0 | 3.6 | | | | |
| NB4 | TOP2A | SA | 100 | 75.4 | 4.1 | 0.004 | 24.6 | | |
| NB4 | TOP2A | BSO | 100 | 116.2 | 8.2 | 0.460 | | - | |
| NB4 | TOP2A | SA+BSO | 100 | 74.7 | 3.4 | 0.024 | | | 25.3 |
| NB4 | TOP2B | None | 10 | 34.4 | 2.1 | | | | |
| NB4 | TOP2B | SA | 10 | 20.7 | 4.0 | 0.011 | 40 | | |
| NB4 | TOP2B | BSO | 10 | 92.4 | 4.0 | <0.001 | | 62.8 | |
| NB4 | TOP2B | SA+BSO | 10 | 22.8 | 3.4 | 0.024 | | | 33.7 |
| NB4 | TOP2B | None | 100 | 100.0 | 3.3 | | | | |
| NB4 | TOP2B | SA | 100 | 56.1 | 8.4 | <0.001 | 43.9 | | |
| NB4 | TOP2B | BSO | 100 | 146.3 | 10.0 | <0.001 | | 31.6 | |
| NB4 | TOP2B | SA+BSO | 100 | 89.8 | 6.2 | 0.900 | | | - |

**Figure 5.3. Glutathione depletion increases etoposide stabilised TOP2-DNA complexes.** NB4 cells were pretreated with SA (200μM, 48hr) or BSO (150μM, 4.5hr) or with both or with neither, followed by the incubation with etoposide (10μM or 100μM) or a vehicle control (0.02% DMSO). Etoposide stabilised TOP2-DNA complexes were quantified for TOP2A (A) or TOP2B (B). Data are expressed relative to the mean value for non-pretreated NB4 cells (black bars) incubated with 100μM etoposide ± S.E.M. **P*<0.05; ***P*<0.01;****P*<0.001. Percentage values are expressed relative to 100μM etoposide. (C) Supporting table shows the percentage of TOP2-DNA complexes relative to the positive control (Non-pretreated NB4 cells with 100μM etoposide) and the significance values for comparison of each pretreatment with non-pretreated NB4 cells after treatment with etoposide.

A

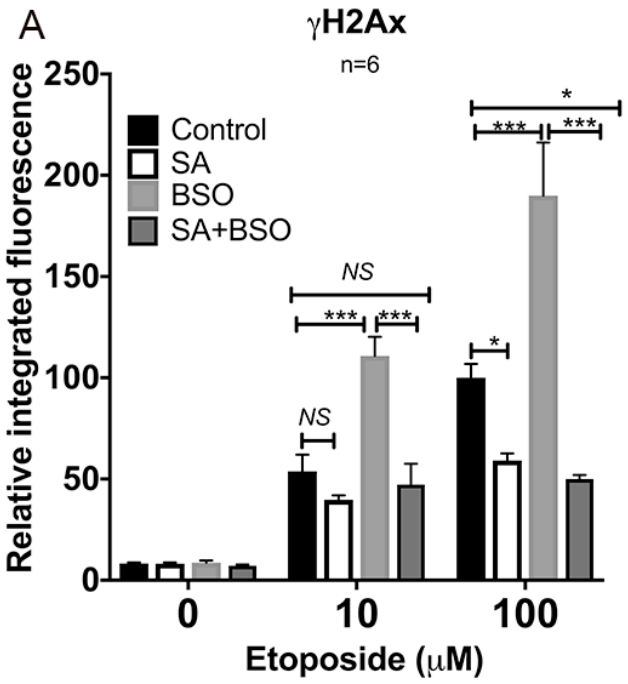


B

| Cell line | Assay | Pre-treatment | Etoposide /μM | %+ve control | SEM | Sig (*P*-value) | % decrease with SA | % increase with BSO | % decrease with SA+BSO |
|---|---|---|---|---|---|---|---|---|---|
| NB4 | γH2Ax | None | 10 | 52 | 6.6 | | | | |
| NB4 | γH2Ax | SA | 10 | 39.7 | 2.2 | 0.993 | 23.7 | | |
| NB4 | γH2Ax | BSO | 10 | 112.6 | 8.6 | <0.001 | | 53.8 | |
| NB4 | γH2Ax | SA+BSO | 10 | 37.7 | 4.5 | 0.964 | | | - |
| NB4 | γH2Ax | None | 100 | 100 | 4.5 | | | | |
| NB4 | γH2Ax | SA | 100 | 65 | 3.8 | 0.032 | 35 | | |
| NB4 | γH2Ax | BSO | 100 | 170.1 | 20.1 | <0.001 | | 70.1 | |
| NB4 | γH2Ax | SA+BSO | 100 | 58.8 | 5 | 0.048 | | | 41.2 |

**Figure 5.4. Glutathione depletion significantly increases etoposide induced global H2Ax phosphorylation.** NB4 cells were pre-treated with SA (200μM, 48hr) or BSO (150μM, 4.5hr) or with both or with neither, followed by the incubation with etoposide (10μM or 100μM) or a vehicle control (0.02% DMSO) and analysed for the level of γH2Ax phosphorylation. Data are expressed relative to the mean value obtained for non-pretreated NB4 cells incubated with 100μM etoposide ± S.E.M. **P*<0.05; ***P*<0.01;****P*<0.001. Percentage values are expressed relative to 100μM etoposide. (B) Supporting table shows the percentage of γH2Ax phosphorylation relative to the positive control (Non-pretreated NB4 cells with 100μM etoposide) and the significance values for comparison of each pretreatment with non-pretreated NB4 cells after treatment with etoposide.

### *5.3.2 Glutathione depletion enhances mitoxantrone induced TOP2 mediated DNA damage.*

MPO-mediated oxidation of mitoxantrone yields a highly electrophilic mitoxantrone quinone-diimine intermediate that can be readily detoxified by glutathione (Figure 5.2) (Blanz *et al.*, 1991). There are no known published studies which have analysed the role of quinone-diimine intermediate or the naphthoquinoxaline in TOP2 poisoning or DSB formation. The TARDIS assay was used to determine the effect of glutathione depletion on the level of mitoxantrone-stabilised TOP2-DNA complexes. Glutathione levels were reduced using BSO (150μM, 4.5hr) in NB4 cells, followed by the incubation with 1μM mitoxantrone for 1hr. BSO treated NB4 cells had significantly higher levels of TOP2A- and TOP2B-DNA complexes induced by 1μM mitoxantrone (29% and 38% more, respectively) (Figure 5.5.A-B). Additionally, the effects of MPO inhibition in combination with the depletion of glutathione were analysed. To inhibit MPO NB4 cells were treated with 200μM SA for 48hr. Pretreatment with SA reduced the level of mitoxantrone stabilised TOP2A- and TOP2B-DNA complexes by 52% (*P=0.002)* and 45% (*P=0.001*) respectively (Figure 5.5A-B). Significantly, the addition of BSO in SA pretreated cells had no affect on the level mitoxantrone induced TOP2 complexes (Figure 5.5A-B). NB4 cells pretreated with SA and BSO had a similar level of stabilised TOP2A- (*P=0.418)* and TOP2B- (*P=0.983)* DNA covalent complexes compared to cells treated with SA. This implies the increase seen with the depletion of glutathione is dependent on MPO-mediated oxidation of mitoxantrone to metabolites that may directly or indirectly poison TOP2.

A similar trend to that observed in the TARDIS assay was observed with the level of mitoxantrone-induced γH2Ax formation, a marker for the level of DBS within a cell. Depletion of glutathione increased the level of mitoxantrone γH2Ax formation by 47% (*P<0.001*) (Figure 5.6), indicating that in the presence of glutathione a significant proportion of mitoxantrone or its metabolites are prevented from inducing DSBs. In the absence of MPO activity using, SA, the level of mitoxantrone induced γH2Ax signal reduced by 44%. The addition of BSO to SA pretreated cells did not increase the level of mitoxantrone-induced γH2Ax formation (36% reduction compared to non-pretreated cells) (Figure 5.6). This suggests the increase in γH2Ax formation

observed in glutathione depleted cells is due to MPO-mediated biotransformation of mitoxantrone.

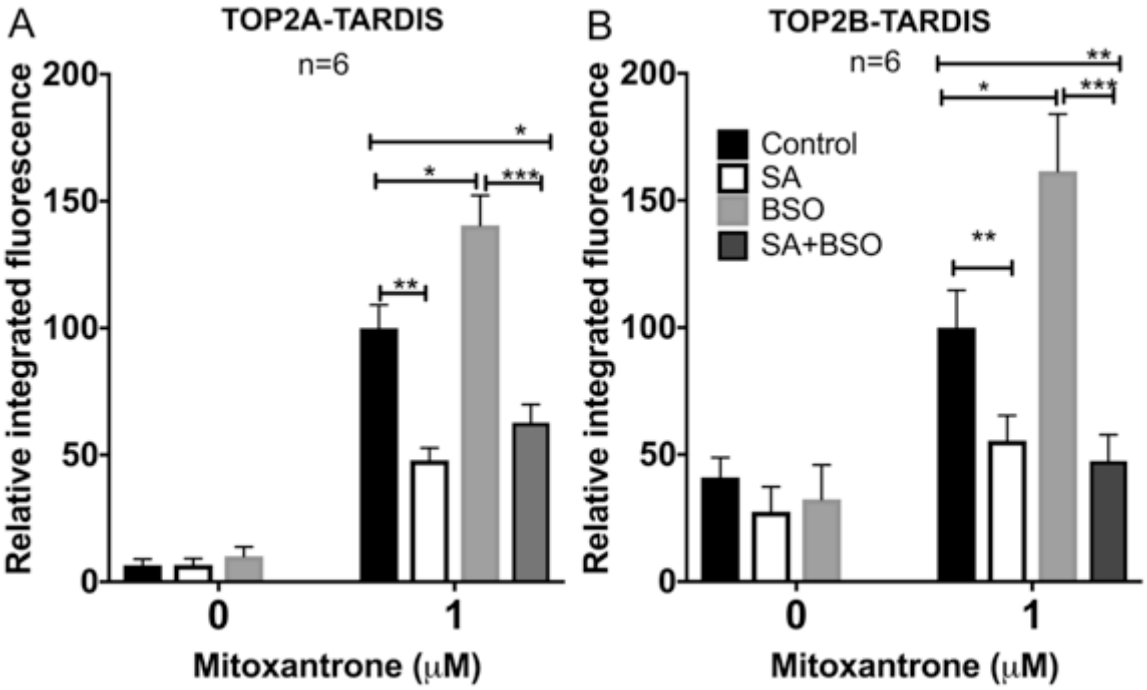


C

| Cell line | TARDIS Assay | Pre-treatment | Mitoxantrone /μM | %+ve control | SEM | Sig (*P*-value) | % decrease with SA | % increase with BSO | % decrease with SA+BSO |
|---|---|---|---|---|---|---|---|---|---|
| NB4 | TOP2A | None | 1 | 100.0 | 9.1 | | | | |
| NB4 | TOP2A | SA | 1 | 48.0 | 4.8 | 0.002 | 52 | | |
| NB4 | TOP2A | BSO | 1 | 140.4 | 11.9 | 0.017 | | 28.8 | |
| NB4 | TOP2A | SA+BSO | 1 | 62.7 | 7.2 | 0.016 | | | 37.3 |
| NB4 | TOP2B | None | 1 | 100.0 | 14.7 | | | | |
| NB4 | TOP2B | SA | 1 | 55.5 | 9.9 | 0.001 | 44.5 | | |
| NB4 | TOP2B | BSO | 1 | 161.5 | 22.5 | 0.039 | | 38 | |
| NB4 | TOP2B | SA+BSO | 1 | 47.5 | 10.4 | 0.004 | | | 52.5 |

**Figure 5.5. Glutathione depletion increases mitoxantrone mediated TOP2-DNA complex stabilisation.** NB4 cells were pretreated with SA (200μM, 48hr), BSO (150μM, 4.5hr) or both or with neither, followed by 1hr incubation with 1μM mitoxantrone. Mitoxantrone stabilised TOP2-DNA complexes were quantified by the TARDIS assay using antibodies specific to (A) TOP2A (4556) or (B) TOP2B (4555). (C) Supporting table shows the percentage of relative to non-pretreated NB4 cells with 1μM mitoxantrone and the significance values for comparison of each pretreatment with non-pretreated NB4 cells after treatment with etoposide. Data are expressed relative to the mean value obtained for non-pretreated NB4 cells (black bar) at 1μM mitoxantrone ± S.E.M. **P*<0.05; ***P*<0.01;****P*<0.001. Percentage values are expressed relative to 1μM mitoxantrone.

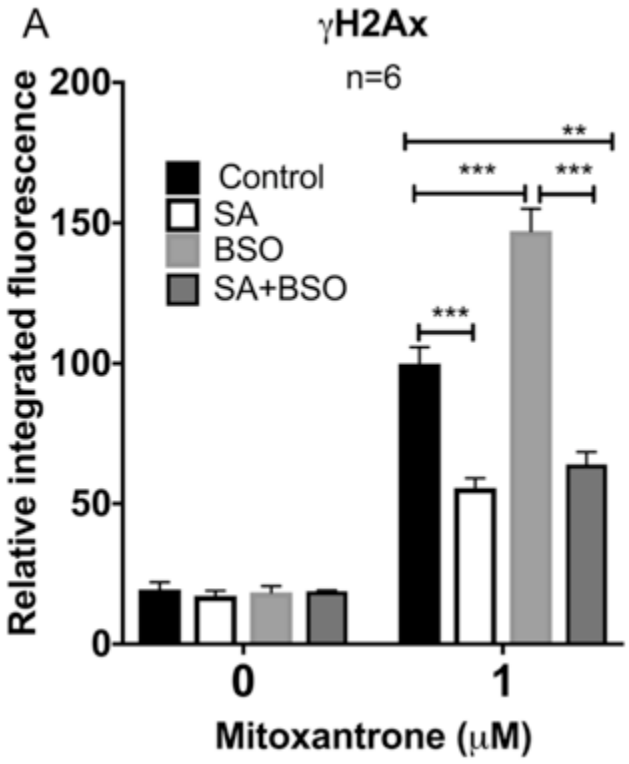


B

| Cell line | Assay | Pre-treatment | Mitoxantrone /μM | %+ve control | SEM | Sig (*P*-value) | % decrease with SA | % increase with BSO | % decrease with SA+BSO |
|---|---|---|---|---|---|---|---|---|---|
| NB4 | γH2Ax | None | 1 | 100 | 5.9 | | | | |
| NB4 | γH2Ax | SA | 1 | 55.7 | 3.4 | <0.001 | 44.3 | | |
| NB4 | γH2Ax | BSO | 1 | 147.1 | 8 | <0.001 | | 47.1 | |
| NB4 | γH2Ax | SA+BSO | 1 | 64.1 | 4.4 | 0.001 | | | 35.9 |

**Figure 5.6. Depletion of glutathione elevates mitoxantrone induced H2Ax phosphorylation.** NB4 cells were pretreated with SA (200μM, 48hr), BSO (150μM, 4.5hr) or both or with neither, followed by 1hr incubation with 1μM mitoxantrone or a vehicle control (0.02% $dH_2O$). Mitoxantrone induced γH2Ax formation was quantified using immunofluorescence. Data are expressed relative to the mean value obtained for non-pretreated NB4 cells (black bars) with 1μM mitoxantrone ± S.E.M. ***P*<0.01; ****P*<0.001, percentage values are expressed relative to 1μM mitoxantrone (C).

### *5.3.3 Etoposide E-ring metabolites.*

The main products of the peroxidase associated oxidation of etoposide at its E-ring are the CYP450 catalysed metabolite, etoposide catechol (O-demethylated at 3' position of E-ring) and the MPO-mediated oxidation product, etoposide quinone (Figure 5.1). Etoposide catechol can be further oxidised by MPO to etoposide

quinone (van Maanen *et al.*, 1988b; Jacob *et al.*, 2013). Etoposide quinone is defined by the presence of the 3' and 4' carbonyl groups on the E-ring and is dark red in colour whereas both etoposide and etoposide catechol are white (solid state) (Fan *et al.*, 2006). Both etoposide catechol and quinone are more effective at poisoning TOP2 in vitro DNA cleavage assays than etoposide (Jacob *et al.*, 2011; Smith *et al.*, 2014b; Gibson *et al.*, 2016). In this study, the TOP2 poisoning ability of 100μM etoposide catechol or etoposide quinone was compared to 100μM etoposide using the TARDIS assay in NB4 cells.

As shown in Figure 5.7 the level of stabilised TOP2A- and TOP2B-DNA complexes induced by etoposide catechol were similar to etoposide (*P=0.860* and *P=0.822* respectively) (Figure 5.7.A-B). Whereas etoposide quinone induced 30% fewer TOP2A- and 46% less TOP2B-DNA complexes, compared to etoposide (Figure 5.7.A-B). These results are different to *in vitro* data, as both etoposide catechol and quinone are more effective in poisoning TOP2 compared to etoposide in vitro (Jacob *et al.*, 2011; Jacob *et al.*, 2013; Smith *et al.*, 2014b). However, the lower TOP2 poisoning ability could be due to reduced cellular and nuclear uptake of the two metabolites and/or conjugation with glutathione, which may reduce the amount of drug that reaches the nucleus.

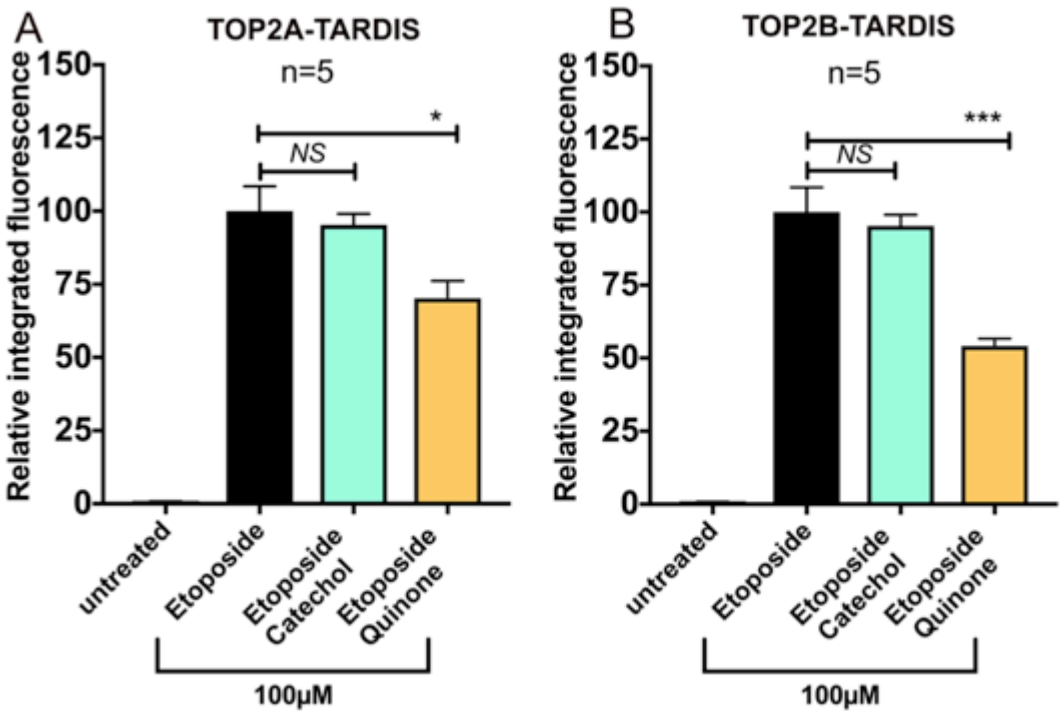


C

| Cell line | TARDIS Assay | Drug /100μM | %+ve control | SEM | Sig (*P*-value) | % difference from Etoposide |
|---|---|---|---|---|---|---|
| NB4 | TOP2A | Etoposide | 100.0 | 8.5 | | |
| NB4 | TOP2A | Etoposide catechol | 95.3 | 3.8 | 0.860 | 4.7 |
| NB4 | TOP2A | Etoposide quinone | 70.2 | 5.9 | 0.020 | 29.8 |
| NB4 | TOP2B | Etoposide | 100.0 | 8.5 | | |
| NB4 | TOP2B | Etoposide catechol | 95.3 | 3.8 | 0.822 | 4.7 |
| NB4 | TOP2B | Etoposide quinone | 54.2 | 2.4 | <0.001 | 45.8 |

**Figure 5.7. TOP2 poisoning by etoposide metabolites, *in cellulo*.** NB4 cells were treated with 100μM etoposide or its metabolites (etoposide catechol or quinone, synthesised by Angelica Mariani, France) for 1hr. Drug stabilised TOP2-DNA complexes were quantified for TOP2A (A) or TOP2B (B). Data are expressed relative to the mean value obtained for NB4 cells incubated with 100μM etoposide ± S.E.M. (C) Percentage values and significance values are expressed relative to 100μM etoposide.

Next, the etoposide metabolites were tested for γH2Ax formation with 100μM drug for 1hr. Both etoposide catechol (*P=0.324)* and etoposide quinone (*P=0.629)* induce similar levels of γH2Ax formation to etoposide (Figure 5.8.A-B). The results obtained for etoposide quinone in the γH2Ax assay do not correlate with the data obtained from the TARDIS assay. This suggests either that (i) etoposide quinone stabilised TOP2-DNA covalent complexes are processed to DSB quicker compared to

etoposide stabilised complexes or (ii) etoposide quinone may induce γH2Ax formation via a route in addition to poisoning TOP2.

A

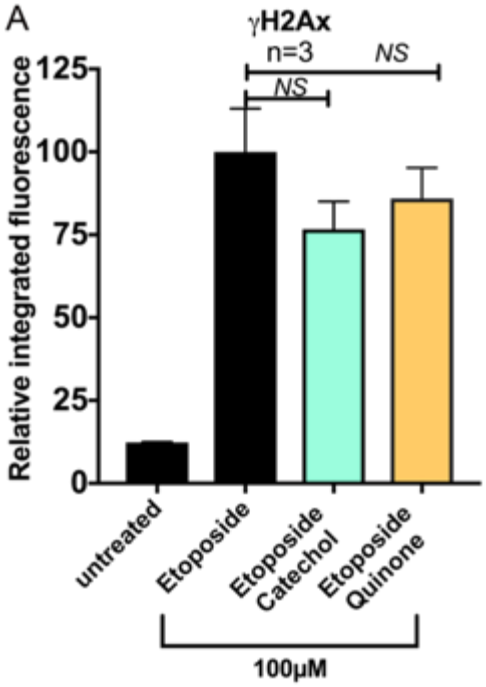


B

| Cell line | Assay | Drug /100μM | %+ve control | SEM | Sig (*P*-value) |
|---|---|---|---|---|---|
| NB4 | γH2Ax | Etoposide | 100 | 13.1 | |
| NB4 | γH2Ax | Etoposide catechol | 76.7 | 8.3 | 0.324 |
| NB4 | γH2Ax | Etoposide quinone | 85.9 | 9.3 | 0.629 |

**Figure 5.8. Etoposide metabolites induce a similar level of γH2Ax phosphorylation.** NB4 cells were treated with 100μM etoposide or its metabolites (etoposide catechol or quinone, synthesised by Angelica Mariani, France) or a vehicle control for 1hr. The level of drug-induced γH2Ax formation was detected using quantitative immunofluorescence. Data are expressed relative to the mean value for NB4 cells incubated with 100μM etoposide ± S.E.M. Percentage values are expressed relative to 100μM etoposide. (C) Percentage values and significance values are expressed relative to 100μM etoposide.

Etoposide catechol is an inherently unstable compound and once exposed to air can quickly oxidise to a red compound, indicating the oxidation to etoposide quinone or a semi-quinone species, therefore it is difficult to conclude whether the data obtained with etoposide catechol is due to the compound itself. Due to this instability of etoposide catechol, no further experiments were conducted with this compound. The data shown using etoposide catechol and quinone in Figures 5.7 and 5.8 were obtained from a different source (synthesised by Angelica Mariani, France) to the

results shown for etoposide quinone in Figures 5.9 and onwards (purchased from Cayman Chemicals, Cambridge, UK).

Etoposide quinone forms adducts with glutathione, this conjugation prevents DNA or cellular damage (Fan *et al.*, 2006). Therefore, experiments were conducted to analyse whether depletion of glutathione using BSO (150μM for 4.5hr) altered the level of etoposide quinone induced TOP2-DNA complexes (using the TARDIS assay) and DSB formation (using γH2Ax quantification) in NB4 cells. In each experiment etoposide was included as a positive control and the mean of medians obtained from integrated fluorescence for 100μM etoposide was used to normalise data from multiple biological replicates (see section 2.14).

Treatment with 10μM etoposide quinone induces substantially lower levels of stabilised TOP2A- (*P=0.002*) and TOP2B-DNA (*P=0.013*) complexes compared to 10μM etoposide (83% and 55% less respectively) (Figure 5.9.A-C). Treatment with BSO in NB4 cells significantly elevated the levels of TOP2A-DNA complexes induced with 10μM and 100μM etoposide quinone (79% and 49% more, respectively) (Figure 5.9.A). Notably, at 100μM etoposide quinone BSO treated cells have 55% more stabilised TOP2A complexes compared to 100μM etoposide in non-BSO treated cells (*P=0.002)* (Figure 5.9.A and C). However, no increase in etoposide quinone (10μM or 100μM) stabilised TOP2B complexes were observed in BSO treated cells (*P=0.718* and *P=0.371* respectively) (Figure 5.9.B).

Similarly, the effects of glutathione depletion were analysed for the level of γH2Ax formation with 10μM or 100μM etoposide quinone in NB4 cells. Etoposide quinone as observed previously, induces a similar level of γH2Ax formation to etoposide at 100μM (Figure 5.10). However, at 10μM etoposide quinone has 42% less γH2Ax formation (*P=0.042)* compared to 10μM etoposide (Figure 5.10. A). Upon treatment with BSO a 57% (*P<0.001*) increase in γH2Ax formation was observed with 10μM etoposide quinone, this exceeds the γH2Ax signal observed with 10μM etoposide *(P=0.034)* (Figure 5.10.A and B). However, BSO did not affect γH2Ax formation at 100μM etoposide quinone (*P=0.993*) (Figure 5.10).

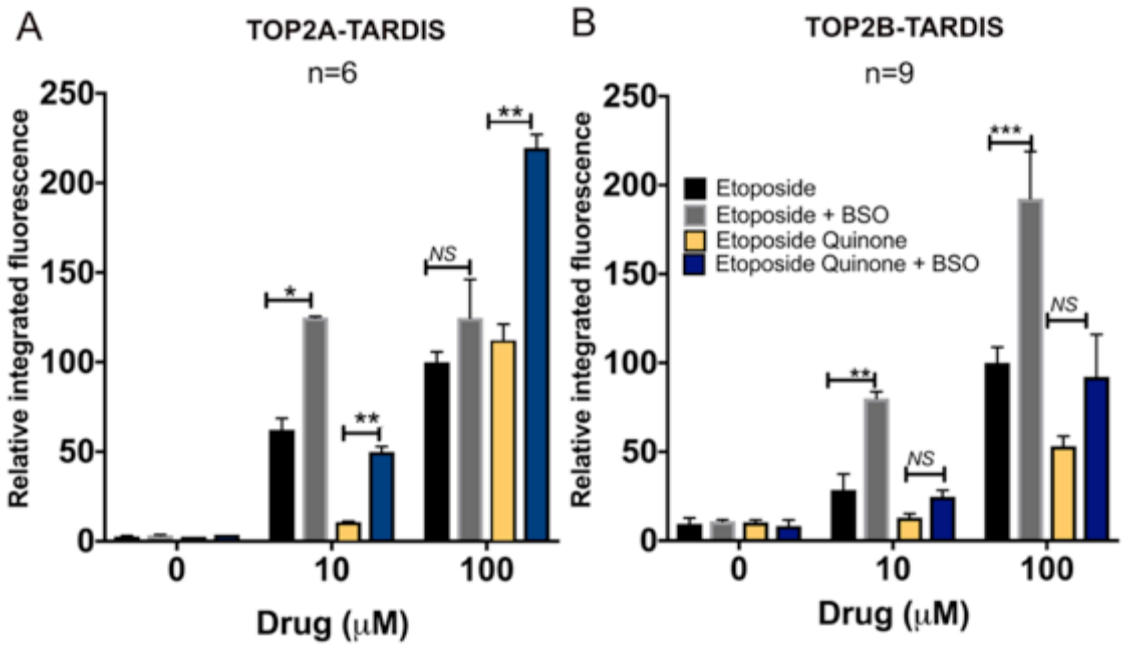


C

| Cell line | TARDIS Assay | Pre-treatment | Etoposide /μM | Etoposide quinone/μM | %+ve control | SEM | Sig (*P*-value) | % increase with BSO |
|---|---|---|---|---|---|---|---|---|
| NB4 | TOP2A | None | 10 | - | 62.2 | 6.3 | | |
| NB4 | TOP2A | BSO | 10 | - | 125.0 | 0.6 | 0.011 | 50 |
| NB4 | TOP2A | None | - | 10 | 10.6 | 0.5 | | |
| NB4 | TOP2A | BSO | - | 10 | 50.0 | 2.9 | 0.005 | 78.8 |
| NB4 | TOP2A | None | 100 | - | 100.0 | 5.8 | | |
| NB4 | TOP2A | BSO | 100 | - | 124.7 | 21.4 | 0.963 | - |
| NB4 | TOP2A | None | - | 100 | 112.1 | 9.1 | | |
| NB4 | TOP2A | BSO | - | 100 | 219.6 | 7.5 | 0.001 | 49 |
| NB4 | TOP2B | None | 10 | - | 28.6 | 8.8 | | |
| NB4 | TOP2B | BSO | 10 | - | 80.1 | 3.8 | 0.001 | 64.3 |
| NB4 | TOP2B | None | - | 10 | 13.0 | 2.1 | | |
| NB4 | TOP2B | BSO | - | 10 | 24.7 | 3.7 | 0.718 | - |
| NB4 | TOP2B | None | 100 | - | 100.0 | 8.9 | | |
| NB4 | TOP2B | BSO | 100 | - | 192.5 | 26.4 | <0.001 | 48 |
| NB4 | TOP2B | None | - | 100 | 53.2 | 5.6 | | |
| NB4 | TOP2B | BSO | - | 100 | 92.1 | 24 | 0.371 | - |

**Figure 5.9. Glutathione depletion increases etoposide quinone stabilised TOP2A-DNA complexes.** NB4 cells were pre-treated with 150μM BSO for 4.5hr followed by 1hr incubation with 10μM or 100μM etoposide or etoposide quinone or a vehicle control (0.02% DMSO). TOP2-DNA complexes were quantified using antibodies specific to TOP2A (A) or TOP2B (B). Data are expressed relative to the mean value for NB4 cells incubated with 100μM etoposide ± S.E.M. **P*<0.05; ***P*<0.01;****P*<0.001. (C) Percentage values are expressed relative to 100μM etoposide in non-BSO treated cells and significance values used difference between non-BSO treated and BSO treated cells for the specified drug. (Etoposide quinone synthesised by Cayman Chemicals, Michigan)

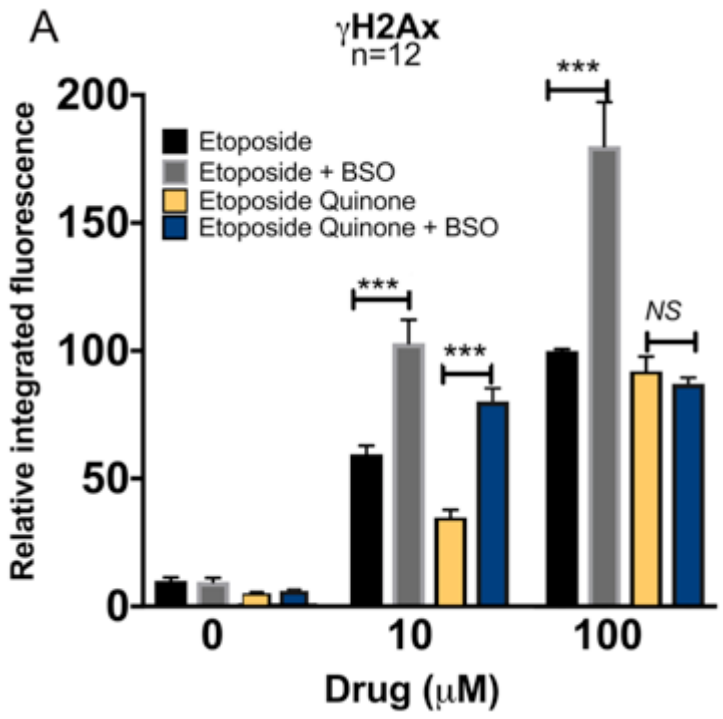


B

| Cell line | Assay | Pre-treatment | Etoposide/ μM | Etoposide quinone/μM | %+ve control | SEM | Sig (*P*-value) | % increase with BSO |
|---|---|---|---|---|---|---|---|---|
| NB4 | γH2Ax | None | 10 | - | 60.0 | 3.3 | | |
| NB4 | γH2Ax | BSO | 10 | - | 106.1 | 12.1 | <0.001 | 43.4 |
| NB4 | γH2Ax | None | - | 10 | 34.8 | 3.0 | | |
| NB4 | γH2Ax | BSO | - | 10 | 80.2 | 5.2 | <0.001 | 56.6 |
| NB4 | γH2Ax | None | 100 | - | 100.0 | 0.7 | | |
| NB4 | γH2Ax | BSO | 100 | - | 180.0 | 17.2 | <0.001 | 40 |
| NB4 | γH2Ax | None | - | 100 | 92.1 | 5.7 | | |
| NB4 | γH2Ax | BSO | - | 100 | 87.1 | 2.4 | 0.993 | - |

**Figure 5.10. Glutathione depletion increases the level of etoposide quinone induced global H2Ax phosphorylation at 10μM.** NB4 cells were pre-treated with BSO (150μM, 4,5hr) followed by the incubation with 10μM or 100μM etoposide or etoposide quinone and analysed for the level of H2Ax phosphorylation. Data are expressed relative to the mean value for NB4 cells incubated with 100μM etoposide ± S.E.M. ****P<0.001*. (B) Percentage values are expressed relative to 100μM etoposide in non-BSO treated cells and significance values used difference between non-BSO treated and BSO treated cells for the specified drug. (Etoposide quinone synthesised from Cayman Chemicals, Michigan).

The data generated shows the depletion of glutathione significantly increases TOP2A poisoning induced at 10μM and 100μM etoposide quinone treatment but did not affect TOP2B poisoning. For DSB induction the depletion of glutathione increases γH2Ax formation at 10μM etoposide quinone but not with 100μM treatment.

### *5.3.4 Longevity of etoposide or etoposide quinone stabilised TOP2-DNA complexes-TARDIS reversal assay.*

The TARDIS assays data shown above (5.3.1 to 5.3.3) and in chapter 4 were utilised to quantify the level of drug-stabilised TOP2-DNA covalent complexes after cells are exposed to a TOP2 poison for 1 hour. Immediately after the 1 hour drug incubation period, cells are processed for the detection of stabilised TOP2-DNA complexes. The TARDIS assay can be modified at the stage of drug incubation to analyse the longevity of drug-stabilised TOP2-DNA complexes at different time-points after drug removal, allowing the determination of the half-life of drug-stabilised TOP2-DNA complexes (Willmore *et al.*, 1998). This assay is therefore referred to as the TARDIS reversal assay. To conduct these experiments, the desired TOP2 poison was incubated in cells for 1 hour followed by the removal of drug from the cell medium. Cells were then placed in fresh drug-free medium and incubated at 37$^{o}$C. At specific time-points after drug removal, the TARDIS assay was conducted using the standard protocol (for further details see sections 2.13.1 to 2.13.7). Previous studies conducted in the Austin lab have shown 50% of etoposide-stabilised TOP2A-DNA complexes reverse within 30-40min. Whereas, for TOP2B the reversal time was 15-20min with almost complete complex reversal achieved within 120mins after drug removal. These previous studies were conducted in MEFs (Errington *et al.*, 2004), CCRF-CEMs (human leukaemia cell line) (Willmore *et al.*, 1998) and K562 cells (Errington *et al.*, 2004; Lee *et al.*, 2016).

The TARDIS reversal assay was conducted to measure the rate of reversal of etoposide stabilised TOP2-DNA covalent complexes in the presence or absence (using BSO) of glutathione in NB4 cells. NB4 cells treated with or without BSO (150μM, 4.5hr) were incubated with 100μM etoposide for 1 hour. The level of etoposide stabilised TOP2A- and TOP2B-DNA complexes were investigated at 0, 30min, 60min and 120min time-points after drug removal. Figures 5.11.A-B represents the level of integrated fluorescence obtained per nucleus for a single biological replicate. The integrated fluorescence values represent the level of stabilised TOP2-DNA covalent complexes for each individual nucleus. Data from an additional two biological replicates were combined using the median value (red line)

to produce the data shown in Figures 5.11.C-D. Firstly, the results in the absence of BSO will be discussed. For TOP2A 72% of etoposide-stabilised complexes resolved within 30min after drug removal (Figure 5.11.A,C and E). At 60min, the average level of integrated fluorescence was comparable to the basal level of TOP2A-DNA complexes within the cell (0min no drug, *P=0.469*) (Figure 5.11.A and C). For TOP2B, a 56% reduction in etoposide-stabilised complexes was achieved after 30min of drug removal and as seen with TOP2A, 60min after etoposide removal the level of TOP2B complexes were comparable to the basal level of TOP2B-DNA complexes (*P=0.500*) (Figure 5.11.B and D). Taken together these results show etoposide stabilised TOP2-DNA complexes have a half-life of less than 30min in NB4 cells.

The addition of BSO to reduce glutathione levels induced a small increase in the level of etoposide-stabilised TOP2B-DNA (*P=0.017*) complexes remaining after drug removal (Figure 5.11.B&D). However, there was less evidence that depletion of glutathione affected the level of stabilised TOP2A-DNA complexes after etoposide removal (*P=0.181*) (Figure 5.11.A&C). These results suggest that glutathione plays a small role in increasing the longevity of stabilised etoposide TOP2B-DNA complexes (Figures 5.11.A-D).

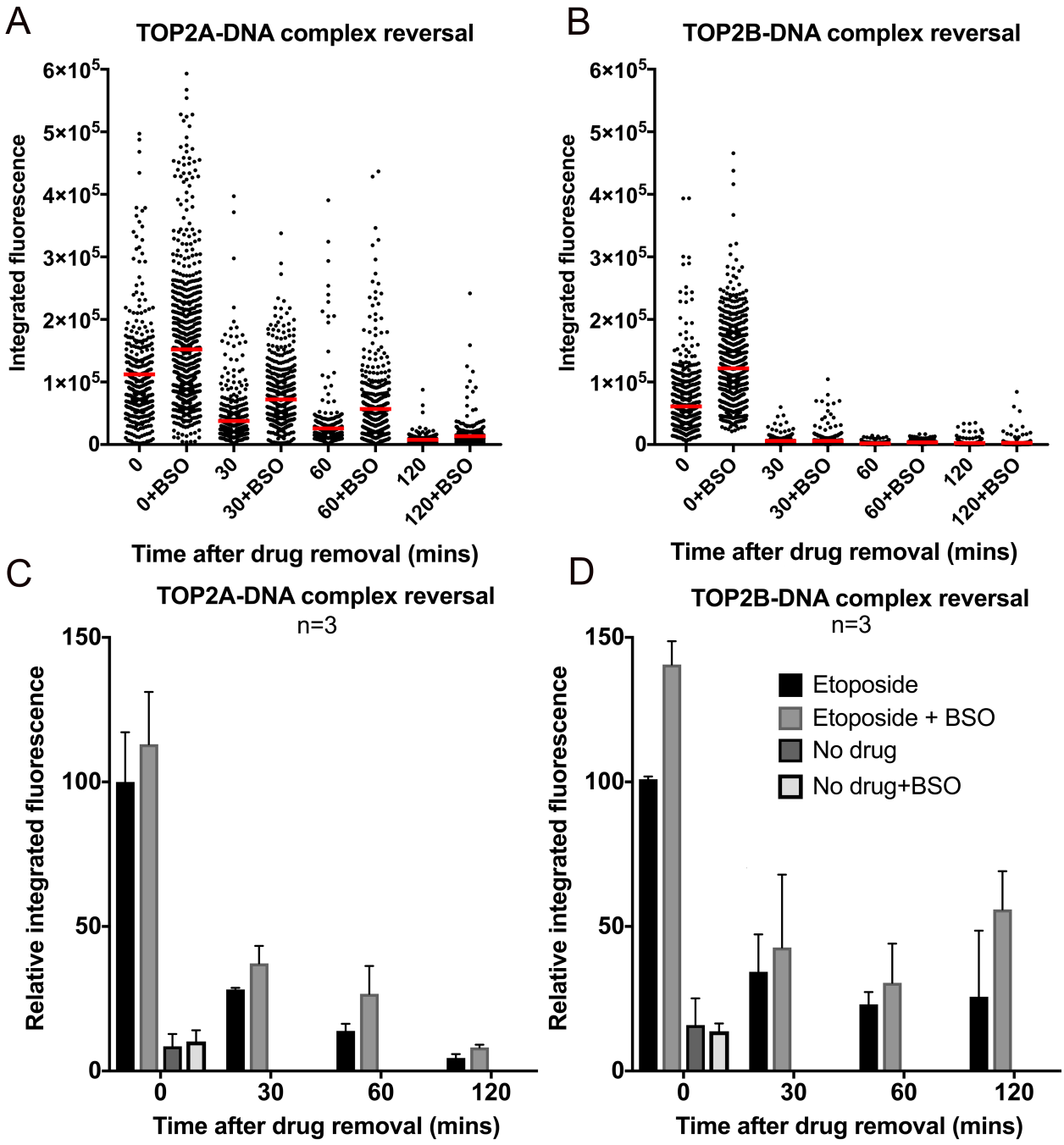


**Figure 5.11. Depletion of glutathione increases the level of etoposide stabilised TOP2B-DNA complexes (*P=0.017*) but not TOP2A-DNA complexes (*P=0.181*) that remain after drug removal.** NB4 cells were pre-treated with BSO (150μM, 4.5hr) followed by treatment with 100μM etoposide or a vehicle control for 1hr. Following this, etoposide containing medium was removed from cells and cells were replaced in fresh non-drug medium (BSO was re-added in cells which had prior BSO treatment). Level of etoposide stabilised TOP2-DNA complexes remaining after drug removal were quantified at the specified time-points for TOP2A (A) or TOP2B (B) n=1, a minimum of 600 cells analysed per treatment. Means of median (red line) were calculated from an additional two experiments. Data are expressed relative to the mean value obtained with 100μM etoposide for non-pretreated NB4 cells or NB4 cells treated with 100μM etoposide in BSO treated cells at the 0min time-point ± S.E.M for TOP2A (C) and TOP2B (D). (E) Supporting table on next page, shows the percentage values relative to either 100μM etoposide in non-pretreated NB4 cells or NB4 cells treated with 100μM etoposide in BSO treated cells. Statistical analysis was conducted using the two-way ANOVA.

E

| Cell line | TARDIS Assay | Pre-treatment | Time after drug removal | %+ve control (100μM non-BSO treated) | %+ve 100μM BSO treated |
|---|---|---|---|---|---|
| NB4 | TOP2A | None | 0 | 100 | |
| NB4 | TOP2A | BSO | 0 | | 100 |
| NB4 | TOP2A | None | 30 | 28.2 | |
| NB4 | TOP2A | BSO | 30 | | 33 |
| NB4 | TOP2A | None | 60 | 13.9 | |
| NB4 | TOP2A | BSO | 60 | | 23.6 |
| NB4 | TOP2A | None | 120 | 4.5 | |
| NB4 | TOP2A | BSO | 120 | | 7.2 |
| NB4 | TOP2B | None | 0 | 100 | |
| NB4 | TOP2B | BSO | 0 | | 100 |
| NB4 | TOP2B | None | 30 | 44.3 | |
| NB4 | TOP2B | BSO | 30 | | 30.4 |
| NB4 | TOP2B | None | 60 | 22.6 | |
| NB4 | TOP2B | BSO | 60 | | 18.7 |
| NB4 | TOP2B | None | 120 | 25.7 | |
| NB4 | TOP2B | BSO | 120 | | 39.7 |

Studies have reported that etoposide quinone behaves as a covalent TOP2 poison (Smith *et al.*, 2014b) therefore, in principle etoposide quinone-stabilised TOP2-DNA complexes could persist for longer than those formed with etoposide, which is an interfacial TOP2 poison. To test this, NB4 cells were treated with 100μM etoposide quinone for 1hr followed by drug removal and analysed for TOP2-DNA covalent complex disappearance for up to 120min after drug removal using the TARDIS assay. Results obtained show that like etoposide, 70% of the TOP2A-DNA complexes (Figure 5.12.A&C) and 50% of TOP2B-DNA complexes induced by etoposide quinone reverse within 30min of drug removal (Figure 5.12.B&D). However in the presence of BSO, to deplete glutathione, the level of etoposide quinone TOP2A *(P=0.019)* and TOP2B-DNA *(P=0.031)* complexes persist for longer in cells at all time-points tested. This can also be seen in the scatterplot data shown in Figures 5.12A-B, that show in the presence of BSO there are a higher proportion of cells compared to non-BSO treated cells which display high level of stabilised complexes after 30min and 60min following drug removal for both TOP2A and TOP2B.

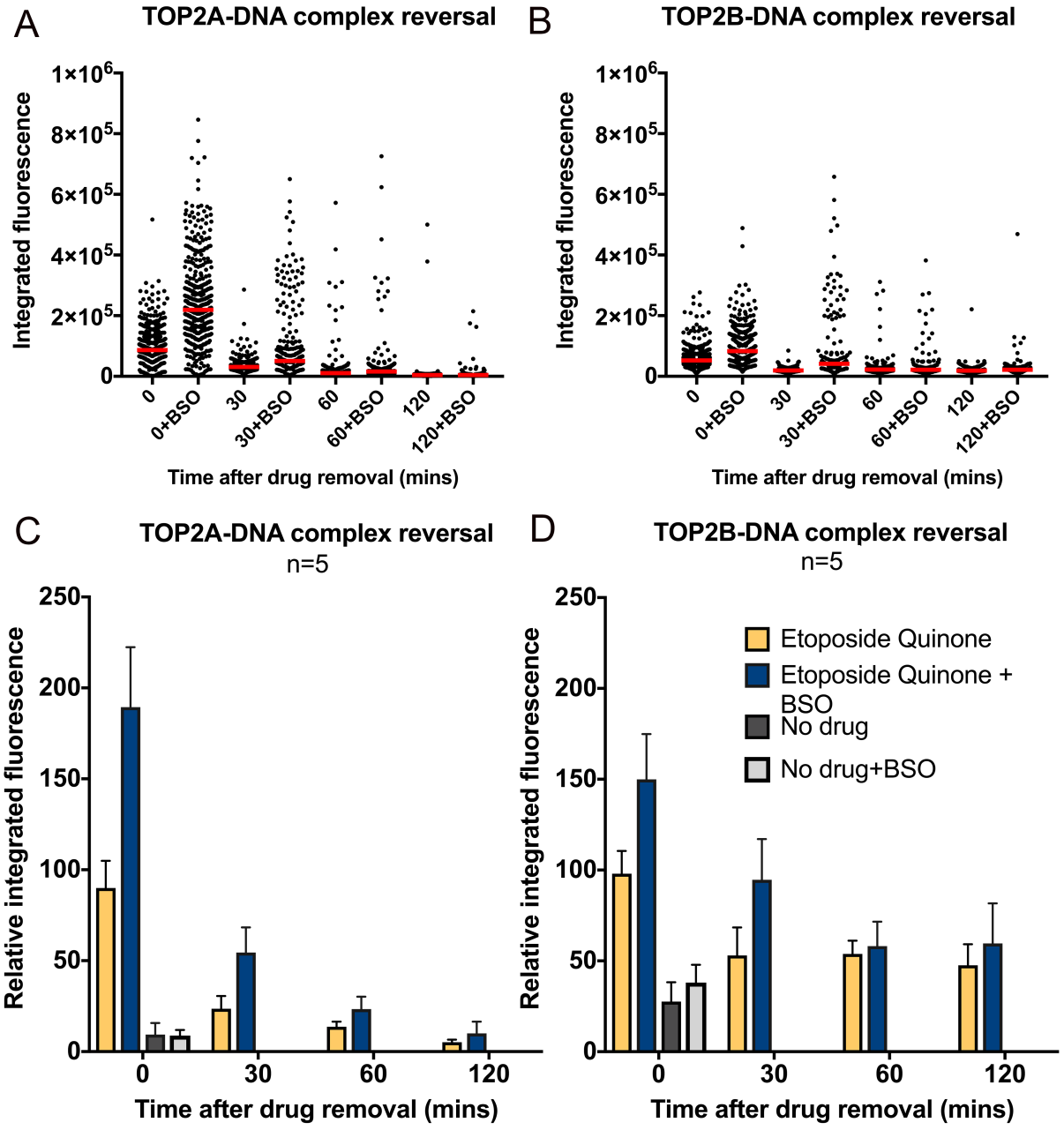
A
TOP2A-DNA complex reversal
Integrated fluorescence
1×10^6
8×10^5
6×10^5
4×10^5
2×10^5
0
0
0+BSO
30
30+BSO
60
60+BSO
120
120+BSO
Time after drug removal (mins)
B
TOP2B-DNA complex reversal
Integrated fluorescence
1×10^6
8×10^5
6×10^5
4×10^5
2×10^5
0
0
0+BSO
30
30+BSO
60
60+BSO
120
120+BSO
Time after drug removal (mins)
C
TOP2A-DNA complex reversal
n=5
Relative integrated fluorescence
250
200
150
100
50
0
0
30
60
120
Time after drug removal (mins)
D
TOP2B-DNA complex reversal
n=5
Relative integrated fluorescence
250
200
150
100
50
0
Etoposide Quinone
Etoposide Quinone + BSO
No drug
No drug+BSO
0
30
60
120
Time after drug removal (mins)

E

| Cell line | TARDIS Assay | Pre-treatment | Time after drug removal | %+ve control | %+ve 100μM BSO treated |
|---|---|---|---|---|---|
| NB4 | TOP2A | None | 0 | 100 | |
| NB4 | TOP2A | BSO | 0 | | 100 |
| NB4 | TOP2A | None | 30 | 23.6 | |
| NB4 | TOP2A | BSO | 30 | | 28.8 |
| NB4 | TOP2A | None | 60 | 13.7 | |
| NB4 | TOP2A | BSO | 60 | | 12.3 |
| NB4 | TOP2A | None | 120 | 5.2 | |
| NB4 | TOP2A | BSO | 120 | | 5.3 |
| NB4 | TOP2B | None | 0 | 100 | |
| NB4 | TOP2B | BSO | 0 | | 100 |
| NB4 | TOP2B | None | 30 | 53 | |
| NB4 | TOP2B | BSO | 30 | | 63.6 |
| NB4 | TOP2B | None | 60 | 53.8 | |
| NB4 | TOP2B | BSO | 60 | | 38.8 |
| NB4 | TOP2B | None | 120 | 47.6 | |
| NB4 | TOP2B | BSO | 120 | | 39.7 |

**Figure 5.12. Glutathione depletion increases the level of stabilised etoposide quinone stabilised TOP2A- (*P=0.019*) and TOP2B- (*P=0.031*) DNA complexes remaining after drug removal.** NB4 cells were treated with 100μM etoposide quinone or a vehicle control for 1hr. Etoposide quinone was subsequently removed from the cell culture medium and cells were replaced in fresh non-drug medium (BSO was re-added in cells which has prior BSO treatment). TOP2-DNA complexes remaining after drug removal were quantified using the TARDIS assay for TOP2A (A) and TOP2B (B) n=1, a minimum of 500 cells analysed per treatment. Means of median (red line) were calculated from an additional four experiments. Data are expressed relative to the mean value obtained with 100μM etoposide for untreated NB4 cells at the 0min time-point ± S.E.M for TOP2A (C) and TOP2B (D). (E) Supporting table shows the percentage values relative to either 100μM etoposide quinone in non-pretreated NB4 cells or NB4 cells treated with 100μM etoposide quinone in BSO treated cells. Statistical analysis was conducted using the two-way ANOVA.

## 5.4 Discussion

Etoposide and mitoxantrone metabolites containing reactive quinone and quinone-diimine groups can be detoxified by glutathione. The MPO-mediated oxidation of etoposide generates etoposide quinone via a semi-quinone species, both of these quinone containing compounds are susceptible to glutathione mediated inactivation. HL60 cell lysates (MPO positive cell line) treated with etoposide revealed the formation of etoposide quinone conjugated with glutathione (Figure 5.1) (Fan *et al.*, 2006). Similarly, MPO mediated oxidation of mitoxantrone results in the formation of the naphthoquinoxaline metabolite via a reactive quinone-diimine, which is also liable to detoxification by glutathione (Blanz *et al.*, 1991) (Figure 5.2). Therefore, the effect of high MPO expression on TOP2 poison-mediated DNA damage in cells may be limited by glutathione. To investigate this, NB4 cells were treated with BSO to inhibit glutathione synthesis. Glutathione depleted cells displayed significantly increased levels of etoposide and mitoxantrone stabilised TOP2-DNA covalent complexes and γH2Ax formation. In glutathione depleted cells 10μM etoposide treatment resulted in TOP2A- and TOP2B-DNA complexes that did not significantly differ to 100μM etoposide treatment in non-glutathione depleted cells (*P=0.919* and *P=0.978* respectively) (Figure 5.3 A-B). A similar effect was observed with 10μM etoposide for γH2Ax formation (Figure 5.4.A). For mitoxantrone, glutathione depletion also increased the level of TOP2A and TOP2B-DNA covalent complexes and γH2Ax formation (Figure 5.5 and 5.6).

Interestingly, the result observed with the depletion of glutathione was dependent on MPO, as treatment with SA (to inhibit MPO activity) decreased the level of etoposide or mitoxantrone mediated damage as measured using the TARDIS assay

and γH2Ax detection assay.

Notably the level of damage observed in SA + BSO treated cells were comparable to that observed in SA treated cells, suggesting that BSO had no affect in cells which do not contain MPO activity. The effect seen in SA pre-treated NB4 cells represents the TOP2 poisoning activity of un-metabolised (by MPO) etoposide or mitoxantrone. These results indicate the TARDIS and γH2Ax signal in glutathione depleted cells are due to the presence of MPO mediated oxidation of etoposide and mitoxantrone to metabolites that poison TOP2 and induce DSB in cells. This was further confirmed by the addition of exogenous etoposide quinone (MPO metabolite), which both poisoned TOP2 and induced γH2Ax formation, which increased upon glutathione depletion (Figure 5.9 and 5.10).

It was hypothesised that as etoposide quinone is able to covalently poison TOP2, the stabilised TOP2-DNA complexes induced by etoposide quinone may have a greater half-life compared to etoposide (Smith *et al.*, 2014b). Etoposide quinone and etoposide stabilised complexes were shown to reverse at similar rates in NB4 cells (Figure 5.11-5.12), this result is in line with in vitro published data (Gibson *et al.*, 2016). Interestingly, the depletion of glutathione delayed TOP2A and TOP2B-DNA complex reversal after etoposide quinone was removed from the drug medium (Figure 5.12A-D). The same was true for the etoposide stabilised TOP2B complexes (Figure 5.11A-D). This suggests the stabilised complexes observed with etoposide quinone may be a mixture of complexes stabilised by the interfacial poisoning mechanism and the covalent poisoning route (see section 1.3.1). TOP2A- or TOP2B-DNA complexes, stabilised by covalent poisoning are predicted to be longer-lived due to the interaction with the protein-DNA complex being stronger compared to drug intercalation into the binary complex.

The substantial increase observed in TOP2 poison mediated damage upon depletion of glutathione is clinically important as patients on high-intensity chemotherapy

regimes have reduced levels of glutathione (Charushila and Subodhini, 2013; Kadam and Abhang, 2015). Therefore the affect seen is BSO-treated cells can reflect the potential genetic damage caused during cytotoxic TOP2 poison therapy in MPO positive cells.

# Chapter 6. Effect of MPO inhibition on anthracycline mediated DNA damage and the role of anthracyclines and mitoxantrone as catalytic TOP2 inhibitors

## 6.1 Introduction

### *6.1.1 Anthracyclines*

The anthracyclines, doxorubicin and epirubicin (Figure.6.1) are widely used in cancer therapy and unlike etoposide are reported to utilise multiple mechanisms for cytotoxicity including, TOP2 poisoning (Capranico *et al.*, 1990a; Capranico *et al.*, 1990b), intercalation with DNA (Agudelo *et al.*, 2014), lipid peroxidation (Winterbourn *et al.*, 1985; Hrelia *et al.*, 2002), formation of DNA adducts (Swift *et al.*, 2006; Coldwell *et al.*, 2008), free radical formation (Sinha *et al.*, 1989; Benchekroun *et al.*, 1993) and apoptotic death via p53 (Magnelli *et al.*, 1995). However, it is debatable whether at the doses given to patients (maximum cumulative dose 450mg/m$^2$ of doxorubicin and 0.9-1g/m$^2$ of epirubicin, NICE Feb 2017 guidelines) and in the presence of glutathione if all these mechanisms of anthracycline-mediated cytotoxicity would take place (Gewirtz, 1999b; Minotti *et al.*, 2004).

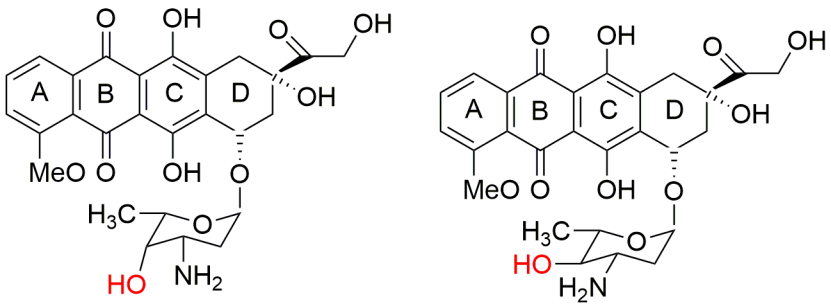


**Figure.6.1 Structures of doxorubicin and epirubicin.**

Studies have been conducted to evaluate the role of peroxidases (MPO and lactoperoxidase) on the oxidation of doxorubicin. Since epirubicin differs only by the position of a hydroxyl group at C-4' in dauosamine (sugar moiety) (axial-to-equatorial epimerization), in principle the mechanism of doxorubicin action would apply to epirubicin (Figure.6.2). MPO can mediate the oxidation of hydroquinone moiety (ring C) to a semi-quinone species (Figure.6.2). This semi-quinone species may further

disproportionate into the parent compound and to a di-quinone species (strong electrophile). Glutathione can conjugate with the semi-quinone species reducing the formation of anthracycline-di-quinone (Reszka *et al.*, 2004). The di-quinone species is potentially cytotoxic to cells however, studies have suggested that this species degrades into two inactive metabolites termed 3-methoxyphthalic acid and 3-methoxysalicylic acid (Reszka *et al.*, 2005; Wagner *et al.*, 2007), this potentially could be a protective measure for cells.

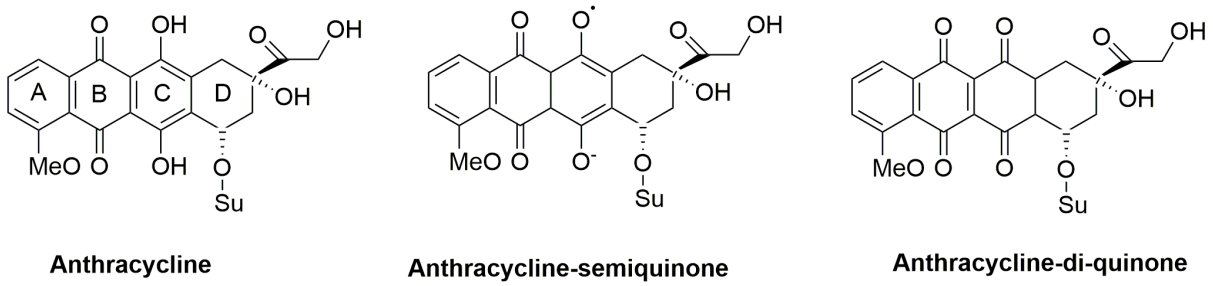


**Figure.6.2 Structures of anthracycline semi-quinone and di-quinone species.** Su denotes the sugar molecule (dauosamine) for doxorubicin or epirubicin. Peroxidases (MPO, LPO) can mediate the oxidation of hydroquinone moiety (ring C) to form a semi-quinone species. The semi-quinone may disproportionate rapidly to the parent compound and to a di-quinone species. Structures of anthracycline semi-quinone and di-quinone obtained from Reszka *et al.,* 2001.

Another mechanism of the biotransformation of doxorubicin and epirubicin is the formation of formaldehyde adducts; doxoform and epiform that can adduct DNA (Fenick *et al.*, 1997; Taatjes *et al.*, 1998) (Figure.6.3). The formation of these conjugates may be dependent on MPO and glutathione. The reason for suggesting this is that MPO can lead to the production of formaldehyde via the oxidation of amino acids (Hazen *et al.*, 1998) whereas glutathione can adduct with formaldehyde reducing the level of intracellular free formaldehyde (Bateman *et al.*, 2007). In this chapter, the effects of active MPO and reduced glutathione on doxorubicin and epirubicin stabilised TOP2-DNA covalent complexes and formation of DSB have been evaluated.

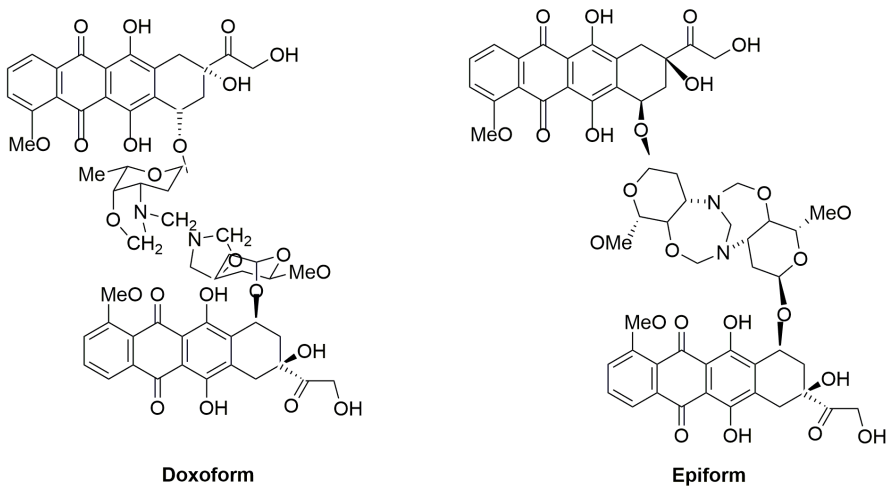


**Figure.6.3 Structures of anthracycline-formaldehyde conjugates.** Doxoform and epiform consist of two parent molecules joined to each other via three methylene groups. At neutral pH these anthracycline-formaldehyde conjugates exist in equilibrium with a mixture of the monomeric and dimeric anthracycline-formaldehyde conjugates without release of the formaldehyde. Both doxoform and epiform can react with DNA to form DNA adducts. Structures of formaldehyde conjugates obtained from Fenwick *et al.,* 1997 and Taatjes *et al.,* 1998.

### *6.1.2 TOP2 Catalytic inhibitors*

Catalytic inhibitors (such as novobiocin, merbarone, bisdioxopiperazines, e.g. ICRF-193, ICRF-187) are distinct from TOP2 poisons in that they do not lead to the accumulation of TOP2-DNA covalent complexes but inhibit at other stages of the TOP2 catalytic cycle (Larsen *et al.*, 2003) (for TOP2 catalytic cycle see section 1.1.3). For example, the bisdioxopiperazines derivatives trap TOP2 in a closed clamp state and inhibit ATP hydrolysis, whereas novobiocin blocks binding of ATP to TOP2 (Sekiguchi *et al.*, 1996; Jensen *et al.*, 2000). In comparison to TOP2 poisons, catalytic inhibitors are generally less cytotoxic and can be used to reduce anthracycline-induced damage or increase the sensitivity to TOP2 poisons. Dexrazoxane (ICRF-187) is sometimes used as a cardioprotective or to prevent tissue necrosis in doxorubicin therapy (Swain *et al.*, 1997; Kane *et al.*, 2008; Asselin *et al.*, 2016). On the other hand, suramin and novobiocin can be used to increase the efficacy of doxorubicin and etoposide (Lorico *et al.*, 1992; Benini *et al.*, 2001; Zhang *et al.*, 2001). However, a given compound does not need to directly interact with the TOP2 protein for it to be considered as a catalytic inhibitor. Examples include the anthracyclines, aclarubicin and idarubicin which inhibit TOP2 poison induced TOP2-DNA complex stabilisation. Studies have suggested that aclarubicin or idarubicin behave as catalytic TOP2 inhibitors by intercalating into DNA, which prevents TOP2

from binding to DNA (Jensen *et al.*, 1990; Sehested and Jensen, 1996; Willmore *et al.*, 2002).

## 6.2 Aims

- To investigate the effect of MPO inhibition and glutathione depletion on anthracycline (doxorubicin and epirubicin) induced DNA damage using the TARDIS and γH2Ax quantitative immunofluorescence assays.
- To establish whether anthracyclines, mitoxantrone or etoposide quinone behave as TOP2 catalytic inhibitors using the TARDIS inhibitor assay.

## 6.3. Results

### *6.3.1 Stabilisation of TOP2-DNA covalent complexes by doxorubicin or epirubicin.*

The TARDIS assay was employed to quantify the level of doxorubicin or epirubicin stabilised TOP2A- or TOP2B-DNA covalent complexes in NB4 cells. The TARDIS assay allows the quantification of TOP2 protein covalently bound to DNA, after the removal of non-covalently bound proteins and cellular constituents from nuclear DNA by SDS-salt extraction (method described in 2.13). Previous studies conducted by the Austin lab have shown treatment with 0.1μM to 10μM doxorubicin in K562 cells induced low levels of complex stabilisation for both TOP2A and for TOP2B; the level of anthracycline induced complexes were not significantly different to the basal level of TOP2B-DNA covalent complexes (Willmore *et al.*, 2002). To test whether the same is applicable in NB4 cells, cells were treated with 0.1μM, 1μM or 10μM doxorubicin or epirubicin for 1hour. Following this, cells were processed to quantify the level of drug-stabilised TOP2-DNA covalent complexes using the TARDIS assay.

The TARDIS assay data obtained for doxorubicin and epirubicin show that both drugs have a similar trend in TOP2A and TOP2B-DNA complex stabilisation to each other (Figure.6.4.A-D). The data shown in Figures 6.4.A-D are represented as scattergrams, each scatter-point depicts the level of integrated fluorescence obtained per nucleus and the red line represents the median value of integrated fluorescence obtained in the cell population. For each treatment a minimum of 300 nuclei were analysed.

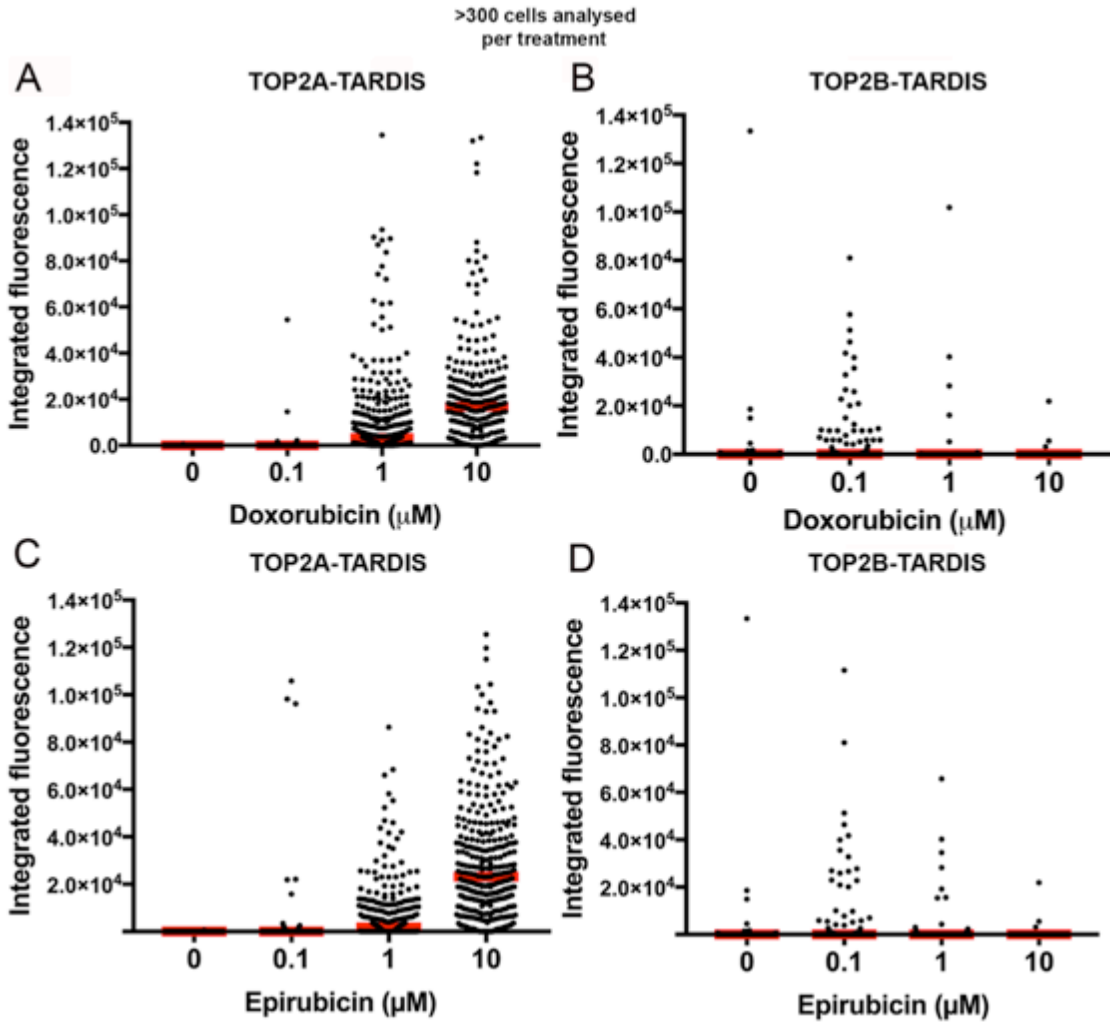


**Figure 6.4. Dose response of doxorubicin or epirubicin mediated TOP2A or TOP2B-DNA complex stabilisation.** NB4 cells were treated with 0.1μM to 10μM of doxorubicin (A&B) or epirubicin (C & D) for 1 hour. Drug-stabilised TOP2-DNA covalent complexes were quantified by the TARDIS assay using antibodies specific to either TOP2A (A & C) or TOP2B (B & D). Data are represented as scattergrams, each point corresponds to the integrated fluorescence obtained for a single nucleus, the median value (red line) of integrated fluorescence obtained for the whole population (n=1).

Doxorubicin produced a dose-dependent increase in TOP2A-DNA covalent complexes (Figure. 6.4.A). However for TOP2B, doxorubicin treatment did not induce a noticeable increase in the median fluorescence signal above the control level (0μM doxorubicin) in NB4 cells (Figure.6.4.B). With 0.1μM doxorubicin, there were a small proportion of cells, with stabilised TOP2B-DNA complexes which were above the basal level of TOP2B complexes, compared to 1μM or 10μM doxorubicin (Figure. 6.4.B), a result which is consistent with previous published data (Willmore *et al.*, 2002). A similar trend for TOP2 poisoning was observed for epirubicin treated NB4 cells (Figure.6.4.C-D). As for doxorubicin, treatment with epirubicin induces a dose-dependent increase in TOP2A complexes but not for TOP2B complexes (Figure.

6.4.C-D). These results indicate both doxorubicin and epirubicin poison TOP2A, but at very low level under the conditions tested.

Next, the level of doxorubicin and epirubicin stabilised TOP2-DNA complexes were tested at various time-points after drug treatment. To investigate this, a time-course experiment was conducted, NB4 cells were treated with 10μM doxorubicin or epirubicin. Following this, cells were processed to quantify for the level of drug-stabilised TOP2A or TOP2B-DNA complexes at 15min, 30min, 60min and 120min of drug treatment. Results shown in Figures 6.5.A-B were obtained from a single biological replicate to conduct analyses, data from an additional two biological replicates were combined using the median value (red line) obtained for each treatment. The mean of the medians obtained with 10μM doxorubicin with 60min treatment was used to normalise data from multiple biological replicates (see section 2.14) (Figure.6.5C-D).

Doxorubicin treated cells show a similar level of TOP2A-DNA complex stabilization at each time-point investigated, due to the low level of signal obtained there are a lot of fluctuations in the data, which is represented by the large standard error (Figure.6.5A&C). At any given time-point after doxorubicin treatment the level of doxorubicin stabilised TOP2A-DNA complexes were not significantly above the basal level of TOP2A-DNA complexes observed in non-drug treated cells (0min) (Figure.6.5C). However, there was an observed increase in the proportion of cells with increased integrated fluorescence from 15min to 60min of doxorubicin incubation (Figure.6.5.A). This heterogeneity in TOP2-DNA complex stabilisation across the cell population was also observed in etoposide and in mitoxantrone treated cells (chapter 4; Figures 4.3 and 4.4). For TOP2B, the level of complex stabilisation observed in doxorubicin treated cells was comparable to the basal level of TOP2B complex stabilisation (0mins) at all time-points tested (Figure.6.5B&D).

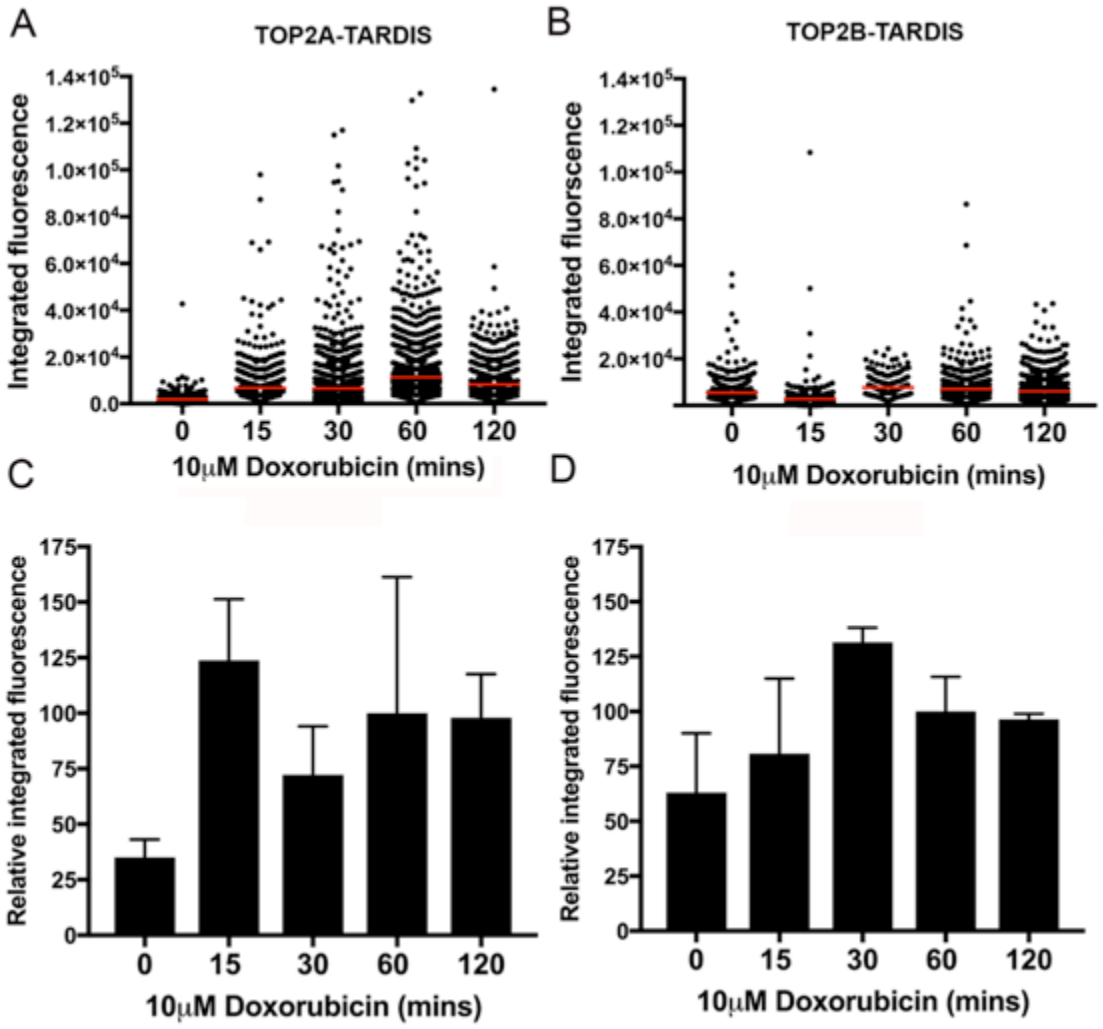


**Figure 6.5. Time course for doxorubicin mediated TOP2A or TOP2B-DNA complex stabilisation.** NB4 cells were treated with 10μM doxorubicin and levels of TOP2A- (A) or TOP2B- (B) DNA stabilised complexes were quantified at the specified time-points using the TARDIS assay (a minimum of 700 cells analysed per treatment). Data obtained from A and B was combined with an additional two experiments using the median values obtained (red line) and represented as histograms for TOP2A (C) and TOP2B (D) (n=3). Data are expressed relative to the mean of the median values obtained for 1hr treatment with 10μM doxorubicin ±S.E.M.

There is a noticeable difference between the integrated fluorescence values obtained in the non-drug treated cells (0μM/0mins) between Figures 6.4 and 6.5. This is due to the differences in background subtraction and the camera exposure value chosen in each experiment. For Figure 6.4, 100μM etoposide was used to set the exposure value of each channel (FITC and DAPI) in the experiment whereas for Figures 6.5 and 6.6, 10μM doxorubicin or epirubicin were used to set exposure values. As 100μM etoposide gives, a high intensity integrated fluorescence signal compared to doxorubicin or epirubicin the exposure value for each channel was lower for data in Figure 6.4.

A time-course TARDIS experiment was conducted using 10μM epirubicin in NB4 cells and the level of TOP2A- or TOP2B-DNA covalent complexes were investigated at 15min, 30min, 60min and 120min after drug exposure. A time-dependent increase in TOP2A-DNA complex stabilisation was observed with epirubicin, with maximum complex stabilisation obtained at 60min of drug exposure (80% above basal levels) (Figure.6.6.C). Additionally, the level of epirubicin stabilised TOP2A-DNA complexes were significantly above the basal level of TOP2A complexes at 30min (*P=0.019*), 60min (*P<0.001*) and 120mins (*P=0.004*). This is different to data obtained using 10μM doxorubicin (Figure 6.5C). For TOP2B, epirubicin treatment did not result in TOP2B signal significantly above basal levels at any of the time-points tested (Figure.6.6.B&D). This is similar to the response obtained with doxorubicin (Figure.6.5.B&D). Additionally, it was observed that epirubicin treatment resulted in less variation between replicate experiments compared to doxorubicin, which is represented by the lower standard error in the data obtained using epirubicin compared to doxorubicin (Figure.6.5C-D and Figure. 6.6C-D). For this reason further TARDIS experiments were conducted using epirubicin and not doxorubicin.

The TARDIS data shown above and in the previous chapters were obtained using isoform specific TOP2 antibodies, raised to the C-terminal domain of either TOP2A or TOP2B (see Table 2.2 for antibody details). The C-terminal region is most diverse between the two isoforms and the site where modifications such as phosphorylation and SUMOylation occur, which potentially block antibody binding (Wells *et al.*, 1995b; Ishida *et al.*, 1996; Yoshida *et al.*, 2016). If modifications to the C-terminus occurred after anthracycline treatment (but not after etoposide treatment) then this could possibly explain the lower TARDIS signal observed with anthracyclines using anti-C-terminal antibodies 4566 (TOP2A) and 4555 (TOP2B). To examine this possibility an antibody raised to N-terminal region of TOP2 was used in the TARDIS assay (antibodies details listed in Table 2.2). However, due to high sequence homology between TOP2A and TOP2B in the N-terminal region (site of catalytic centers), this antibody does not distinguish between the isoforms of TOP2.

To conduct this TARDIS experiment, NB4 cells were treated with 10μM doxorubicin or epirubicin for 1hour. In addition, cells were separately treated with 20μM mitoxantrone or etoposide (10μM or 100μM). Figure 6.7. shows both doxorubicin and epirubicin induce TOP2-DNA complex stabilisation which is similar to that obtained in

non-drug treated cells (*P=0.846* and *P=0.999* respectively). Whereas both mitoxantrone and 10μM etoposide induce TOP2-DNA complexe levels that are significantly above the basal level of TOP2-DNA complexes (*P=0.0171* and *P=0.001* respectively). This data generated using the N-terminal TOP2 antibody was obtained under conditions where both doxorubicin and epirubicin induced low levels of TOP2-DNA complex stabilisation using TOP2-CTD antibodies 4566 (TOP2A) and 4555 (TOP2B) (see table 2.2. for antibody details). Therefore, it is unlikely that the low level of TOP2-DNA complexes induced by anthracyclines observed in the TARDIS assay is due to post-translational modifications at the C-terminus of TOP2.

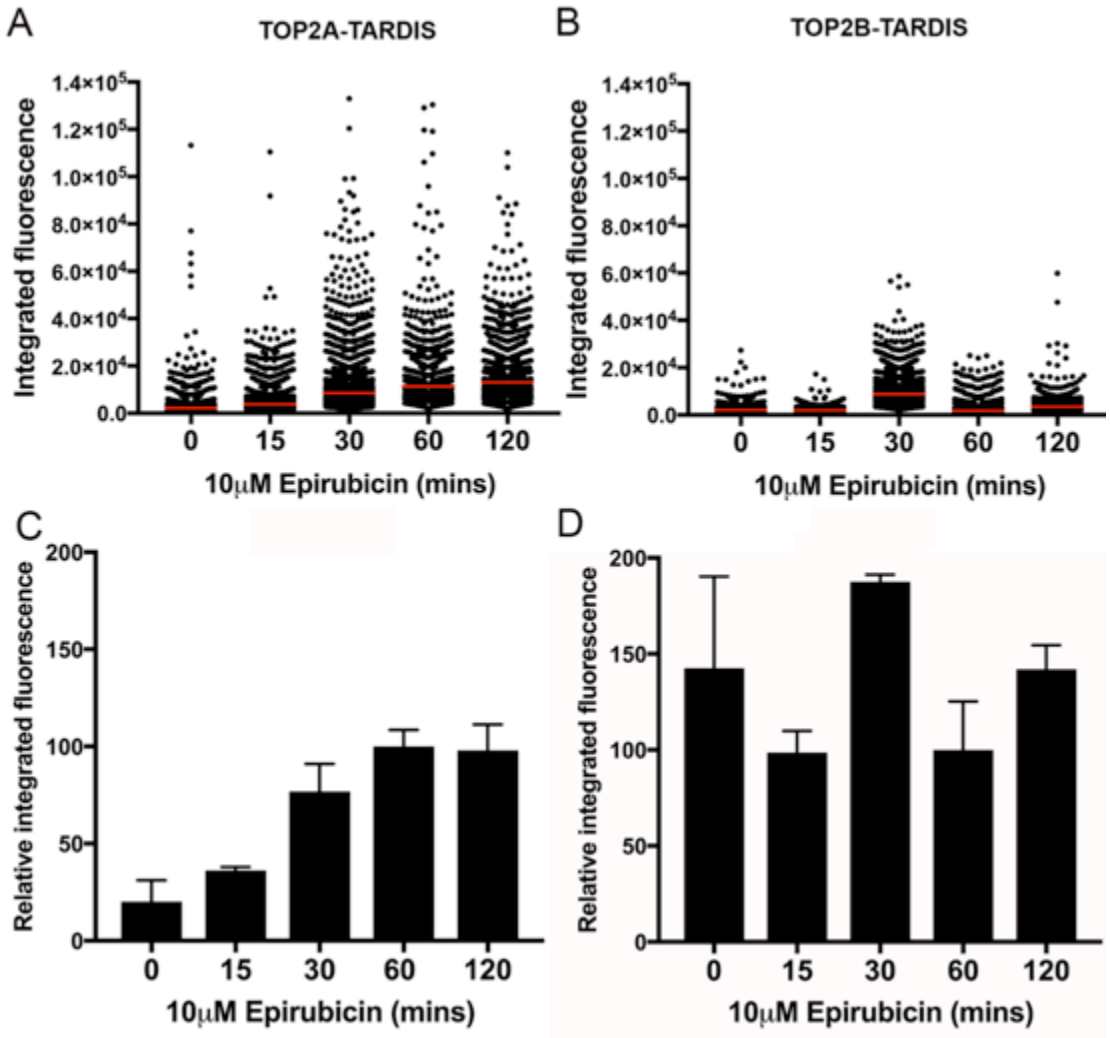


**Figure 6.6. Time course for epirubicin mediated TOP2A or TOP2B-DNA complex stabilisation.** NB4 cells were treated with 10μM epirubicin and probed for the level of TOP2A- (A) or TOP2B- (B) DNA covalent complexes at the specified timepoints (a minimum of 700 cells analysed per treatment). Data from additional two biological replicates were combined using the mean of median values (shown as a red line in A&B) and represented as histograms. Data are expressed relative to the mean value obtained with 10μM epirubicin at 1hr from three separate experiments ±S.E.M.

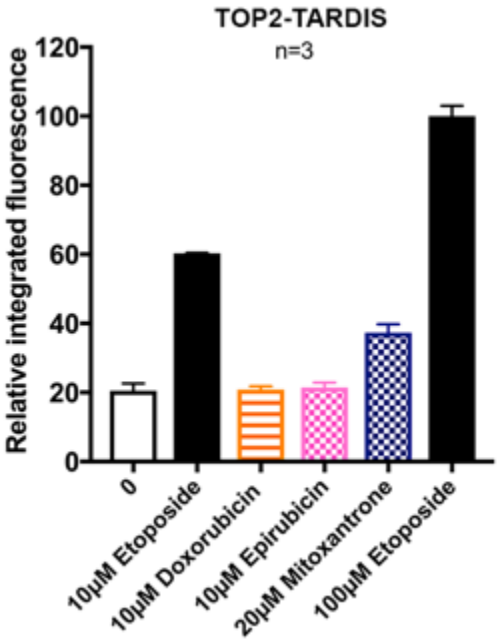


**Figure 6.7. Probing for the level TOP2-DNA covalent complex stabilisation using TOP2 antibody raised to N-terminal domain of bovine TOP2.** Cells were treated with the specified TOP2 poisons for 1 hour and probed for the level of drug-stabilised TOP2 complexes by the TARDIS assay using an antibody (4882) raised to the N-terminal (140kDa) of bovine TOP2. Data are expressed relative to 100μM etoposide ±S.E.M.

### *6.3.2. Inhibition of MPO reduces the level of epirubicin-stabilised TOP2A-DNA complexes.*

MPO has been implicated in the oxidation of anthracyclines, the precise consequence of this oxidation is unclear. In this chapter, the role of MPO on epirubicin induced TOP2-DNA covalent complex stabilisation was investigated. To inhibit MPO activity, NB4 cells were pre-treated with 200μM SA for 48hr (see section 3.3.5) followed by the incubation with 10μM epirubicin for 1 hour. Pretreatment with SA reduced the levels of epirubicin stabilised TOP2A-DNA complexes by 40% (*P=0.006*), but as observed previously, epirubicin did not induce TOP2B-DNA complex stabilisation above basal levels (Figure 6.8A-B).

Glutathione can conjugate with the peroxidase-mediated oxidation metabolites of anthracyclines and therefore the presence of glutathione may reduce the level of TOP2 poisoning in cells. To investigate this, glutathione levels were reduced in NB4 cells using 150μM BSO for 4.5hr (see section 3.3.9). Following this, cells were incubated with 10μM epirubicin for 1hour and tested for the level of TOP2A-DNA or TOP2B-DNA complex stabilisation using the TARDIS assay. BSO treatment had no effect on epirubicin stabilised TOP2A- or TOP2B-DNA complexes (*P=0.820* and

*P=0.330* respectively) (Figure 6.8.A-B). For TOP2A the pre-treatment with SA and BSO resulted in a 29% decrease in epirubicin stabilised complexes compared to non-pretreated cells (Figure 6.8.A). Notably the level of epirubicin induced TOP2A-DNA complexes in SA+BSO pretreated cells were comparable to those obtained in SA pretreated cells (*P= 0.150*) (Figure 6.8.A). Taken together the data generated shows MPO activity contributes to epirubicin induced TOP2A-DNA complex stabilisation but the depletion of glutathione does not affect epirubicin TOP2 poisoning ability. The results obtained for glutathione are in-line with in vitro experiments conducted using doxorubicin, which showed depletion of glutathione (using BSO) does not affect the level TOP2-DNA complex stabilisation induced by doxorubicin (Bonner *et al.*, 1992).

A

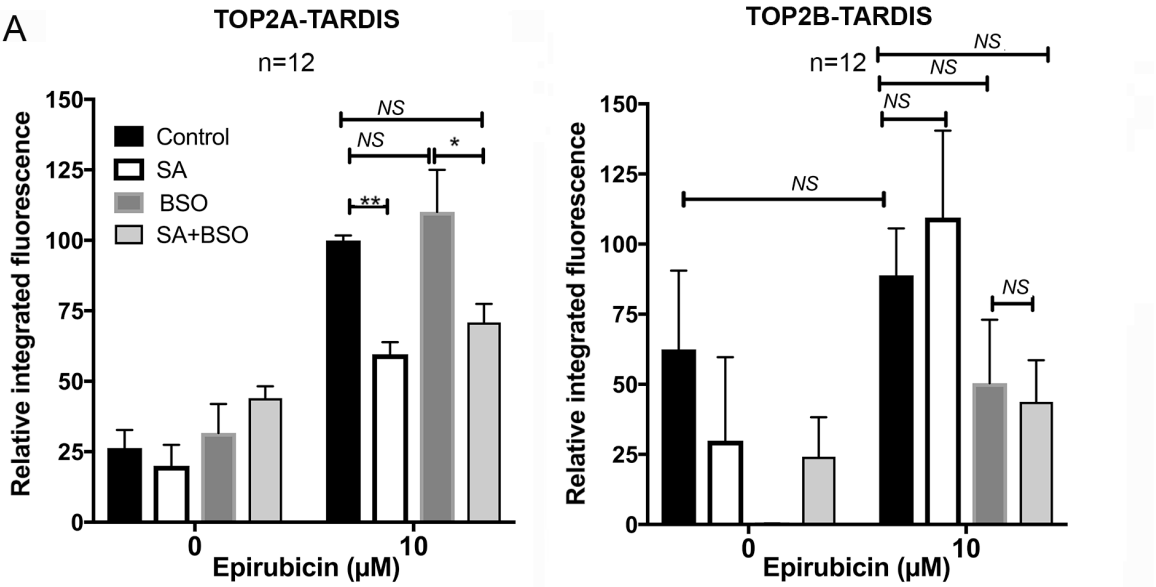


C

| Cell line | TARDIS Assay | Pre-treatment | Epirubicin/ μM | %+ve control | SEM | Sig (*P*-value) | % reduction by SA | % reduction by SA+BSO |
|---|---|---|---|---|---|---|---|---|
| NB4 | TOP2A | None | 10 | 100 | 1.7 | | | |
| NB4 | TOP2A | SA | 10 | 59.6 | 4.3 | 0.006 | 40.4 | |
| NB4 | TOP2A | BSO | 10 | 110.1 | 14.9 | 0.82 | | |
| NB4 | TOP2A | SA+BSO | 10 | 70.9 | 6.5 | 0.070 | | 29.1 |
| NB4 | TOP2B | None | 10 | 100 | 2.7 | | | |
| NB4 | TOP2B | SA | 10 | 109.5 | 31 | 0.990 | | |
| NB4 | TOP2B | BSO | 10 | 50.4 | 22.7 | 0.330 | | |
| NB4 | TOP2B | SA+BSO | 10 | 43.7 | 14.9 | 0.230 | | |

**Figure 6.8. Inhibition of MPO reduces epirubicin stabilised TOP2A-DNA covalent complexes.** NB4 cells were pre-treated with 200μM SA for 48hr or 150μM BSO for 4.5 hours, or with both or with neither followed by 1hr incubation with 10μM epirubicin. Cells were processed and analysed for the level of epirubicin stabilised TOP2-DNA covalent complexes for TOP2A (A) or TOP2B (B). Data are expressed relative to the mean value obtained with 10μM epirubicin in non-pre-treated cells (black bar). (C) Percentage values showing the mean level of TOP2-DNA complex stabilisation compared to 10μM epirubicin in non-pretreated cells. Statistical analysis was performed by the one-way ANOVA with post hoc Tukey's multiple comparison test. * *P* <0.05; ** *P <0.01.*

### *6.3.3. γH2Ax formation in doxorubicin or epirubicin treated NB4 cells.*

Doxorubicin and epirubicin elicit the formation of γH2Ax foci, which indicates production of DSBs within a cell (Kurz *et al.*, 2004; Monteiro *et al.*, 2013). The induction of γH2Ax foci upon treatment with doxorubicin or epirubicin is partly dependent on TOP2A (Yan *et al.*, 2009) but additional mechanisms such as redox cycling may also contribute to γH2Ax formation. To measure the level of DSB induced by doxorubicin or epirubicin, NB4 cells were treated with a range of concentrations of either doxorubicin or epirubicin for 1hour. Following this, the drug was removed from the cell medium and cells were fixed onto slides, permeabilised and probed for the level of γH2Ax formation using quantitative immunofluorescence (method described 2.11). For each treatment a minimum of 700 cells were analysed and data are represented as scattergrams. Each data-point represents the level of integrated fluorescence obtained per cell, which is indicative of the level of γH2Ax formation in each cell.

Data presented in Figure 6.9.A-B, show both doxorubicin and epirubicin elicit a dose-dependent increase in γH2Ax formation (Figure.6.9A-B). A low level of γH2Ax was observed in the non-drug treated NB4 cells, this basal level of γH2Ax formation is presumably caused during normal cellular processes (McManus and Hendzel, 2005; An *et al.*, 2010). The intensity of integrated fluorescence is distributed heterogeneously in the cell population, a response which is similar to that observed in the TARDIS assay (Figure.6.4). Due to this heterogeneity across the cell population, the median value (red line) of integrated fluorescence was used to combine replicate experiments to present data as histograms shown in Figure 6.9.C-D.

For doxorubicin, a dose of 10μM doxorubicin was required to achieve γH2Ax formation above the basal level (0μM) (*P>0.001*) (Figure.6.9C). In epirubicin treated cells, the response to treatment is dose dependent but between 10μM and 20μM, there was no observed change in integrated fluorescence. However, in contrast to doxorubicin, 1μM epirubicin treatment (*P=0.027*) is sufficient to produce a response above basal levels (Figure. 6.9D). This suggests that epirubicin is more potent than doxorubicin at inducing DSB within cells.

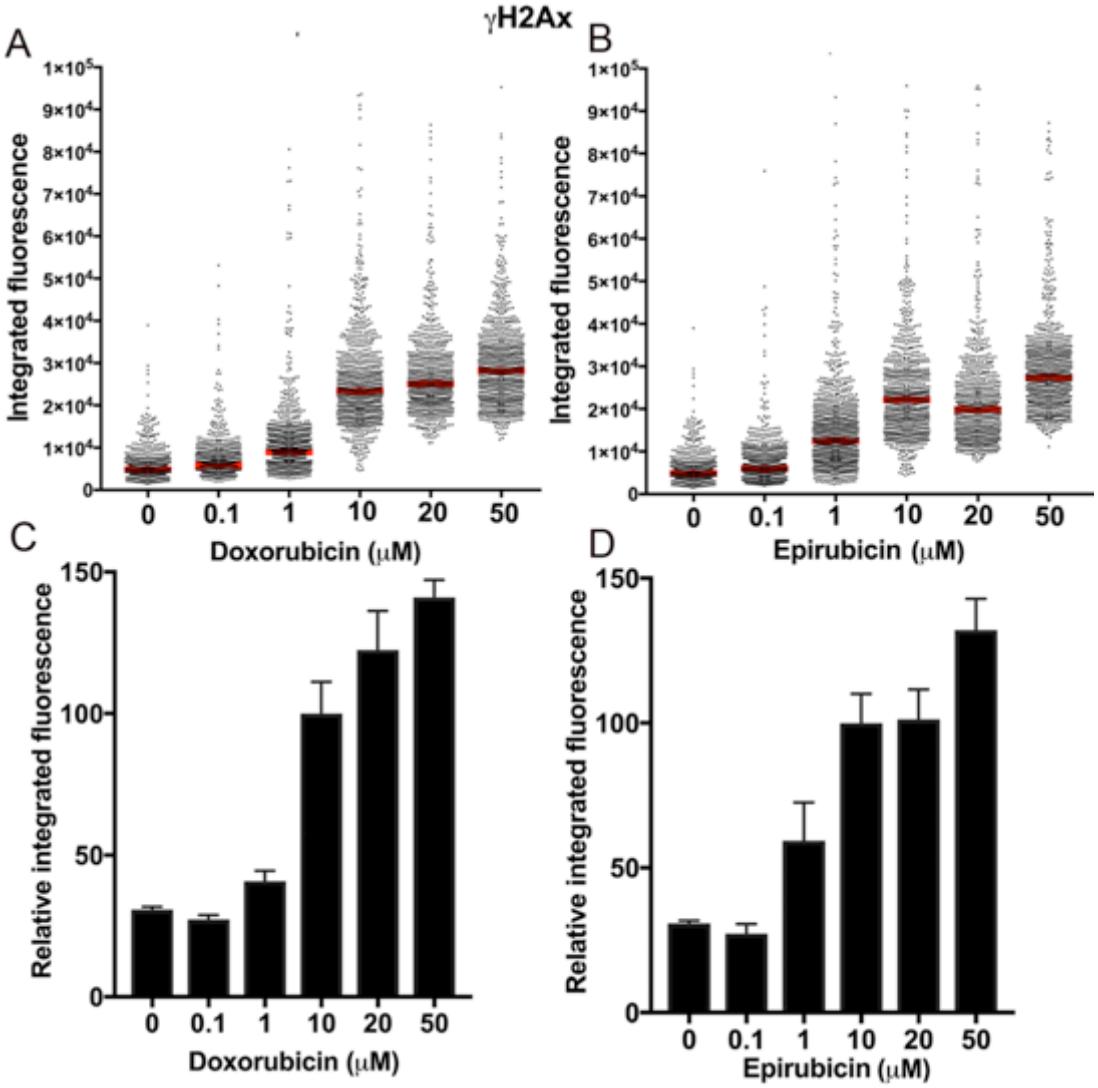


**Figure 6.9. Dose response of doxorubicin or epirubicin- induced γH2Ax formation.** NB4 cells were treated with the specified concentrations of doxorubicin (A) or epirubicin (B) for 1 hour and probed for the level of γH2Ax formation using quantitative immunofluorescence (A & B) n=1. In figures A and B, each point on the scattergram represents the level of integrated fluorescence (i.e. level of γH2Ax signal) obtained per cell. Data from a further three experiments were combined using the mean of the medians (median value shown as a red line in A & B) to generate the histograms shown in C & D. Data are expressed relative to 10μM of doxorubicin (C) or 10μM epirubicin (D) ±S.E.M (n=4).

### *6.3.4. The effect of MPO inhibition and glutathione depletion on doxorubicin and epirubicin induced γH2Ax formation.*

As described in section 6.3.2, inhibition of MPO activity significantly reduced the level of epirubicin induced TOP2A-DNA covalent complexes in NB4 cells (Figure.6.8A). Therefore, I investigated whether inhibition of MPO also affected the level of γH2Ax formation after treatment with 10μM epirubicin or doxorubicin. To inhibit MPO, cells were pretreated with 200μM SA for 48hr followed by incubation with 10μM doxorubicin or epirubicin. Pretreatment with SA significantly reduced the level of both

doxorubicin (Figure.6.10A) and epirubicin (Figure.6.10.B) induced γH2Ax formation (reduction by 36% and 28% respectively) (Figure.6.10.C). As SA pre-treatment reduced the level of epirubicin stabilised TOP2A-DNA covalent complexes by 40% this suggests the formation of DSB in epirubicin treated cells may at least be partly due to the processing of stabilised TOP2A-DNA covalent complexes to DSB. For doxorubicin, a TARDIS signal above basal TOP2-DNA complex stabilisation was not obtained, despite the robust γH2Ax phosphorylation using the same drug concentration. This may suggest that doxorubicin induces predominantly DSB via a different mechanism to poisoning TOP2.

Both doxorubicin and epirubicin undergo redox cycling within cells, it is plausible that reduced glutathione may reduce the action of both the anthracyclines and therefore, reduce the level of DSB in cells upon exposure to doxorubicin or epirubicin. NB4 cells were pre-treated with 150μM BSO for 4.5hr to deplete cells of total and reduced glutathione. BSO treated cells had 28% more doxorubicin-induced γH2Ax formation (*P=0.044*) compared to non-BSO pre-treated cells (Figure.6.10A). Similarly, BSO treatment induced a 28% increase in epirubicin induced γH2Ax formation *(P=0.001)* (Figure.6.10.B). To investigate if the affect observed in glutathione-depleted cells is due to MPO, NB4 cells were first pre-treated with SA followed by treatment with BSO. In SA+BSO pre-treated cells, incubation with either doxorubicin or epirubicin reduced the level of γH2Ax formation to a level that was no longer significantly different to SA treated cells (*P=0.239* and *P=0.524* respectively) (Figure.6.10.A-B). This indicates the elevated levels of doxorubicin or epirubicin induced γH2Ax formation in glutathione depleted cells is dependent upon MPO mediated oxidation of doxorubicin and epirubicin to semi-quinone and di-quinone species.

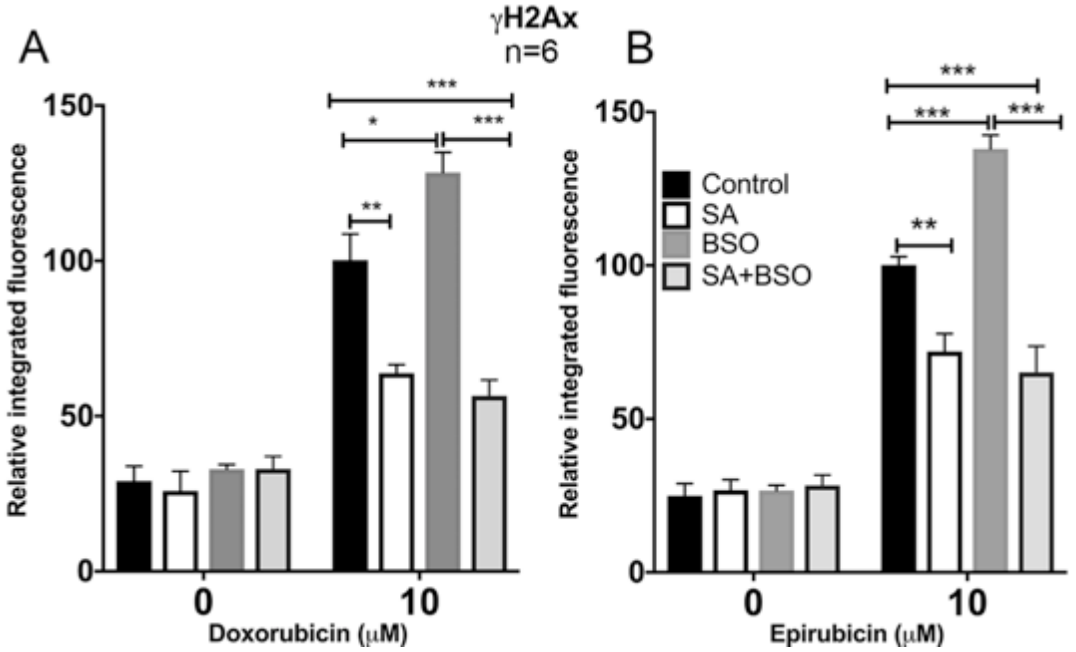


C

| Cell line | Assay | Pre-treatment | Doxorubicin/ μM | %+ve control | SEM | Sig (*P*-value) | % reduction by SA | % increase by BSO | % reduction by SA+BSO |
|---|---|---|---|---|---|---|---|---|---|
| NB4 | γH2Ax | None | 10 | 100 | 8.4 | | | | |
| NB4 | γH2Ax | SA | 10 | 63.8 | 2.8 | 0.094 | 36.2 | | |
| NB4 | γH2Ax | BSO | 10 | 120.1 | 10.1 | 0.044 | | 28.4 | |
| NB4 | γH2Ax | SA+BSO | 10 | 56.5 | 5.1 | 0.019 | | | 43.5 |

D

| Cell line | Assay | Pre-treatment | Epirubicin/ μM | %+ve control | SEM | Sig (*P*-value) | % reduction by SA | % increase by BSO | % reduction by SA+BSO |
|---|---|---|---|---|---|---|---|---|---|
| NB4 | γH2Ax | None | 10 | 100 | 2.8 | | | | |
| NB4 | γH2Ax | SA | 10 | 72 | 5.8 | 0.013 | 28 | | |
| NB4 | γH2Ax | BSO | 10 | 138 | 4.5 | 0.001 | | 27.5 | |
| NB4 | γH2Ax | SA+BSO | 10 | 65.1 | 8.5 | 0.002 | | | 35 |

**Figure 6.10. The effect of inhibiting MPO and depleting glutathione on the level of doxorubicin (A) and epirubicin (B) induced γH2Ax formation.** NB4 cells were pre-treated with SA (200μM, 48hr) or BSO (150μM, 4.5hr) or with both or with neither followed by the treatment with 10μM doxorubicin (A) or epirubicin (B) for 1 hour. Cells were then processed to quantify the level of γH2Ax phosphorylation using immunofluorescence. Data are expressed relative to 10μM doxorubicin (A) or 10μM epirubicin (B) ±S.E.M. (C-D) Percentage values are shown relative to the mean of 10μM doxorubicin (C) or 10μM epirubicin in non-pretreated cells. Statistical analysis was performed by the one-way ANOVA with post hoc Tukey's multiple comparison test. * *P* <0.05; ** *P <0.01; ***P<0.001.*

### *6.3.5 Catalytic inhibition of TOP2 by anthracyclines and mitoxantrone*

The anthracyclines, aclarubicin and idarubicin behave as catalytic inhibitors of TOP2 and reduce TOP2 poison induced TOP2-DNA covalent complex stabilisation. The route of catalytic inhibition by aclarubicin or idarubicin is thought to be via DNA intercalation preventing the binding of TOP2 (Ferrazzi *et al.*, 1991; Jensen and Sehested, 1997). Therefore it was investigated whether the anthracyclines; doxorubicin and epirubicin and the anthracenedione, mitoxantrone behave as catalytic inhibitors of TOP2 as these drugs can intercalate into DNA. To conduct these experiments the TARDIS assay was modified at the stage of drug incubation to explore whether a particular compound behaves as a TOP2 catalytic inhibitor. This will be referred to as the TARDIS inhibitor assay (method described in 2.13.1 to 2.13.8). In this assay the proposed catalytic inhibitor is added to the cells for 1 hour. Following this, a known TOP2 poison (etoposide) is added to cells for an additional 1 hour. During the incubation with etoposide the catalytic inhibitor remains in the cell culture medium. If the compound catalytically inhibits TOP2, then the level of etoposide stabilised TOP2-DNA covalent complexes will be reduced compared to the etoposide alone positive control.

NB4 cells were incubated separately with the proposed catalytic inhibitors (doxorubicin, epirubicin or mitoxantrone) for 1 hour followed by the incubation with 10μM or 100μM etoposide. The dose chosen for mitoxantrone was 20μM as at this concentration mitoxantrone reduced levels of TOP2A and TOP2B-DNA complex stabilisation compared to 1μM mitoxantrone treatment (see section 4.3.1). In addition, 100μM ICRF-193, an established catalytic inhibitor of TOP2 was used as positive control. Previous studies conducted in the Austin lab showed that 100μM ICRF-193 inhibited etoposide induced TOP2A and TOP2B-DNA covalent complex stabilisation in MEFs (Errington, 2001) .

Figure 6.11A-D shows the pre-treatment with the ICRF-193 or proposed catalytic inhibitor doxorubicin, epirubicin or mitoxantrone substantially reduces the level of etoposide stabilised TOP2A- and TOP2B-DNA covalent complexes across the whole cell population, this is true for both 10μM and 100μM etoposide. Notably the TOP2B signal obtained with 10μM etoposide in the presence of catalytic inhibitors is comparable to the basal level of TOP2B-DNA complex stabilisation observed in non-

drug treated cells (0μM). (Figure.6.11.B). Data from a five additional biological replicates were combined using the median values (red line-Figure. 6.11.A-C) to produce data for statistical analysis and is shown in Figure 6.12.

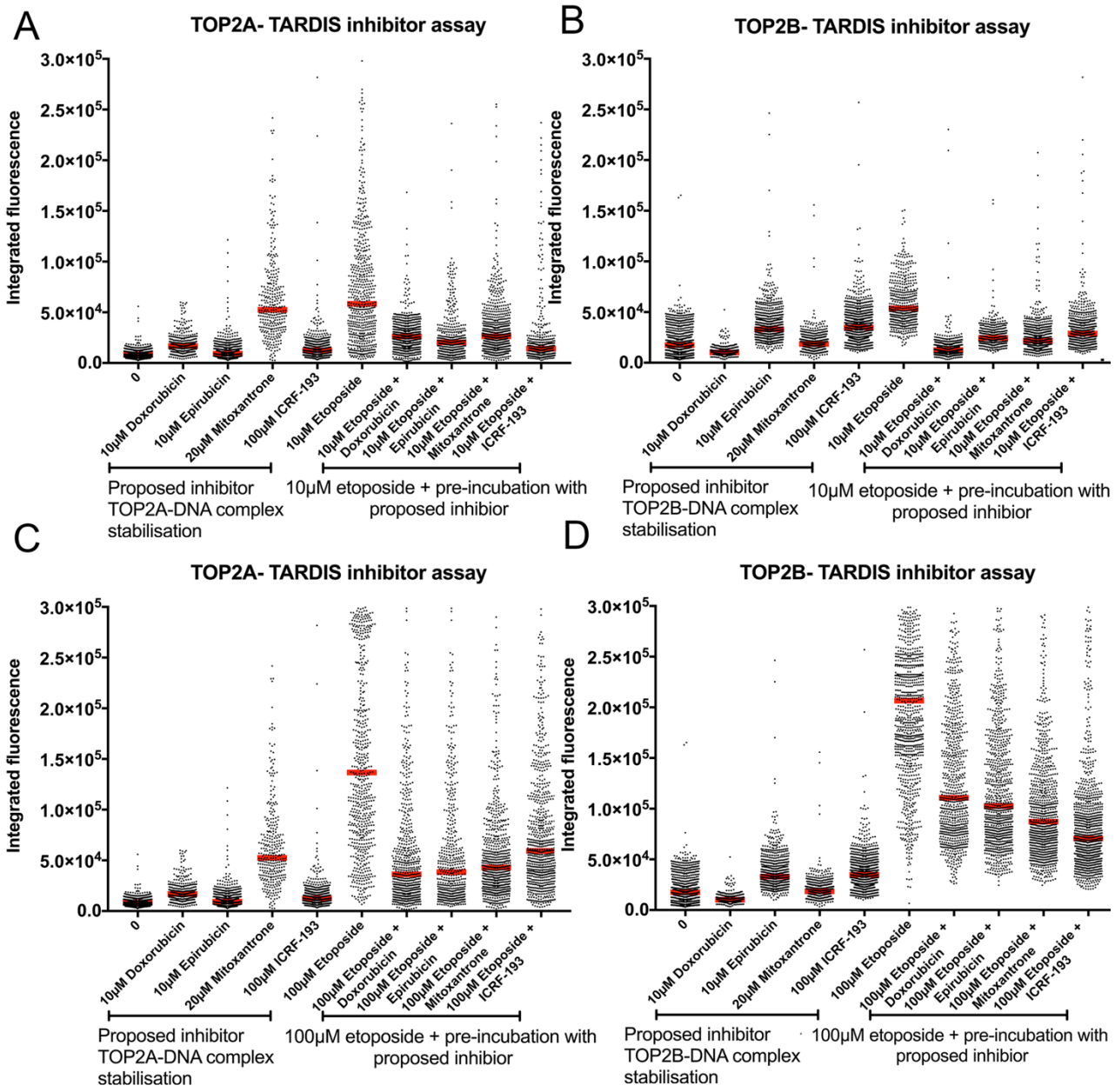


**Figure 6.11. Inhibition of etoposide-stabilised TOP2A (A and C) and TOP2B (B and D) DNA covalent complexes by anthracyclines or mitoxantrone.** NB4 cells were pre-incubated with either 10μM of doxorubicin or epirubicin or 20μM mitoxantrone or 100μM ICRF-193 (positive control) for 1 hr. Following this, cells were treated with 10μM (Ju *et al.*) or 100μM (C-D) etoposide or a vehicle control (0.02% DMSO) for 1hr. Etoposide stabilised complexes were quantified for TOP2A (A and C) or TOP2B (B and D) using TARDIS assay. Data are expressed as scattergrams obtained from a single biological replicate, where the red line represents medium line of integrated fluorescence (a minimum of 600 cell analysed per treatment).

Pre-treatment with 10μM doxorubicin resulted in 40% (*P<0.001*) reduction in TOP2A-DNA complexes induced by 100μM etoposide, this signal obtained was no longer different to that observed with 10μM etoposide for non-pretreated cells (*P=0.750*) (Figure.6.12.A). However, at 10μM etoposide a reduction of 70% (*P<0.001*) in TOP2A-DNA complexes was observed with the prior treatment with doxorubicin (Figure.6.12.A). For TOP2B, pre-treatment with doxorubicin resulted in 38% (*P<0.001*) and 47% (*P<0.001*) reduction in etoposide stabilised TOP2B-DNA complexes at 10μM and 100μM etoposide respectively (Figure.6.12.B). Notably with doxorubicin treatment, the levels of TOP2B complexes induced with 10μM etoposide were comparable to the level of basal TOP2B-DNA complexes observed in non-drug treated cells (*P=0.226*) (Figure.6.12.B).

The addition of epirubicin prior to treatment with etoposide, reduced the levels of etoposide stabilised TOP2A complexes by 60% with 10μM etoposide (*P<0.001*) and 49% with 100μM etoposide (*P<0.001*) (Figure.6.12.A and C). The level of TOP2A-DNA complexes induced with 100μM etoposide in 10μM epirubicin pre-treated cells was comparable to the level of TOP2A complexes observed with 10μM etoposide in non-pretreated cells (*P=0.997*) (Figure.6.12A). The same was true for TOP2B, prior treatment with 10μM epirubicin reduced the level of TOP2B-DNA complexes with 100μM etoposide, to a level which was no longer significantly different to 10μM etoposide treatment in non-pretreated cells (*P=0.323*) (Figure.6.12.B). Similarly, to doxorubicin pre-treatment, the pre-treatment with epirubicin reduced the levels of etoposide (10μM) stabilised TOP2B complexes to a level that was no longer significantly different to the basal level of TOP2B-DNA complexes (*P=0.960*) (Figure.6.12B).

The suggestion made in chapter 4 (4.3.1) that mitoxantrone could behave as a TOP2 poison at lower doses (0.1μM-10μM) and as a TOP2 catalytic inhibitor at higher doses is supported by the data obtained in Figures 6.11 to 6.12A-C. Pretreatment with 20μM mitoxantrone resulted in a significant reduction in etoposide complex stabilisation for both TOP2A and TOP2B at both 10μM (70% and 44%) and 100μM (61% and 63%) etoposide (Figure.6.12A-C). Interestingly, pretreatment with mitoxantrone resulted in a level of etoposide stabilised TOP2A complexes with 10μM etoposide being lower than those obtained with 20μM mitoxantrone alone for TOP2A (*P<0.001*). Additionally, TOP2A-DNA complexes obtained with the pre-incubation of

mitoxantrone at 100μM etoposide were significantly lower than the level of complex stabilisation obtained with 10μM etoposide in non-pretreated cells (23% lower, *P=0.030*) (Figure.6.12.A).

As ICRF-193 is a catalytic inhibitor of TOP2, it is not anticipated that ICRF-193 alone will poison TOP2, however it was observed that 100μM ICRF-193 induced a small increase in integrated fluorescence values, consistent with a low level of TOP2A poisoning (*P<0.001*); this has been previously reported in vitro (Jensen *et al.*, 2000; Huang *et al.*, 2001). The degree of TOP2A poisoning obtained with 100μM ICRF-193 is comparable to 10μM epirubicin (*P=0.941*). Pre-treatment with ICRF-193 resulted in reduced levels of etoposide complex stabilisation for both TOP2A and TOP2B at both 10μM (67% and 55%) and 100μM (34% and 64%) etoposide (Figure.6.12A-C). NB4 cells contain MPO, and as anthracyclines and mitoxantrone are affected by MPO activity, it was thought that the effects observed for catalytic inhibition in NB4 cells may affected by the action of MPO. To test this a replicate experiment was performed in K562 cells, which are negative for MPO expression. As shown in Figure 6.13A-B doxorubicin, epirubicin and mitoxantrone behave as catalytic inhibitors in K562 cells. Notably the affect seen in K562 cells is more pronounced with 100μM etoposide treatment compared to NB4 cells for TOP2B (Figure.6.13.B-C and 6.14.B-C). At 100μM etoposide the pre-treatment with the proposed catalytic inhibitors resulted in a level of TOP2B complex stabilisation being lower than that obtained with 10μM etoposide (Figure.6.14.B). As a result, pretreatment with doxorubicin or epirubicin resulted in the TOP2B-DNA complex level obtained with 100μM etoposide being 59% (*P=0.012*) and 48% (*P=0.044*) lower than the signal obtained with 10μM etoposide for non-pretreated cells (Figure.6.14.B). Pre-treatment with 20μM mitoxantrone at 100μM etoposide also resulted in a 59% (*P=0.012*) reduction of TOP2B-DNA complexes compared to 10μM etoposide (Figure.6.14.B-C).

In contrast, using each proposed catalytic inhibitor or ICRF-193 the level of reduction obtained after treatment with 100μM etoposide for TOP2A was greater in NB4 cells (Figure.6.12.A) than K562 cells (Figure.6.14.A). As a result, mitoxantrone pre-treatment in NB4 cells resulted in 63% (*P<0.001*) reduction in TOP2A-DNA complex stabilisation at 100μM etoposide whereas in K562 cells the level of reduction was 38% (*P=0.014*) (Figure.6.14.A and C). Similarly, for doxorubicin pre-treatment in NB4 cells, the level of TOP2A-DNA complexes at 100μM reduced by 47% *(P<0.001*)

(Figure 6.12.A and C) and for K562 cells the reduction was 20% (*P=0.002*) (Figure.6.14.A and C).

Taken together the data obtained show that doxorubicin, epirubicin and mitoxantrone behave as catalytic inhibitors of TOP2 and reduce TOP2 poison action, which is independent on the expression of active MPO.

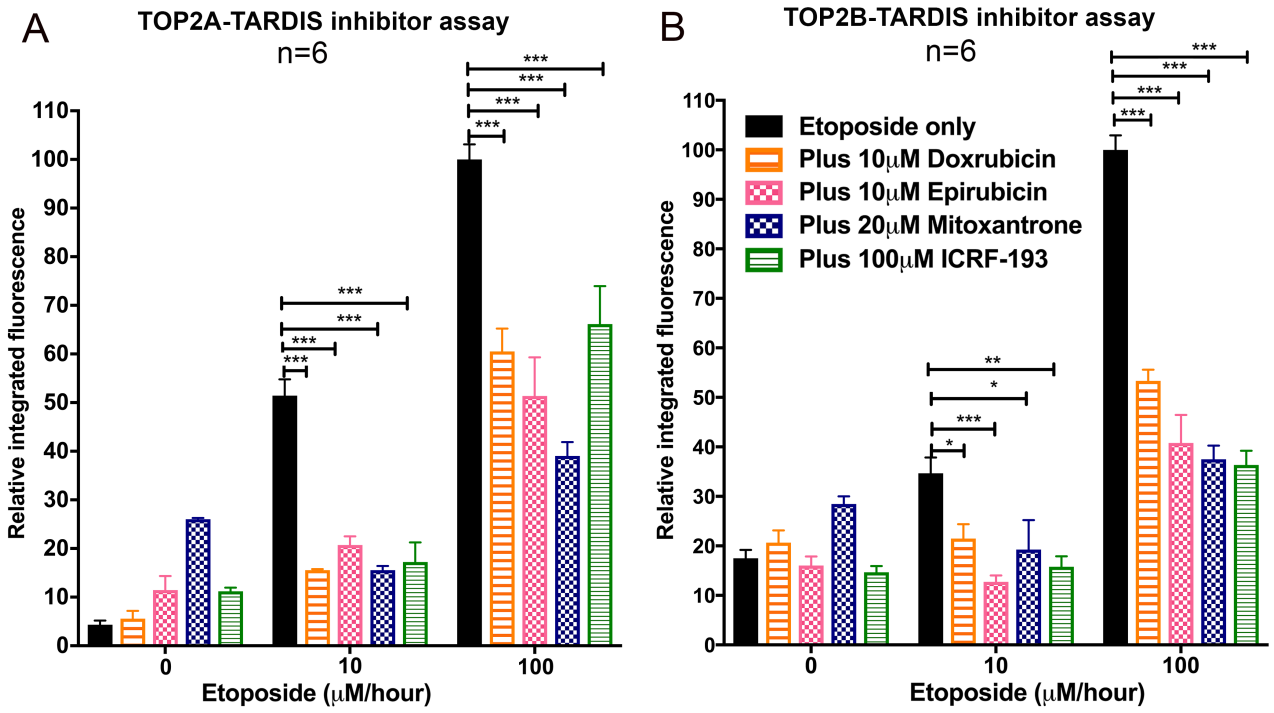

C

| Cell line | TARDIS Assay | Pre-treatment | Etoposide /μM | %+ve control | SEM | Sig (*P*-value) | % reduction by pre-treatment |
|---|---|---|---|---|---|---|---|
| NB4 | TOP2A | None | 10 | 51.4 | 3.4 | | |
| NB4 | TOP2A | 10μM Doxorubicin | 10 | 15.5 | 0.2 | <0.001 | 70 |
| NB4 | TOP2A | 10μM Epirubicin | 10 | 20.7 | 1.7 | <0.001 | 60 |
| NB4 | TOP2A | 20μM Mitoxantrone | 10 | 15.6 | 0.8 | <0.001 | 70 |
| NB4 | TOP2A | 100μM ICRF-193 | 10 | 17.2 | 4 | <0.001 | 66.5 |
| NB4 | TOP2A | None | 100 | 100 | 3.1 | | |
| NB4 | TOP2A | 10μM Doxorubicin | 100 | 60.5 | 4.7 | <0.001 | 39.5 |
| NB4 | TOP2A | 10μM Epirubicin | 100 | 51.4 | 8 | <0.001 | 48.6 |
| NB4 | TOP2A | 20μM Mitoxantrone | 100 | 39.1 | 2.8 | <0.001 | 60.9 |
| NB4 | TOP2A | 100μM ICRF-193 | 100 | 66.2 | 7.8 | <0.001 | 33.8 |
| NB4 | TOP2B | None | 10 | 34.7 | 3.2 | | |
| NB4 | TOP2B | 10μM Doxorubicin | 10 | 21.5 | 2.9 | <0.001 | 38 |
| NB4 | TOP2B | 10μM Epirubicin | 10 | 12.7 | 1.3 | <0.001 | 63.4 |
| NB4 | TOP2B | 20μM Mitoxantrone | 10 | 19.3 | 6 | 0.05 | 44.4 |
| NB4 | TOP2B | 100μM ICRF-193 | 10 | 15.8 | 2.1 | 0.004 | 54.5 |
| NB4 | TOP2B | None | 100 | 100 | 3 | | |
| NB4 | TOP2B | 10μM Doxorubicin | 100 | 53.3 | 2.3 | <0.001 | 46.7 |
| NB4 | TOP2B | 10μM Epirubicin | 100 | 40.8 | 5.7 | <0.001 | 59.2 |
| NB4 | TOP2B | 20μM Mitoxantrone | 100 | 37.5 | 2.7 | <0.001 | 62.8 |
| NB4 | TOP2B | 100μM ICRF-193 | 100 | 36.3 | 2.9 | <0.001 | 63.7 |

**Figure 6.12. Inhibition of etoposide-stabilised TOP2A (A) and TOP2B (B) DNA covalent complexes by anthracyclines or mitoxantrone**. NB4 cells were pre-incubated with either 10μM of doxorubicin or epirubicin or 20μM mitoxantrone or 100μM ICRF-193 (positive control) for 1 hr. Following this, cells were treated with 10μM or 100μM etoposide or a vehicle control (0.02% DMSO) for 1hr. Etoposide stabilised complexes were quantified for TOP2A (A) or TOP2B (B) by TARDIS assay. Data are expressed relative to 100μM etoposide in non-pre-treated cells ±S.E.M. (C) Percentage values are relative to the mean value obtained with 100μM etoposide in non-pretreated cells. Statistical analysis was performed by the one-way ANOVA with post hoc Tukey's multiple comparison test. * *P* <0.05; ** *P <0.01; ***P<0.001*

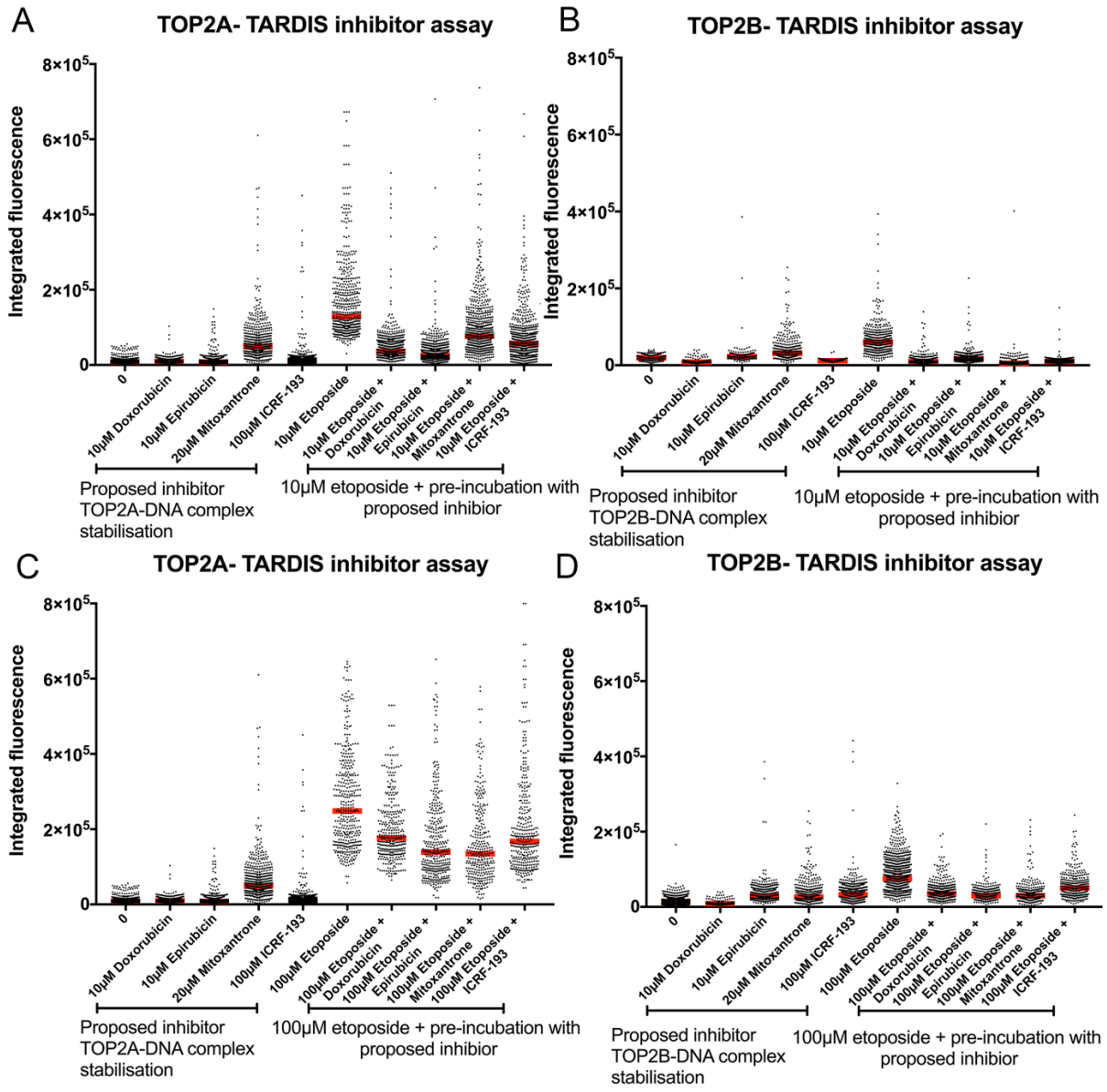


**Figure 6.13. Inhibition of etoposide-stabilised TOP2A (A and C) and TOP2B (B and D) DNA covalent complexes by anthracyclines or mitoxantrone in K562 cells.** K562 cells were pre-incubated with either 10μM of antracyclines (doxorubicin or epirubicin) or 20μM mitoxantrone or 100μM ICRF-193 (positive control) for 1 hr followed by the addition of 10μM (Ju *et al.*) or 100μM (C-D) etoposide and probed for the level of etoposide stabilised TOP2A (A and C) or TOP2B (B and D) complexes using the TARDIS assay. Data are represented as scattergrams where each point represents the integrated fluorescence (i.e TOP2-DNA complex stabilisation) obtained in each individual nuclei (a minimum of 600 cells analysed per treatment).

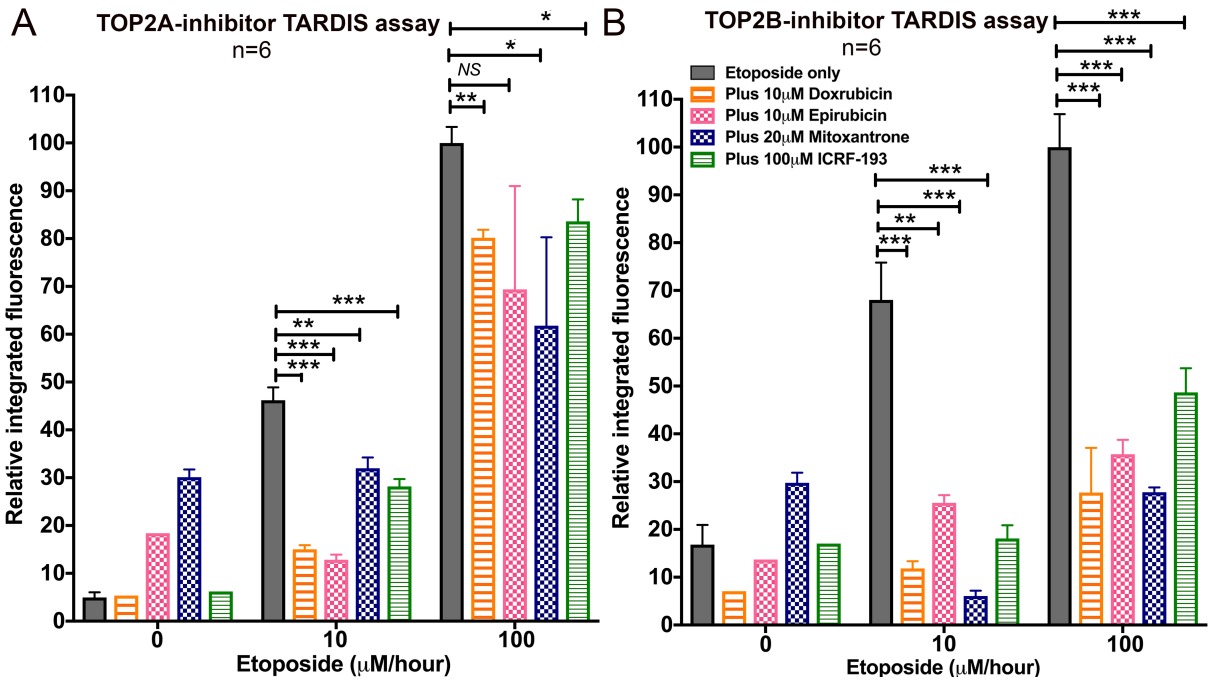


C

| Cell line | TARDIS Assay | Pre-treatment | Etoposide /μM | %+ve control | SEM | Sig (*P*-value) | % reduction by pre-treatment |
|---|---|---|---|---|---|---|---|
| K562 | TOP2A | None | 10 | 46.2 | 2.7 | | |
| K562 | TOP2A | 10μM Doxorubicin | 10 | 15 | 0.8 | <0.001 | 67.5 |
| K562 | TOP2A | 10μM Epirubicin | 10 | 12.9 | 1.1 | <0.001 | 72.1 |
| K562 | TOP2A | 20μM Mitoxantrone | 10 | 32 | 2.2 | 0.003 | 30.7 |
| K562 | TOP2A | 100μM ICRF-193 | 10 | 28.2 | 1.5 | <0.001 | 39 |
| K562 | TOP2A | None | 100 | 100 | 3.3 | | |
| K562 | TOP2A | 10μM Doxorubicin | 100 | 80.2 | 1.7 | 0.002 | 19.8 |
| K562 | TOP2A | 10μM Epirubicin | 100 | 69.4 | 21.2 | 0.259 | 30.6 |
| K562 | TOP2A | 20μM Mitoxantrone | 100 | 61.8 | 18.5 | 0.014 | 38.2 |
| K562 | TOP2A | 100μM ICRF-193 | 100 | 83.6 | 4.6 | 0.047 | 16.4 |
| K562 | TOP2B | None | 10 | 68 | 7.8 | | |
| K562 | TOP2B | 10μM Doxorubicin | 10 | 11.9 | 1.5 | <0.001 | 82.5 |
| K562 | TOP2B | 10μM Epirubicin | 10 | 25.6 | 1.6 | <0.001 | 62.4 |
| K562 | TOP2B | 20μM Mitoxantrone | 10 | 6.1 | 1.1 | 0.012 | 91 |
| K562 | TOP2B | 100μM ICRF-193 | 10 | 18.1 | 2.8 | <0.001 | 73.3 |
| K562 | TOP2B | None | 100 | 100 | 6.9 | | |
| K562 | TOP2B | 10μM Doxorubicin | 100 | 27.7 | 9.3 | <0.001 | 72.3 |
| K562 | TOP2B | 10μM Epirubicin | 100 | 35.7 | 3 | <0.001 | 64.3 |
| K562 | TOP2B | 20μM Mitoxantrone | 100 | 27.8 | 1 | <0.001 | 72.2 |
| K562 | TOP2B | 100μM ICRF-193 | 100 | 48.7 | 5 | <0.001 | 51.3 |

**Figure 6.14. Inhibition of etoposide-stabilised TOP2A (A) and TOP2B (B) DNA covalent complexes by anthracyclines or mitoxantrone in K562 cells**. K562 cells were pre-incubated with either 10μM of antracyclines or 20μM mitoxantrone or 100μM ICRF-193 (positive control) for 1 hr, followed by addition of 10μM or 100μM etoposide and probed for the level of etoposide stabilised TOP2A (A) or TOP2B (B) complexes. (C) Percentage values are shown relative to the mean value obtained with 100μM etoposide in non-pretreated cells. Data are expressed relative to 100μM etoposide (non-pretreated) ±S.E.M. Statistical analysis was performed by the one-way ANOVA with post hoc Tukey's multiple comparison test. * *P* <0.05; ** *P <0.01; ***P<0.001*

From the data obtained using the TARDIS inhibitor assay, I hypothesised that in the presence of catalytic inhibitors the level of etoposide induced γH2Ax formation would be reduced. To test this, NB4 cells were pre-incubated with either 10μM doxorubicin or epirubicin, or 20μM mitoxantrone for 1 hour followed by the addition of 10μM or 100μM etoposide for an additional 1 hour. ICRF-193 (100μM) was used as positive control in this experiment. NB4 cells were processed to analyse for the level of γH2Ax formation using quantitative immunofluorescence.

For doxorubicin and epirubicin the results differ (Figure.6.15A-B & 6.16). Pre-treatment with 10μM doxorubicin did not significantly alter the level of γH2Ax formation at 10μM (*P=0.950*) or 100μM (*P=0.600*) etoposide, suggesting the addition of doxorubicin does not significantly reduce etoposide DSB formation in cells (Figure.6.16). Treatment with 10μM epirubicin alone results in 20% greater γH2Ax formation compared to 10μM doxorubicin (Figure.6.16). Upon treatment with 10μM or 100μM etoposide the γH2Ax formation induced is comparable to response obtained with epirubicin alone (*P=0.821* and *P=0.993* respectively) (Figure.6.16). This suggests that etoposide does not induce additional DSB breaks in cells treated with epirubicin due to reduction in etoposide induced TOP2-DNA complex stabilisation.

Treatment with 100μM ICRF-193 alone in NB4 cells did not result in γH2Ax formation. Prior treatment with ICRF-193 did reduce the level of etoposide induced γH2Ax formation at 10μM and 100μM etoposide (67% and 39% less respectively) (Figure.6.16).

Prior treatment with 20μM mitoxantrone resulted in the greatest inhibition of etoposide induced γH2Ax formation (Figure.6.15 and Figure.6.16). With 10μM etoposide, the pre-treatment with mitoxantrone reduced the level of γH2Ax formation by 79% (*P<0.001*). Interestingly a greater reduction of 89% was observed with mitoxantrone pre-treatment at 100μM etoposide, this signal was comparable to that obtained with 10μM etoposide in mitoxantrone pretreated cells (*P=0.502*) (Figure.6.16.A-B). Interestingly, at both doses of etoposide the pretreatment with mitoxantrone resulted in the level of γH2Ax signal being comparable to basal levels (Figure.6.16.A).

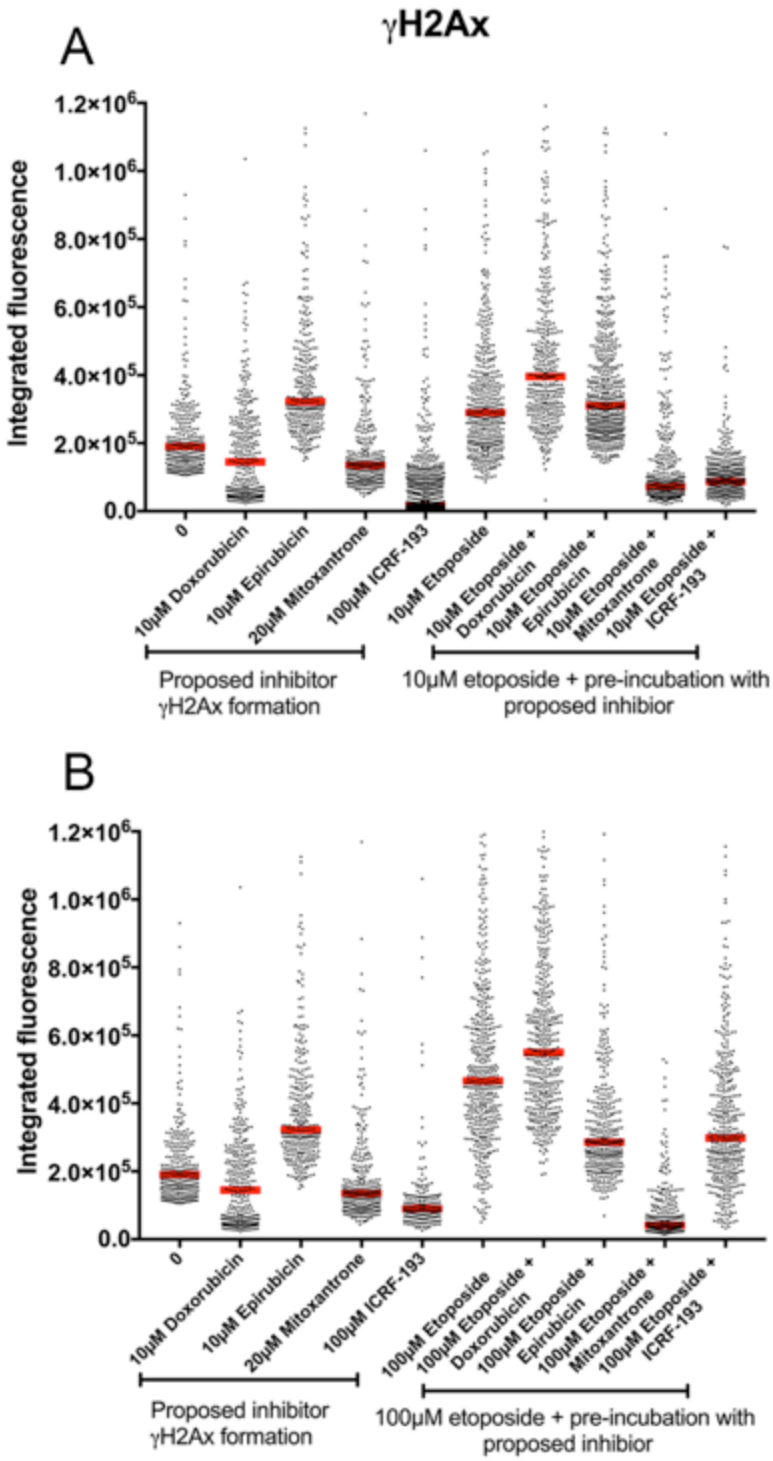


**Figure 6.15. Effect on etoposide-induced γH2Ax by pretreatment anthracyclines or mitoxantrone in NB4 cells.** NB4 cells were pre-incubated with either doxorubicin, epirubicin or mitoxantrone or ICRF-193 (positive control) for 1 hr. Following this, cells were treated with with 10μM (A) or 100μM (B) etoposide or a vehicle control (0.02% DMSO) for 1hr and probed for the level of γH2Ax formation using quantitative immunofluorescence.

A

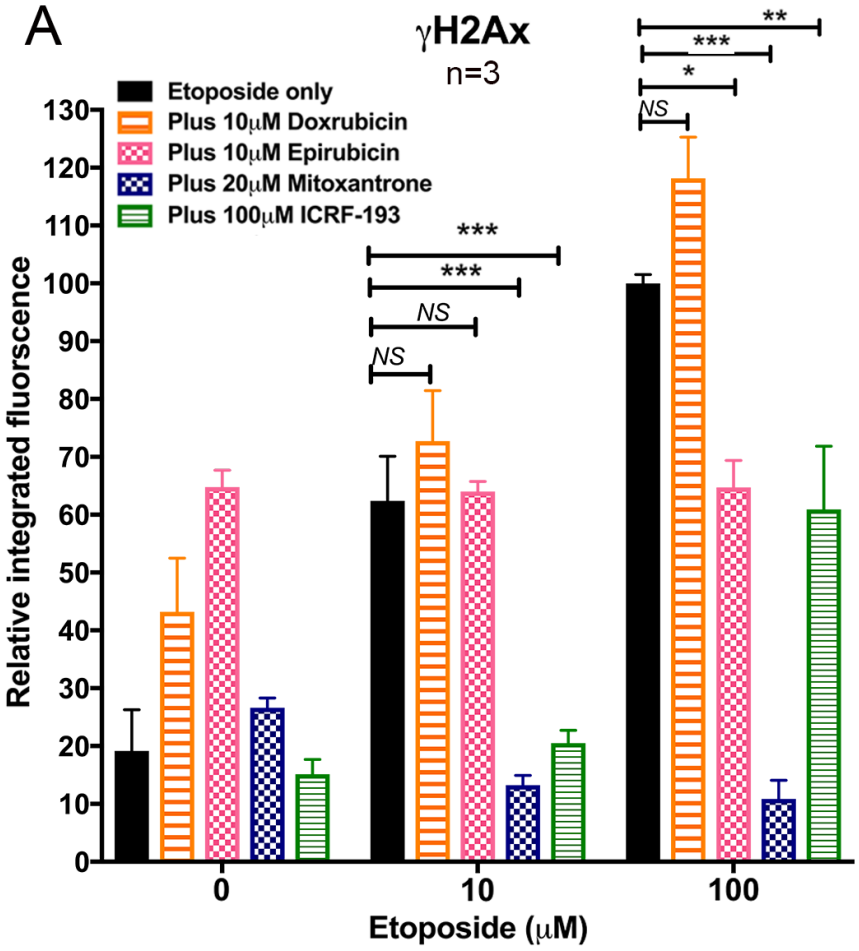


B

| Cell line | Assay | Pre-treatment | Etoposide /μM | %+ve control | SEM | Sig (*P*-value) | % reduction by pre-treatment |
|---|---|---|---|---|---|---|---|
| NB4 | γH2Ax | None | 10 | 62.4 | 7.7 | | |
| NB4 | γH2Ax | 10μM Doxorubicin | 10 | 72.7 | 8.8 | 0.950 | |
| NB4 | γH2Ax | 10μM Epirubicin | 10 | 64 | 1.7 | >0.999 | |
| NB4 | γH2Ax | 20μM Mitoxantrone | 10 | 13.2 | 1.7 | <0.001 | 78.8 |
| NB4 | γH2Ax | 100μM ICRF-193 | 10 | 20.5 | 2.2 | <0.001 | 67.1 |
| NB4 | γH2Ax | None | 100 | 100 | 3 | | |
| NB4 | γH2Ax | 10μM Doxorubicin | 100 | 118.2 | 7.1 | 0.600 | |
| NB4 | γH2Ax | 10μM Epirubicin | 100 | 64.7 | 4.7 | 0.020 | 35.3 |
| NB4 | γH2Ax | 20μM Mitoxantrone | 100 | 10.9 | 3.2 | <0.001 | 89.1 |
| NB4 | γH2Ax | 100μM ICRF-193 | 100 | 60.9 | 11 | 0.007 | 39.1 |

**Figure 6.16. Effect on etoposide-induced γH2Ax by pre-treatment anthracyclines or mitoxantrone in NB4 cells.** NB4 cells were pre-incubated with either doxorubicin, epirubicin or mitoxantrone or ICRF-193 (positive control) for 1 hr. Following this, cells were treated with with 10μM or 100μM etoposide or a vehicle control (0.02% DMSO) for 1hr and probed for the level of γH2Ax formation using quantitative immunofluorescence. Data are expressed relative to 100μM etoposide ±S.E.M. (B) Supporting data table shows the percentage values relative to the mean value obtained with 100μM etoposide in non-pretreated cells. Statistical analysis was performed by the one-way ANOVA with post hoc Tukey's multiple comparison test. * *P* <0.05; ** *P <0.01; ***P<0.001.*

### *6.3.6. Role of etoposide quinone as a TOP2 covalent inhibitor.*

In vitro studies have reported that etoposide quinone both poisons TOP2 and inhibits DNA binding to TOP2 (Smith *et al.*, 2014b; Gibson *et al.*, 2016). Etoposide quinone is an MPO catalysed metabolite of etoposide. Etoposide quinone is defined by the presence of carbonyl groups at the 3' and 4' positions of the E-ring. In the previous chapter (see section 5.3.3 to 5.3.4) the role of etoposide quinone as a TOP2 poison was investigated and data showed that etoposide quinone poisons both TOP2A and TOP2B in perhaps a similar mechanism to etoposide. In this chapter the role of etoposide quinone as a catalytic inhibitor was investigated using the TARDIS inhibitor assay (see section 6.3.5 and 2.13). For this 10μM etoposide quinone was incubated in NB4 cells for 1 hour prior to addition with 10μM or 100μM etoposide. The dose of 10μM etoposide quinone was chosen, as at this dose there was low level of TOP2 poisoning observed (5.3.3).

As seen in Figure 6.17A, 10μM etoposide quinone does not induce TOP2A-DNA complexes which are significantly above the basal level of TOP2A complexes observed in non-drug treated cells (*P=0.992*). However, the pre-treatment with etoposide quinone significantly reduces the level of etoposide (10μM) stabilised TOP2A complexes by 32% (*P=0.038*), but no significant affect was observed at 100μM etoposide (*P=0.056*) (Figure.6.17.A and C). For TOP2B, etoposide quinone did not reduce the level of TOP2 poisoning induced by either 10μM or 100μM etoposide (Figure.6.17.B). Indeed, at 100μM etoposide the pre-treatment of etoposide quinone resulted in greater TOP2B-DNA complex stabilisation of 38% (*P=0.005*) (Figure.6.17.B and C). This suggests that etoposide quinone behaves as a catalytic inhibitor of TOP2A but not for TOP2B. 100μM etoposide treatment seems to out-compete the catalytic inhibitor capacity of 10μM etoposide quinone.

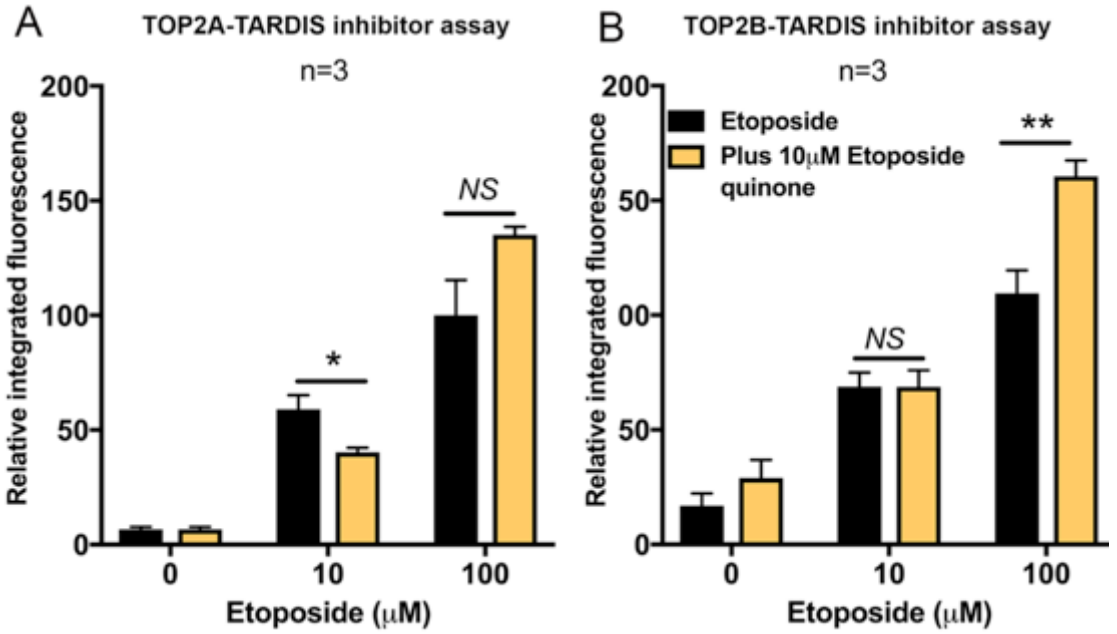


C

| Cell line | Assay | Pre-treatment | Etoposide /μM | %+ve control | SEM | Sig (*P*-value) | % reduction by pre-treatment |
|---|---|---|---|---|---|---|---|
| NB4 | TOP2A-CC | None | 10 | 59 | 6.2 | | |
| NB4 | TOP2A-CC | 10μM Etoposide quinone | 10 | 40.2 | 2 | 0.038 | 31.8 |
| NB4 | TOP2A-CC | None | 100 | 100 | 15.4 | | |
| NB4 | TOP2A-CC | 10μM Etoposide quinone | 100 | 135.2 | 3.5 | 0.056 | |
| NB4 | TOP2B-CC | None | 10 | 68.8 | 6.2 | | |
| NB4 | TOP2B-CC | 10μM Etoposide quinone | 10 | 68.7 | 7.2 | >0.999 | |
| NB4 | TOP2B-CC | None | 100 | 100 | 6.4 | | |
| NB4 | TOP2B-CC | 10μM Etoposide quinone | 100 | 160.5 | 6.9 | 0.005 | |

**Figure 6.17. Effect of etoposide quinone pretreatment on the level of etoposide stabilised TOP2A (A) and TOP2B (B) covalent complexes in NB4 cells.** Cells were pre-treated with 10μM etoposide quinone (Cayman Chemicals) for 1 hour followed by the incubation with 10μM or 100μM etoposide. Cells were then processed for the level of etoposide stabilised TOP2A or TOP2B using the TARDIS assay. Data are expressed relative to the mean value obtained with 100μM etoposide for pre-treated NB4 cells (black bars) ±S.E.M. (C) Percentage values are shown relative to mean value obtained for 100μM etoposide in non-pretreated cells. Statistical analysis was performed using the Student's t-test. * *P* <0.05; ** *P <0.01..*

## 6.4 Discussion

The anthracyclines doxorubicin and epirubicin are known to have potentially multiple mechanisms for cytotoxicity. However, it is unknown whether under the doses administered in chemotherapy regimes doxorubicin or epirubicin are able to accumulate in cells to have multiple routes of damage causing DNA DSB. As shown

in this chapter, both doxorubicin and epirubicin cause a dose dependent increase in DNA DSB formation as assayed by the quantification of γH2Ax formation (Figure.6.9A-D). Additionally active MPO expression and depletion of glutathione enhanced the level of γH2Ax formation in doxorubicin or epirubicin treated cells (Figure.6.10A-B). Notably the elevation in γH2Ax formation in glutathione-depleted cells was dependent on active MPO expression. This supports the idea that MPO mediates the formation of doxorubicin or epirubicin semi-quinone species that further disproportionates to a di-quinone species leading to DNA DSB formation (Reszka *et al.*, 2005). In the presence of glutathione, the semi-quinone and di-quinone species could conjugate with glutathione leading to their detoxification. In addition, as MPO can catalyse the production of formaldehyde, the formation of doxoform and epiform could contribute to the γH2Ax formation observed in NB4 cells. If doxoform or epiform were produced in cells then DNA damage would be caused by the formation of DNA cross-links via a combination of covalent bonding (by formaldehyde), DNA intercalation and hydrogen bonding (by the anthracycline) (Fenick *et al.*, 1997).

Both doxorubicin and epirubicin displayed low potency towards TOP2 poisoning (Figure.6.4 to 6.6.) yet displayed effective TOP2 catalytic inhibitor functionality by inhibiting etoposide induced TOP2A- and TOP2B-DNA complex stabilisation (Figure.6.11-6.14). Additionally mitoxantrone pre-treatment also effectively inhibited etoposide TOP2A and TOP2B complex formation. It is not clear how doxorubicin, epirubicin or mitoxantrone behave as TOP2 catalytic inhibitors. Studies have suggested that anthracycline based TOP2 catalytic inhibition act by DNA intercalation which blocks TOP2 binding to DNA (Sorensen *et al.*, 1992; Sehested and Jensen, 1996). Mitoxantrone can be activated by peroxidases or formaldehyde to form DNA adducts which may also block TOP2 binding (Panousis *et al.*, 1994; Panousis *et al.*, 1997; Parker *et al.*, 1999; Parker *et al.*, 2000; Parker *et al.*, 2001). Additionally as mitoxantrone is able to condense nuclei acids, this may also block TOP2 binding to DNA (Kapuscinski and Darzynkiewicz, 1986; Hajihassan and Rabbani-Chadegani, 2009). However, as both the anthracyclines and mitoxantrone are able to poison TOP2 it is possible that these drugs interact with TOP2 and inhibit the enzyme directly. As etoposide quinone is reported to inhibit TOP2 due to presence of *ortho*-quinone on the E-ring (Lindsey *et al.*, 2005; Bender and Osheroff, 2007; Jacob *et al.*,

2011), it could be feasible that the anthracyclines and mitoxantrone use their quinone moieties to adduct TOP2.

Whilst doxorubicin, epirubicin and mitoxantrone followed the same trend in the reduction of etoposide induced TOP2-DNA complex stabilisation, the trend in inhibition of etoposide induced γH2Ax formation was different for each drug (Figure.6.15-6.16). Prior treatment with doxorubicin did not affect etoposide induced γH2Ax formation whereas epirubicin treatment inhibited the γH2Ax formation by etoposide. Mitoxantrone pre-treatment reduced the level of etoposide induced γH2Ax formation to basal levels (0μM) and was the most effective inhibitor of etoposide induced DSB formation. Clinically this is important as mitoxantrone, epirubicin and doxorubicin are separately used in chemotherapy regimes involving etoposide. For example in chemotherapy regimes termed, MEC, PACE, VIDE and IEV involve etoposide (represented by E or V) used in combination therapy with mitoxantrone (represented by M), doxorubicin (represented by A or D) or epirubicin (represented by E in IEV). The data shown in this chapter suggests that using etoposide in conjugation with anthracyclines or mitoxantrone will reduce etoposide activity in cells.

# Chapter 7. Discussion

## 7.1 The effect of myeloperoxidase expression on TOP2 poison-mediated DNA damage.

Topoisomerase II (TOP2) poisons are effective cytotoxic agents used to treat a wide range of neoplasms including solid cancers and haematological malignancies. However, TOP2 poison therapy is associated with a small but increasing risk of developing therapy related acute myeloid leukaemia, characterised by recurrent balanced chromosome translocations commonly involving the *MLL (KMT2A)* gene at 11q23 or *t(15,17)(PML-RARA)*, *t(8,21)(RUNX1-RUNX1T1/ETO)*, or inv*(16)(p13;q22)(CBFB-MYH11),* and are generally associated with a poor prognosis compared to *de novo* AML (Leone *et al.*, 2010; Kayser *et al.*, 2011; Cowell and Austin, 2012).

The development of therapy related leukaemia is a rare but life threating complication side effect from primary therapy. Although mechanisms leading to t-AML have not been fully elucidated, measures to protect hematopoietic progenitors from genotoxic damage caused during primary therapy would be of clinical benefit. Whereas the development of t-AML reflects genotoxic damage caused by TOP2 poisons, another side effect of TOP2 poison therapy is myelosuppression (bone marrow suppression), defined by the reduction in blood cell activity due to decreased production in blood cells.

Myeloperoxidase (MPO) is expressed in myeloid progenitor cells and is capable of catalysing the oxidation of TOP2 poisons including etoposide, mitoxantrone and anthracyclines to metabolites with altered DNA damaging properties and potentially genotoxic in nature. Therefore, the presence of MPO could increase myeloid cell susceptibility to TOP2 poison induced genetic and/or cytotoxic damage. This hypothesis is supported by data reported in this thesis which shows inhibition of MPO using succinylacetone (SA) significantly reduces the level of TOP2 poison induced TOP2-DNA damage (tested using etoposide, mitoxantrone, epirubicin) and γH2Ax formation (tested using etoposide, mitoxantrone, doxorubicin or epirubicin) in NB4 cells.

To further, confirm the data generated using SA in NB4 cells, two small molecule direct inhibitors of MPO were used; PF1355 (Phase I clinical trials completed) and MPOi-II. Results generated with both inhibitors showed specific inhibition of MPO greatly reduced the level of TOP2 poison induced DNA damage for both etoposide and mitoxantrone. Similarly, induction of exogenous expression of MPO into K562 cells (non-MPO expressers) significantly increased the level of etoposide- or mitoxantrone induced TOP2 mediated damage. An example of this is one $K562^{MPO}$ cell line that only exhibited 18% MPO activity compared to NB4 cells displayed up to 50% more stabilised TOP2-DNA complexes compared to parental cell lines (Table 4.1 and Figure 4.7.A-C). This result highlights that MPO expressed at moderate levels can significantly enhance TOP2 poison mediated damage.

The TOP2 poisons, etoposide and mitoxantrone effectively target both isoforms of TOP2, stabilising TOP2A- and TOP2B-DNA covalent complexes that could be detected and quantified using the TARDIS assay. However, under the conditions tested epirubicin did not induce detectable TOP2B-DNA complexes. For etoposide and mitoxantrone, suppression of MPO activity resulted in a greater reduction in the level of drug stabilised TOP2B-DNA complexes compared to TOP2A. Interesting at lower doses of etoposide or mitoxantrone the inhibition of MPO resulted in the level of drug stabilised TOP2B-DNA complexes that was comparable to the level of complexes observed in non-drug treated cells. This result is of interest as recent evidence points a greater role for TOP2B in TOP2 poison mediated carcinogenesis and in the induction of DNA breaks at regions in genes involved in t-AML (Azarova *et al.*, 2007; Haffner *et al.*, 2010; Cowell *et al.*, 2012; Smith *et al.*, 2014a).

Another factor that may increase patient susceptibility to t-AML or myelosuppression is the level glutathione present within cells. Studies have reported that following high-level chemotherapy regimens patients have reduced plasma glutathione (Charushila and Subodhini, 2013; Kadam and Abhang, 2015). Low glutathione results in a reduction in the body's capability to detoxify reactive oxide species and xenobiotics. Glutathione can protect cells from the MPO catalysed production of TOP2 poison metabolites by formation of glutathione conjugates that are subsequently excreted from the body (Blanz *et al.*, 1991; Mewes *et al.*, 1993; Zheng *et al.*, 2006). As observed in NB4 cells the depletion of glutathione using buthionine sulfoximine (BSO) greatly elevated the level of etoposide, mitoxantrone, doxorubicin and

epirubicin induced γH2Ax formation and TOP2-DNA complex stabilisation (etoposide and mitoxantrone only). However, the elevated response to glutathione depletion was only observed in NB4 cells with MPO activity. Glutathione depletion did not affect the level of TOP2 poisoning or γH2Ax formation in cells with suppression of MPO activity. This suggests glutathione acts to reduce the damage caused by MPO catalysed metabolites of TOP2 poisons.

The role of MPO and neutrophils in inflammatory disorders is of clinical interest and has led to the development of novel specific MPO inhibitors. In the work reported here, two such inhibitors PF1355 and MPOi-II were shown to effectively reduce etoposide and mitoxantrone induced TOP2-DNA complexes and γH2Ax formation. Therefore, it is feasible that compounds like PF1355 and MPOi-II could be tailored into primary chemotherapy regimens to reduce damage caused to myeloid progenitors, to decrease the occurrence of t-AML and myelosuppression. The use of glutathione supplements (ClinicalTrials.gov ID NCT01044277) could additionally protect myeloid cells from damage caused by MPO catalysed metabolites of TOP2 poisons.

### 7.2 The role of doxorubicin, epirubicin and mitoxantrone as catalytic inhibitors of TOP2.

In the latter section of this thesis, the effects of anthracyclines (doxorubicin and epirubicin) and mitoxantrone (anthracenedione) as TOP2 catalytic inhibitors were investigated. When testing the effects of MPO inhibition on TOP2 poison stabilised TOP2-DNA complexes, there were difficulties in observing a signal for TOP2-DNA stabilised complexes for doxorubicin and epirubicin and at higher concentrations of mitoxantrone. A similar observation was previously observed using mouse embryonic fibroblast cell line using doxorubicin and in vitro studies showed at high antracyclines concentrations the level of TOP2 mediated cleavage of plasmid DNA was inhibited (Tewey *et al.*, 1984; Capranico *et al.*, 1990a; Capranico *et al.*, 1990b; Willmore *et al.*, 2002). This led to the hypothesis that doxorubicin, epirubicin and mitoxantrone may behave as catalytic inhibitors of TOP2. A TOP2 catalytic inhibitor is defined as a compound that can interfere with TOP2's catalytic cycle to prevent the formation of TOP2-DNA covalent complexes (Sehested and Jensen, 1996). To test whether a proposed drug behaves as a catalytic inhibitor, cells were incubated with the drug in

question for one hour prior to the addition of etoposide and detection for the level TOP2-DNA complexes using the TARDIS assay. If the drug behaves as a TOP2 catalytic inhibitor, then the immunofluorescence TARDIS signal is reduced compared to the signal obtained with etoposide alone, due to reduced formation of TOP2-DNA covalent complexes.

Doxorubicin, epirubicin and mitoxantrone inhibited etoposide's TOP2 poisoning activity and γH2Ax formation and this did not require the action of MPO. This effect is likely due to the ability of anthracyclines and mitoxantrone to intercalate between DNA base pairs, which prevent TOP2 binding to DNA.

There are no strong consensus sequences for TOP2 mediated cleavage, although preferred *in vitro* DNA cleavage sites have been described, and there is some preference for A/T sites (Capranico and Binaschi, 1998). In addition, TOP2 does show preference for DNA structures and preferentially binds to helix-helix juxtapositions (Zechiedrich and Osheroff, 1990; West and Austin, 1999). Doxorubicin and epirubicin display a preference for binding to A/T nucleotides resulting in DNA adducts (Capranico *et al.*, 1990a; Capranico *et al.*, 1990b). This action of anthracyclines may create local structures within the DNA molecule that disfavour the binding of TOP2. Additionally as doxorubicin, epirubicin and mitoxantrone contain a hydroquinone moiety within their structures, they could potentially bind to free thiol or amine residues on TOP2 and inhibit TOP2 directly, a mechanism similar to that observed for etoposide quinone (MPO catalysed metabolite) (Gibson *et al.*, 2016).

Therefore, adding etoposide into cells with anthracycline or anthracenedione agents reduces etoposide action and this could potentially result in more 'free' etoposide to undergo oxidative activation by peroxidases such as MPO. This result is of interest as etoposide is regularly used in combination with anthracyclines or mitoxantrone for treatment in refractory AML, myeloma, plasma cell leukaemia, Ewing's sarcoma and refractory non-Hodgkin/Hodgkin lymphoma.

**Future work**

The data generated show that MPO expression enhances TOP2 poison mediated damage and the inhibition MPO activity using three chemically distinct inhibitors can reduce excessive TOP2 poison mediated DNA damage. This study could be

extended to analyse the effects of MPO expression on TOP2 poison mediated cytotoxicity in myeloid cells to assess whether MPO expression could be a contributor to TOP2 poison induced myelosuppression. The same approach could be used to assess whether using anthracyclines or mitoxantrone in combination with etoposide effects level of cell death. Additionally, it would be interesting to investigate if MPO affects the level of TOP2 poison mediated breaks within breakpoint regions in genes implicated in t-AML either in cell lines or in primary bone marrow cells. This study has the potential to be extended into primary hematopoietic cells, to determine if MPO expression contributes to TOP2-mediated DNA damage. Notably the protein expression of MPO is readily detectable in primary $CD34^{+}$ bone marrow blood progenitor cells (Atwal *et al.*, 2017) and there is potential that the hypothesis tested here may also hold true in cells where a leukaemic stem cell is likely to arise from. Therefore, this hypothesis could be tested in an ex vivo system, experimentally using the methods described in chapters 3, 4 and 5.

# Appendices

Figure i. Mass spectroscopy data for etoposide quinone

Figure ii. Mass spectroscopy data for etoposide catechol

Figure iii. Elemental Composition Report for etoposide quinone and etoposide catechol

Figure iv. Insert cDNA sequence for MPO in expression vector RC216029.

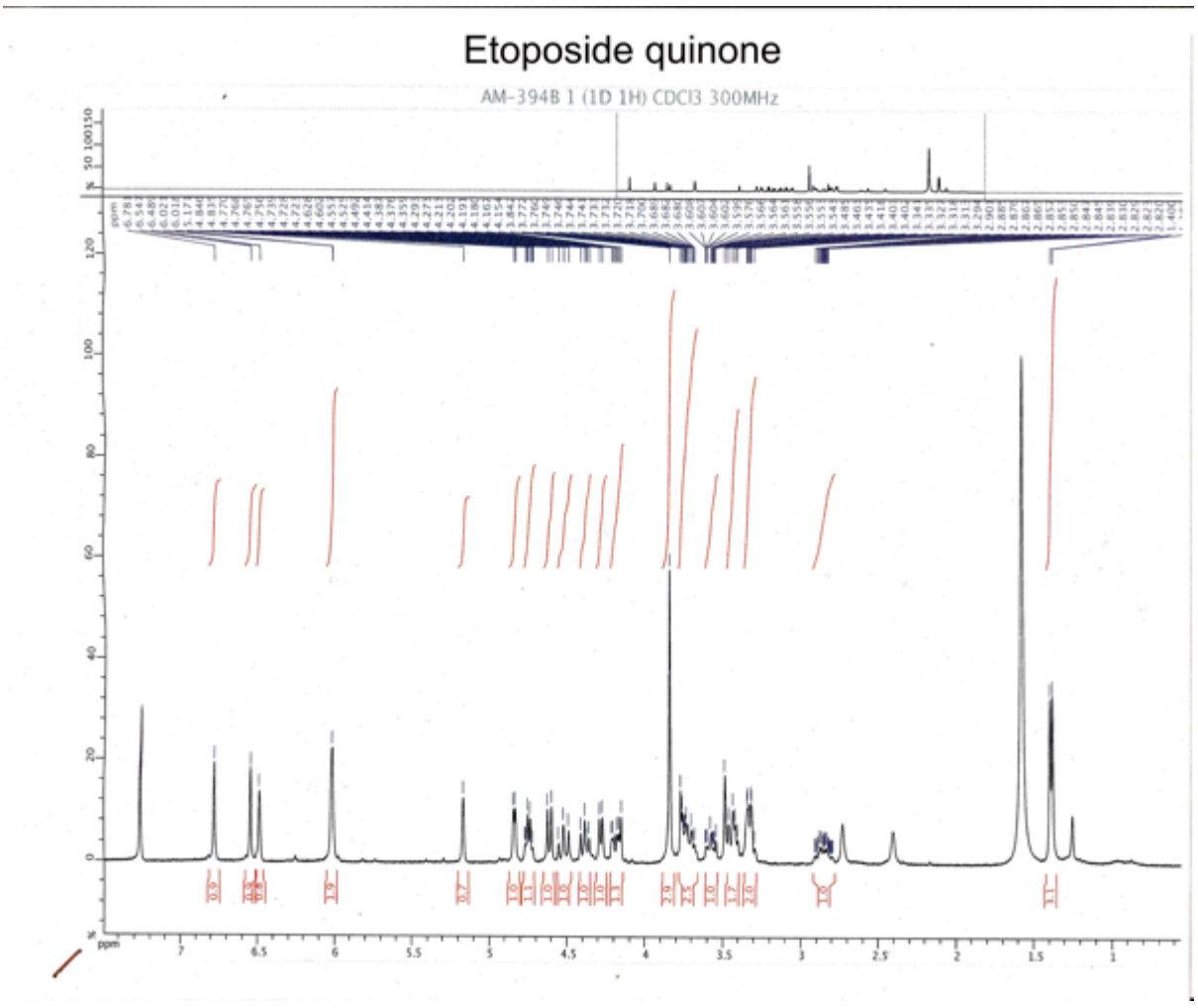


**Figure i.** Mass spectroscopy data for etoposide quinone, synthesised by Angelica Mariani, France

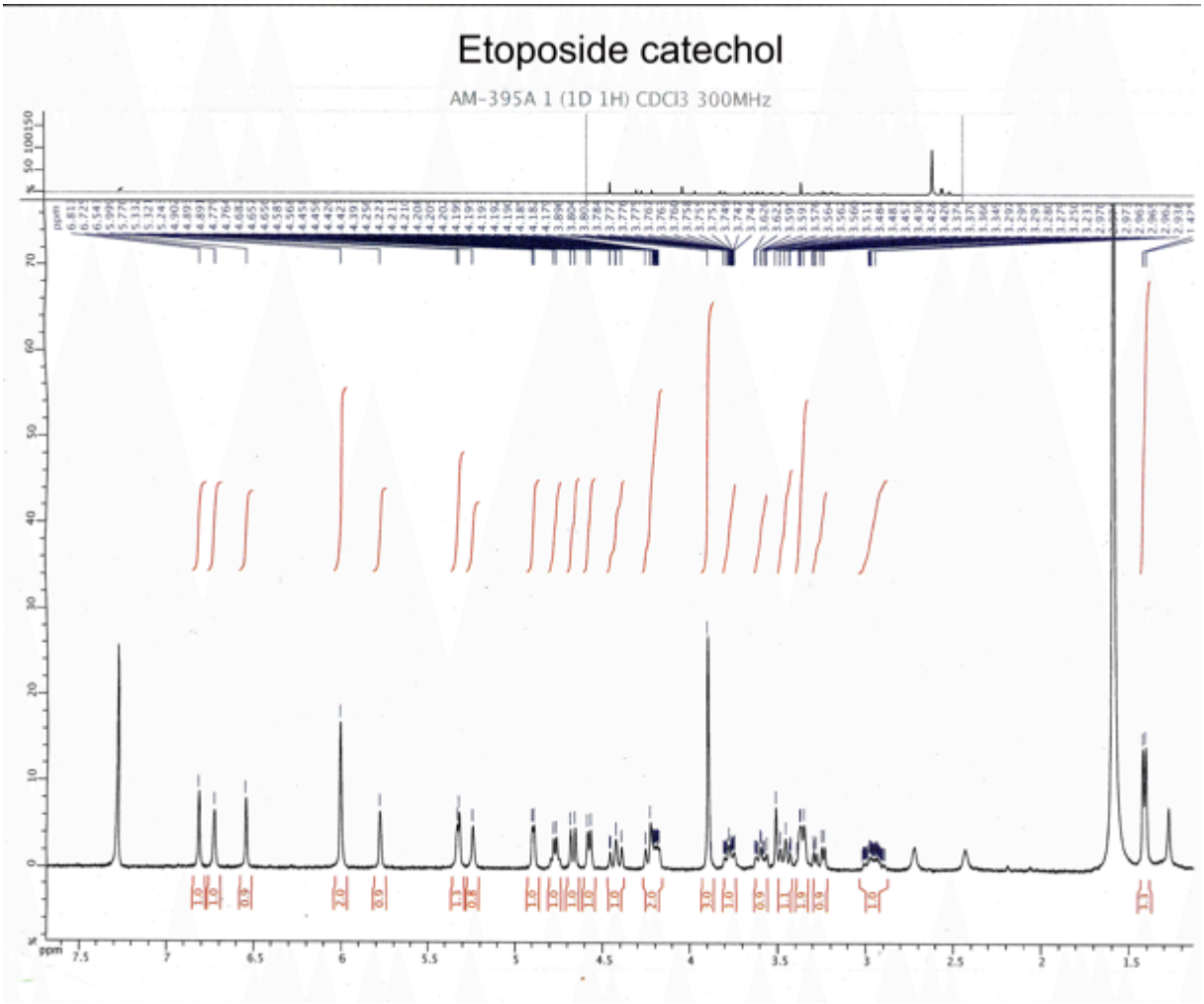


**Figure ii.** Mass spectroscopy data for etoposide catechol, synthesised by Angelica Mariani, France.

## Etoposide quinone

**Elemental Composition Report** Page 1

**Single Mass Analysis**
Tolerance = 5.0 PPM / DBE: min = -1.5, max = 100.0
Element prediction: Off
Number of isotope peaks used for i-FIT = 9

Monoisotopic Mass, Even Electron Ions
16 formula(e) evaluated with 1 results within limits (up to 50 best isotopic matches for each mass)
Elements Used:
C: 0-28 H: 0-30 O: 0-15
16-Jul-2014 10:49:32 AM-394 LCT Premier XE KE483
RODRIGUEZ_mariani68-1 22 (0.590) Cm (17:29) 1: TOF MS ES+
2.16e+005

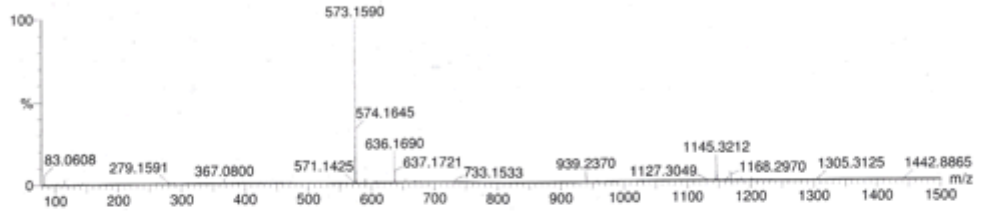


| | | | | | | | |
|---|---|---|---|---|---|---|---|
| Minimum: | | | | -1.5 | | | |
| Maximum: | | 5.0 | 5.0 | 100.0 | | | |
| Mass | Calc. Mass | mDa | PPM | DBE | i-FIT | i-FIT (Norm) | Formula |
| 573.1590 | 573.1608 | -1.8 | -3.1 | 14.5 | 1255.5 | 0.0 | C28 H29 O13 |

## Etoposide catechol

**Elemental Composition Report** Page 1

**Single Mass Analysis**
Tolerance = 5.0 PPM / DBE: min = -1.5, max = 100.0
Element prediction: Off
Number of isotope peaks used for i-FIT = 9

Monoisotopic Mass, Even Electron Ions
16 formula(e) evaluated with 0 results within limits (up to 50 best isotopic matches for each mass)
Elements Used:
C: 0-28 H: 0-29 O: 0-15
17-Jul-2014 11:52:25 AM-395 LCT Premier XE KE483
RODRIGUEZ_mariani69-1 20 (0.543) Cm (15:32) 2: TOF MS ES-
3.69e+005

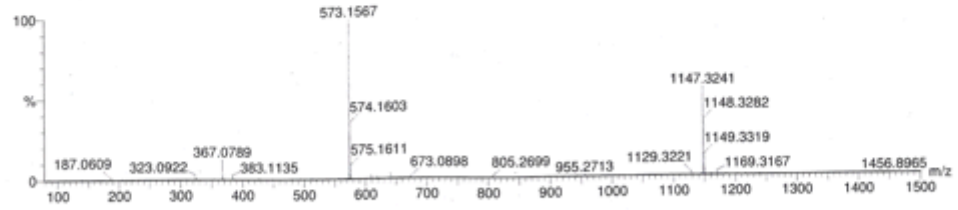


| | | | | | | | |
|---|---|---|---|---|---|---|---|
| Minimum: | | | | -1.5 | | | |
| Maximum: | | 5.0 | 5.0 | 100.0 | | | |
| Mass | Calc. Mass | mDa | PPM | DBE | i-FIT | i-FIT (Norm) | Formula |
| 573.1567 | --- | | | | | | |

**Figure iii.** Elemental composition report for etoposide quinone (upper panel) and etoposide catechol (lower panel), synthesised by Angelica Mariani.

Orange=Cloning site Blue=ORF Green=Tag(s)

```
   1 TTTTGTAATA CGACTCACTA TAGGGCGGCC GGGAATTCGT CGACTGGATC
  51 CGGTACCGAG GAGATCTGCC GCCGCGATCG CCATGGGGGT TCCCTTCTTC
 101 TCTTCTCTCA GATGCATGGT GGACTTAGGA CCTTGCTGGG CTGGGGGTCT
 151 CACTGCAGAG ATGAAGCTGC TTCTGGCCCT AGCAGGGCTC CTGGCCATTC
 201 TGGCCACGCC CCAGCCCTCT GAAGGTGCTG CTCCAGCTGT CCTGGGGGAG
 251 GTGGACACCT CGTTGGTGCT GAGCTCCATG GAGGAGGCCA AGCAGCTGGT
 301 GGACAAGGCC TACAAGGAGC GGCGGGAAAG CATCAAGCAG CGGCTTCGCA
 351 GCGGCTCAGC CAGCCCCATG GAACTCCTAT CCTACTTCAA GCAGCCGGTG
 401 GCAGCCACCA GGACGGCGGT GAGGGCCGCT GACTACCTGC ACGTGGCTCT
 451 AGACCTGCTG GAGAGGAAGC TGCGGTCCCT GTGGCGAAGG CCATTCAATG
 501 TCACTGATGT GCTGACGCCC GCCCAGCTGA ATGTGTTGTC CAAGTCAAGC
 551 GGCTGCGCCT ACCAGGACGT GGGGGTGACT TGCCCGGAGC AGGACAAATA
 601 CCGCACCATC ACCGGGATGT GCAACAACAG ACGCAGCCCC ACGCTGGGGG
 651 CCTCCAACCG TGCCTTTGTG CGCTGGCTGC CGGCGGAGTA TGAGGACGGC
 701 TTCTCTCTTC CCTACGGCTG GACGCCCGGG GTCAAGCGCA ACGGCTTCCC
 751 GGTGGCTCTG GCTCGCGCGG TCTCCAACGA GATCGTGCGC TTCCCCACTG
 801 ATCAGCTGAC TCCGGACCAG GAGCGCTCAC TCATGTTCAT GCAATGGGGC
 851 CAGCTGTTGG ACCACGACCT CGACTTCACC CCTGAGCCGG CCGCCCGGGC
 901 CTCCTTCGTC ACTGGCGTCA ACTGCGAGAC CAGCTGCGTT CAGCAGCCGC
 951 CCTGCTTCCC GCTCAAGATC CCGCCCAATG ACCCCCGCAT CAAGAACCAA
1001 GCCGACTGCA TCCCGTTCTT CCGCTCCTGC CCGGCTTGCC CCGGGAGCAA
1051 CATCACCATC CGCAACCAGA TCAACGCGCT CACTTCCTTC GTGGACGCCA
1101 GCATGGTGTA CGGCAGCGAG GAGCCCCTGG CCAGGAACCT GCGCAACATG
1151 TCCAACCAGC TGGGGCTGCT GGCCGTCAAC CAGCGCTTCC AAGACAACGG
1201 CCGGGCCCTG CTGCCCTTTG ACAACCTGCA CGATGACCCC TGTCTCCTCA
1251 CCAACCGCTC AGCGCGCATC CCCTGCTTCC TGGCAGGGGA CACCCGTTCC
1301 AGTGAGATGC CCGAGCTCAC CTCCATGCAC ACCCTCTTAC TTCGGGAGCA
1351 CAACCGGCTG GCCACAGAGC TCAAGAGCCT GAACCCTAGG TGGGATGGGG
1401 AGAGGCTCTA CCAGGAAGCC CGGAAGATCG TGGGGGCCAT GGTCCAGATC
1451 ATCACTTACC GGGACTACCT GCCCCTGGTG CTGGGGCCAA CGGCCATGAG
1501 GAAGTACCTG CCCACGTACC GTTCCTACAA TGACTCAGTG GACCCACGCA
1551 TCGCCAACGT CTTCACCAAT GCCTTCCGCT ACGGCCACAC CCTCATCCAA
1601 CCCTTCATGT TCCGCCTGGA CAATCGGTAC CAGCCCATGG AACCCAACCC
1651 CCGTGTCCCC CTCAGCAGGG TCTTTTTTGC CTCCTGGAGG GTCGTGCTGG
1701 AAGGTGGCAT TGACCCCATC CTCCGGGGCC TCATGGCCAC CCCTGCCAAG
```

```
1751 CTGAATCGTC AGAACCAAAT TGCAGTGGAT GAGATCCGGG AGCGATTGTT
1801 TGAGCAGGTC ATGAGGATTG GGCTGGACCT GCCTGCTCTG AACATGCAGC
1851 GCAGCAGGGA CCACGGCCTC CCAGGATACA ATGCCTGGAG GCGCTTCTGT
1901 GGGCTCCCGC AGCCTGAAAC TGTGGGCCAG CTGGGCACGG TGCTGAGGAA
1951 CCTGAAATTG GCGAGGAAAC TGATGGAGCA GTATGGCACG CCCAACAACA
2001 TCGACATCTG GATGGGCGGC GTGTCCGAGC CTCTGAAGCG CAAAGGCCGC
2051 GTGGGCCCAC TCCTCGCCTG CATCATCGGT ACCCAGTTCA GGAAGCTCCG
2101 GGATGGTGAT CGGTTTTGGT GGGAGAACGA GGGTGTGTTC AGCATGCAGC
2151 AGCGACAGGC CCTGGCCCAG ATCTCATTGC CCCGGATCAT CTGCGACAAC
2201 ACAGGCATCA CCACCGTGTC TAAGAACAAC ATCTTCATGT CCAACTCATA
2251 TCCCCGGGAC TTTGTCAACT GCAGTACACT TCCTGCATTG AACCTGGCTT
2301 CCTGGAGGGA AGCCTCCACG CGTACGCGGC CGCTCGAGCA GAAACTCATC
2351 TCAGAAGAGG ATCTGGCAGC AAATGATATC CTGGATTACA AGGATGACGA
2401 CGATAAGGTT TAA
```

**Figure iv**. Insert cDNA sequence for MPO in expression vector RC216029.

# References


Adachi, N., Miyaike, M., Ikeda, H. and Kikuchi, A. (1992) 'Characterization of cDNA encoding the mouse DNA topoisomerase II that can complement the budding yeast top2 mutation', *Nucleic Acids Research*, 20(20), pp. 5297-5303.

Adachi, N., Miyaike, M., Kato, S., Kanamaru, R., Koyama, H. and Kikuchi, A. (1997) 'Cellular distribution of mammalian DNA topoisomerase II is determined by its catalytically dispensable C-terminal domain', *Nucleic Acids Research*, 25(15), pp. 3135-3142.

Adam, M., Gajdova, S., Kolarova, H., Kubala, L., Lau, D., Geisler, A., Ravekes, T., Rudolph, V., Tsao, P.S., Blankenberg, S., Baldus, S. and Klinke, A. (2014) 'Red blood cells serve as intravascular carriers of myeloperoxidase', *Journal of Molecular and Cellular Cardiology*, 74(0), pp. 353-363.

Agudelo, D., Bourassa, P., Berube, G. and Tajmir-Riahi, H.A. (2014) 'Intercalation of antitumor drug doxorubicin and its analogue by DNA duplex: structural features and biological implications', *Int J Biol Macromol*, 66, pp. 144-50.

Álvarez-Quilón, A., Serrano-Benítez, A., Ariel Lieberman, J., Quintero, C., Sánchez-Gutiérrez, D., Escudero, L.M. and Cortés-Ledesma, F. (2014) 'ATM specifically mediates repair of double-strand breaks with blocked DNA ends', *Nat Commun*, 5, p. 3347.

An, J., Huang, Y.C., Xu, Q.Z., Zhou, L.J., Shang, Z.F., Huang, B., Wang, Y., Liu, X.D., Wu, D.C. and Zhou, P.K. (2010) 'DNA-PKcs plays a dominant role in the regulation of H2AX phosphorylation in response to DNA damage and cell cycle progression', *BMC Mol Biol*, 11, p. 18.

Anderson, M.M., Hazen, S.L., Hsu, F.F. and Heinecke, J.W. (1997) 'Human neutrophils employ the myeloperoxidase-hydrogen peroxide-chloride system to convert hydroxy-amino acids into glycolaldehyde, 2-hydroxypropanal, and acrolein. A mechanism for the generation of highly reactive alpha-hydroxy and alpha,beta-unsaturated aldehydes by phagocytes at sites of inflammation', *J Clin Invest*, 99(3), pp. 424-32.

Aravind, L., Leipe, D.D. and Koonin, E.V. (1998) 'Toprim--a conserved catalytic domain in type IA and II topoisomerases, DnaG-type primases, OLD family nucleases and RecR proteins', *Nucleic Acids Res*, 26(18), pp. 4205-13.

Asou, H., Tashiro, S., Hamamoto, K., Otsuji, A., Kita, K. and Kamada, N. (1991) 'Establishment of a Human Acute Myeloid Leukemia Cell Line (Kasumi-1) With 8;2 1 Chromosome Translocation', *Blood*, 77(9), pp. 2031-2036.

Asselin, B.L., Devidas, M., Chen, L., Franco, V.I., Pullen, J., Borowitz, M.J., Hutchison, R.E., Ravindranath, Y., Armenian, S.H., Camitta, B.M. and Lipshultz, S.E.

(2016) 'Cardioprotection and Safety of Dexrazoxane in Patients Treated for Newly Diagnosed T-Cell Acute Lymphoblastic Leukemia or Advanced-Stage Lymphoblastic Non-Hodgkin Lymphoma: A Report of the Children's Oncology Group Randomized Trial Pediatric Oncology Group 9404', *J Clin Oncol*, 34(8), pp. 854-62.

Atwal, M., Lishman, E.L., Austin, C.A. and Cowell, I.G. (2017) 'Myeloperoxidase Enhances Etoposide and Mitoxantrone-Mediated DNA Damage: A Target for Myeloprotection in Cancer Chemotherapy', *Mol Pharmacol*, 91(1), pp. 49-57.

Augusto, O., Cavalieri, E.L., Rogan, E.G., RamaKrishna, N.V. and Kolar, C. (1990) 'Formation of 8-methylguanine as a result of DNA alkylation by methyl radicals generated during horseradish peroxidase-catalyzed oxidation of methylhydrazine', *J Biol Chem*, 265(36), pp. 22093-6.

Austin, C.A. and Fisher, L.M. (1990) 'Isolation and characterization of a human cDNA clone encoding a novel DNA topoisomerase II homologue from HeLa cells', *FEBS Lett*, 266(1-2), pp. 115-7.

Austin, C.A., Marsh, K.L., Wasserman, R.A., Willmore, E., Sayer, P.J., Wang, J.C. and Fisher, L.M. (1995) 'Expression, domain structure, and enzymatic properties of an active recombinant human DNA topoisomerase II beta', *J Biol Chem*, 270(26), pp. 15739-46.

Austin, C.A., Sng, J.H., Patel, S. and Fisher, L.M. (1993) 'Novel HeLa topoisomerase II is the IIβ isoform: complete coding sequence and homology with other type II topoisomerases', *BBA - Gene Structure and Expression*, 1172(3), pp. 283-291.

Azarova, A.M., Lyu, Y.L., Lin, C.P., Tsai, Y.C., Lau, J.Y., Wang, J.C. and Liu, L.F. (2007) 'Roles of DNA topoisomerase II isozymes in chemotherapy and secondary malignancies', *Proc Natl Acad Sci U S A*, 104(26), pp. 11014-9.

Bateman, R., Rauh, D. and Shokat, K.M. (2007) 'Glutathione traps formaldehyde by formation of a bicyclo[4.4.1]undecane adduct', *Organic & biomolecular chemistry*, 5(20), pp. 3363-3367.

Benchekroun, M.N., Sinha, B.K. and Robert, J. (1993) 'Doxorubicin-induced oxygen free radical formation in sensitive and doxorubicin-resistant variants of rat glioblastoma cell lines', *FEBS Letters*, 326(1), pp. 302-305.

Bender, R.P., Ham, A.J. and Osheroff, N. (2007) 'Quinone-induced enhancement of DNA cleavage by human topoisomerase IIalpha: adduction of cysteine residues 392 and 405', *Biochemistry*, 46(10), pp. 2856-64.

Bender, R.P. and Osheroff, N. (2007) 'Mutation of Cysteine Residue 455 to Alanine in Human Topoisomerase IIα Confers Hypersensitivity to Quinones: Enhancing DNA Scission by Closing the N-Terminal Protein Gate', *Chemical Research in Toxicology*, 20(6), pp. 975-981.

Benini, S., Manara, M.C., Baldini, N., Cerisano, V., Massimo, S., Mercuri, M., Lollini, P.L., Nanni, P., Picci, P. and Scotlandi, K. (2001) 'Inhibition of insulin-like growth

factor I receptor increases the antitumor activity of doxorubicin and vincristine against Ewing's sarcoma cells', *Clin Cancer Res*, 7(6), pp. 1790-7.

Berger, J.M., Gamblin, S.J., Harrison, S.C. and Wang, J.C. (1996a) 'Structure and mechanism of DNA topoisomerase II', *Nature*, 379(6562), pp. 225-232.

Berger, J.M., Gamblin, S.J., Harrison, S.C. and Wang, J.C. (1996b) 'Structure and mechanism of DNA topoisomerase II', *Nature*, 379(6562), pp. 225-32.

Bermejo, R., Capra, T., Gonzalez-Huici, V., Fachinetti, D., Cocito, A., Natoli, G., Katou, Y., Mori, H., Kurokawa, K., Shirahige, K. and Foiani, M. (2009) 'Genome-Organizing Factors Top2 and Hmo1 Prevent Chromosome Fragility at Sites of S phase Transcription', *Cell*, 138(5), pp. 870-884.

Biterova, E.I. and Barycki, J.J. (2010) 'Structural basis for feedback and pharmacological inhibition of Saccharomyces cerevisiae glutamate cysteine ligase', *J Biol Chem*, 285(19), pp. 14459-66.

Blanz, J., Mewes, K., Ehninger, G., Proksch, B., Waidelich, D., Greger, B. and Zeller, K.P. (1991) 'Evidence for oxidative activation of mitoxantrone in human, pig, and rat', *Drug Metab Dispos*, 19(5), pp. 871-80.

Block, A.W., Carroll, A.J., Hagemeijer, A., Michaux, L., van Lom, K., Olney, H.J. and Baer, M.R. (2002) 'Rare recurring balanced chromosome abnormalities in therapy-related myelodysplastic syndromes and acute leukemia: report from an international workshop', *Genes Chromosomes Cancer*, 33(4), pp. 401-12.

Bonner, J.A., Christianson, T.J. and Lawrence, T.S. (1992) 'Interaction of buthionine sulfoximine and the stabilization of DNA-topoisomerase II complexes by doxorubicin', *Int J Radiat Oncol Biol Phys*, 22(3), pp. 519-23.

Branzei, D. and Foiani, M. (2010) 'Maintaining genome stability at the replication fork', *Nat Rev Mol Cell Biol*, 11(3), pp. 208-19.

Brill, S.J., DiNardo, S., Voelkel-Meiman, K. and Sternglanz, R. (1987) 'Need for DNA topoisomerase activity as a swivel for DNA replication for transcription of ribosomal RNA', *Nature*, 326(6111), pp. 414-6.

Bromberg, K.D., Burgin, A.B. and Osheroff, N. (2003) 'A two-drug model for etoposide action against human topoisomerase IIalpha', *J Biol Chem*, 278(9), pp. 7406-12.

Bromberg, K.D., Vélez-Cruz, R., Burgin, A.B. and Osheroff, N. (2004) 'DNA Ligation Catalyzed by Human Topoisomerase IIα', *Biochemistry*, 43(42), pp. 13416-13423.

Bruck, T.B. and Bruck, D.W. (2011) 'Oxidative metabolism of the anti-cancer agent mitoxantrone by horseradish, lacto-and lignin peroxidase', *Biochimie*, 93(2), pp. 217-26.

Bruck, T.B. and Harvey, P.J. (2003) 'Oxidation of mitoxantrone by lactoperoxidase', *Biochim Biophys Acta*, 1649(2), pp. 154-63.

Buchenau, P., Saumweber, H. and Arndt-Jovin, D.J. (1993) 'Consequences of topoisomerase II inhibition in early embryogenesis of Drosophila revealed by in vivo confocal laser scanning microscopy', *Journal of Cell Science*, 104(4), pp. 1175-85.

Bunch, H., Lawney, B.P., Lin, Y.F., Asaithamby, A., Murshid, A., Wang, Y.E., Chen, B.P. and Calderwood, S.K. (2015) 'Transcriptional elongation requires DNA break-induced signalling', *Nat Commun*, 6, p. 10191.

Burner, U., Obinger, C., Paumann, M., Furtmuller, P.G. and Kettle, A.J. (1999) 'Transient and steady-state kinetics of the oxidation of substituted benzoic acid hydrazides by myeloperoxidase', *J Biol Chem*, 274(14), pp. 9494-502.

Calderwood, S.K. (2016) 'A critical role for topoisomerase IIb and DNA double strand breaks in transcription', *Transcription*, 7(3), pp. 75-83.

Capranico, G. and Binaschi, M. (1998) 'DNA sequence selectivity of topoisomerases and topoisomerase poisons', *Biochim Biophys Acta*, 1400(1-3), pp. 185-94.

Capranico, G., Kohn, K.W. and Pommier, Y. (1990a) 'Local sequence requirements for DNA cleavage by mammalian topoisomerase II in the presence of doxorubicin', *Nucleic Acids Res*, 18(22), pp. 6611-9.

Capranico, G., Zunino, F., Kohn, K.W. and Pommier, Y. (1990b) 'Sequence-selective topoisomerase II inhibition by anthracycline derivatives in SV40 DNA: relationship with DNA binding affinity and cytotoxicity', *Biochemistry*, 29(2), pp. 562-9.

Carpena, X., Vidossich, P., Schroettner, K., Calisto, B.M., Banerjee, S., Stampler, J., Soudi, M., Furtmuller, P.G., Rovira, C., Fita, I. and Obinger, C. (2009) 'Essential role of proximal histidine-asparagine interaction in mammalian peroxidases', *J Biol Chem*, 284(38), pp. 25929-37.

Cartoni, A., Menna, P., Salvatorelli, E., Braghiroli, D., Giampietro, R., Animati, F., Urbani, A., Del Boccio, P. and Minotti, G. (2004) 'Oxidative Degradation of Cardiotoxic Anticancer Anthracyclines to Phthalic Acids: NOVEL FUNCTION FOR FERRYLMYOGLOBIN', *Journal of Biological Chemistry*, 279(7), pp. 5088-5099.

Chang, C.-J., Goulding, S., Earnshaw, W.C. and Carmena, M. (2003) 'RNAi analysis reveals an unexpected role for topoisomerase II in chromosome arm congression to a metaphase plate', *Journal of Cell Science*, 116(23), pp. 4715-4726.

Charushila, Y.K. and Subodhini, A.A. (2013) 'Evaluation of serum levels of reduced glutathione, glutathione-s-transferase and nitric oxide in breast cancer patients undergoing adjuvant chemotherapy', *IJCRR*, 5(13), pp. 51-57.

Chatterjee, A. (2013) 'Reduced Glutathione: A Radioprotector or a Modulator of DNA-Repair Activity?', *Nutrients*, 5(2), pp. 525-542.

Chen, G.L., Yang, L., Rowe, T.C., Halligan, B.D., Tewey, K.M. and Liu, L.F. (1984) 'Nonintercalative antitumor drugs interfere with the breakage-reunion reaction of

mammalian DNA topoisomerase II', *Journal of Biological Chemistry*, 259(21), pp. 13560-6.

Chikamori, K., Grabowski, D.R., Kinter, M., Willard, B.B., Yadav, S., Aebersold, R.H., Bukowski, R.M., Hickson, I.D., Andersen, A.H., Ganapathi, R. and Ganapathi, M.K. (2003) 'Phosphorylation of Serine 1106 in the Catalytic Domain of Topoisomerase IIα Regulates Enzymatic Activity and Drug Sensitivity', *Journal of Biological Chemistry*, 278(15), pp. 12696-12702.

Christensen, M.O., Larsen, M.K., Barthelmes, H.U., Hock, R., Andersen, C.L., Kjeldsen, E., Knudsen, B.R., Westergaard, O., Boege, F. and Mielke, C. (2002) 'Dynamics of human DNA topoisomerases IIalpha and IIbeta in living cells', *J Cell Biol*, 157(1), pp. 31-44.

Chung, T.D., Drake, F.H., Tan, K.B., Per, S.R., Crooke, S.T. and Mirabelli, C.K. (1989) 'Characterization and immunological identification of cDNA clones encoding two human DNA topoisomerase II isozymes', *Proc Natl Acad Sci U S A*, 86(23), pp. 9431-5.

Classen, S., Olland, S. and Berger, J.M. (2003) 'Structure of the topoisomerase II ATPase region and its mechanism of inhibition by the chemotherapeutic agent ICRF-187', *Proc Natl Acad Sci U S A*, 100(19), pp. 10629-34.

Coldwell, K.E., Cutts, S.M., Ognibene, T.J., Henderson, P.T. and Phillips, D.R. (2008) 'Detection of Adriamycin–DNA adducts by accelerator mass spectrometry at clinically relevant Adriamycin concentrations', *Nucleic Acids Research*, 36(16), pp. e100-e100.

Corbett, A.H., Fernald, A.W. and Osheroff, N. (1993) 'Protein kinase C modulates the catalytic activity of topoisomerase II by enhancing the rate of ATP hydrolysis: evidence for a common mechanism of regulation by phosphorylation', *Biochemistry*, 32(8), pp. 2090-7.

Corbett, A.H., Zechiedrich, E.L. and Osheroff, N. (1992) 'A role for the passage helix in the DNA cleavage reaction of eukaryotic topoisomerase II. A two-site model for enzyme-mediated DNA cleavage', *J Biol Chem*, 267(2), pp. 683-6.

Cornarotti, M., Tinelli, S., Willmore, E., Zunino, F., Fisher, L.M., Austin, C.A. and Capranico, G. (1996) 'Drug sensitivity and sequence specificity of human recombinant DNA topoisomerases IIalpha (p170) and IIbeta (p180)', *Mol Pharmacol*, 50(6), pp. 1463-71.

Cowell, I.G. and Austin, C.A. (2012) 'Mechanism of generation of therapy related leukemia in response to anti-topoisomerase II agents', *Int J Environ Res Public Health*, 9(6), pp. 2075-91.

Cowell, I.G., Okorokov, A.L., Cutts, S.A., Padget, K., Bell, M., Milner, J. and Austin, C.A. (2000) 'Human Topoisomerase IIα and IIβ Interact with the C-Terminal Region of p53', *Experimental Cell Research*, 255(1), pp. 86-94.

Cowell, I.G., Sondka, Z., Smith, K., Lee, K.C., Manville, C.M., Sidorczuk-Lesthuruge, M., Rance, H.A., Padget, K., Jackson, G.H., Adachi, N. and Austin, C.A. (2012) 'Model for MLL translocations in therapy-related leukemia involving topoisomerase IIβ-mediated DNA strand breaks and gene proximity', *Proceedings of the National Academy of Sciences*, 109(23), pp. 8989-8994.

Cowell, I.G., Tilby, M.J. and Austin, C.A. (2011) 'An overview of the visualisation and quantitation of low and high MW DNA adducts using the trapped in agarose DNA immunostaining (TARDIS) assay', *Mutagenesis*, 26(2), pp. 253-60.

Cowell, I.G., Willmore, E., Chalton, D., Marsh, K.L., Jazrawi, E., Fisher, L.M. and Austin, C.A. (1998) 'Nuclear Distribution of Human DNA Topoisomerase IIβ: A Nuclear Targeting Signal Resides in the 116-Residue C-Terminal Tail', *Experimental Cell Research*, 243(2), pp. 232-240.

Cutts, S.M., Nudelman, A., Rephaeli, A. and Phillips, D.R. (2005) 'The power and potential of doxorubicin-DNA adducts', *IUBMB Life*, 57(2), pp. 73-81.
Cuvier, O. and Hirano, T. (2003) 'A role of topoisomerase II in linking DNA replication to chromosome condensation', *The Journal of Cell Biology*, 160(5), pp. 645-655.

Dahlgren, C. and Karlsson, A. (1999) 'Respiratory burst in human neutrophils', *J Immunol Methods*, 232(1-2), pp. 3-14.

Deponte, M. (2013) 'Glutathione catalysis and the reaction mechanisms of glutathione-dependent enzymes', *Biochimica et Biophysica Acta (BBA) - General Subjects*, 1830(5), pp. 3217-3266.

Deweese, J.E., Burch, A.M., Burgin, A.B. and Osheroff, N. (2009a) 'Use of Divalent Metal Ions in the DNA Cleavage Reaction of Human Type II Topoisomerases', *Biochemistry*, 48(9), pp. 1862-1869.

Deweese, J.E., Guengerich, F.P., Burgin, A.B. and Osheroff, N. (2009b) 'Metal Ion Interactions in the DNA Cleavage/Ligation Active Site of Human Topoisomerase IIα', *Biochemistry*, 48(38), pp. 8940-8947.

Deweese, J.E. and Osheroff, N. (2009) 'The DNA cleavage reaction of topoisomerase II: wolf in sheep's clothing', *Nucleic Acids Res*, 37(3), pp. 738-48.

Dong, J.Q., Varma, M.V., Wolford, A., Ryder, T., Di, L., Feng, B., Terra, S.G., Sagawa, K. and Kalgutkar, A.S. (2016) 'Pharmacokinetics and Disposition of the Thiouracil Derivative PF-06282999, an Orally Bioavailable, Irreversible Inactivator of Myeloperoxidase Enzyme, Across Animals and Humans', *Drug Metabolism and Disposition*, 44(2), pp. 209-219.

Dong, K.C. and Berger, J.M. (2007) 'Structural basis for gate-DNA recognition and bending by type IIA topoisomerases', *Nature*, 450(7173), pp. 1201-1205.
Drake, F.H., Hofmann, G.A., Bartus, H.F., Mattern, M.R., Crooke, S.T. and Mirabelli, C.K. (1989) 'Biochemical and pharmacological properties of p170 and p180 forms of topoisomerase II', *Biochemistry*, 28(20), pp. 8154-60.

Drew, R. and Miners, J.O. (1984) 'The effects of buthionine sulphoximine (BSO) on glutathione depletion and xenobiotic biotransformation', *Biochem Pharmacol*, 33(19), pp. 2989-94.

Dykhuizen, E.C., Hargreaves, D.C., Miller, E.L., Cui, K., Korshunov, A., Kool, M., Pfister, S., Cho, Y.J., Zhao, K. and Crabtree, G.R. (2013) 'BAF complexes facilitate decatenation of DNA by topoisomerase IIalpha', *Nature*, 497(7451), pp. 624-7.

Earnshaw, W.C. and Heck, M.M. (1985) 'Localization of topoisomerase II in mitotic chromosomes', *J Cell Biol*, 100(5), pp. 1716-25.

Errington, F., Willmore, E., Leontiou, C., Tilby, M.J. and Austin, C.A. (2004) 'Differences in the longevity of topo IIalpha and topo IIbeta drug-stabilized cleavable complexes and the relationship to drug sensitivity', *Cancer Chemother Pharmacol*, 53(2), pp. 155-62.

Errington, F., Willmore, E., Tilby, M.J., Li, L., Li, G., Li, W., Baguley, B.C. and Austin, C.A. (1999) 'Murine transgenic cells lacking DNA topoisomerase IIbeta are resistant to acridines and mitoxantrone: analysis of cytotoxicity and cleavable complex formation', *Mol Pharmacol*, 56(6), pp. 1309-16.

Evison, B.J., Sleebs, B.E., Watson, K.G., Phillips, D.R. and Cutts, S.M. (2015) 'Mitoxantrone, More than Just Another Topoisomerase II Poison', *Med Res Rev*.

Fachinetti, D., Bermejo, R., Cocito, A., Minardi, S., Katou, Y., Kanoh, Y., Shirahige, K., Azvolinsky, A., Zakian, V.A. and Foiani, M. (2010) 'Replication Termination at Eukaryotic Chromosomes Is Mediated by Top2 and Occurs at Genomic Loci Containing Pausing Elements', *Molecular Cell*, 39(4), pp. 595-605.

Fan, J.R., Peng, A.L., Chen, H.C., Lo, S.C., Huang, T.H. and Li, T.K. (2008) 'Cellular processing pathways contribute to the activation of etoposide-induced DNA damage responses', *DNA Repair (Amst)*, 7(3), pp. 452-63.

Fan, Y., Schreiber, E.M., Giorgianni, A., Yalowich, J.C. and Day, B.W. (2006) 'Myeloperoxidase-Catalyzed Metabolism of Etoposide to Its Quinone and Glutathione Adduct Forms in HL60 Cells', *Chemical Research in Toxicology*, 19(7), pp. 937-943.

Farr, C.J., Antoniou-Kourounioti, M., Mimmack, M.L., Volkov, A. and Porter, A.C. (2014) 'The alpha isoform of topoisomerase II is required for hypercompaction of mitotic chromosomes in human cells', *Nucleic Acids Res*, 42(7), pp. 4414-26.

Fass, D., Bogden, C.E. and Berger, J.M. (1999) 'Quaternary changes in topoisomerase II may direct orthogonal movement of two DNA strands', *Nat Struct Mol Biol*, 6(4), pp. 322-326.

Faulds, D., Balfour, J.A., Chrisp, P. and Langtry, H.D. (1991) 'Mitoxantrone. A review of its pharmacodynamic and pharmacokinetic properties, and therapeutic potential in the chemotherapy of cancer', *Drugs*, 41(3), pp. 400-49.

Felix, C.A., Kolaris, C.P. and Osheroff, N. (2006) 'Topoisomerase II and the etiology of chromosomal translocations', *DNA Repair (Amst)*, 5(9-10), pp. 1093-108.

Fenick, D.J., Taatjes, D.J. and Koch, T.H. (1997) 'Doxoform and Daunoform: Anthracycline−Formaldehyde Conjugates Toxic to Resistant Tumor Cells', *Journal of Medicinal Chemistry*, 40(16), pp. 2452-2461.

Fernández, X., Díaz-Ingelmo, O., Martínez-García, B. and Roca, J. (2014) 'Chromatin regulates DNA torsional energy via topoisomerase II-mediated relaxation of positive supercoils', *The EMBO Journal*, 33(13), pp. 1492-1501.

Ferrazzi, E., Woynarowski, J.M., Arakali, A., Brenner, D.E. and Beerman, T.A. (1991) 'DNA damage and cytotoxicity induced by metabolites of anthracycline antibiotics, doxorubicin and idarubicin', *Cancer Commun*, 3(6), pp. 173-80.

Fiedler, T.J., Davey, C.A. and Fenna, R.E. (2000) 'X-ray Crystal Structure and Characterization of Halide-binding Sites of Human Myeloperoxidase at 1.8 Å Resolution', *Journal of Biological Chemistry*, 275(16), pp. 11964-11971.

Fox, M.E. and Smith, P.J. (1990) 'Long-Term Inhibition of DNA Synthesis and the Persistence of Trapped Topoisomerase II Complexes in Determining the Toxicity of the Antitumor DNA Intercalators mAMSA and Mitoxantrone', *Cancer Research*, 50(18), pp. 5813-5818.

Frederick, C.A., Williams, L.D., Ughetto, G., van der Marel, G.A., van Boom, J.H., Rich, A. and Wang, A.H. (1990) 'Structural comparison of anticancer drug-DNA complexes: adriamycin and daunomycin', *Biochemistry*, 29(10), pp. 2538-49.

Furtmuller, P.G., Arnhold, J., Jantschko, W., Pichler, H. and Obinger, C. (2003) 'Redox properties of the couples compound I/compound II and compound II/native enzyme of human myeloperoxidase', *Biochem Biophys Res Commun*, 301(2), pp. 551-7.

Furtmüller, P.G., Zederbauer, M., Jantschko, W., Helm, J., Bogner, M., Jakopitsch, C. and Obinger, C. (2006) 'Active site structure and catalytic mechanisms of human peroxidases', *Archives of Biochemistry and Biophysics*, 445(2), pp. 199-213.

Gallagher, S., Kefford, R.F. and Rizos, H. (2005) 'Enforced expression of p14ARF induces p53-dependent cell cycle arrest but not apoptosis', *Cell Cycle*, 4(3), pp. 465-72.

Gantchev, T.G. and Hunting, D.J. (1997) 'Enhancement of etoposide (VP-16) cytotoxicity by enzymatic and photodynamically induced oxidative stress', *Anticancer Drugs*, 8(2), pp. 164-73.

Gantchev, T.G. and Hunting, D.J. (1998) 'The ortho-quinone metabolite of the anticancer drug etoposide (VP-16) is a potent inhibitor of the topoisomerase II/DNA cleavable complex', *Mol Pharmacol*, 53(3), pp. 422-8.

Gewirtz, D. (1999a) 'A critical evaluation of the mechanisms of action proposed for the antitumor effects of the anthracycline antibiotics adriamycin and daunorubicin', *Biochemical Pharmacology*, 57(7), pp. 727-741.

Gewirtz, D.A. (1999b) 'A critical evaluation of the mechanisms of action proposed for the antitumor effects of the anthracycline antibiotics adriamycin and daunorubicin', *Biochem Pharmacol*, 57(7), pp. 727-41.

Gibson, E.G., King, M.M., Mercer, S.L. and Deweese, J.E. (2016) 'Two-Mechanism Model for the Interaction of Etoposide Quinone with Topoisomerase IIalpha', *Chem Res Toxicol*, 29(9), pp. 1541-8.

Giger, U. and Meyer, U.A. (1983) 'Effect of succinylacetone on heme and cytochrome P450 synthesis in hepatocyte culture', *FEBS Lett*, 153(2), pp. 335-8.

Gilroy, K.L. and Austin, C.A. (2011) 'The impact of the C-terminal domain on the interaction of human DNA topoisomerase II alpha and beta with DNA', *PLoS One*, 6(2), p. e14693.

Goenrich, M., Bartoschek, S., Hagemeier, C.H., Griesinger, C. and Vorholt, J.A. (2002) 'A glutathione-dependent formaldehyde-activating enzyme (Gfa) from Paracoccus denitrificans detected and purified via two-dimensional proton exchange NMR spectroscopy', *J Biol Chem*, 277(5), pp. 3069-72.

Gonzalez, R.E., Lim, C.-U., Cole, K., Bianchini, C.H., Schools, G.P., Davis, B.E., Wada, I., Roninson, I.B. and Broude, E.V. (2011) 'Effects of conditional depletion of topoisomerase II on cell cycle progression in mammalian cells', *Cell Cycle*, 10(20), pp. 3505-3514.

Goswami, P.C., Roti Roti, J.L. and Hunt, C.R. (1996) 'The cell cycle-coupled expression of topoisomerase IIalpha during S phase is regulated by mRNA stability and is disrupted by heat shock or ionizing radiation', *Mol Cell Biol*, 16(4), pp. 1500-8.

Greene, J. and Hennessy, B. (2014) 'The role of anthracyclines in the treatment of early breast cancer', *J Oncol Pharm Pract*.

Griffith, O.W. (1982) 'Mechanism of action, metabolism, and toxicity of buthionine sulfoximine and its higher homologs, potent inhibitors of glutathione synthesis', *J Biol Chem*, 257(22), pp. 13704-12.

Griffith, O.W., Anderson, M.E. and Meister, A. (1979) 'Inhibition of glutathione biosynthesis by prothionine sulfoximine (S-n-propyl homocysteine sulfoximine), a selective inhibitor of gamma-glutamylcysteine synthetase', *J Biol Chem*, 254(4), pp. 1205-10.

Griffith, O.W. and Meister, A. (1979) 'Potent and specific inhibition of glutathione synthesis by buthionine sulfoximine (S-n-butyl homocysteine sulfoximine)', *J Biol Chem*, 254(16), pp. 7558-60.

Grishkovskaya, I., Paumann-Page, M., Tscheliessnig, R., Stampler, J., Hofbauer, S., Soudi, M., Sevcnikar, B., Oostenbrink, C., Furtmuller, P.G., Djinovic-Carugo, K., Nauseef, W.M. and Obinger, C. (2017) 'Structure of human promyeloperoxidase (proMPO) and the role of the propeptide for processing and maturation', *J Biol Chem*, 292(20), pp. 8244-8261.

Habig, W.H., Pabst, M.J. and Jakoby, W.B. (1974) 'Glutathione S-transferases. The first enzymatic step in mercapturic acid formation', *J Biol Chem*, 249(22), pp. 7130-9.

Haffner, M.C., Aryee, M.J., Toubaji, A., Esopi, D.M., Albadine, R., Gurel, B., Isaacs, W.B., Bova, G.S., Liu, W., Xu, J., Meeker, A.K., Netto, G., De Marzo, A.M., Nelson, W.G. and Yegnasubramanian, S. (2010) 'Androgen-induced TOP2B-mediated double-strand breaks and prostate cancer gene rearrangements', *Nat Genet*, 42(8), pp. 668-75.

Haim, N., Nemec, J., Roman, J. and Sinha, B.K. (1987a) 'In vitro metabolism of etoposide (VP-16-213) by liver microsomes and irreversible binding of reactive intermediates to microsomal proteins', *Biochem Pharmacol*, 36(4), pp. 527-36.

Haim, N., Nemec, J., Roman, J. and Sinha, B.K. (1987b) 'Peroxidase-catalyzed metabolism of etoposide (VP-16-213) and covalent binding of reactive intermediates to cellular macromolecules', *Cancer Res*, 47(22), pp. 5835-40.

Haim, N., Roman, J., Nemec, J. and Sinha, B.K. (1986) 'Peroxidative free radical formation and O-demethylation of etoposide(VP-16) and teniposide(VM-26)', *Biochem Biophys Res Commun*, 135(1), pp. 215-20.

Hajihassan, Z. and Rabbani-Chadegani, A. (2009) 'Studies on the binding affinity of anticancer drug mitoxantrone to chromatin, DNA and histone proteins', *J Biomed Sci*, 16, p. 31.

Hande, K.R. (1998) 'Etoposide: four decades of development of a topoisomerase II inhibitor', *Eur J Cancer*, 34(10), pp. 1514-21.

Hansson, M., Olsson, I. and Nauseef, W.M. (2006) 'Biosynthesis, processing, and sorting of human myeloperoxidase', *Arch Biochem Biophys*, 445(2), pp. 214-24.

Harker, W.G., Slade, D.L., Drake, F.H. and Parr, R.L. (1991) 'Mitoxantrone resistance in HL-60 leukemia cells: reduced nuclear topoisomerase II catalytic activity and drug-induced DNA cleavage in association with reduced expression of the topoisomerase II beta isoform', *Biochemistry*, 30(41), pp. 9953-61.

Harker, W.G., Slade, D.L., Parr, R.L., Feldhoff, P.W., Sullivan, D.M. and Holguin, M.H. (1995a) 'Alterations in the topoisomerase II alpha gene, messenger RNA, and subcellular protein distribution as well as reduced expression of the DNA topoisomerase II beta enzyme in a mitoxantrone-resistant HL-60 human leukemia cell line', *Cancer Res*, 55(8), pp. 1707-16.

Harker, W.G., Slade, D.L., Parr, R.L. and Holguin, M.H. (1995b) 'Selective use of an alternative stop codon and polyadenylation signal within intron sequences leads to a

truncated topoisomerase II alpha messenger RNA and protein in human HL-60 leukemia cells selected for resistance to mitoxantrone', *Cancer Res*, 55(21), pp. 4962-71.

Harrison, J.E. and Schultz, J. (1976) 'Studies on the chlorinating activity of myeloperoxidase', *J Biol Chem*, 251(5), pp. 1371-4.

Hasan, S.K., Mays, A.N., Ottone, T., Ledda, A., La Nasa, G., Cattaneo, C., Borlenghi, E., Melillo, L., Montefusco, E., Cervera, J., Stephen, C., Satchi, G., Lennard, A., Libura, M., Byl, J.A., Osheroff, N., Amadori, S., Felix, C.A., Voso, M.T., Sperr, W.R., Esteve, J., Sanz, M.A., Grimwade, D. and Lo-Coco, F. (2008) 'Molecular analysis of t(15;17) genomic breakpoints in secondary acute promyelocytic leukemia arising after treatment of multiple sclerosis', *Blood*, 112(8), pp. 3383-90.

Hasan, S.K., Ottone, T., Schlenk, R.F., Xiao, Y., Wiemels, J.L., Mitra, M.E., Bernasconi, P., Di Raimondo, F., Stanghellini, M.T., Marco, P., Mays, A.N., Dohner, H., Sanz, M.A., Amadori, S., Grimwade, D. and Lo-Coco, F. (2010) 'Analysis of t(15;17) chromosomal breakpoint sequences in therapy-related versus de novo acute promyelocytic leukemia: association of DNA breaks with specific DNA motifs at PML and RARA loci', *Genes Chromosomes Cancer*, 49(8), pp. 726-32.

Hazen, S.L., d'Avignon, A., Anderson, M.M., Hsu, F.F. and Heinecke, J.W. (1998) 'Human neutrophils employ the myeloperoxidase-hydrogen peroxide-chloride system to oxidize alpha-amino acids to a family of reactive aldehydes. Mechanistic studies identifying labile intermediates along the reaction pathway', *J Biol Chem*, 273(9), pp. 4997-5005.

Heck, M.M., Hittelman, W.N. and Earnshaw, W.C. (1988) 'Differential expression of DNA topoisomerases I and II during the eukaryotic cell cycle', *Proc Natl Acad Sci U S A*, 85(4), pp. 1086-90.

Heng, X., Jin, G., Zhang, X., Yang, D., Zhu, M., Fu, S., Li, X. and Le, W. (2012) 'Nurr1 regulates Top IIbeta and functions in axon genesis of mesencephalic dopaminergic neurons', *Mol Neurodegener*, 7, p. 4.

Hinchman, C.A., Matsumoto, H., Simmons, T.W. and Ballatori, N. (1991) 'Intrahepatic conversion of a glutathione conjugate to its mercapturic acid. Metabolism of 1-chloro-2,4-dinitrobenzene in isolated perfused rat and guinea pig livers', *J Biol Chem*, 266(33), pp. 22179-85.

Ho, C.K., Law, S.L., Chiang, H., Hsu, M.L., Wang, C.C. and Wang, S.Y. (1991) 'Inhibition of microtubule assembly is a possible mechanism of action of mitoxantrone', *Biochem Biophys Res Commun*, 180(1), pp. 118-23.

Holm, C., Goto, T., Wang, J.C. and Botstein, D. (1985) 'DNA topoisomerase II is required at the time of mitosis in yeast', *Cell*, 41(2), pp. 553-63.

Hopkinson, R.J., Barlow, P.S., Schofield, C.J. and Claridge, T.D. (2010) 'Studies on the reaction of glutathione and formaldehyde using NMR', *Org Biomol Chem*, 8(21), pp. 4915-20.

Hopkinson, R.J., Leung, I.K.H., Smart, T.J., Rose, N.R., Henry, L., Claridge, T.D.W. and Schofield, C.J. (2015) 'Studies on the Glutathione-Dependent Formaldehyde-Activating Enzyme from Paracoccus denitrificans', *PLOS ONE*, 10(12), p. e0145085.
Hrelia, S., Fiorentini, D., Maraldi, T., Angeloni, C., Bordoni, A., Biagi, P.L. and Hakim, G. (2002) 'Doxorubicin induces early lipid peroxidation associated with changes in glucose transport in cultured cardiomyocytes', *Biochim Biophys Acta*, 1567(1-2), pp. 150-6.

Hu, Z.B., Ma, W., Uphoff, C.C., Metge, K., Gignac, S.M. and Drexler, H.G. (1993) 'Myeloperoxidase: expression and modulation in a large panel of human leukemia-lymphoma cell lines', *Blood*, 82(5), pp. 1599-607.

Huang, K.C., Gao, H., Yamasaki, E.F., Grabowski, D.R., Liu, S., Shen, L.L., Chan, K.K., Ganapathi, R. and Snapka, R.M. (2001) 'Topoisomerase II poisoning by ICRF-193', *J Biol Chem*, 276(48), pp. 44488-94.

Huang, X., Traganos, F. and Darzynkiewicz, Z. (2003) 'DNA damage induced by DNA topoisomerase I- and topoisomerase II-inhibitors detected by histone H2AX phosphorylation in relation to the cell cycle phase and apoptosis', *Cell Cycle*, 2(6), pp. 614-9.

Huret, J. (2004) 't(9;22)(q34;q11) in treatment related leukemia', *Atlas Genet Cytogenet Oncol Haematol.*, 8(1), pp. 26-26.

Inoue, T., Swain, A., Nakanishi, Y. and Sugiyama, D. (2014) 'Multicolor analysis of cell surface marker of human leukemia cell lines using flow cytometry', *Anticancer Res*, 34(8), pp. 4539-50.

Ishida, R., Iwai, M., Marsh, K.L., Austin, C.A., Yano, T., Shibata, M., Nozaki, N. and Hara, A. (1996) 'Threonine 1342 in human topoisomerase IIalpha is phosphorylated throughout the cell cycle', *J Biol Chem*, 271(47), pp. 30077-82.

Jacob, D.A., Gibson, E.G., Mercer, S.L. and Deweese, J.E. (2013) 'Etoposide Catechol Is an Oxidizable Topoisomerase II Poison', *Chemical Research in Toxicology*, 26(8), pp. 1156-1158.

Jacob, D.A., Mercer, S.L., Osheroff, N. and Deweese, J.E. (2011) 'Etoposide Quinone Is a Redox-Dependent Topoisomerase II Poison', *Biochemistry*, 50(25), pp. 5660-5667.

Jenkins, J.R., Ayton, P., Jones, T., Davies, S.L., Simmons, D.L., Harris, A.L., Sheer, D. and Hickson, I.D. (1992) 'Isolation of cDNA clones encoding the beta isozyme of human DNA topoisomerase II and localisation of the gene to chromosome 3p24', *Nucleic Acids Res*, 20(21), pp. 5587-92.

Jensen, H.A., Yourish, H.B., Bunaciu, R.P., Varner, J.D. and Yen, A. (2015) 'Induced myelomonocytic differentiation in leukemia cells is accompanied by noncanonical transcription factor expression', *FEBS Open Bio*, 5, pp. 789-800.

Jensen, L.H., Nitiss, K.C., Rose, A., Dong, J., Zhou, J., Hu, T., Osheroff, N., Jensen, P.B., Sehested, M. and Nitiss, J.L. (2000) 'A Novel Mechanism of Cell Killing by Anti-topoisomerase II Bisdioxopiperazines', *Journal of Biological Chemistry*, 275(3), pp. 2137-2146.

Jensen, P.B. and Sehested, M. (1997) 'DNA topoisomerase II rescue by catalytic inhibitors: a new strategy to improve the antitumor selectivity of etoposide', *Biochem Pharmacol*, 54(7), pp. 755-9.

Jensen, P.B., Sorensen, B.S., Demant, E.J., Sehested, M., Jensen, P.S., Vindelov, L. and Hansen, H.H. (1990) 'Antagonistic effect of aclarubicin on the cytotoxicity of etoposide and 4'-(9-acridinylamino)methanesulfon-m-anisidide in human small cell lung cancer cell lines and on topoisomerase II-mediated DNA cleavage', *Cancer Res*, 50(11), pp. 3311-6.

Johnson, R.K., Zee-Cheng, R.K., Lee, W.W., Acton, E.M., Henry, D.W. and Cheng, C.C. (1979) 'Experimental antitumor activity of aminoanthraquinones', *Cancer Treat Rep*, 63(3), pp. 425-39.

Ju, B.-G., Lunyak, V.V., Perissi, V., Garcia-Bassets, I., Rose, D.W., Glass, C.K. and Rosenfeld, M.G. (2006a) 'A Topoisomerase IIß-Mediated dsDNA Break Required for Regulated Transcription', *Science*, 312(5781), pp. 1798-1802.

Ju, B.G., Lunyak, V.V., Perissi, V., Garcia-Bassets, I., Rose, D.W., Glass, C.K. and Rosenfeld, M.G. (2006b) 'A topoisomerase IIbeta-mediated dsDNA break required for regulated transcription', *Science*, 312(5781), pp. 1798-802.

Kadam, C.Y. and Abhang, S.A. (2015) 'Correlation of Serum levels of Reduced Glutathione and Glutathione dependent Enzymes with Cytochrome c after 1st cycle of adjuvant Chemotherapy in Breast Cancer.', *Research Journal of Recent Sciences*, 4, pp. 55-60.

Kagan, V.E., Kuzmenko, A.I., Tyurina, Y.Y., Shvedova, A.A., Matsura, T. and Yalowich, J.C. (2001) 'Pro-oxidant and antioxidant mechanisms of etoposide in HL-60 cells: role of myeloperoxidase', *Cancer Res*, 61(21), pp. 7777-84.

Kagan, V.E., Yalowich, J.C., Borisenko, G.G., Tyurina, Y.Y., Tyurin, V.A., Thampatty, P. and Fabisiak, J.P. (1999) 'Mechanism-based chemopreventive strategies against etoposide-induced acute myeloid leukemia: free radical/antioxidant approach', *Mol Pharmacol*, 56(3), pp. 494-506.

Kagan, V.E., Yalowich, J.C., Day, B.W., Goldman, R., Gantchev, T.G. and Stoyanovsky, D.A. (1994) 'Ascorbate is the primary reductant of the phenoxyl radical of etoposide in the presence of thiols both in cell homogenates and in model systems', *Biochemistry*, 33(32), pp. 9651-60.

Kalyanaraman, B., Nemec, J. and Sinha, B.K. (1989) 'Characterization of free radicals produced during oxidation of etoposide (VP-16) and its catechol and quinone derivatives. An ESR Study', *Biochemistry*, 28(11), pp. 4839-46.

Kane, R.C., McGuinn, W.D., Dagher, R., Justice, R. and Pazdur, R. (2008) 'Dexrazoxane (Totect™): FDA Review and Approval for the Treatment of Accidental Extravasation Following Intravenous Anthracycline Chemotherapy', *The Oncologist*, 13(4), pp. 445-450.

Kapuscinski, J. and Darzynkiewicz, Z. (1986) 'Relationship between the pharmacological activity of antitumor drugs Ametantrone and mitoxantrone (Novatrone) and their ability to condense nucleic acids', *Proc Natl Acad Sci U S A*, 83(17), pp. 6302-6.

Kato, S., Burke, P.J., Fenick, D.J., Taatjes, D.J., Bierbaum, V.M. and Koch, T.H. (2000) 'Mass spectrometric measurement of formaldehyde generated in breast cancer cells upon treatment with anthracycline antitumor drugs', *Chem Res Toxicol*, 13(6), pp. 509-16.

Kayser, S., Dohner, K., Krauter, J., Kohne, C.H., Horst, H.A., Held, G., von Lilienfeld-Toal, M., Wilhelm, S., Kundgen, A., Gotze, K., Rummel, M., Nachbaur, D., Schlegelberger, B., Gohring, G., Spath, D., Morlok, C., Zucknick, M., Ganser, A., Dohner, H. and Schlenk, R.F. (2011) 'The impact of therapy-related acute myeloid leukemia (AML) on outcome in 2853 adult patients with newly diagnosed AML', *Blood*, 117(7), pp. 2137-45.

Kettle, A.J., Gedye, C.A. and Winterbourn, C.C. (1997) 'Mechanism of inactivation of myeloperoxidase by 4-aminobenzoic acid hydrazide', *Biochem J*, 321 ( Pt 2), pp. 503-8.

Kim, H.J., Khalimonchuk, O., Smith, P.M. and Winge, D.R. (2012) 'Structure, function, and assembly of heme centers in mitochondrial respiratory complexes', *Biochim Biophys Acta*, 1823(9), pp. 1604-16.

Kim, K.H., Kanbe, T., Akashi, T., Mizuguchi, I. and Kikuchi, A. (2002) 'Identification of a single nuclear localization signal in the C-terminal domain of an Aspergillus DNA topoisomerase II', *Molecular Genetics and Genomics*, 268(3), pp. 287-297.

Kim, Y.R., Eom, J.I., Kim, S.J., Jeung, H.K., Cheong, J.W., Kim, J.S. and Min, Y.H. (2010) 'Myeloperoxidase expression as a potential determinant of parthenolide-induced apoptosis in leukemia bulk and leukemia stem cells', *J Pharmacol Exp Ther*, 335(2), pp. 389-400.

Klebanoff, S.J. (2005) 'Myeloperoxidase: friend and foe', *J Leukoc Biol*, 77(5), pp. 598-625.

Knaapen, A.M., Schins, R.P., Borm, P.J. and van Schooten, F.J. (2005) 'Nitrite enhances neutrophil-induced DNA strand breakage in pulmonary epithelial cells by inhibition of myeloperoxidase', *Carcinogenesis*, 26(9), pp. 1642-8.

Koeffler, H. and Golder, D. (1978) 'Acute myelogenous leukemia: a human cell line responsive to colony-stimulating activity.', *Science*, 200, pp. 1153-4.

Kolodziejczyk, P., Reszka, K. and Lown, J.W. (1988) 'Enzymatic oxidative activation and transformation of the antitumor agent mitoxantrone', *Free Radic Biol Med*, 5(1), pp. 13-25.

Kozuki, T., Chikamori, K., Surleac, M.D., Micluta, M.A., Petrescu, A.J., Norris, E.J., Elson, P., Hoeltge, G.A., Grabowski, D.R., Porter, A.C.G., Ganapathi, R.N. and Ganapathi, M.K. (2017) 'Roles of the C-terminal domains of topoisomerase IIalpha and topoisomerase IIbeta in regulation of the decatenation checkpoint', *Nucleic Acids Res*, 45(10), pp. 5995-6010.

Kregiel, D., Berlowska, J. and Ambroziak, W. (2008) 'Succinate Dehydrogenase Activity Assay in situ with Blue Tetrazolium Salt in Crabtree-Positive Saccharomyces cerevisiae Strain', *Food Technol. Biotechnol.*, 46(4), pp. 376-380.

Kurz, E.U., Douglas, P. and Lees-Miller, S.P. (2004) 'Doxorubicin Activates ATM-dependent Phosphorylation of Multiple Downstream Targets in Part through the Generation of Reactive Oxygen Species', *Journal of Biological Chemistry*, 279(51), pp. 53272-53281.

Lanotte, M., Martin-Thouvenin, V., S.Najman, Balerini, P., Valensi, F. and Berger, R. (1991) 'NB4, a Maturation Inducible Cell Line With t(15;17) Marker Isolated From a Human Acute Promyelocytic Leukemia (M3)', *Blood*, 77(5), pp. 1080-1086.

Laponogov, I., Veselkov, D.A., Crevel, I.M., Pan, X.S., Fisher, L.M. and Sanderson, M.R. (2013) 'Structure of an 'open' clamp type II topoisomerase-DNA complex provides a mechanism for DNA capture and transport', *Nucleic Acids Res*, 41(21), pp. 9911-23.

Larsen, A.K., Escargueil, A.E. and Skladanowski, A. (2003) 'Catalytic topoisomerase II inhibitors in cancer therapy', *Pharmacology & Therapeutics*, 99(2), pp. 167-181.

Lau, D., Mollnau, H., Eiserich, J.P., Freeman, B.A., Daiber, A., Gehling, U.M., Brümmer, J., Rudolph, V., Münzel, T., Heitzer, T., Meinertz, T. and Baldus, S. (2005) 'Myeloperoxidase mediates neutrophil activation by association with CD11b/CD18 integrins', *Proceedings of the National Academy of Sciences of the United States of America*, 102(2), pp. 431-436.

Lee, K.C., Bramley, R.L., Cowell, I.G., Jackson, G.H. and Austin, C.A. (2016) 'Proteasomal inhibition potentiates drugs targeting DNA topoisomerase II', *Biochem Pharmacol*, 103, pp. 29-39.

Lee, K.C., Padget, K., Curtis, H., Cowell, I.G., Moiani, D., Sondka, Z., Morris, N.J., Jackson, G.H., Cockell, S.J., Tainer, J.A. and Austin, C.A. (2012a) 'MRE11 facilitates the removal of human topoisomerase II complexes from genomic DNA', *Biology Open*.

Lee, S., Jung, S.R., Heo, K., Byl, J.A., Deweese, J.E., Osheroff, N. and Hohng, S. (2012b) 'DNA cleavage and opening reactions of human topoisomerase IIalpha are regulated via Mg2+-mediated dynamic bending of gate-DNA', *Proc Natl Acad Sci U S A*, 109(8), pp. 2925-30.

Leone, G., Fianchi, L., Pagano, L. and Voso, M.T. (2010) 'Incidence and susceptibility to therapy-related myeloid neoplasms', *Chem Biol Interact*, 184(1-2), pp. 39-45.

Leone, G., Pagano, L., Ben-Yehuda, D. and Voso, M.T. (2007) 'Therapy-related leukemia and myelodysplasia: susceptibility and incidence', *Haematologica*, 92(10), pp. 1389-98.

Li, H., Wang, Y. and Liu, X. (2008) 'Plk1-dependent Phosphorylation Regulates Functions of DNA Topoisomerase IIα in Cell Cycle Progression', *Journal of Biological Chemistry*, 283(10), pp. 6209-6221.

Li, Y., Hao, H., Tzatzalos, E., Lin, R.-K., Doh, S., Liu, L.F., Lyu, Y.L. and Cai, L. (2014) 'Topoisomerase IIbeta is required for proper retinal development and survival of postmitotic cells', *Biology Open*, 3(2), pp. 172-184.

Lindsey, R.H., Bender, R.P. and Osheroff, N. (2005) 'Effects of Benzene Metabolites on DNA Cleavage Mediated by Human Topoisomerase IIα: 1,4-Hydroquinone Is a Topoisomerase II Poison', *Chemical Research in Toxicology*, 18(4), pp. 761-770.

Lindsey, R.H., Pendleton, M., Ashley, R.E., Mercer, S.L., Deweese, J.E. and Osheroff, N. (2014) 'The Catalytic Core of Human Topoisomerase IIalpha: Insights into Enzyme-DNA Interactions and Drug Mechanism', *Biochemistry*, 53(41), pp. 6595-6602.

Linka, R.M., Porter, A.C., Volkov, A., Mielke, C., Boege, F. and Christensen, M.O. (2007) 'C-terminal regions of topoisomerase IIalpha and IIbeta determine isoform-specific functioning of the enzymes in vivo', *Nucleic Acids Res*, 35(11), pp. 3810-22.

Liu, L.F. and Wang, J.C. (1987) 'Supercoiling of the DNA template during transcription', *Proc Natl Acad Sci U S A*, 84(20), pp. 7024-7.

Loike, J.D. and Horwitz, S.B. (1976) 'Effects of podophyllotoxin and VP-16-213 on microtubule assembly in vitro and nucleoside transport in HeLa cells', *Biochemistry*, 15(25), pp. 5435-43.

Lorico, A., Rappa, G. and Sartorelli, A.C. (1992) 'Novobiocin-induced accumulation of etoposide (VP-16) in WEHI-3B D+ leukemia cells', *Int J Cancer*, 52(6), pp. 903-9.

Lovett, B.D., Lo Nigro, L., Rappaport, E.F., Blair, I.A., Osheroff, N., Zheng, N., Megonigal, M.D., Williams, W.R., Nowell, P.C. and Felix, C.A. (2001a) 'Near-precise interchromosomal recombination and functional DNA topoisomerase II cleavage sites at MLL and AF-4 genomic breakpoints in treatment-related acute lymphoblastic leukemia with t(4;11) translocation', *Proceedings of the National Academy of Sciences*, 98(17), pp. 9802-9807.

Lovett, B.D., Strumberg, D., Blair, I.A., Pang, S., Burden, D.A., Megonigal, M.D., Rappaport, E.F., Rebbeck, T.R., Osheroff, N., Pommier, Y.G. and Felix, C.A. (2001b) 'Etoposide metabolites enhance DNA topoisomerase II cleavage near leukemia-associated MLL translocation breakpoints', *Biochemistry*, 40(5), pp. 1159-70.

Lozzio, C.B. and Lozzio, B.B. (1975) 'Human Chronic Myelogenous Leukemia Cell-Line with Postive Philadelphia Chromosome', *Blood*, 45(3), pp. 321-334.

Lucas, I., Germe, T., Chevrier-Miller, M. and Hyrien, O. (2001) 'Topoisomerase II can unlink replicating DNA by precatenane removal', *The EMBO Journal*, 20(22), pp. 6509-6519.

Lushchak, V.I. (2012) 'Glutathione homeostasis and functions: potential targets for medical interventions', *J Amino Acids*, 2012, p. 736837.

MacLeod, R.A. and Drexler, H.G. (2008) 'Leukaemia cell lines are robust in vitro models', *Br J Haematol*, 142(1), pp. 137-8; author reply 138-41.

Madabhushi, R., Gao, F., Pfenning, Andreas R., Pan, L., Yamakawa, S., Seo, J., Rueda, R., Phan, T.X., Yamakawa, H., Pao, P.-C., Stott, Ryan T., Gjoneska, E., Nott, A., Cho, S., Kellis, M. and Tsai, L.-H. (2015) 'Activity-Induced DNA Breaks Govern the Expression of Neuronal Early-Response Genes', *Cell*, 161(7), pp. 1592-1605.

Magnelli, L., Cinelli, M. and Chiarugi, V. (1995) 'Phorbol Esters Attenuate the Expression of p53 in Cells Treated with Doxorubicin and Protect ts-p53/K562 from Apoptosis', *Biochemical and Biophysical Research Communications*, 215(2), pp. 641-645.

Malle, E., Furtmuller, P.G., Sattler, W. and Obinger, C. (2007) 'Myeloperoxidase: a target for new drug development?', *Br J Pharmacol*, 152(6), pp. 838-54.

Mans, D.R., Retel, J., van Maanen, J.M., Lafleur, M.V., van Schaik, M.A., Pinedo, H.M. and Lankelma, J. (1990) 'Role of the semi-quinone free radical of the anti-tumour agent etoposide (VP-16-213) in the inactivation of single- and double-stranded phi X174 DNA', *Br J Cancer*, 62(1), pp. 54-60.

Manville, C.M., Smith, K., Sondka, Z., Rance, H., Cockell, S., Cowell, I.G., Lee, K.C., Morris, N.J., Padget, K., Jackson, G.H. and Austin, C.A. (2015) 'Genome-wide ChIP-seq analysis of human TOP2B occupancy in MCF7 breast cancer epithelial cells', *Biology Open*, 4(11), pp. 1436-1447.

Mays, A.N., Osheroff, N., Xiao, Y., Wiemels, J.L., Felix, C.A., Byl, J.A., Saravanamuttu, K., Peniket, A., Corser, R., Chang, C., Hoyle, C., Parker, A.N., Hasan, S.K., Lo-Coco, F., Solomon, E. and Grimwade, D. (2010) 'Evidence for direct involvement of epirubicin in the formation of chromosomal translocations in t(15;17) therapy-related acute promyelocytic leukemia', *Blood*, 115(2), pp. 326-30.

McClendon, A.K., Gentry, A.C., Dickey, J.S., Brinch, M., Bendsen, S., Andersen, A.H. and Osheroff, N. (2008) 'Bimodal Recognition of DNA Geometry by Human Topoisomerase IIα: Preferential Relaxation of Positively Supercoiled DNA Requires Elements in the C-Terminal Domain', *Biochemistry*, 47(50), pp. 13169-13178.

McClendon, A.K. and Osheroff, N. (2006) 'The Geometry of DNA Supercoils Modulates Topoisomerase-Mediated DNA Cleavage and Enzyme Response to Anticancer Drugs', *Biochemistry*, 45(9), pp. 3040-3050.

McManus, K.J. and Hendzel, M.J. (2005) 'ATM-dependent DNA damage-independent mitotic phosphorylation of H2AX in normally growing mammalian cells', *Mol Biol Cell*, 16(10), pp. 5013-25.

McNamara, S., Wang, H., Hanna, N. and Miller, W.H., Jr. (2008) 'Topoisomerase IIbeta negatively modulates retinoic acid receptor alpha function: a novel mechanism of retinoic acid resistance', *Mol Cell Biol*, 28(6), pp. 2066-77.

Meczes, E.L., Gilroy, K.L., West, K.L. and Austin, C.A. (2008) 'The impact of the human DNA topoisomerase II C-terminal domain on activity', *PLoS One*, 3(3), p. e1754.

Menna, P., Salvatorelli, E. and Minotti, G. (2007) 'Doxorubicin Degradation in Cardiomyocytes', *Journal of Pharmacology and Experimental Therapeutics*, 322(1), p. 408.

Metzler, K.D., Fuchs, T.A., Nauseef, W.M., Reumaux, D., Roesler, J., Schulze, I., Wahn, V., Papayannopoulos, V. and Zychlinsky, A. (2011) 'Myeloperoxidase is required for neutrophil extracellular trap formation: implications for innate immunity', *Blood*, 117(3), pp. 953-9.

Metzler, Kathleen D., Goosmann, C., Lubojemska, A., Zychlinsky, A. and Papayannopoulos, V. (2014) 'A Myeloperoxidase-Containing Complex Regulates Neutrophil Elastase Release and Actin Dynamics during NETosis', *Cell Reports*, 8(3), pp. 883-896.

Mewes, K., Blanz, J., Ehninger, G., Gebhardt, R. and Zeller, K.P. (1993) 'Cytochrome P-450-induced cytotoxicity of mitoxantrone by formation of electrophilic intermediates', *Cancer Res*, 53(21), pp. 5135-42.

Meyer, K.N., Kjeldsen, E., Straub, T., Knudsen, B.R., Hickson, I.D., Kikuchi, A., Kreipe, H. and Boege, F. (1997) 'Cell cycle-coupled relocation of types I and II topoisomerases and modulation of catalytic enzyme activities', *J Cell Biol*, 136(4), pp. 775-88.

Minnich, V., Smith, M.B., Brauner, M.J. and Majerus, P.W. (1971) 'Glutathione biosynthesis in human erythrocytes. I. Identification of the enzymes of glutathione synthesis in hemolysates', *J Clin Invest*, 50(3), pp. 507-13.

Minocha, A. and Long, B.H. (1984) 'Inhibition of the DNA catenation activity of type II topoisomerase by VP16-213 and VM26', *Biochem Biophys Res Commun*, 122(1), pp. 165-70.

Minotti, G., Menna, P., Salvatorelli, E., Cairo, G. and Gianni, L. (2004) 'Anthracyclines: molecular advances and pharmacologic developments in antitumor activity and cardiotoxicity', *Pharmacol Rev*, 56(2), pp. 185-229.

Mirski, S.E., Gerlach, J.H. and Cole, S.P. (1999) 'Sequence determinants of nuclear localization in the alpha and beta isoforms of human topoisomerase II', *Exp Cell Res*, 251(2), pp. 329-39.

Mirski, S.E.L., Bielawski, J.C. and Cole, S.P.C. (2003) 'Identification of functional nuclear export sequences in human topoisomerase IIα and β', *Biochemical and Biophysical Research Communications*, 306(4), pp. 905-911.

Mistry, A.R., Felix, C.A., Whitmarsh, R.J., Mason, A., Reiter, A., Cassinat, B., Parry, A., Walz, C., Wiemels, J.L., Segal, M.R., Ades, L., Blair, I.A., Osheroff, N., Peniket, A.J., Lafage-Pochitaloff, M., Cross, N.C., Chomienne, C., Solomon, E., Fenaux, P. and Grimwade, D. (2005) 'DNA topoisomerase II in therapy-related acute promyelocytic leukemia', *N Engl J Med*, 352(15), pp. 1529-38.

Miyamoto, Y., Kanayama, A., Inoue, J.-I., Konishi, Y.S. and Shimizu, M. (2003) 'Taurine Is Involved in Oxidation of IκBα at Met45', in Lombardini, J.B., Schaffer, S.W. and Azuma, J. (eds.) *Taurine 5: Beginning the 21st Century*. Boston, MA: Springer US, pp. 373-380.

Mondal, N. and Parvin, J.D. (2001) 'DNA topoisomerase IIalpha is required for RNA polymerase II transcription on chromatin templates', *Nature*, 413(6854), pp. 435-8.

Mondal, N., Zhang, Y., Jonsson, Z., Dhar, S.K., Kannapiran, M. and Parvin, J.D. (2003) 'Elongation by RNA polymerase II on chromatin templates requires topoisomerase activity', *Nucleic Acids Res*, 31(17), pp. 5016-24.

Montaudon, D., Pourquier, P., Denois, F., de Tinguy-Moreaud, E., Lagarde, P. and Robert, J. (1997) 'Differential stabilization of topoisomerase-II-DNA cleavable complexes by doxorubicin and etoposide in doxorubicin-resistant rat glioblastoma cells', *Eur J Biochem*, 245(2), pp. 307-15.

Monteiro, L.J., Khongkow, P., Kongsema, M., Morris, J.R., Man, C., Weekes, D., Koo, C.Y., Gomes, A.R., Pinto, P.H., Varghese, V., Kenny, L.M., Charles Coombes, R., Freire, R., Medema, R.H. and Lam, E.W.F. (2013) 'The Forkhead Box M1 protein regulates BRIP1 expression and DNA damage repair in epirubicin treatment', *Oncogene*, 32(39), pp. 4634-4645.

Mukundan, H., Bahadur, A.K., Kumar, A., Sardana, S., Naik, S.L., Ray, A. and Sharma, B.K. (1999) 'Glutathione level and its relation to radiation therapy in patients with cancer of uterine cervix', *Indian J Exp Biol*, 37(9), pp. 859-64.

Murao, S., Stevens, F.J., Ito, A. and Huberman, E. (1988) 'Myeloperoxidase: a myeloid cell nuclear antigen with DNA-binding properties', *Proceedings of the National Academy of Sciences*, 85(4), pp. 1232-1236.

Nagra, R.M., Becher, B., Tourtellotte, W.W., Antel, J.P., Gold, D., Paladino, T., Smith, R.A., Nelson, J.R. and Reynolds, W.F. (1997) 'Immunohistochemical and genetic evidence of myeloperoxidase involvement in multiple sclerosis', *J Neuroimmunol*, 78(1-2), pp. 97-107.

Nakazato, T., Sagawa, M., Yamato, K., Xian, M., Yamamoto, T., Suematsu, M., Ikeda, Y. and Kizaki, M. (2007) 'Myeloperoxidase is a key regulator of oxidative stress mediated apoptosis in myeloid leukemic cells', *Clin Cancer Res*, 13(18 Pt 1), pp. 5436-45.

Nauseef, W.M., Cogley, M. and McCormick, S. (1996) 'Effect of the R569W missense mutation on the biosynthesis of myeloperoxidase', *J Biol Chem*, 271(16), pp. 9546-9.

Nauseef, W.M., McCormick, S. and Yi, H. (1992) 'Roles of heme insertion and the mannose-6-phosphate receptor in processing of the human myeloid lysosomal enzyme, myeloperoxidase', *Blood*, 80(10), pp. 2622-33.

Nauseef, W.M., McCormick, S.J. and Clark, R.A. (1995) 'Calreticulin functions as a molecular chaperone in the biosynthesis of myeloperoxidase', *J Biol Chem*, 270(9), pp. 4741-7.

Nauseef, W.M., McCormick, S.J. and Goedken, M. (1998) 'Coordinated participation of calreticulin and calnexin in the biosynthesis of myeloperoxidase', *J Biol Chem*, 273(12), pp. 7107-11.

Nitiss, J.L. (2009a) 'DNA topoisomerase II and its growing repertoire of biological functions', *Nat Rev Cancer*, 9(5), pp. 327-37.

Nitiss, J.L. (2009b) 'Targeting DNA topoisomerase II in cancer chemotherapy', *Nat Rev Cancer*, 9(5), pp. 338-50.

Null, A.P., Hudson, J. and Gorbsky, G.J. (2002) 'Both alpha and beta isoforms of mammalian DNA topoisomerase II associate with chromosomes in mitosis', *Cell Growth Differ*, 13(7), pp. 325-33.

Panousis, C., Kettle, A.J. and Phillips, D.R. (1994) 'Oxidative metabolism of mitoxantrone by the human neutrophil enzyme myeloperoxidase', *Biochem Pharmacol*, 48(12), pp. 2223-30.

Panousis, C., Kettle, A.J. and Phillips, D.R. (1997) 'Neutrophil-mediated activation of mitoxantrone to metabolites which form adducts with DNA', *Cancer Lett*, 113(1-2), pp. 173-8.

Papayannopoulos, V., Metzler, K.D., Hakkim, A. and Zychlinsky, A. (2010) 'Neutrophil elastase and myeloperoxidase regulate the formation of neutrophil extracellular traps', *J Cell Biol*, 191(3), pp. 677-91.

Parker, B.S., Buley, T., Evison, B.J., Cutts, S.M., Neumann, G.M., Iskander, M.N. and Phillips, D.R. (2004) 'A molecular understanding of mitoxantrone-DNA adduct formation: effect of cytosine methylation and flanking sequences', *J Biol Chem*, 279(18), pp. 18814-23.

Parker, B.S., Cullinane, C. and Phillips, D.R. (1999) 'Formation of DNA adducts by formaldehyde-activated mitoxantrone', *Nucleic Acids Res*, 27(14), pp. 2918-23.

Parker, B.S., Cutts, S.M., Cullinane, C. and Phillips, D.R. (2000) 'Formaldehyde activation of mitoxantrone yields CpG and CpA specific DNA adducts', *Nucleic Acids Res*, 28(4), pp. 982-90.

Parker, B.S., Cutts, S.M. and Phillips, D.R. (2001) 'Cytosine methylation enhances mitoxantrone-DNA adduct formation at CpG dinucleotides', *J Biol Chem*, 276(19), pp. 15953-60.

Paul, F., Arkin, Y., Giladi, A., Jaitin, D.A., Kenigsberg, E., Keren-Shaul, H., Winter, D., Lara-Astiaso, D., Gury, M., Weiner, A., David, E., Cohen, N., Lauridsen, F.K., Haas, S., Schlitzer, A., Mildner, A., Ginhoux, F., Jung, S., Trumpp, A., Porse, B.T., Tanay, A. and Amit, I. (2015) 'Transcriptional Heterogeneity and Lineage Commitment in Myeloid Progenitors', *Cell*, 163(7), pp. 1663-77.

Pember, S.O., Fuhrer-Krusi, S.M., Barnes, K.C. and Kinkade, J.M., Jr. (1982) 'Isolation of three native forms of myeloperoxidase from human polymorphonuclear leukocytes', *FEBS Lett*, 140(1), pp. 103-8.

Pember, S.O., Shapira, R. and Kinkade, J.M., Jr. (1983) 'Multiple forms of myeloperoxidase from human neutrophilic granulocytes: evidence for differences in compartmentalization, enzymatic activity, and subunit structure', *Arch Biochem Biophys*, 221(2), pp. 391-403.

Pendleton, M., Lindsey, R.H., Jr., Felix, C.A., Grimwade, D. and Osheroff, N. (2014) 'Topoisomerase II and leukemia', *Ann N Y Acad Sci*, 1310, pp. 98-110.
Perez-Arnaiz, C., Busto, N., Leal, J.M. and Garcia, B. (2014) 'New insights into the mechanism of the DNA/doxorubicin interaction', *J Phys Chem B*, 118(5), pp. 1288-95.

Perillo, B., Ombra, M.N., Bertoni, A., Cuozzo, C., Sacchetti, S., Sasso, A., Chiariotti, L., Malorni, A., Abbondanza, C. and Avvedimento, E.V. (2008) 'DNA oxidation as triggered by H3K9me2 demethylation drives estrogen-induced gene expression', *Science*, 319(5860), pp. 202-6.

Peter, B.J., Ullsperger, C., Hiasa, H., Marians, K.J. and Cozzarelli, N.R. (1998) 'The structure of supercoiled intermediates in DNA replication', *Cell*, 94(6), pp. 819-27.

Piedrafita, F.J., Molander, R.B., Vansant, G., Orlova, E.A., Pfahl, M. and Reynolds, W.F. (1996) 'An Alu element in the myeloperoxidase promoter contains a composite SP1-thyroid hormone-retinoic acid response element', *J Biol Chem*, 271(24), pp. 14412-20.

Pinnix, I.B., Guzman, G.S., Bonkovsky, H.L., Zaki, S.R. and Kinkade, J.M. (1994) 'The Post-translational Processing of Myeloperoxidase Is Regulated by the Availability of Heme', *Archives of Biochemistry and Biophysics*, 312(2), pp. 447-458.

Pommier, Y. and Marchand, C. (2012) 'Interfacial inhibitors: targeting macromolecular complexes', *Nat Rev Drug Discov*, 11(1), pp. 25-36.

Post, G.C., Barthel, B.L., Burkhart, D.J., Hagadorn, J.R. and Koch, T.H. (2005) 'Doxazolidine, a Proposed Active Metabolite of Doxorubicin That Cross-links DNA', *Journal of Medicinal Chemistry*, 48(24), pp. 7648-7657.

Povirk, L.F. (2012) 'Processing of Damaged DNA Ends for Double-Strand Break Repair in Mammalian Cells', *ISRN Molecular Biology*, 2012, pp. 1-16.

Psaila, B., Barkas, N., Iskander, D., Roy, A., Anderson, S., Ashley, N., Caputo, V.S., Lichtenberg, J., Loaiza, S., Bodine, D.M., Karadimitris, A., Mead, A.J. and Roberts, I. (2016) 'Single-cell profiling of human megakaryocyte-erythroid progenitors identifies distinct megakaryocyte and erythroid differentiation pathways', *Genome Biology*, 17(1), p. 83.

Ray, S., Panova, T., Miller, G., Volkov, A., Porter, A.C., Russell, J., Panov, K.I. and Zomerdijk, J.C. (2013) 'Topoisomerase IIalpha promotes activation of RNA polymerase I transcription by facilitating pre-initiation complex formation', *Nat Commun*, 4, p. 1598.

Reszka, K., Hartley, J.A., Kolodziejczyk, P. and Lown, J.W. (1989) 'Interaction of the peroxidase-derived metabolite of mitoxantrone with nucleic acids. Evidence for covalent binding of 14C-labeled drug', *Biochem Pharmacol*, 38(23), pp. 4253-60.

Reszka, K., Kolodziejczyk, P. and Lown, J.W. (1986) 'Horseradish peroxidase-catalyzed oxidation of mitoxantrone: spectrophotometric and electron paramagnetic resonance studies', *J Free Radic Biol Med*, 2(1), pp. 25-32.

Reszka, K.J., Britigan, L.H., Rasmussen, G.T., Wagner, B.A., Burns, C.P. and Britigan, B.E. (2004) 'Acetaminophen stimulates the peroxidative metabolism of anthracyclines', *Arch Biochem Biophys*, 427(1), pp. 16-29.

Reszka, K.J., McCormick, M.L. and Britigan, B.E. (2001) 'Peroxidase- and nitrite-dependent metabolism of the anthracycline anticancer agents daunorubicin and doxorubicin', *Biochemistry*, 40(50), pp. 15349-61.

Reszka, K.J., Wagner, B.A., Teesch, L.M., Britigan, B.E., Spitz, D.R. and Burns, C.P. (2005) 'Inactivation of anthracyclines by cellular peroxidase', *Cancer Res*, 65(14), pp. 6346-53.

Reynolds, W.F., Rhees, J., Maciejewski, D., Paladino, T., Sieburg, H., Maki, R.A. and Masliah, E. (1999) 'Myeloperoxidase polymorphism is associated with gender specific risk for Alzheimer's disease', *Exp Neurol*, 155(1), pp. 31-41.

Riordan, C.G. and Wei, P. (1994) 'Methyl Radical-Initiated DNA Cleavage Facilitated by a Discrete Organometallic Complex', *Journal of the American Chemical Society*, 116(5), pp. 2189-2190.

Ross, W., Rowe, T., Glisson, B., Yalowich, J. and Liu, L. (1984) 'Role of topoisomerase II in mediating epipodophyllotoxin-induced DNA cleavage', *Cancer Res*, 44(12 Pt 1), pp. 5857-60.

Rucker, F.G., Sander, S., Dohner, K., Dohner, H., Pollack, J.R. and Bullinger, L. (2006) 'Molecular profiling reveals myeloid leukemia cell lines to be faithful model systems characterized by distinct genomic aberrations', *Leukemia*, 20(6), pp. 994-1001.

Ruggeri, R.B., Buckbinder, L., Bagley, S.W., Carpino, P.A., Conn, E.L., Dowling, M.S., Fernando, D.P., Jiao, W., Kung, D.W., Orr, S.T., Qi, Y., Rocke, B.N., Smith, A., Warmus, J.S., Zhang, Y., Bowles, D., Widlicka, D.W., Eng, H., Ryder, T., Sharma, R., Wolford, A., Okerberg, C., Walters, K., Maurer, T.S., Zhang, Y., Bonin, P.D., Spath, S.N., Xing, G., Hepworth, D., Ahn, K. and Kalgutkar, A.S. (2015) 'Discovery of 2-(6-(5-Chloro-2-methoxyphenyl)-4-oxo-2-thioxo-3,4-dihydropyrimidin-1(2H)-yl)acet amide (PF-06282999): A Highly Selective Mechanism-Based Myeloperoxidase Inhibitor for the Treatment of Cardiovascular Diseases', *J Med Chem*, 58(21), pp. 8513-28.

Santo, A., Chacim, S., Ferreira, I., Leite, L., Moreira, C., Pereira, D., Dantas Brito, M.D., Nunes, M., Domingues, N., Oliveira, I., Moreira, I., Martins, A., Viterbo, L., Mariz, J.M. and Medeiros, R. (2016) 'Effect of therapy-related acute myeloid leukemia on the outcome of patients with acute myeloid leukemia', *Oncol Lett*, 12(1), pp. 262-268.

Schakowski, F., Buttgereit, P., Mazur, M., Märten, A., Schöttker, B., Gorschlüter, M. and Schmidt-Wolf, I.G.H. (2004) 'Novel non-viral method for transfection of primary leukemia cells and cell lines', *Genetic Vaccines and Therapy*, 2, pp. 1-1.

Scharf, S., Zech, J., Bursen, A., Schraets, D., Oliver, P.L., Kliem, S., Pfitzner, E., Gillert, E., Dingermann, T. and Marschalek, R. (2006) 'Transcription linked to recombination: a gene-internal promoter coincides with the recombination hot spot II of the human MLL gene', *Oncogene*, 26(10), pp. 1361-1371.

Schmidt, B.H., Burgin, A.B., Deweese, J.E., Osheroff, N. and Berger, J.M. (2010) 'A novel and unified two-metal mechanism for DNA cleavage by type II and IA topoisomerases', *Nature*, 465(7298), pp. 641-4.

Schmidt, B.H., Osheroff, N. and Berger, J.M. (2012) 'Structure of a topoisomerase II-DNA-nucleotide complex reveals a new control mechanism for ATPase activity', *Nat Struct Mol Biol*, 19(11), pp. 1147-54.

Schultz, M.C., Brill, S.J., Ju, Q., Sternglanz, R. and Reeder, R.H. (1992) 'Topoisomerases and yeast rRNA transcription: negative supercoiling stimulates initiation and topoisomerase activity is required for elongation', *Genes Dev*, 6(7), pp. 1332-41.

Sehested, M. and Jensen, P.B. (1996) 'Mapping of DNA topoisomerase II poisons (etoposide, clerocidin) and catalytic inhibitors (aclarubicin, ICRF-187) to four distinct steps in the topoisomerase II catalytic cycle', *Biochem Pharmacol*, 51(7), pp. 879-86.

Seita, J. and Weissman, I.L. (2010) 'Hematopoietic stem cell: self-renewal versus differentiation', *Wiley Interdiscip Rev Syst Biol Med*, 2(6), pp. 640-53.

Sekiguchi, J., Stivers, J.T., Mildvan, A.S. and Shuman, S. (1996) 'Mechanism of Inhibition of Vaccinia DNA Topoisomerase by Novobiocin and Coumermycin', *Journal of Biological Chemistry*, 271(4), pp. 2313-2322.

Sinha, B.K., Kumar, A., Bhattacharjee, S., Espey, M.G. and Mason, R.P. (2013) 'Effect of nitric oxide on the anticancer activity of the topoisomerase-active drugs

etoposide and adriamycin in human melanoma cells', *J Pharmacol Exp Ther*, 347(3), pp. 607-14.

Sinha, B.K., Mimnaugh, E.G., Rajagopalan, S. and Myers, C.E. (1989) 'Adriamycin Activation and Oxygen Free Radical Formation in Human Breast Tumor Cells: Protective Role of Glutathione Peroxidase in Adriamycin Resistance', *Cancer Research*, 49(14), p. 3844.

Sinha, B.K., Politi, P.M., Eliot, H.M., Kerrigan, D. and Pommier, Y. (1990) 'Structure-activity relations, cytotoxicity and topoisomerase II dependent cleavage induced by pendulum ring analogues of etoposide', *Eur J Cancer*, 26(5), pp. 590-3.

Slany, R.H. (2009) 'The molecular biology of mixed lineage leukemia', *Haematologica*, 94(7), pp. 984-993.

Smith, K.A., Cowell, I.G., Zhang, Y., Sondka, Z. and Austin, C.A. (2014a) 'The role of topoisomerase II beta on breakage and proximity of RUNX1 to partner alleles RUNX1T1 and EVI1', *Genes Chromosomes Cancer*, 53(2), pp. 117-28.

Smith, N.A., Byl, J.A.W., Mercer, S.L., Deweese, J.E. and Osheroff, N. (2014b) 'Etoposide Quinone Is a Covalent Poison of Human Topoisomerase IIβ', *Biochemistry*, 53(19), pp. 3229-3236.

Snoke, J.E., Yanari, S. and Bloch, K. (1953) 'Synthesis of glutathione from gamma-glutamylcysteine', *J Biol Chem*, 201(2), pp. 573-86.

Sorensen, B.S., Sinding, J., Andersen, A.H., Alsner, J., Jensen, P.B. and Westergaard, O. (1992) 'Mode of action of topoisomerase II-targeting agents at a specific DNA sequence. Uncoupling the DNA binding, cleavage and religation events', *J Mol Biol*, 228(3), pp. 778-86.

Soubeyrand, S., Pope, L. and Haché, R.J.G. (2010) 'Topoisomerase IIα-dependent induction of a persistent DNA damage response in response to transient etoposide exposure', *Molecular Oncology*, 4(1), pp. 38-51.

Soubhye, J., Aldib, I., Elfving, B., Gelbcke, M., Furtmuller, P.G., Podrecca, M., Conotte, R., Colet, J.M., Rousseau, A., Reye, F., Sarakbi, A., Vanhaeverbeek, M., Kauffmann, J.M., Obinger, C., Neve, J., Prevost, M., Zouaoui Boudjeltia, K., Dufrasne, F. and Van Antwerpen, P. (2013) 'Design, synthesis, and structure-activity relationship studies of novel 3-alkylindole derivatives as selective and highly potent myeloperoxidase inhibitors', *J Med Chem*, 56(10), pp. 3943-58.

Soubhye, J., Prevost, M., Van Antwerpen, P., Zouaoui Boudjeltia, K., Rousseau, A., Furtmuller, P.G., Obinger, C., Vanhaeverbeek, M., Ducobu, J., Neve, J., Gelbcke, M. and Dufrasne, F.O. (2010) 'Structure-based design, synthesis, and pharmacological evaluation of 3-(aminoalkyl)-5-fluoroindoles as myeloperoxidase inhibitors', *J Med Chem*, 53(24), pp. 8747-59.

Sundin, O. and Varshavsky, A. (1980) 'Terminal stages of SV40 DNA replication proceed via multiply intertwined catenated dimers', *Cell*, 21(1), pp. 103-14.

Sundin, O. and Varshavsky, A. (1981) 'Arrest of segregation leads to accumulation of highly intertwined catenated dimers: dissection of the final stages of SV40 DNA replication', *Cell*, 25(3), pp. 659-69.

Sunter, N.J., Cowell, I.G., Willmore, E., Watters, G.P. and Austin, C.A. (2010) 'Role of Topoisomerase IIbeta in DNA Damage Response following IR and Etoposide', *J Nucleic Acids*, 2010, p. 710589.

Super, H.J., McCabe, N.R., Thirman, M.J., Larson, R.A., Le Beau, M.M., Pedersen-Bjergaard, J., Philip, P., Diaz, M.O. and Rowley, J.D. (1993) 'Rearrangements of the MLL gene in therapy-related acute myeloid leukemia in patients previously treated with agents targeting DNA- topoisomerase II', *Blood*, 82(12), p. 3705.

Swain, S.M., Whaley, F.S., Gerber, M.C., Weisberg, S., York, M., Spicer, D., Jones, S.E., Wadler, S., Desai, A., Vogel, C., Speyer, J., Mittelman, A., Reddy, S., Pendergrass, K., Velez-Garcia, E., Ewer, M.S., Bianchine, J.R. and Gams, R.A. (1997) 'Cardioprotection with dexrazoxane for doxorubicin-containing therapy in advanced breast cancer', *J Clin Oncol*, 15(4), pp. 1318-32.

Swift, L.P., Rephaeli, A., Nudelman, A., Phillips, D.R. and Cutts, S.M. (2006) 'Doxorubicin-DNA adducts induce a non-topoisomerase II-mediated form of cell death', *Cancer Res*, 66(9), pp. 4863-71.

Taagepera, S., Rao, P.N., Drake, F.H. and Gorbsky, G.J. (1993) 'DNA topoisomerase II alpha is the major chromosome protein recognized by the mitotic phosphoprotein antibody MPM-2', *Proc Natl Acad Sci U S A*, 90(18), pp. 8407-11.

Taatjes, D.J., Fenick, D.J. and Koch, T.H. (1998) 'Epidoxoform: a hydrolytically more stable anthracycline-formaldehyde conjugate toxic to resistant tumor cells', *J Med Chem*, 41(8), pp. 1306-14.

Tavormina, P.A., Come, M.G., Hudson, J.R., Mo, Y.Y., Beck, W.T. and Gorbsky, G.J. (2002) 'Rapid exchange of mammalian topoisomerase II alpha at kinetochores and chromosome arms in mitosis', *J Cell Biol*, 158(1), pp. 23-9.

Tewey, K.M., Rowe, T.C., Yang, L., Halligan, B.D. and Liu, L.F. (1984) 'Adriamycin-induced DNA damage mediated by mammalian DNA topoisomerase II', *Science*, 226(4673), pp. 466-8.

Thakurela, S., Garding, A., Jung, J., Schubeler, D., Burger, L. and Tiwari, V.K. (2013) 'Gene regulation and priming by topoisomerase IIalpha in embryonic stem cells', *Nat Commun*, 4, p. 2478.

Thorndike, J. and Beck, W.S. (1977) 'Production of formaldehyde from N5-methyltetrahydrofolate by normal and leukemic leukocytes', *Cancer Res*, 37(4), pp. 1125-32.

Tiden, A.K., Sjogren, T., Svensson, M., Bernlind, A., Senthilmohan, R., Auchere, F., Norman, H., Markgren, P.O., Gustavsson, S., Schmidt, S., Lundquist, S., Forbes, L.V., Magon, N.J., Paton, L.N., Jameson, G.N., Eriksson, H. and Kettle, A.J. (2011)

'2-thioxanthines are mechanism-based inactivators of myeloperoxidase that block oxidative stress during inflammation', *J Biol Chem*, 286(43), pp. 37578-89.

Tiwari, V.K., Burger, L., Nikoletopoulou, V., Deogracias, R., Thakurela, S., Wirbelauer, C., Kaut, J., Terranova, R., Hoerner, L., Mielke, C., Boege, F., Murr, R., Peters, A.H.F.M., Barde, Y.-A. and Schübeler, D. (2012) 'Target genes of Topoisomerase IIβ regulate neuronal survival and are defined by their chromatin state', *Proceedings of the National Academy of Sciences*, 109(16), pp. E934–E943.

Toldo, S., Goehe, R.W., Lotrionte, M., Mezzaroma, E., Sumner, E.T., Biondi-Zoccai, G.G.L., Seropian, I.M., Van Tassell, B.W., Loperfido, F., Palazzoni, G., Voelkel, N.F., Abbate, A. and Gewirtz, D.A. (2013) 'Comparative Cardiac Toxicity of Anthracyclines In Vitro and In Vivo in the Mouse', *PLoS ONE*, 8(3), p. e58421.

Trotter, K.W., King, H.A. and Archer, T.K. (2015) 'Glucocorticoid Receptor Transcriptional Activation via the BRG1-Dependent Recruitment of TOP2beta and Ku70/86', *Mol Cell Biol*, 35(16), pp. 2799-817.

Tsai-Pflugfelder, M., Liu, L.F., Liu, A.A., Tewey, K.M., Whang-Peng, J., Knutsen, T., Huebner, K., Croce, C.M. and Wang, J.C. (1988) 'Cloning and sequencing of cDNA encoding human DNA topoisomerase II and localization of the gene to chromosome region 17q21-22', *Proc Natl Acad Sci U S A*, 85(19), pp. 7177-81.

Tschudy, D.P., Hess, R.A. and Frykholm, B.C. (1981) 'Inhibition of delta-aminolevulinic acid dehydrase by 4,6-dioxoheptanoic acid', *J Biol Chem*, 256(19), pp. 9915-23.

Tuduri, S., Crabbe, L., Conti, C., Tourriere, H., Holtgreve-Grez, H., Jauch, A., Pantesco, V., De Vos, J., Thomas, A., Theillet, C., Pommier, Y., Tazi, J., Coquelle, A. and Pasero, P. (2009) 'Topoisomerase I suppresses genomic instability by preventing interference between replication and transcription', *Nat Cell Biol*, 11(11), pp. 1315-24.

Tulpule, K. and Dringen, R. (2013) 'Formaldehyde in brain: an overlooked player in neurodegeneration?', *J Neurochem*, 127(1), pp. 7-21.

Tuteja, N., Phan, T.N., Tuteja, R., Ochem, A. and Falaschi, A. (1997) 'Inhibition of DNA unwinding and ATPase activities of human DNA helicase II by chemotherapeutic agents', *Biochem Biophys Res Commun*, 236(3), pp. 636-40.

Uemura, T. and Tanagida, M. (1986) 'Mitotic spindle pulls but fails to separate chromosomes in type II DNA topoisomerase mutants: uncoordinated mitosis', *Embo j*, 5(5), pp. 1003-10.

van der Veen, B.S., de Winther, M.P. and Heeringa, P. (2009) 'Myeloperoxidase: molecular mechanisms of action and their relevance to human health and disease', *Antioxid Redox Signal*, 11(11), pp. 2899-937.

van Leeuwen, J.E. and Kearse, K.P. (1996) 'Deglucosylation of N-linked glycans is an important step in the dissociation of calreticulin-class I-TAP complexes', *Proc Natl Acad Sci U S A*, 93(24), pp. 13997-4001.

van Maanen, J.M., Lafleur, M.V., Mans, D.R., van den Akker, E., de Ruiter, C., Kootstra, P.R., Pappie, D., de Vries, J., Retel, J. and Pinedo, H.M. (1988a) 'Effects of the ortho-quinone and catechol of the antitumor drug VP-16-213 on the biological activity of single-stranded and double-stranded phi X174 DNA', *Biochem Pharmacol*, 37(19), pp. 3579-89.

van Maanen, J.M.S., Retèl, J., de Vries, J. and Pinedo, H.M. (1988b) 'Mechanism of Action of Antitumor Drug Etoposide: A Review', *Journal of the National Cancer Institute*, 80(19), pp. 1526-1533.

Villablanca, J.G., Volchenboum, S.L., Cho, H., Kang, M.H., Cohn, S.L., Anderson, C.P., Marachelian, A., Groshen, S., Tsao-Wei, D., Matthay, K.K., Maris, J.M., Hasenauer, C.E., Czarnecki, S., Lai, H., Goodarzian, F., Shimada, H. and Reynolds, C.P. (2016) 'A Phase I New Approaches to Neuroblastoma Therapy Study of Buthionine Sulfoximine and Melphalan With Autologous Stem Cells for Recurrent/Refractory High-Risk Neuroblastoma', *Pediatr Blood Cancer*, 63(8), pp. 1349-56.

Vlasova, II, Feng, W.H., Goff, J.P., Giorgianni, A., Do, D., Gollin, S.M., Lewis, D.W., Kagan, V.E. and Yalowich, J.C. (2011) 'Myeloperoxidase-dependent oxidation of etoposide in human myeloid progenitor CD34+ cells', *Mol Pharmacol*, 79(3), pp. 479-87.

Vyas, D.M., Kadow, J.F., LeBoulluec, K.L., Saulnier, M.G. and Doyle, T.W. (1992) 'Etoposide(VP16): Chemical reactivity of etoposide ortho-quinone with amines and thiols', *Bioorganic & Medicinal Chemistry Letters*, 2(9), pp. 1111-1114.

Wagner, B.A., Teesch, L.M., Buettner, G.R., Britigan, B.E., Burns, C.P. and Reszka, K.J. (2007) 'Inactivation of anthracyclines by serum heme proteins', *Chem Res Toxicol*, 20(6), pp. 920-6.

Wang, A.H., Gao, Y.G., Liaw, Y.C. and Li, Y.K. (1991) 'Formaldehyde cross-links daunorubicin and DNA efficiently: HPLC and X-ray diffraction studies', *Biochemistry*, 30(16), pp. 3812-5.

Wang, J.C. (2002) 'Cellular roles of DNA topoisomerases: a molecular perspective', *Nat Rev Mol Cell Biol*, 3(6), pp. 430-40.

Ward, J., Spath, S.N., Pabst, B., Carpino, P.A., Ruggeri, R.B., Xing, G., Speers, A.E., Cravatt, B.F. and Ahn, K. (2013) 'Mechanistic Characterization of a 2-Thioxanthine Myeloperoxidase Inhibitor and Selectivity Assessment Utilizing Click Chemistry–Activity-Based Protein Profiling', *Biochemistry*, 52(51), pp. 9187-9201.

Wei, H., Ruthenburg, A.J., Bechis, S.K. and Verdine, G.L. (2005) 'Nucleotide-dependent domain movement in the ATPase domain of a human type IIA DNA topoisomerase', *J Biol Chem*, 280(44), pp. 37041-7.

Weiss, S.J., Klein, R., Slivka, A. and Wei, M. (1982) 'Chlorination of Taurine by Human Neutrophils: Evidence for Hypochlorous Acid Generation', *Journal of Clinical Investigation*, 70(3), pp. 598-607.

Wells, N.J., Fry, A.M., Guano, F., Norbury, C. and Hickson, I.D. (1995a) 'Cell cycle phase-specific phosphorylation of human topoisomerase II alpha. Evidence of a role for protein kinase C', *J Biol Chem*, 270(47), pp. 28357-63.

Wells, N.J., Fry, A.M., Guano, F., Norbury, C. and Hickson, I.D. (1995b) 'Cell Cycle Phase-specific Phosphorylation of Human Topoisomerase IIα: EVIDENCE OF A ROLE FOR PROTEIN KINASE C', *Journal of Biological Chemistry*, 270(47), pp. 28357-28363.

Wendorff, T.J., Schmidt, B.H., Heslop, P., Austin, C.A. and Berger, J.M. (2012) 'The structure of DNA-bound human topoisomerase II alpha: conformational mechanisms for coordinating inter-subunit interactions with DNA cleavage', *J Mol Biol*, 424(3-4), pp. 109-24.

West, K.L. and Austin, C.A. (1999) 'Human DNA topoisomerase IIβ binds and cleaves four-way junction DNA in vitro', *Nucleic Acids Research*, 27(4), pp. 984-992.

West, K.L., Meczes, E.L., Thorn, R., Turnbull, R.M., Marshall, R. and Austin, C.A. (2000) 'Mutagenesis of E477 or K505 in the B‘ Domain of Human Topoisomerase IIβ Increases the Requirement for Magnesium Ions during Strand Passage', *Biochemistry*, 39(6), pp. 1223-1233.

West, K.L., Turnbull, R.M., Willmore, E., Lakey, J.H. and Austin, C.A. (2002) 'Characterisation of the DNA-dependent ATPase activity of human DNA topoisomerase IIbeta: mutation of Ser165 in the ATPase domain reduces the ATPase activity and abolishes the in vivo complementation ability', *Nucleic Acids Res*, 30(24), pp. 5416-24.

Wigley, D.B., Davies, G.J., Dodson, E.J., Maxwell, A. and Dodson, G. (1991) 'Crystal structure of an N-terminal fragment of the DNA gyrase B protein', *Nature*, 351(6328), pp. 624-9.

Willmore, E., Errington, F., Tilby, M.J. and Austin, C.A. (2002) 'Formation and longevity of idarubicin-induced DNA topoisomerase II cleavable complexes in K562 human leukaemia cells', *Biochem Pharmacol*, 63(10), pp. 1807-15.

Willmore, E., Frank, A.J., Padget, K., Tilby, M.J. and Austin, C.A. (1998) 'Etoposide targets topoisomerase IIalpha and IIbeta in leukemic cells: isoform-specific cleavable complexes visualized and quantified in situ by a novel immunofluorescence technique', *Mol Pharmacol*, 54(1), pp. 78-85.

Winter, J., Ilbert, M., Graf, P.C., Ozcelik, D. and Jakob, U. (2008) 'Bleach activates a redox-regulated chaperone by oxidative protein unfolding', *Cell*, 135(4), pp. 691-701.

Winterbourn, C.C. (2002) 'Biological reactivity and biomarkers of the neutrophil oxidant, hypochlorous acid', *Toxicology*, 181-182, pp. 223-7.

Winterbourn, C.C., Gutteridge, J.M.C. and Halliwell, B. (1985) 'Doxorubicin-dependent lipid peroxidation at low partial pressures of O2', *Journal of Free Radicals in Biology & Medicine*, 1(1), pp. 43-49.

Woessner, R.D., Mattern, M.R., Mirabelli, C.K., Johnson, R.K. and Drake, F.H. (1991) 'Proliferation- and cell cycle-dependent differences in expression of the 170 kilodalton and 180 kilodalton forms of topoisomerase II in NIH-3T3 cells', *Cell Growth Differ*, 2(4), pp. 209-14.

Wozniak, A.J. and Ross, W.E. (1983) 'DNA damage as a basis for 4'-demethylepipodophyllotoxin-9-(4,6-O-ethylidene-beta-D-glucopyranoside) (etoposide) cytotoxicity', *Cancer Res*, 43(1), pp. 120-4.

Wu, C.C., Li, T.K., Farh, L., Lin, L.Y., Lin, T.S., Yu, Y.J., Yen, T.J., Chiang, C.W. and Chan, N.L. (2011) 'Structural basis of type II topoisomerase inhibition by the anticancer drug etoposide', *Science*, 333(6041), pp. 459-62.

Wu, C.C., Li, Y.C., Wang, Y.R., Li, T.K. and Chan, N.L. (2013) 'On the structural basis and design guidelines for type II topoisomerase-targeting anticancer drugs', *Nucleic Acids Res*, 41(22), pp. 10630-40.

Wu, H.Y., Shyy, S.H., Wang, J.C. and Liu, L.F. (1988) 'Transcription generates positively and negatively supercoiled domains in the template', *Cell*, 53(3), pp. 433-40.

Wu, K.Z., Wang, G.N., Fitzgerald, J., Quachthithu, H., Rainey, M.D., Cattaneo, A., Bachi, A. and Santocanale, C. (2016) 'DDK dependent regulation of TOP2A at centromeres revealed by a chemical genetics approach', *Nucleic Acids Res*, 44(18), pp. 8786-8798.

Yamada, M., Mori, M. and Sugimura, T. (1981) 'Purification and characterization of small molecular weight myeloperoxidase from human promyelocytic leukemia HL-60 cells', *Biochemistry*, 20(4), pp. 766-71.

Yan, H., Tammaro, M. and Liao, S. (2016) 'Collision of Trapped Topoisomerase 2 with Transcription and Replication: Generation and Repair of DNA Double-Strand Breaks with 5' Adducts', *Genes (Basel)*, 7(7), p. 13.

Yan, T., Deng, S., Metzger, A., Gödtel-Armbrust, U., Porter, A.C.G. and Wojnowski, L. (2009) 'Topoisomerase IIα-dependent and -independent apoptotic effects of dexrazoxane and doxorubicin', *Molecular Cancer Therapeutics*, 8(5), pp. 1075-1085.

Yip, B.H. and So, C.W. (2013) 'Mixed lineage leukemia protein in normal and leukemic stem cells', *Exp Biol Med (Maywood)*, 238(3), pp. 315-23.

Yoshida, M.M., Ting, L., Gygi, S.P. and Azuma, Y. (2016) 'SUMOylation of DNA topoisomerase IIα regulates histone H3 kinase Haspin and H3 phosphorylation in mitosis', *The Journal of Cell Biology*, 213(6), pp. 665-678.

Zandvliet, D.W.J., Hanby, A.M., Austin, C.A., Marsh, K.L., Clark, I.B.N., Wright, N.A. and Poulsom, R. (1996) 'Analysis of foetal expression sites of human type II DNA topoisomerase α and β mRNAs by in situ hybridisation', *Biochimica et Biophysica Acta (BBA) - Gene Structure and Expression*, 1307(2), pp. 239-247.

Zechiedrich, E.L. and Osheroff, N. (1990) 'Eukaryotic topoisomerases recognize nucleic acid topology by preferentially interacting with DNA crossovers', *Embo j*, 9(13), pp. 4555-62.

Zee-Cheng, R.K. and Cheng, C.C. (1978) 'Antineoplastic agents. Structure-activity relationship study of bis(substituted aminoalkylamino)anthraquinones', *J Med Chem*, 21(3), pp. 291-4.

Zgliczynski, J.M., Stelmaszynska, T., Ostrowiski, W., Naskalski, J. and Sznajd, J. (1968) 'Myeloperoxidase of human leukaemic leucocytes. Oxidation of amino acids in the presence of hydrogen peroxide', *Eur J Biochem*, 4(4), pp. 540-7.

Zhang, A., Lyu, Y.L., Lin, C.P., Zhou, N., Azarova, A.M., Wood, L.M. and Liu, L.F. (2006) 'A protease pathway for the repair of topoisomerase II-DNA covalent complexes', *J Biol Chem*, 281(47), pp. 35997-6003.

Zhang, Y., Song, S., Yang, F., Au, J.L. and Wientjes, M.G. (2001) 'Nontoxic doses of suramin enhance activity of doxorubicin in prostate tumors', *J Pharmacol Exp Ther*, 299(2), pp. 426-33.

Zheng, N., Felix, C.A., Pang, S., Boston, R., Moate, P., Scavuzzo, J. and Blair, I.A. (2004) 'Plasma etoposide catechol increases in pediatric patients undergoing multiple-day chemotherapy with etoposide', *Clin Cancer Res*, 10(9), pp. 2977-85.

Zheng, N., Pang, S., Oe, T., Felix, C.A., Wehrli, S. and Blair, I.A. (2006) 'Characterization of an etoposide-glutathione conjugate derived from metabolic activation by human cytochrome p450', *Curr Drug Metab*, 7(8), pp. 897-911.

Zheng, W., Warner, R., Ruggeri, R., Su, C., Cortes, C., Skoura, A., Ward, J., Ahn, K., Kalgutkar, A., Sun, D., Maurer, T.S., Bonin, P.D., Okerberg, C., Bobrowski, W., Kawabe, T., Zhang, Y., Coskran, T., Bell, S., Kapoor, B., Johnson, K. and Buckbinder, L. (2015) 'PF-1355, a Mechanism-Based Myeloperoxidase Inhibitor, Prevents Immune Complex Vasculitis and Anti–Glomerular Basement Membrane Glomerulonephritis', *Journal of Pharmacology and Experimental Therapeutics*, 353(2), pp. 288-298.

Zhitkovich, A. and Costa, M. (1992) 'A simple, sensitive assay to detect DNA-protein crosslinks in intact cells and in vivo', *Carcinogenesis*, 13(8), pp. 1485-9.

Zhuo, X., Zheng, N., Felix, C.A. and Blair, I.A. (2004) 'Kinetics and regulation of cytochrome P450-mediated etoposide metabolism', *Drug Metab Dispos*, 32(9), pp. 993-1000.